MUSTANG - A MUltiple Space and Time scale Approach for the quaNtification of deep saline formations for CO2 storaGe

Final Report
Summary of Project R&T Findings

Auli Niemi, Uppsala University (coordinator),
MUSTANG PSC [1]
and MUSTANG partners[2]

September 2014

[1]**MUSTANG Project Steering Committee**: Mikael Erlström, Martin Sauter, Philippe Gouze, Jacob Bear, Jacob Bensabat, Henry Power, Jesús Carrera, Beatriz Medina, Yvi le Guen, Roger Herbert

[2]**MUSTANG partners**: Christopher Juhlin, Fritjof Fagerlund, Kristina Rasmusson, Maria Rasmusson, Tian Liang, Nicoleta Enescu, Fuguo Tong, Farzad Basirat, Saba Joodaki, Zhibing Yang, Chin-Fu Tsang, Yvonne Tsang, Roger Herbert (Uppsala University, Sweden), Jacob Bensabat, Sagi Dor (EWRE, Israel), Martin Sauter, Iulia Ghergut, Mario Schaffer, Tobias Licha, Friedrich Maier, Alexandru Tatomir, Sagi Dror,Torsten Lange (University Goettingen, Germany), Jesús Carrera, Carlos Ayora, Francisco Batlle, Jordi Cama, Francesca de Gaspari, Luis Manuel de Vries, Gabriela Dávila, Marco Dentz, María García Ríos, Albert Nardi, Sebastia Olivella, Tobias Roetting, Maarten Saaltink, Orlando Silva, Luit Jan Slooten, Josep Soler, Victor Vilarrasa, Linda Luguot, Lurdes Martinez Landa (IDAEA-CSIC-UPC, Spain), Jacob Bear, Myra Kitron-Belinkov (Israel Institute of Technology, Israel), Henry Power, Kenneth Andrew Cliffe, David Stevens (Universty of Nottingham, England), Philippe Gouze, Philippe Pezard (CNRS, France), Christopher McDermott, Katriona Edlmann, Stuart Hazeldine (Univeristy of Edinburgh, Scotland), Manfred W. Wuttke, Hans Sulzbacher (Leibniz Institute for Applied Geophysics, Germany), Andrew W Woods, (BP Institute, University of Cambridge, England), Daniel Scradeanu, Radu Gogu, (University of Bucharest, Romania), Gabriele Wiegand, Nicolaus Dahmen (KIT, Germany), Calin Cosma (Vibrometric, Finland), Beatriz Medina, Jordi Bruno (Amphos, Spain), Mikael Erlström, (Geological Survey of Sweden), Vladimir Shtivelman, Michael Gendler, Igor Goldberg (The Geophysical Institute of Israel, Israel), Luxembourg, Eli Kemer (Lapidoth Oil Prospectors Corporation, Israel), Laurent Depraz (Imageau, France), Yvi le Guen, Oliver Poupard (Oxand SA, France)

Table of Contents

1. Introduction

This report summarizes the main scientific and technical results of the MUSTANG project. The results are presented by Work Package. The references are not included for space considerations but can be found on the project web-site and in the 'publications' part of this final report. Besides this summary report, a good overview of project achievements can be obtained from the proceedings of the project final meeting held in Uppsala, May 26-27, 2014 (Deliverables D1015)

D1015: Proceedings of the MUSTANG Closing Meeting Uppsala, May 26-27th, 2014
Part 1: Summary of Panel Discussion and Invited Presentations
D1015: Proceedings of the MUSTANG Closing Meeting Uppsala, May 26-27th, 2014
Part 2: Summary of MUSTANG work Presentations
In these proceedings as well as on MUSTANG webb-site (www.co2mustang.eu) all the presentations are given, thus providing a good overview of the work done.

2. WP 02 - Site Characterization (SGU, UU, UB, CSIC, GII, LIAG)

The overall objective of the Site Characterization Work Package (WP02) has been

- to gather available data from the five different test sites included in the project, the South Scania (Sweden), Horstberg (Germany), Valcele (Romania), Heletz (Israel) and Hontomín (Spain). The gathered data should be relevant to the evaluation of the sites in terms of storage of CO_2 and provide input to the site-specific dynamic simulation models.
- to develop 3D geological models for each test site, and
- to prepare the necessary input data sets for the dynamic simulation models of each test site to be used in WPs on modelling and impact evaluation

The five sites display a wide diversity in location, geology, reservoir properties and depths (Figure 1-1). The sites differ, beside the above mentioned factors, in the quality and quantity of available data. Some sites, like the Heletz site in Israel is highly characterized while others like the Hontomín site in Spain is in the exploration phase. This is clearly reflected in the variable amount of available geological information that has been evaluated and scrutinized from each site.

2.1 Summary of activities

A large effort has been put on the construction of 3D geological/structural models of the sites, and as for the Valcele and Heletz sites, also the spatial distributions of porosity and permeability. Examples of the 3D geological models are shown in Figure

1-1. A substantial part of the work was also in compilation and interpretation of available data into property values and parameters, for the different reservoir and cap-rock units identified and described in the 3D models (Deliverable D022).

During the first phase of the project main focus was put on constructing a framework and screening the type and amount of data available for each site. Emphasis was put on the construction of appropriate templates that would assist the data gathering and assembly, with special emphasis of the data requirements for the assessment of deep saline formations for storage of CO_2 (Deliverable D021).

The subsequent phases focused on compiling the deliverables D023: Report on property values and parameters, related uncertainties and D024: Data files describing the conceptual model for each test site for the computational model and communication of the data analyzed to the respective modeling teams (WP 07) carrying out the dynamic reservoir simulations. In addition, many of the partners involved in the site characterization work package have, during the later stage of the Mustang project, contributed and co-authored a number of papers and presentations where site specific geological settings are presented together with results from different CO_2 modeling scenarios.

2.1.1. Report on property values and parameters, related uncertainties

The characterization is mainly based on existing data from older exploration programs for hydrocarbon exploration or geothermal purposes. This has resulted in data sets which do not completely fill the needs for the numerical simulation of CO_2-storage potential. Data gaps are identified during the compilation of the available information. For most of the sites analyzed there is presently no possibility to supplement the data as sample material (cores, formation fluids etc.) are lacking. In addition, many parameters such as rock stress and hydraulic conditions are only possible to assess from in situ measurements, i.e. during drilling or test operations. For the Heletz and Hontomín sites the drilling of new wells has been/will facilitate the compilation of more comprehensive data bases than was originally available.

The work performed has resulted in a set of summary tables, which describe the available data for each site and unit layer. The unit layers consist of a number of identified reservoir (traps) and cap-rock (seal) units. The parameters included in the tables are described in Deliverables D021 and D022 and defined as the most important input parameters to the dynamic reservoir modeling. The D023 deliverable constitutes together with the reports of the 3D structures the most important and extensive results of WP02.

2.1.2 Data files describing the conceptual model for each test site for the computational model

Most of the work performed involved gathering, compiling and describing existing data. Even though much of this work was initiated during the first 18 months, complementary and continuous transfer and communication of various data sets was made to the numerical modeling teams (Work Package WP07), especially concerning the Heletz and South Scania test site. The ongoing work at the Hontomin site has also resulted in valuable updated 3D models of this site.

The gathered data from the different sites has in addition been communicated with the work package dealing with the Decision Support System (WP09).

The available data sets have been comprehensively described in D024 where type of data, data format, availability, maintenance, and data hosting organisation for the different sites are presented. This meta-data is intended to be a guidance document giving an overview of the data sets, which facilitates the process of data retrieval for various studies.

The information from each site is classified into:

1. Surface data: Geographic, geologic and other thematic maps
2. Seismic and structural data, and 3D information
3. Well reports and wire-line logs
4. Physical and chemical parameters
5. Geological setting – key publications:

An example of data summary is given in table 1-1.

2.2 Main results

The site characterization work of the different sites has resulted in a broad knowledge regarding the complexity of compiling existing data from previous investigations into a framework of needed information regarding characterization of CO_2 storage sites. The experience achieved from the quite different geological settings and characterization work of these sites is essential in assessing their usefulness as storage sites for CO_2.

The main achievements are summarised as follows:

- Construction of a framework, guidelines and templates regarding the geological characterization of potential sites for CO_2 storage.
- Essential parameters needed for the numerical modeling have been identified and available data compiled.
- Structural 3D geological models of all sites have been constructed and experience from this work can be transferred to other CO_2 site characterization projects.
- Experience from performing geological characterization with respect to CO_2 storage in a wide range of geological settings and amount available data has been obtained.
- Wide range of data has been gathered which will complement the overall knowledge base concerning potential CO_2 storage aquifers.
- Identification of data gaps reveals a general lack and need for more information on the cap rock intervals.
- Explanation and validation of geological information to the modeling, i.e. intercommunication between geologists and engineers, has been greatly emphasized, therefore hopefully resulting better and well-motivated dynamic reservoir models in terms of typically difficult issues such as boundary conditions and heterogeneity.

Figure 1-1. Summary of geological characteristics of the five Mustang sites.

	South Scania	Horstberg	Valcele	Hontomín	Heletz
Character	Multilayered sequence of heterogeneous as well as uniform aquifers	Deep, low permeable aquifers High temperature	Oil and gas field Complex structural setting Large data set	Exploration site Pre-investigation phase	Abandoned oil field Well known geology Field test site
Structure	Subhorisontal	Inversion structure	Multitrap folds	Closed dome	Anticline fold
No. wells	16 (2^1)	2	71[2] (241[3])	1 (3^4)	40
Site model, km^2	Regional c. 1000 Local: c. 10	c. 50	c. 5	c. 15	c. 20
Depth range, of potential storage layers	1100–1950 m	3700–4000 m	1100–2200 m	1200–1600 m	1380–1560 m
Age	E. Cretaceous-Jurassic	Early Triassic	Neogene	Jurassic	Cretaceous
Thicknesses of potential storage layers	4–55 m	13–40 m	20–30 m	n.d.	0.6–21
Main rock type	Sandstone	Sandstone	Sandstone	Limestone/dolomite	Sandstone
Main seal rock type	Claystone Argillaceous limestone	Claystone	Marlstone Clay	Marl	Limestone Shale, marl
Porosity, %	20–29	5–10	20–28	n.d.	16–20
Permeability, mD	10–4000	<10	15–500	n.d.	100–250

Figure 1-2. Examples of 3D visualization of the different sites

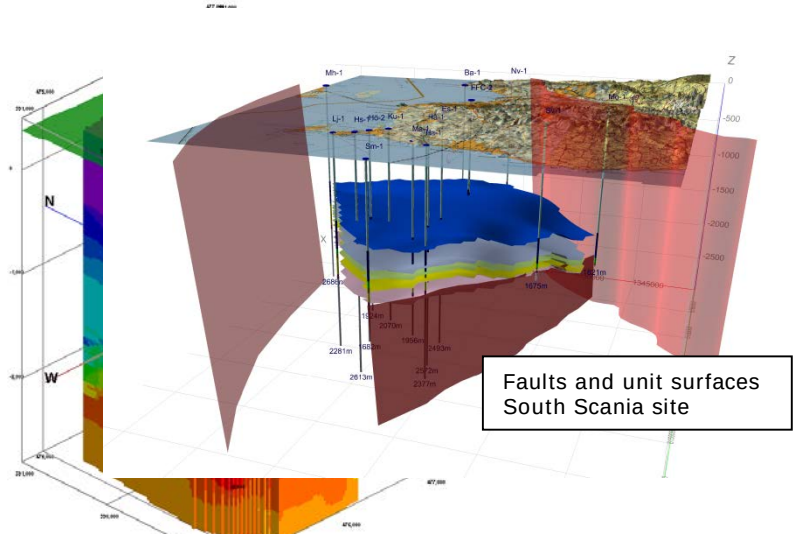

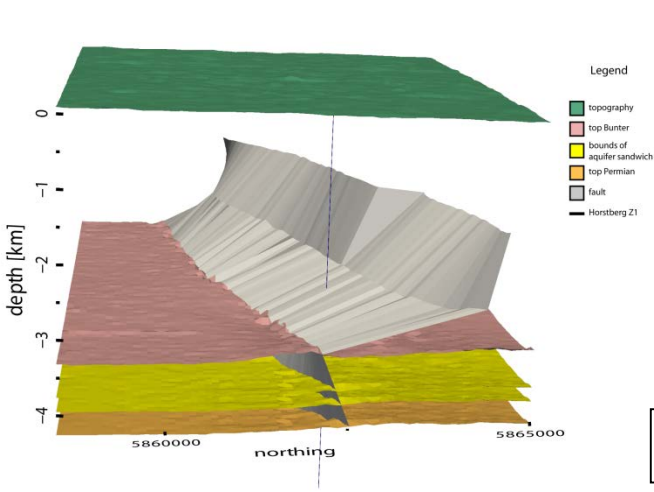

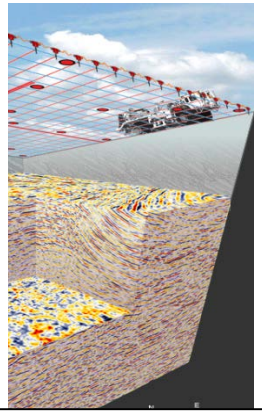

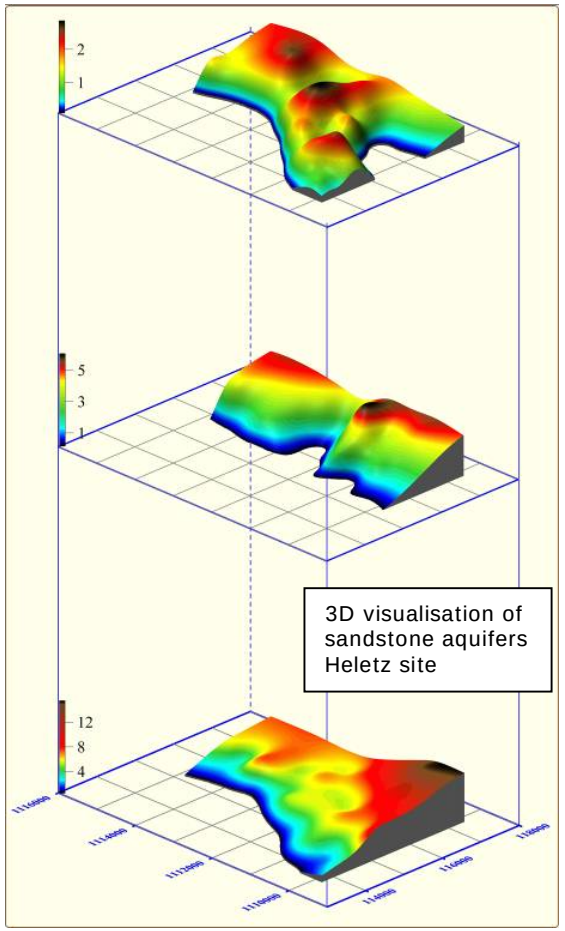

Table 1-1 Example of summary table including data sets, formats, availability and hosting organization for the Heletz site.

Data set	Data type	Format	Host and maintenance	Contact	Availability
Surface data					
Topographic map	Analogue and digital	jpg GIS	GII	www.gii.co.il vladi@gii.co.il	Public
Air photo	Analogue and digital	jpg GIS	GII	-"-	Public
Location of wells and seismic lines (coordinates and maps)	Analogue and digital	jpg Excel	GII	-"-	Public
General geological information					
Geological description of the site	Digital	doc, pdf	GII	-"-	Public
Description of aquifers in the Heletz area	Digital	doc, pdf	GII	-"-	Public
General lithostratigraphic section	Analogue and digital	jpg grf	GII	-"-	Public, presented in D023
Well and seismic data					
Drilling reports	Analogue	jpg	GII	-"-	Public
Well testing reports	Analogue and digital	Excel	GII	-"-	Public
Wire-line logs	Analogue and digital	LAS	GII	-"-	Public
Composite logs	Analogue	jpg	GII	-"-	Public
Expanded composite logs in 3 wells (H-18, H-38 and HE-A1)	Analogue	jpg	GII	-"-	Public
Core analysis	Digital	Excel	GII	-"-	Public
Well log analysis	Digital	Excel	GII	-"-	Public
Permeability vs Porosity – regional relationship	Analogue	jpg	GII	-"-	Public
Estimated porosity and permeability	Digital	Excel	GII	-"-	Public

3. WP 03 – Field quantification techniques

The overall objective of MUSTANG WP 03 was to provide

- innovative, CCS-adapted, field measurement techniques to assess the suitability of a deep geologic saline formation for CO2 storage,
- technologies for monitoring the fate of CO2 during the injection and migration phases in a saline aquifer,
- and finally to recommend suitable and cost-effectives technologies that could be applied for the **MMV** (Measurement Monitoring Verification) process.

3.1 Design and dimensioning of combined HTT experiments for the target formations (UGOE, LIAG)

The key findings of UGOE have been reported in deliverables D35, D38, D61, D62 and in the progress reports.

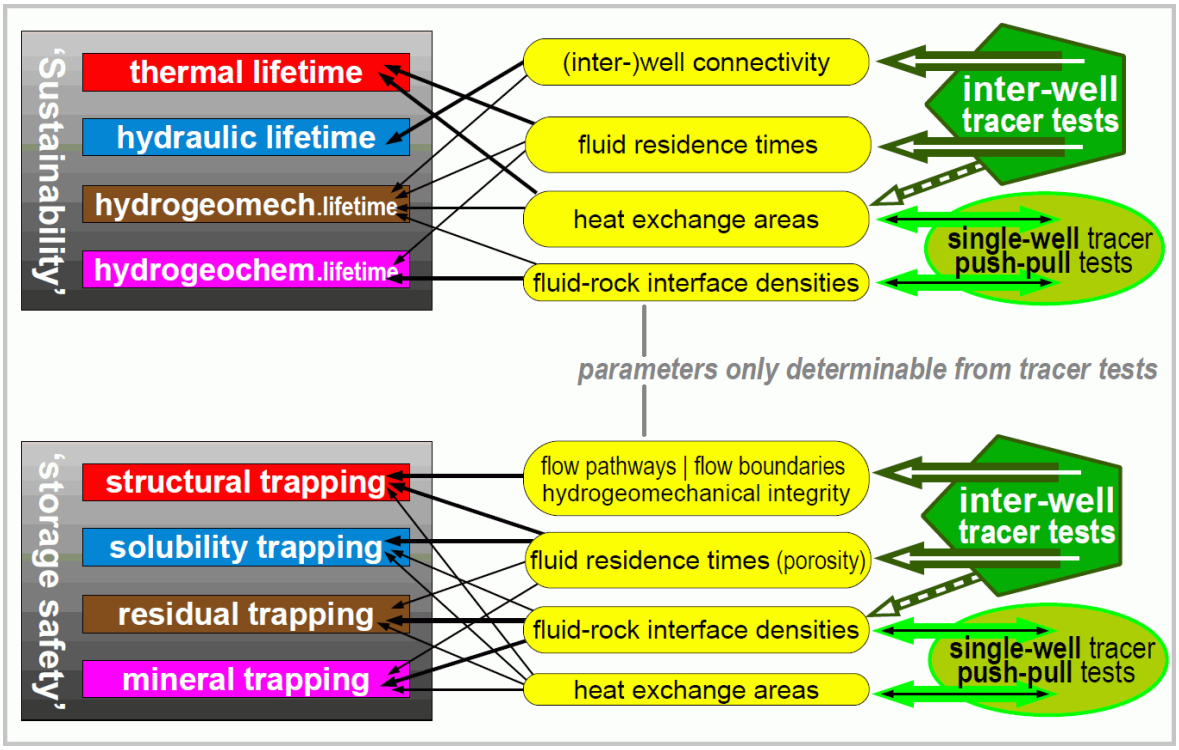

Figure 3-1: Overview of georeservoir and CCS lifetime-controlling parameters that essentially relate to fluid transport processes, and thus can only be measured from tracer tests (IW, or SW).

3.1.1 Merging SW and IW into one forced-gradient dipole test at the Heletz site

The major CO2 injection experiment at Heletz was supposed to be preceded and accompanied by a sequence of single-well (SW) and inter-well (IW) tracer tests, aimed at characterizing transport properties of the target storage formation, in accordance to a number of general and specific principles (Ghergut et al. 2013ac). Instead of the rather luxurious {SW1, IW1, SW2, IW2} test sequence described in Deliverables D6.1, D6.2, D3.5, we also propose a drastically economized tracer test concept (Behrens et al. 2014), which lets the sampling stages of SW and IW tests merge into a single fluid production stage, and relies on a forced-gradient dipole flow field at any time of the overall test (fig. 3-2). Besides cost reduction, this economized design also improves on operational aspects, as well as on issues of parameter ambiguity and of scale disparity between SW and IW flow fields:

(i) the new design renders SW test results more representative for the aquifer sector ('angle') actually interrogated by the IW dipole test (cf. fig. 3-3);

(ii) the new design saves time and costs on the SW test (fluid sampling for SW 'pull' now being conducted simultaneously with IW-related sampling and monitoring), while allowing for a considerably longer duration of SW 'pull' signals than had originally been intended, whose late-time tailings help improve the quantification of non-advective processes and parameters, which are of great relevance to mid- and long-term trapping mechanisms ('residual trapping', 'mineral trapping');

(iii) the quasi-concomitant execution of fluid injection/production for the IW and SW tests considerably reduces the overall hydraulic imbalance that was originally associated with the SW test, thus preventing formation damage and supporting hydrogeomechanical stability;

(iv) the new design reduces the imbalance between injected and produced fluid volumes at any time to a minimum, thus eliminating the need for large-capacity tanks (and water supply) to provide 'push' fluid for injection and to store 'pull' fluid during production within the SW test (saving on costs again).

Consistently with the recommended low injection rates, the triple-scale SW test defined in fig.3-2 is not meant to detect THCM-induced changes to hydrogeological properties of the target storage formation. Instead, it is expected to provide information on hydrogeological heterogeneity, in terms of a possibly scale-dependent, equivalent 'Peclet number', SW test sensitivity to this parameter being approximately similar to that of fig.3-4, with slight improvement: ~erfc(Pe1/2...), for Peclet numbers, versus ~erfc(.../R1/4), for retardation factors.

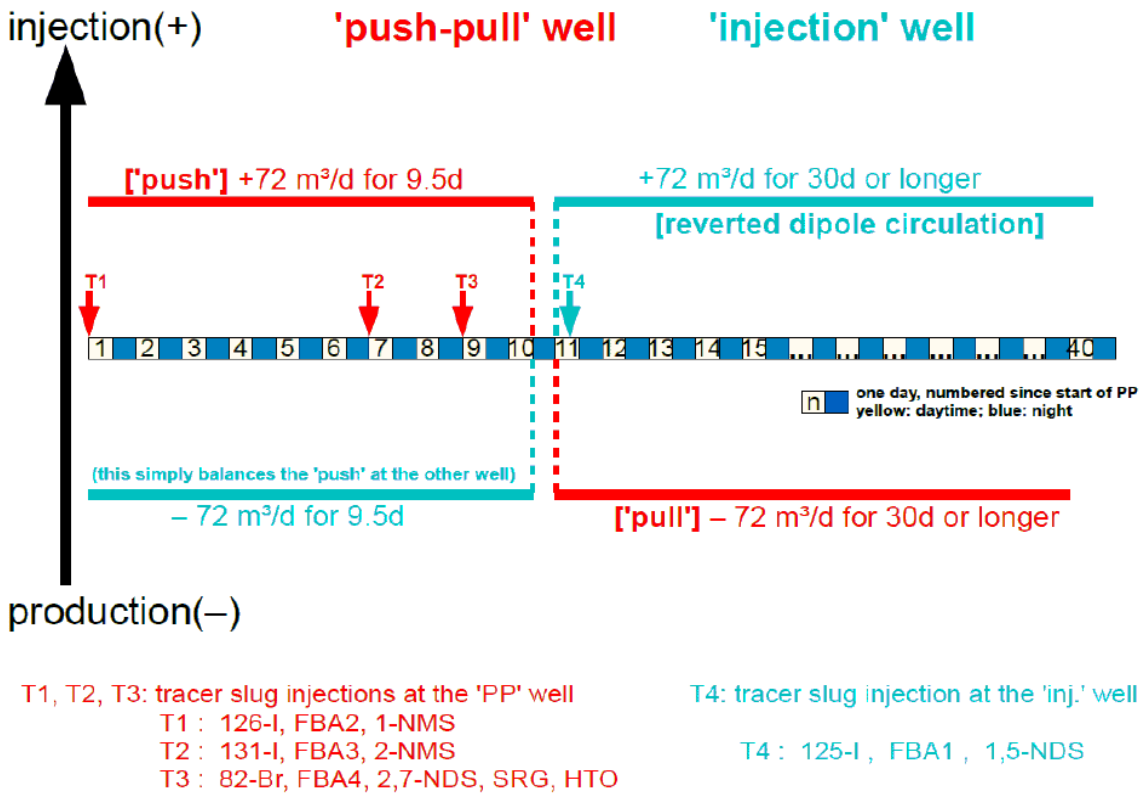

Figure 2-2: Merged SW and IW test design for the Heletz site within the MUSTANG project

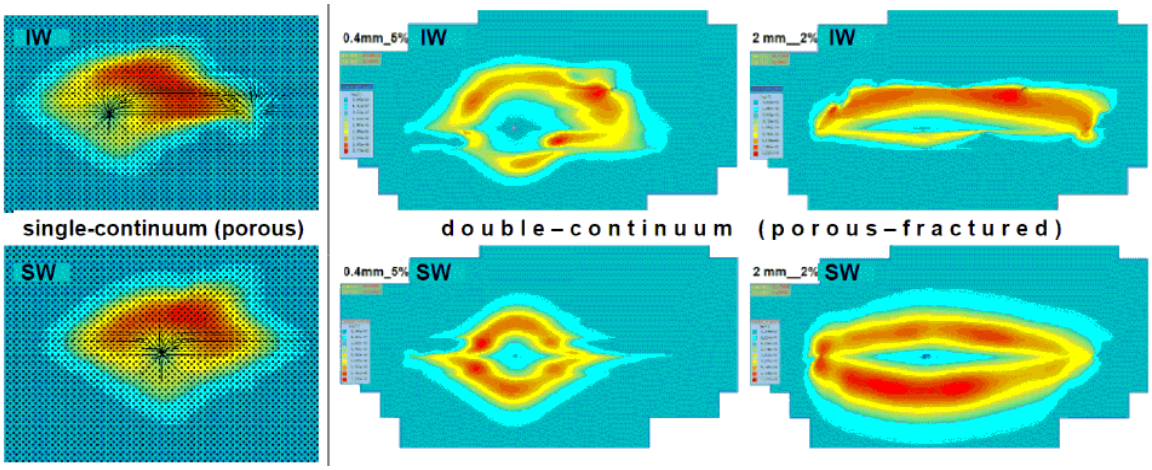

Figure 3-3: Comparison of reservoir regions captured by a dipole versus a monopole test, in a homogeneous single-continuum versus a porous-fractured reservoir.

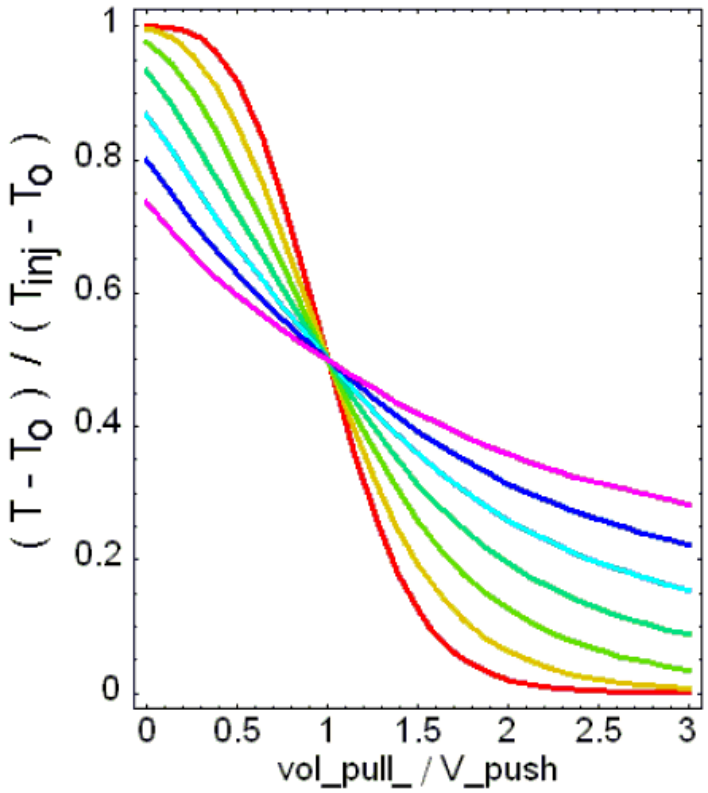

Figure 3-4: 'Pull' signals from heat SW push-then-pull tests in a single-continuum reservoir, for various values of the thermal retardation factor's relative change factor, increasing from f = 1 (red, meaning no change) to f = 1000 (magenta). Only relative changes can be determined from this kind of tests, and high f values are purely theoretical.

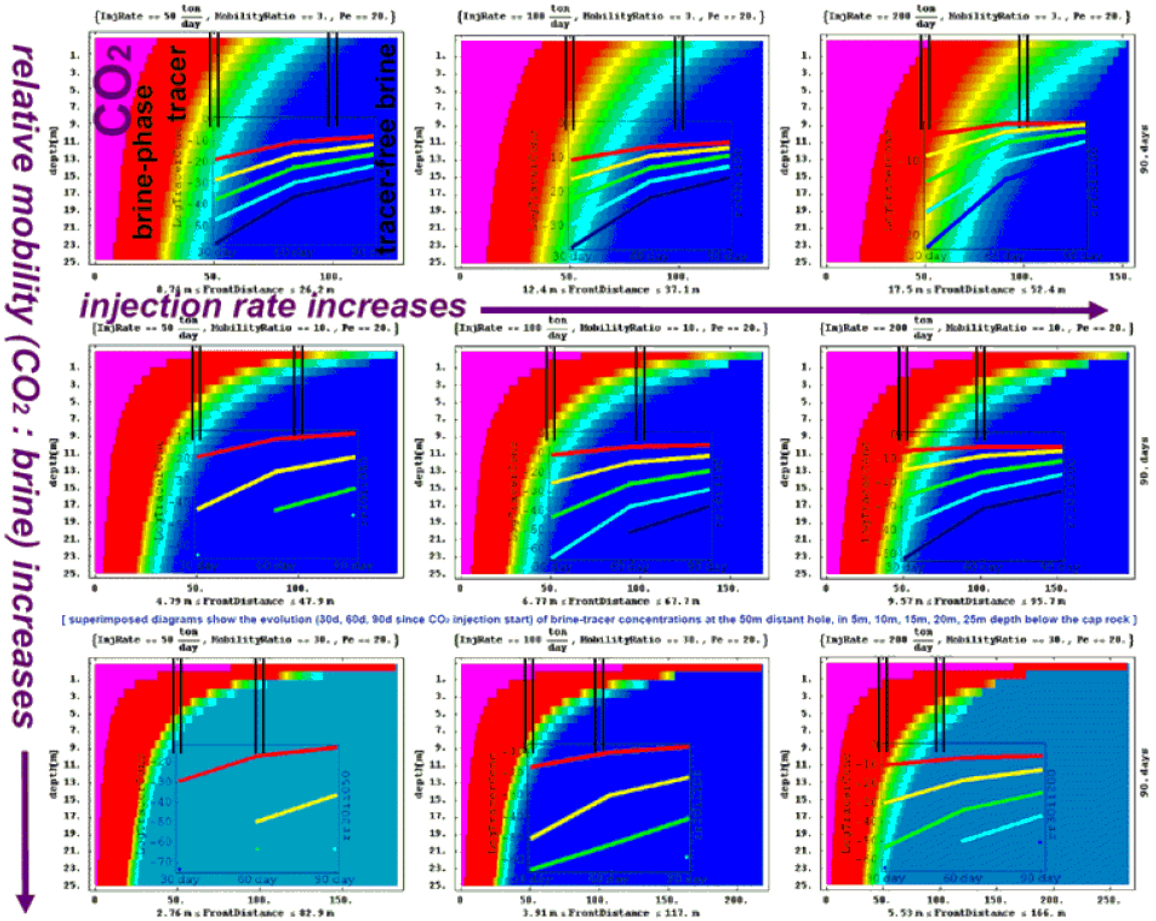

Figure 3-5: Brine-phase tracer spreading during a so-called 'brine displacement' test in conjunction with CO2 injection.

Additionally, experiences made with detecting and quantifying certain organic tracer species in fluid samples from IW tracer tests conducted in the Upper Rhine Rift Valley (2007, 2009, 2011) lead to suggesting new procedures for tracer prequantification to be applied 'on site' (uphole and/or downhole, more or less 'in situ') alongside with the ongoing programs of fluid monitoring during dipole circulation. Also, passive in-situ sampling is especially recommended with a view at very high dilution of brine-phase tracers expected for the so-called 'brine displacement' test stage (fig. 3-5). A further difficulty pertains to 'selecting' adequate tracers. Within German Academia, there seems to be a precept of using only tracers that can be measured by the same people, or same-department colleagues of the people who initiated and conducted the tracer experiments. This precept irrationally limits the choice of 'available' tracers with physico-chemical properties suitable to the intended test purposes. A host of financial, administrative, cultural, ideological, and sometimes also technical barriers obstruct a sane cooperation between colleagues who would have been able to detect and quantify a particular tracer species, and colleagues who would have liked to use that particular tracer species within a particular experiment. With the tracer cocktail suggested in fig. 3-2, we assume that those barriers will not be encountered within the MUSTANG project.

3.1.2 Conceptualized relation of single-well/inter-well tracer tests to the target information required for georeservoir management

Sensitivity analysis of flow and transport parameters in the dipole configuration for Heletz

One step in the design process of the tracer tests to be conducted in the pre-injection of CO2 stage is the inter-well (IW) tracer test. We have a closer look at the IW or dipole experiment and its dependency on various flow and transport parameters. Understanding the individual parameter sensitivities is important to adjust the constraints of the tracer test that has to be pre-designed appropriately, like the fluid turnover rate, the injection-fluid availability and conditioning facilities, fluid disposal capacity, the test duration, tracer quantities/ species available, tracer metering costs, etc. That is accomplished through a sensitivity analysis of the BTC associated with different flow and transport parameters: effective transport porosity, intrinsic permeability, numerical discretization scheme and size of the finite elements.

The focus was to investigate the individual sensitivities of the selected target parameters by means of numerical modelling for an inter-well tests configuration. Furthermore, two computer models were developed for simulating flow and transport in deep geological reservoirs, which were implemented within different frameworks. The goal is to examine the variability in the model predictions obtained with different modelling tools and perform a benchmark. The comparison of the modelling results shows good agreement and increases the confidence and accuracy of predictions.

The collection of BTCs corresponding to different porosities, intrinsic permeability, injection and extraction rates of water and other parameters helps to design the tracer experiments and to decide the best CO2 injection strategy.

- **Numerical simulation environment:** Two simulation programs have been used to implement and compute the flow and transport of tracer in porous media. The first one, DuMu^x (Flemisch et al. 2011), is a free, open-source numerical simulator using the vertex centred finite volume method (Helmig 1997) for the spatial discretization techniques. The second simulator is COMSOL Multiphysics a proprietary software using finite element method. Both DuMu^x and COMSOL have been verified and validated in many benchmark studies. The numerical model comparison has increased the confidence in the predictions to the tracer experiments. Their results are in relatively good agreement.
- **Site specific tracer tests at Heletz:** The planned tracer test experiments at the Heletz site involve currently two wells, one injection well and one monitoring and extraction well. A more detailed description of the comprehensive tracer test planning and modelling can be found in (Bensabat et al. 2011; Niemi et al. 2012) or in MUSTANG deliverables D35, D61, and D62. While the distance between the wells is 50 m, the cumulative sandstone width is approximately 10.6 m. The permeability range of the sandstone is between 1 and 400 mD (millidarcy) whereas, for the shale it is about 0.001 mD. Besides vertical heterogeneity, the sandstone has a coarse aspect and often is loosely cemented. The effective transport porosity is between 10% and 30% for the sand stone and 0.1% for the shale. The diffusion coefficient is chosen constant 1e-9 [m^2/s]. The tortuosity factor is given with the Millington and Quirk model.
- **Pressure sensitivity to intrinsic permeability:** The pressure response with regard to the variation of intrinsic permeability is important for establishing the injection rate during the tracer tests and to prevent fracturing. Figure 3-5 indicates the pressures in a homogeneous reservoir with different permeabilities. In the traditional sense of a

hydraulic pulse testing water is injected into the reservoir and the pressure profiles are plotted as shown in **Figure 3-5**. Lower permeabilities correspond to higher pressures whereas the BTCs overlap (**Figure 3-7**). A permeability field is generated using a Gaussian uniform distribution. The calculated velocities are shown in **Figure 3-8**. The profile of the BTC is not sensitive to the contrast in intrinsic permeabilities but to the distribution of heterogeneities.

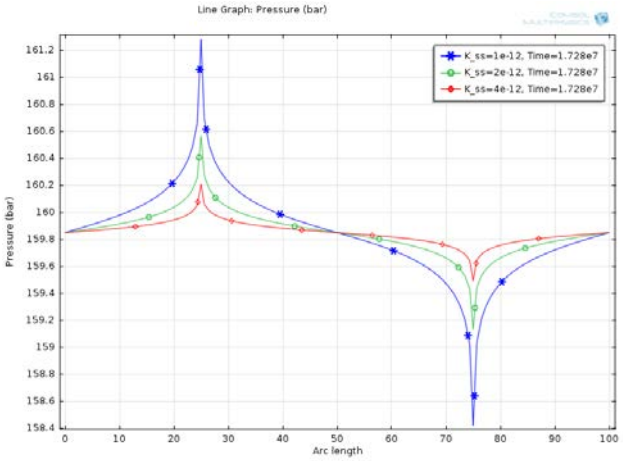

Figure 3-6: Pressure profile response related to intrinsic permeability of the reservoir

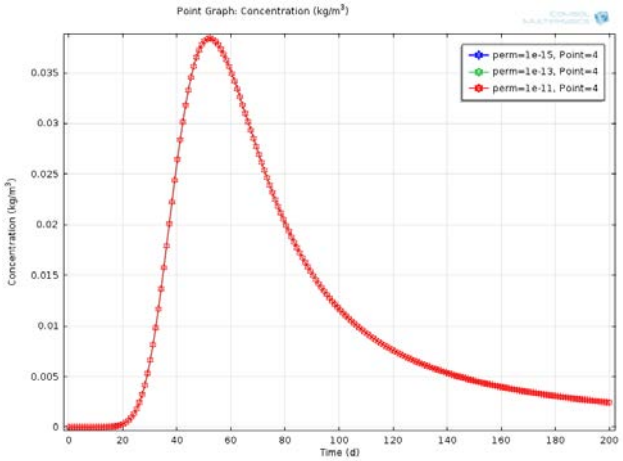

Figure 3-7: BTC comparison for different uniform distributions of permeabilities

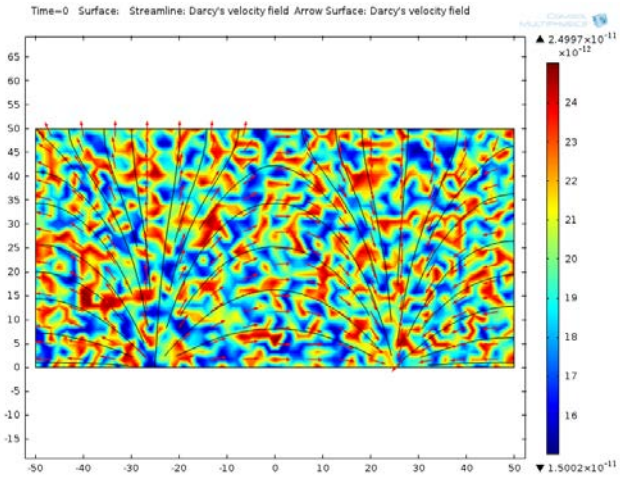

Figure 3-8: Streamline Darcy velocity field resulted from a uniform distribution of intrinsic permeabilities

- **Parametric study with regard to effective transport porosity:** The peak arrival time and the shape of the BTC are changing with the effective transport porosity (Fig 3-9). The results obtained with DuMu^x implementation and COMSOL implementation are shown in **Figure 3-9**, respectively **Figure 3-10**. Furthermore the two can be compared with each other. Even though there are slight differences in the peak concentrations, the arrival time and BTC profile are in good agreement. The injection and extraction rates are 5 [m^3/h].

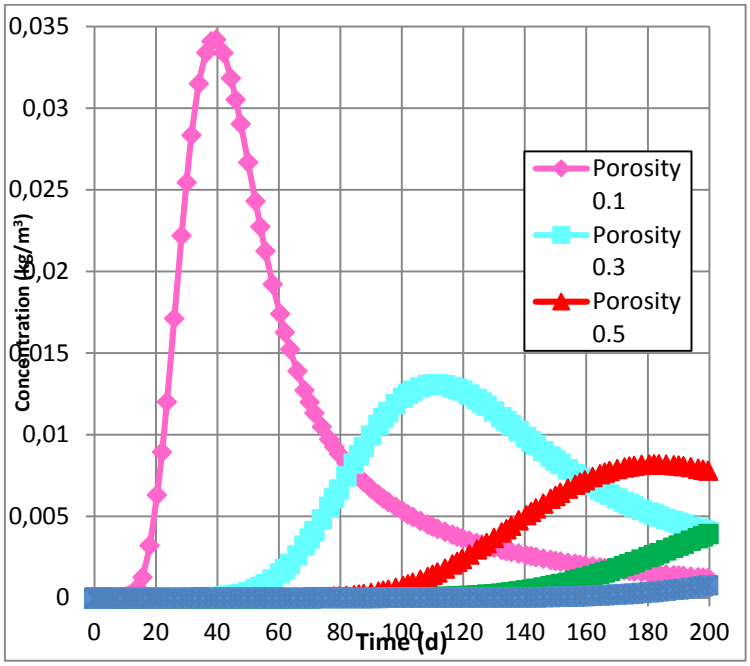

Figure 3-9: DuMux BTC variation with change in porosity

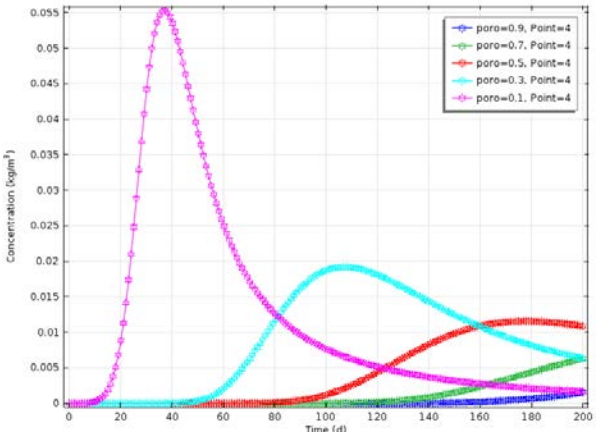

Figure 3-10: COMSOL BTCs variation with change in porosity

- **Peak arrival time with regard to injection and extraction rates:** The pumps required for dimensioning the IW tracer tests have to be chosen according to the injection and extraction rates. These rates have a direct influence on the shape of BTC (see **Figure 3-10**) and the peak arrival (**Table 1**). Two scenarios have been considered, the first one considers that water is injected and extracted with the same rates and is noted "WithExtr.", and the second assumes that at the monitoring well there is no extraction, shown in the "NoExtr." column. The porosity parameter is kept constant 14.3% and only the pumping and extraction rates are varied. The peak arrival time with extraction is approximately three times faster than in the scenario without extraction. This indicates that any extraction pump that has a rate between 0 (no extraction) and the rate equal to injection will produce a BTC with the peak arrival time between the two values. The analysis of the BTCs cannot determine specific location of the flow path distributions and implicitly the heterogeneities of the geo-reservoir. They appear as volume averaged properties which cannot be uniquely inverted. Therefore the tracer analysis has to be combined with geophysical methods and hydraulic tests.

Table 3-1: Peak arrival variation with regard to injection-extraction rate

Q [m^3/h]	Peak arrival [day]	
	WithExtr	NoExtr.
5	52.4	151
4	64	188
3	86	256
2	127	378
1	254	

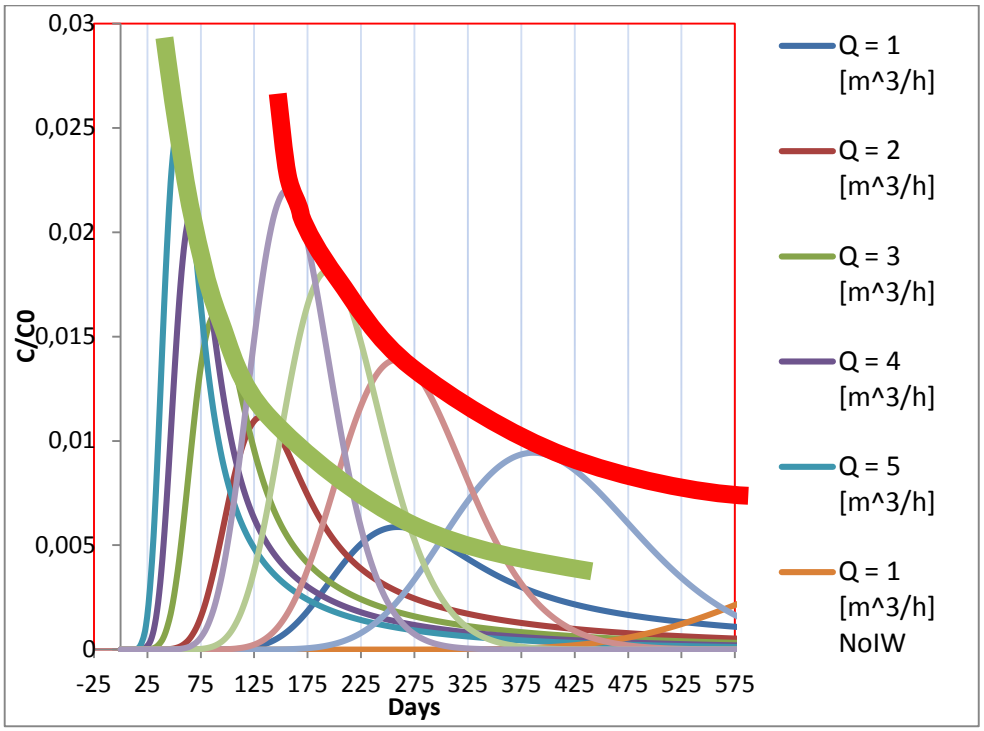

Figure 3-11: Variation of BTCs with pumping rates

3.1.3 Two-well test sequence for quantifying residual and dissolution trapping

A two-well test sequence aimed at quantifying field values of both residual and dissolution trapping of CO2 was developed. The test was applied to the Heletz experimental CO2 injection site, using numerical modelling. The sequence includes a hydraulic test to measure residual scCO2 saturation and a novel tracer technique, together with measurements of abstracted fluid compositions for quantification of the rate of CO2 dissolution in the reservoir. The proposed negligible solubility tracer (NST) technique uses a tracer with negligible aqueous solubility, which is injected with the scCO2 and enriched in the scCO2 phase as CO2 dissolves. A clear relationship exists between the NST enrichment in the supercritical (sc) CO2 phase and the dissolution of mobile scCO2 in the formation for a wide range of different groundwater flow fields and dissolution patterns represented by the different modelling scenarios (Fagerlund et al., 2013). Hence, it was shown that this tracer can provide direct information about the dissolution of mobile scCO2. Example of simulation results is shown in WP 06.

Furthermore it was shown that the rate of abstracted dissolved CO2 can be used to predict the total rate of CO2 dissolution, provided that the amount of dissolved CO2 in the formation stabilizes. It was concluded that the combination of these measurements is a promising tool for detailed field-scale characterization of residual and dissolution trapping processes. More detailed information is given by Fagerlund et al. (2013).

3.1.4 Semi-analytical approximation to tracer signals

- A semi-analytical approximation to tracer signals was proposed (Ghergut et al. 2013) with the advantage of expressing the tracer signals in terms of fluid volume recovery

fraction rather than time. This makes the inter-well tracer tests independent upon the distance between wells and upon the injection/ production rates.

- Tracer signals were simulated for Heletz for different hydrostratigraphy scenarios using three types of tracers to be used both in inter-well and single-well push-pull tests (**Figure 3-12**).
- The inter-well tests are sensitive to storage capacity but suffer from ambiguity between longitudinal and vertical heterogeneity and from all-parameter ambiguity at early times.

3.2 Implementation of HTT methods for field sites

3.2.1 IW and SW test simulations for the Heletz site: main findings

For the Heletz site, a number of up to nine alternating sandstone and shale layers were assumed, whose permeabilities contrast by factors ~103–104, and whose transport-effective porosities range from 3–5% (shale) to 11–18% (sandstone), according to Fagerlund et al. (2011), Bensabat et al. (2011) who had proposed five different hydrostratigraphy scenarios: a so-called 'best estimate' (BE, with 9 different layers whose permeability and porosity values were derived by standard inversion protocols from available poro-perm and hydraulic test data), a 'single-layer' equivalent (SL), a version of SL with doubled porosity (SL2), and two variations of BE amplifying the permeability contrast factor between contributing layers by 4 and by 8, respectively (BE4, BE8). With these hydrostratigraphy scenarios, tracer signals were simulated for three types of tracers, to be used in both IW and SW push-pull tests:

- conservative solute tracers (including fluid salinity as a particular case),
- equilibrium-sorptive tracers, whose distribution coefficients (between brine and sandstone rock surface) must be assessed independently from these very tests (sorptive tracers being assumed to adsorb onto sandstone rock surfaces, but not onto shale's),
- heat as a tracer (with fluid temperature as the measurable signal quantity).

Simulation results are summarized in **Figure 3-12**, for IW tests, and **Figure 3-13**, for SW tests. As expected, tracer signals from inter-well tests are quite sensitive to the total storage capacity (measured primarily by transport-effective porosities ε), but suffer from a certain ambiguity between longitudinal heterogeneity (measured by a Peclet number Pe) and vertical heterogeneity (expressed by the different hydrostratigraphy scenarios Prf(z), as detailed above). At early times (volume recovery fraction <0.3), IW tracer signal inversion suffers from ambiguity between all parameters: porosity, longitudinal dispersion, vertical heterogeneity. Ambiguity between porosity and longitudinal dispersion diminishes with increasing observation time; also, it can be eliminated by using fluid temperature signals, and/or sorptive tracers, alongside with conservative tracers. On the other hand, the ambiguity between vertical heterogeneity and longitudinal dispersion can be eliminated from IW signal inversions, by exploiting the insensitivity of SW tracer pull signals towards vertical heterogeneity. In turn, SW tracer signal inversion suffers from ambiguity between porosity and radial dispersion; this ambiguity can be reduced by using sorptive tracers (whose sorption distribution coefficients must be known independently of the very SW test), and/or fluid temperature signals (sufficient temperature contrast provided between the injected fluid and the target formation).

Table 2 lists the species and quantities of sensible chemical-tracer combinations that can be used at the Heletz site in order to achieve 'ambiguity reduction' in the sense explained above. All those species were assumed to be environmentally benign (cf. Behrens et al. 2001). Expectations regarding tracer adsorption onto sandstone (while not onto shale) were derived

from Behrens (1986); expectations as to a possible temperature dependence of sorption properties from Maggs (1969), Teutenberg (2010).

To be noted, unlike with **Figure 3-12**, porosities with **Figure 3-13** should not be regarded as unknown, because they cannot be determined from SW tests alone. Finally, it remains to ask: does the Heletz stratigraphy, in conjunction with the maximum duration of intended SW and IW tests, fit the assumptions that justified neglecting the effects matrix diffusion? This question remains to be answered by the field tracer tests themselves.

3.2.2 Protocol for the field experiment at Heletz (EWRE, UGOE, ETH, UU)

- A protocol for the first field experiments at Heletz was created. It consists of the following HTT tests: step testing, pulse testing, push-pull tracer test, borehole thermal recovery test, flowing fluid electrical conductivity, chemical characterization of the formation fluid, flowing fluid electric conductivity. The protocol is not currently published being available only for the MUSTANG partners.

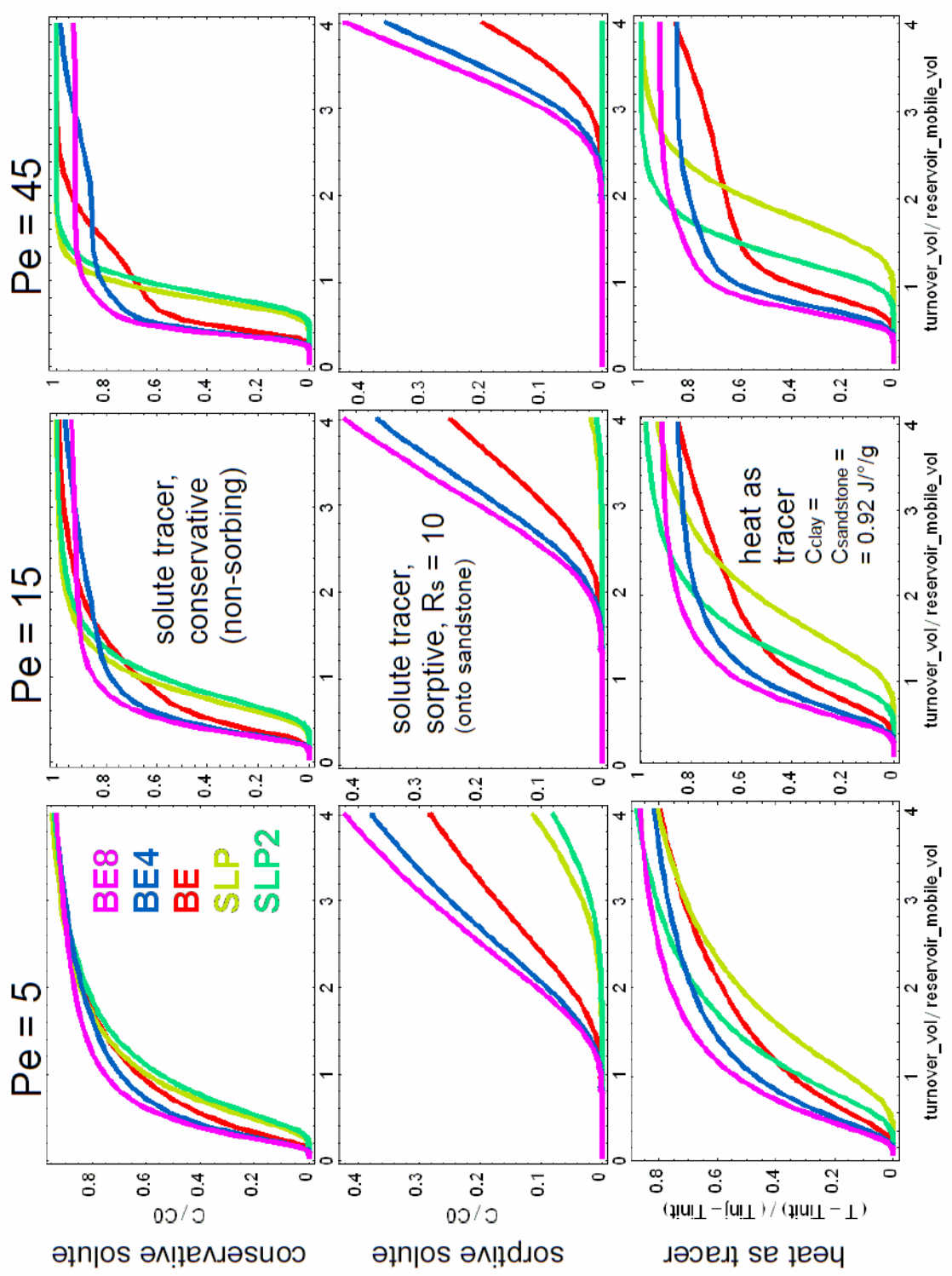

Figure 3-12. Simulated IW test signals, using conservative and sorptive solutes, or fluid temperature as a tracer, for different degrees of longitudinal heterogeneity (measured by Peclet number), vertical heterogeneity (indicated by different colors within each plot) and reservoir size (expressed by the scaling of the time equivalent axis)

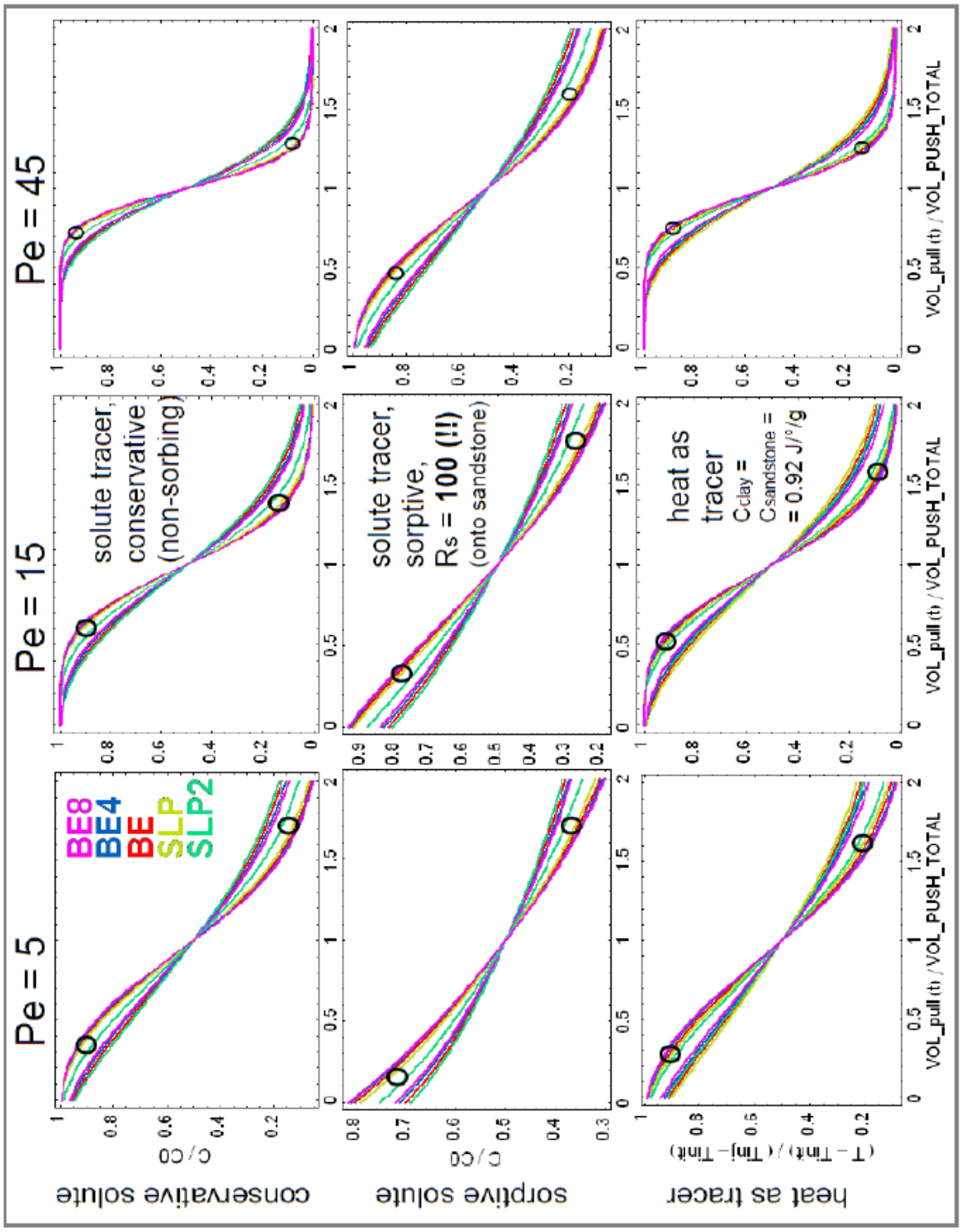

Figure 3-13. Simulated SW test signals, using conservative and sorptive solutes, or fluid temperature as a tracer, for different degrees of longitudinal heterogeneity (measured by Peclet number), vertical heterogeneity (indicated by different colors within each plot) and reservoir size (expressed by the scaling of the time equivalent axis)

Table 3-2. Liquid-phase tracer species and quantities recommended for use at the Heletz site.

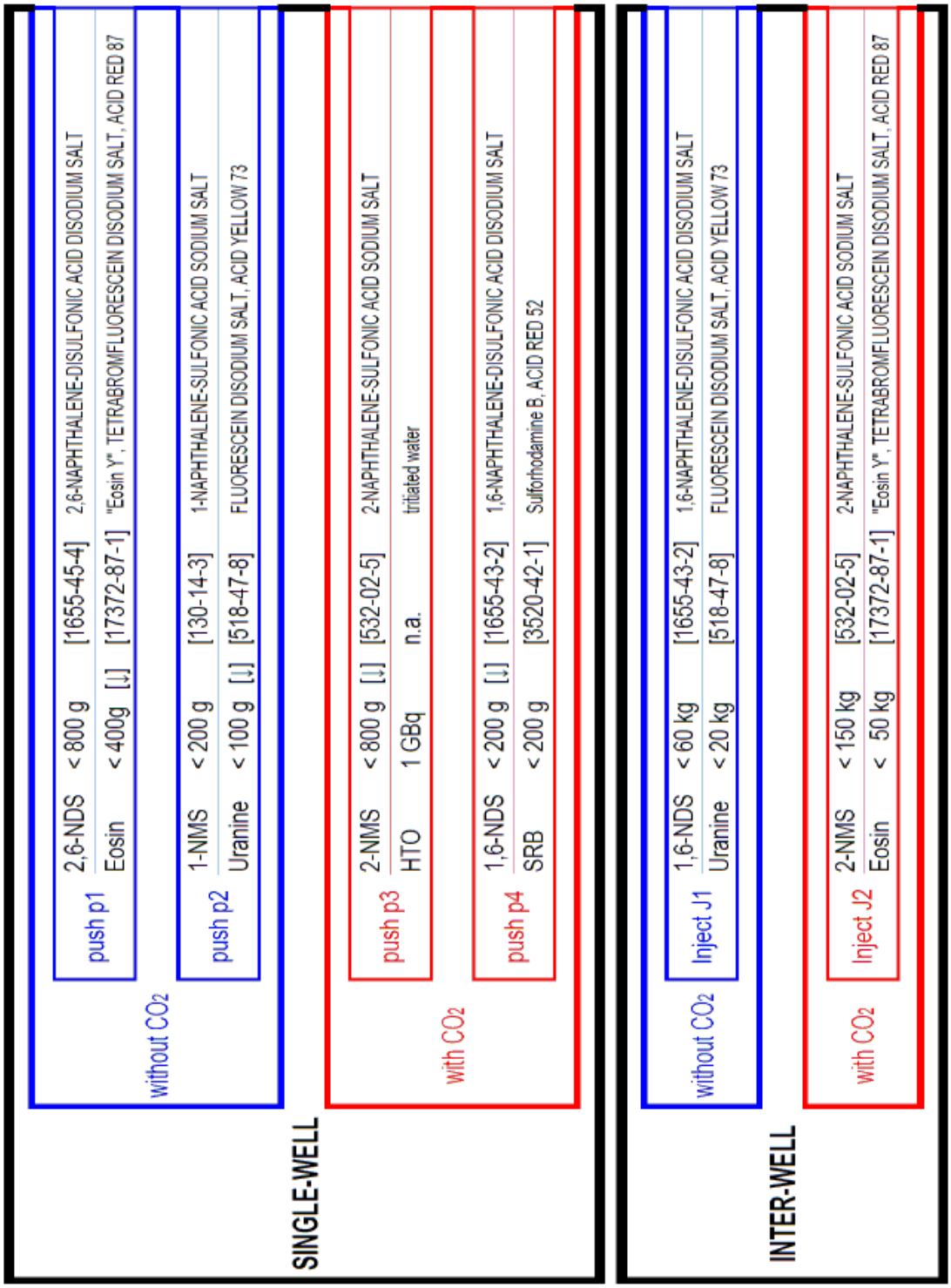

3.3 Laboratory investigations on hydraulic and tracer behaviour

3.3.1 Tracer development

The development of kinetic KIS tracers is reported in WP 04.

3.3.2 Hydraulic experiments to determine the hydraulic conductivity

The hydraulic conductivity of the sandstone in the target layer is to be determined. Pressure drop ranges of the PERO device (Figure 3-15) are up to 10 bars using air as pressure source. The core sizes have a diameter of 4-5 cm and 9-10 cm length. The device had to be modified to fit the core dimensions taken from Heletz.

- During the Haifa meeting in September 2012 samples from the wells Heletz 18A and Heletz 18B were distributed to the project partners for characterization of both, the reservoir and the cap rock of the sandstone reservoir in the Heletz Formation. UGOE received a small number of core subsamples to determine hydraulic properties and if possible evaluate the sorption characteristics with respect to the tracers that would be selected for the tracer experiments. The available core material however, was not sufficient to study transport behavior by means of column experiments.

- Two strategies were followed to obtain results for the hydraulic properties of the reservoir rock as soon as possible to be applicable in the various tasks in WP3 and WP6. On the one hand, a permeameter from PERO Gesellschaft für Mess- und Steuerungstechnik mbH, Sickte, Germany was installed and pre-tested at UGOE. Because the device was not suited for core diameters of less than 10 cm it was adapted first to the diameter of 4 cm of the Heletz core samples.

3.3.3. High resolution micro-CT

- In cooperation with Dr. Matthias Halisch (LIAG) high resolution micro-CT scans have been performed on the sandstone cores from Heletz (Figure 3-13). The probes have provided the hydraulic conductivities
- Although, the core analysis was prepared at UGOE, it was eventually decided to perform all tests at LIAG, Hannover, because of their technical capabilities as well as experience with respect to problematic core material. The core material was problematic with respect to a low degree of cementation, which would make permeability testing using the water based permeameter at UGEO a difficult task. In addition, subsequent investigations on the material were likely to be impossible. Beside the pore scale analysis using computer tomography gas permeabilities were determined at ambient pressure so far. While this report was in preparation work continued to run permeability experiments at higher pressures. New high pressure rubber cuffs were purchased to conduct these experiments at LIAG, Hannover. The maximum pressure that can be reached before core failure is unpredictable because of the limited stability of the sample material.

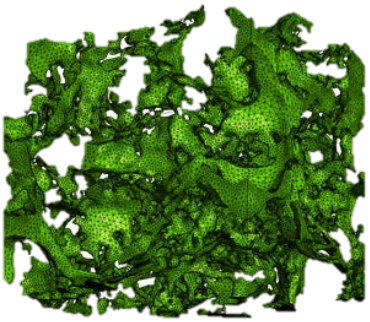

Figure 3-14. Pore structure of Heletz sandstone

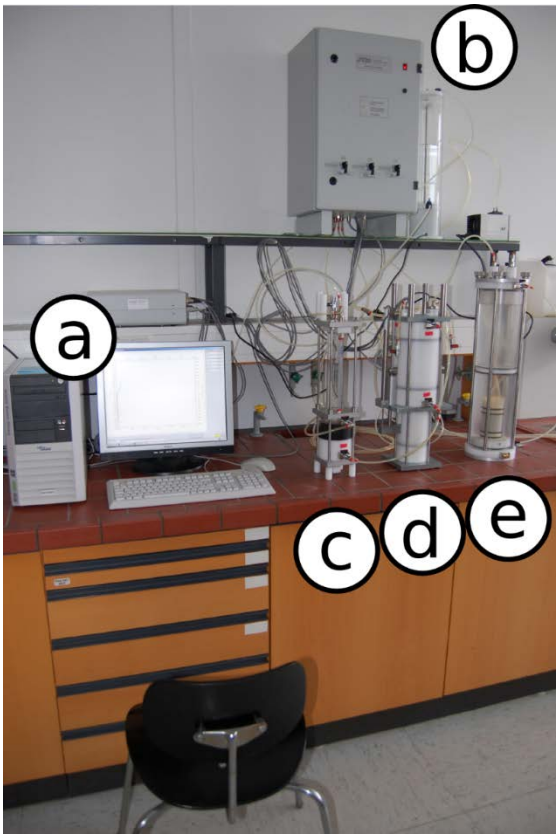

Figure 3-15. PERO device for measuring hydraulic conductivity in the laboratory on the sandstone cores. permeameter to determine hydraulic conductivities developed by PERO Gesellschaft für Mess- und Steuerungstechnik GmbH, Sickte, Germany. The components of the device are indicated by small letters in the picture: a) computer with software interface to run the experiments, and store and evaluate data; logic controller unit above the PC monitor, b) pressure control unit and water reservoir on its right side, c) graduated burette to record the core saturation volume, d) pressure balance to apply adjustable, stable pressure differences at high pressure levels between inlet and outlet of the pressure cell; the water flow rate is determined by recording the movement of the piston inside the balance over time, e) pressure

cell with core sample – water circulation system through the core is separated from the cell pressure by latex tubes.

Figure 3-16: Core samples of sandstone from Helet (H18A and H18B).

Table 2-3. Permeability measurements in millidarcy (mD) on the sandstone cores from H18A and H18B from Heletz

#	Fine core (H18A), Direction I	Fine core (H18A), Direction II	Coarse core (H18B), Direction I	Coarse core (H18B), Direction II
1	449	469	339	351
2	441	465	358	343
3	431	467	355	343
4	459	453	349	342
5	449	449	343	341
6	440	456	341	339
7	426	442	348	338
8	441	453	346	335
9	455	442	348	331
10	439	447	344	329

3.4 Seismic modelling to determine source-receiver geometry

3.4.1 Background

The seismic development has been documented in Deliverables D031, D033 and D036.

Approximately 1400 tons of CO2 are planned to be injected at the Heletz site at a depth of approximately 1550 m over a 2-3 week period in early 2013. The estimated thickness of the

injection horizon is 5 to 6 m and the estimated average porosity is 15%. The diameter of the plume is expected to be of the order of 100 m. Based on modelling studies (Alonaizi et al., 2011; D033), it is doubtful that a plume of this size can be detected with standard surface seismic measurements. Noise and repeatability become significant issues. However, the modelling does indicate that if highly repeatable and low noise data can be acquired then there is a chance to see the plume. Therefore, we have designed an acquisition strategy where the seismic experiment is repeated numerous times with an acquisition geometry that is as close as possible the same each time.

3.4.2 Seismic source development

The initial objective was to develop a near surface 'permanent' source to be tested during the main field test of the Mustang project, at the Heletz site. However, later in the project it has been considered that placing a permanent prototype source at a predetermined fixed location would make problematic if not impossible the detection by seismics of such a small CO2 plume as derived through modelling. New directions of interest and priorities also appeared in the course of the project, such as increased emphasis on low frequencies.

A prototype low frequency surface seismic source has been built based on the VIBSIST concept. The prototype is mobile, to serve the current needs of the project, but the same concept can be used for permanent subsurface installations

The acoustic impedance contrast at the source/ground contact is significantly reduced by using high density liquids and/or rubber compounds. As a result, the source signature becomes a wide band critically damped transient, which is conveyed with high efficiency to the ground.

The study of the high density fluids as conveyors of seismic energy from the source to the ground has not been reported previously and is, therefore, presented in some detail deliverable D036.

3.4.3 Borehole digital receivers

Considering the modelling results (D033) it became clear that borehole seismic measurements should augment any surface investigations in order to increase the chances of detection of a small CO2 plume, such as one with diameter of ~100m.

Digital receivers, the RD-XYZ, with 4-components/level were developed by Vibrometric, independently of the MUSTANG project. However, in order for the new tool to be useful for the planned field tests within this project, the 4th component can be a hydrophone or a 1 Hz geophone, which can provide a LF solution. The tool is designed to be a very low noise one, with an 8-step gain control down-hole. It has individually programmable amplifiers and 24-bit down-hole A/D conversion for up to 96-levels on a wireline cable. Its modules are interchangeable, with software-driven reconfiguration.

Together with EWRE and Solexperts, significant effort has been made during the design of the smart casing for the Heletz wells, so that the RD-XYZ may be temporarily installed in these wells. Geophones are planned to be installed to a maximal depth of 1600 m. Vibrometric is in charge to deliver and to install the geophone string. The following requirements were considered to ensure that geophones may be used at Heletz:

- The geophones must be in contact with the casing
- The geophone string must be movable in order to cover a large depth interval by moving the string between measurements.
- Free space must exist for a geophone outer diameter (54 mm)

- Space for a cable of 20 mm diameter must exist

Figure 3-17 shows the installation layout, where a v-shaped guidance aluminium profile mounted to the twin tubing assures the orientation of the geophone probes. Solexperts proposed

Vibrometric to equip the geophone probes with two sliding elements. One side of the sliding element fits into the v-profile. The other side is equipped with wheels rolling on the casing. Springs are attached to the arms holding the wheels. Due to the springs the wheels are pushed to the casing. The well completion has been later modified and a tube dedicated to the geophone installation has been included. This tube is cemented inside the casing and therefore provides a

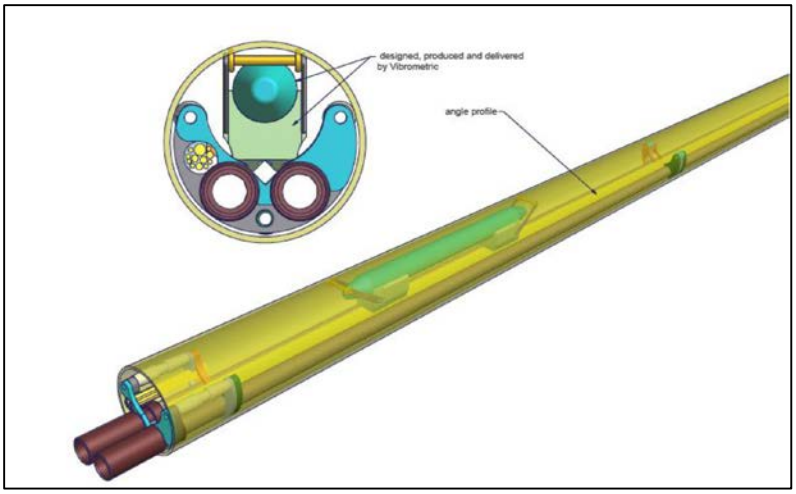

Figure 3-17: Installation scenario for the RD-XYZ digital downhole receivers.

more stable acoustic contact of the geophones clamped inside the tube to the formation.

3.4.4 Field tests, acquisition strategy

Surface seismic data (both active and passive) will be recorded during the injection period. During the injection period, active source data will be recorded on a daily basis along a fixed 2D receiver spread (Figure 3-18), giving a series of about 10 repeats during the injection period. This may allow small changes in the reservoir to be monitored at fine temporal resolution. In addition to recording the active source data, all stations will also record on a continuous basis during injection when active data are not being recorded. The continuous recordings can be used to possibly detect micro-seismicity and for generating virtual source gather seismograms, using correlation techniques, that can be further processed.

UU will bring 48 single-component wireless units and 24 three-component wireless units with integrated low frequency MEMS sensors attached. 10 Hz geophones will be connected to the single-component units. All sensors will be buried at about 30-50 cm depth, ensuring good coupling and reduced noise conditions. The units will be powered by 12 volt batteries that will be purchased in advance in Israel. All other equipment necessary for recording will be transported to Israel from Uppsala. The newly developed VIBSIST-500-LF will be used as the source during the injection period. It is estimated that each source point will take 3 minutes to acquire on average. If the source is activated at every receiver point then the daily acquisition

time is about 4 hours for the active source component. This leaves time to use the source the rest of the day for borehole seismic measurements.

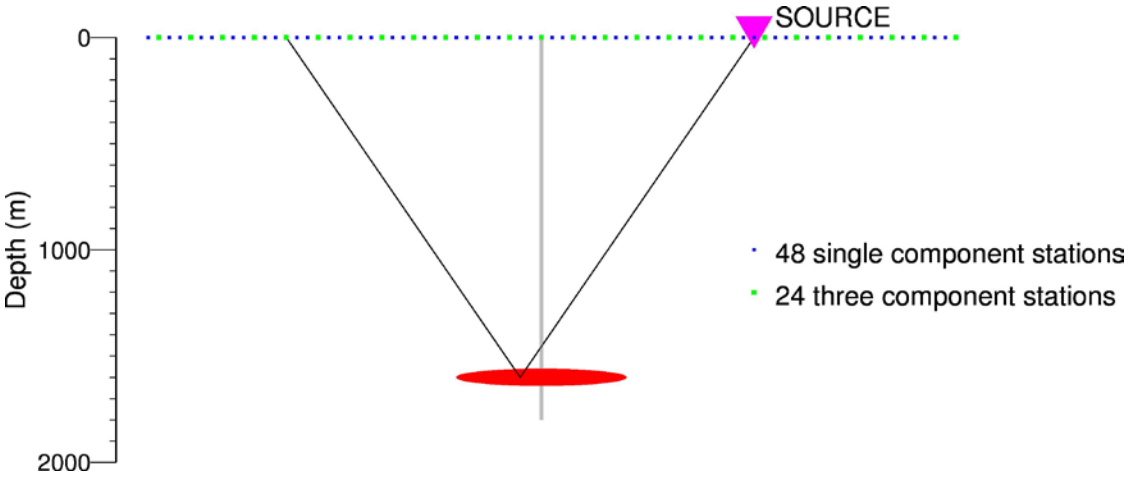

Figure 3-18: Acquisition geometry sketch for the surface seismic recording. Receivers are spaced 50 m apart and the source will be shot through the spread on a daily basis.

3.5 Electrical monitoring

The electrical observatory has been tested in the field with full capacity of the electronic transmission system in November and December of 2012. The full description of the Maguenone experiement is given in WP 06. Here only some observations of the electrical monitoring are made.

A detailed study of desaturation/saturation processes in t (Ihe 3 m thick conglomerate reservoir located at 15 m depth has been conducted, using high-frequency probing, during N2 injection in November of 2012 and during CO_2 injection in January of 2013.

For the study of desaturation/saturation during the two gas injection (November and January) on the Maguelone site, imaGeau was in charge of:

- the resistivity profiles acquisition during several days before the gas injection in order to set up a baseline
- the configuration of the electrical observatory for a high frequency acquisition (a resistivity profile each two hours) during the gas injection and several days afterwards by remote control
- the checking of the data transmission to the remote server
- the data processing (data filtering, analyze….)
- the realization of resistivity images (R(z,t)) of desaturation/saturation processes during the gas injection

All the processing data and ours analyzes (resistivity images) have been delivered to the CNRS for cross analyses with others measurements.

3.5.1 Resistivity baseline

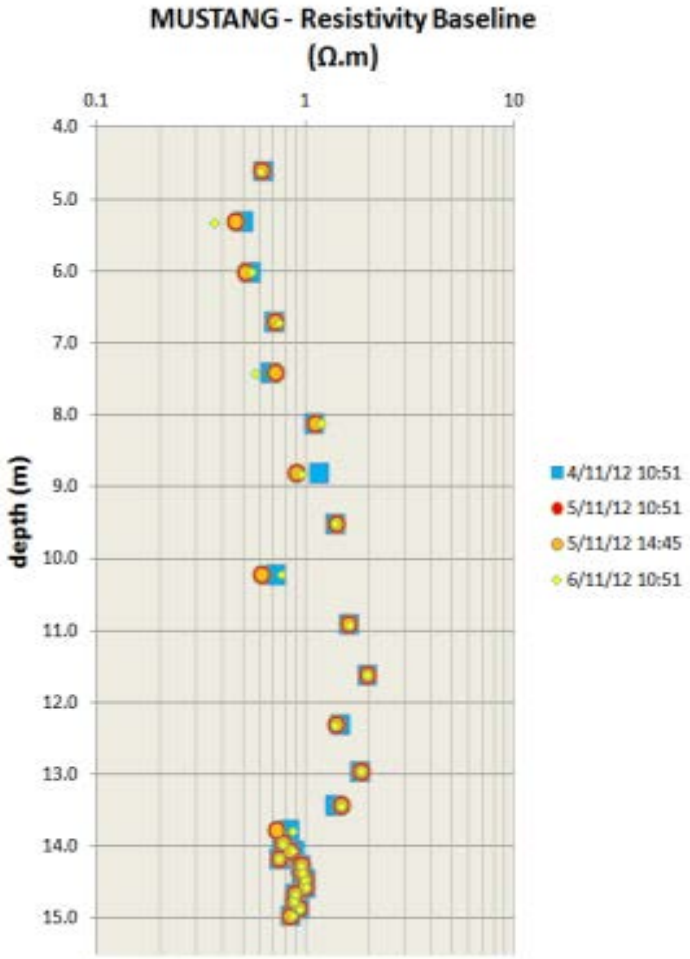

Figure 3-3: View of resistivity profiles in depth at different dates to establish the baseline

Several acquisitions have been acquired during 3 days before the injection experiment.

The accurate repeatability of the measure has been checked. These profiles have been used as baseline before gas injection experiment.

3.5.2 N2 injection in November of 2012

Resistivity image

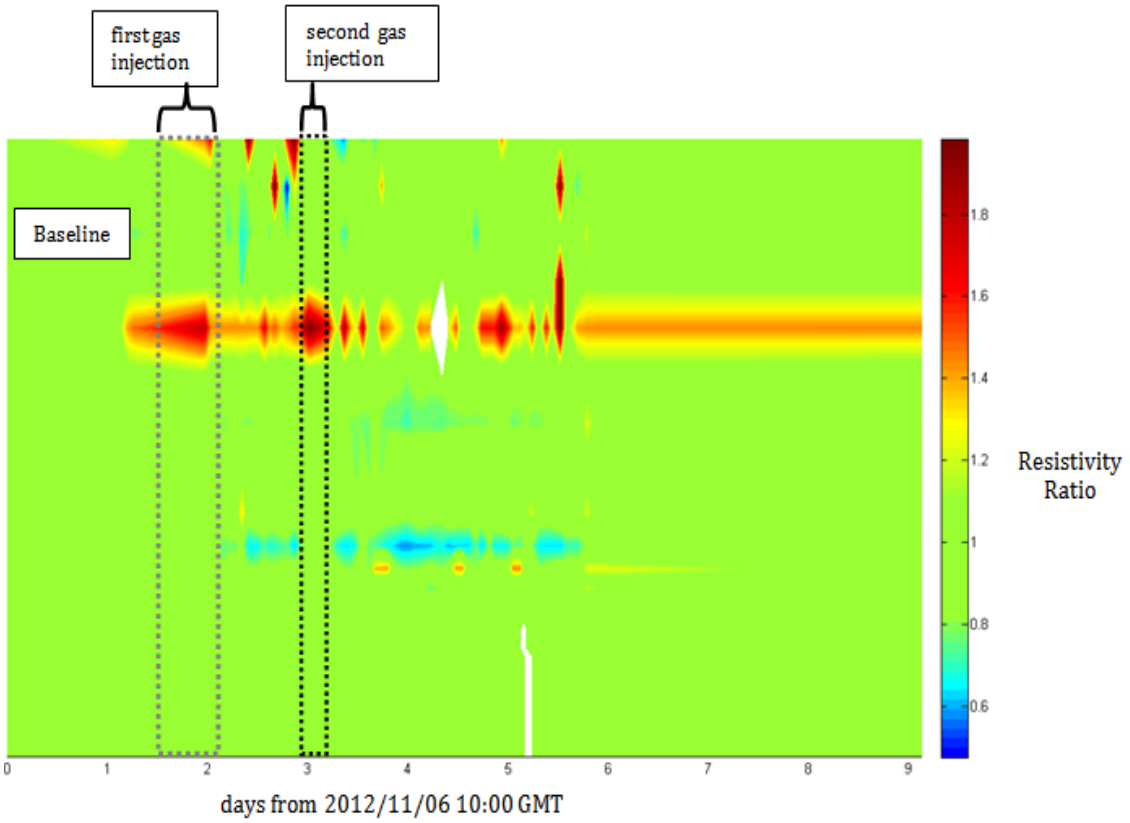

Figure 3-4: Evolution of resistivity in depth and time during N2 injection (the resistivity ratio is calculated with R(z,t)/R(z,t0), t0 is the baseline).

During N_2 injection, the resistivity increases in the 8 m reservoir due to desaturation process. The evolution of resistivity is very low in the 15m reservoir oppositely as expected.

The gas seems to stay in the 8m reservoir during several days.

CO_2 injection in January of 2013

Resistivity image

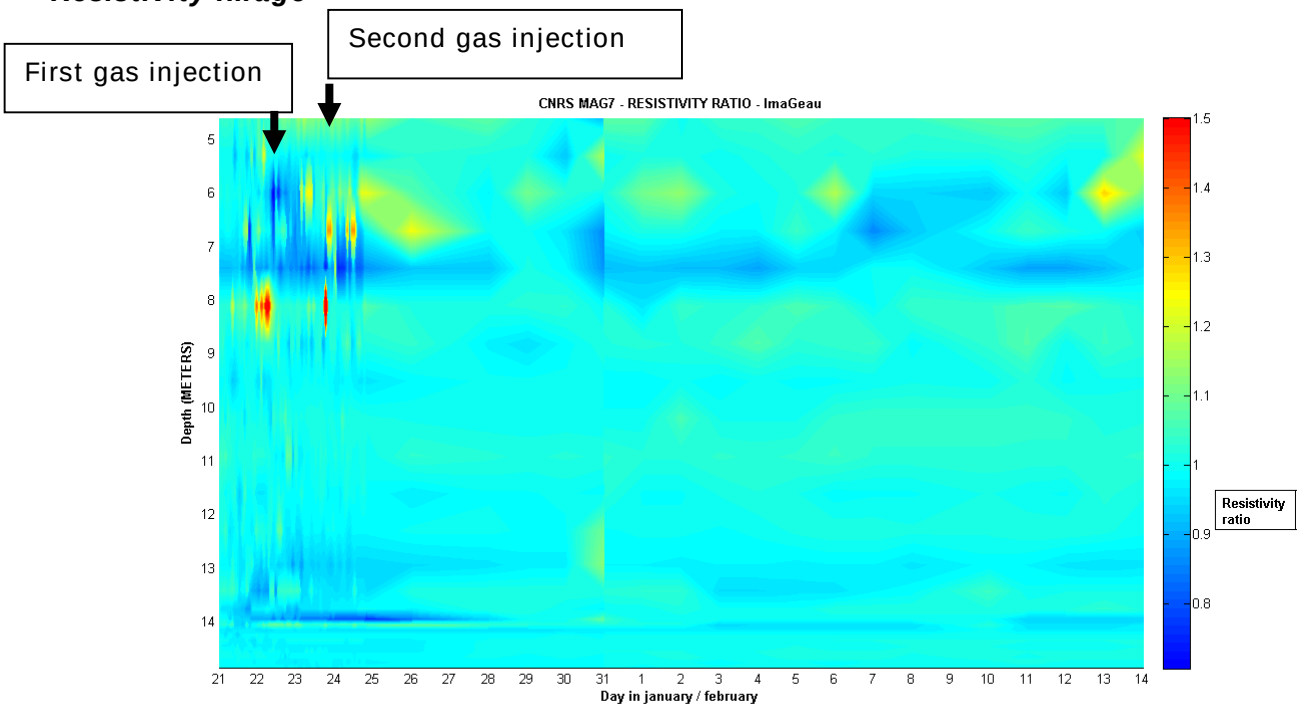

Figure 3-5: Evolution of resistivity in depth and time during CO2 injection (the resistivity ratio is calculated with R(z,t)/R(z,t0), t0 is the baseline).

During CO_2 injection, the resistivity increases rapidly during the gas injection in the 8m reservoir due to desaturation process, and decreases at 7.5m and 14 m depth. This evolution could be due to CO_2 dissolution that increases the water conductivity.The Maguelone experiment is described in full in WP 6 where also the electrical monitoring is discussed.

3.6 Concluding remarks

In Deliverable 3.8 the findings of field methods are summarized, including the work in this WP 03, WP 04 and WP 06 and some recommendations of method use are given. In the same report, the general Best Practice is reviewed.

4. WP 04 – Laboratory experiments and natural analogies

The objectives of this WP are

- Providing support to the theoretical improvement of reservoir-scale modeling, including parameter upscaling, by characterizing mass transfer mechanisms and identifying controlling parameters from core-sample scale to reservoir scale.
- Parameterizing the thermo-hydro-mechanical & chemical - THMC - processes associated with the migration of supercritical and dissolved CO2 in the aquifers and through the seal.
- Producing a comprehensive, self-consistent, experiment and field observation data base for validating models

The tasks and contributing partners are:

1) Identification of the hydro-chemical alteration of claystone/mudrock and evaporate cap-rocks due to CO2 seepage in hydraulic discontinuities (CNRS, UEDIN)

1.1 Flow behavior of single phase CO2-enriched brine and scCO2/brine mixture through fractured cap-rock.
1.2 Permeability changes induced by multi-phase flow of CO2/brine through reactivated fractured cap-rock.

2) THMC parameterization of non-homogeneous dissolution processes expected in the vicinity of the injection. (CNRS)

3) Determination of the parameters which are essential for constraining SACS-adapted numerical models.

3.1 Kinetic control of interfacial processes in scCO2/brine/rock systems during & after injection(s) (UGOE)
3.2 Thermodynamic properties of CO2 solubility in brine and design of on-site pumping and sampling equipment for Heletz experiment (replaces the original task - Thermodynamic properties of CO2 solubility in brine (KIT)
3.3 Effective dissolution-precipitation rates and proper parameterization in the system CO2-enriched brine/rock, i.e. far-field conditions (CNRS)

4) THMC analysis of seal integrity in CO2 analogues (UEDIN)

4.1 Field Investigation
4.2 Fluid and rock analysis

4.1 WP 04 - Summary of work

4.1.1 Task 1: Identification of the hydro-chemical alteration of claystone / mudrock and evaporate cap-rocks due to CO2 seepage in hydraulic discontinuities.

UEDIN and CNRS are contributing this task. To fulfil these tasks UEDIN and CNRS have undertaken experimental work, modelling work and analogue work relating to the integrity of caprocks. At each stage we have attempted to reconstruct in situ conditions of reservoir pressure, temperature and fluid chemistry. Our emphasis has been on the investigation of thermal, hydraulic, mechanical and chemical interactions. The progress made in the last 18months is as follows:

- To complete the MUSTANG experimental undertakings bespoke experimental equipment has been designed and built both at Edinburgh University CNRS Montpellier.

High pressure and temperature flow rig (UEDIN) designed to deliver up to 69MPa (10,000psi) confining pressure and fluid pressure has been designed and built for the MUSTANG project. It delivers up to 80°C fluid and rock temperatures, supercritical CO_2 and brine fluid flow (both single and multi-phase) with fluid flow rates from 0.1g/min to 10g/min. It can facilitate tracer loops to add gas, liquid or solid tracers (or other markers) and is directly linked to a Mass Spectrometer. The rig uses 38mm diameter cylindrical rock samples that can be initially saturated with range of fluids including oils and brines, see Figure 4-1.

High pressure batch vessels (UEDIN): Pressure vessels have been designed and constructed for static exposure of rock to $scCO_2$ at in-situ fluid pressure and temperature. They have been designed to deliver up to 20MPa (3,000psi) fluid pressure, up to 100°C temperatures – held constant in an oven and these temperatures and pressures allow CO_2 to enter its supercritical state. It also allows additional saturating fluid on powdered or chipped rock samples. XRD is undertaken before and after to monitor any mineral changes.

High pressure and temperature flow rig (CNRS) See description in *Task 2 Summary of Work* below.

A set of experiments have been performed and results published.

- CO2 flow through experiments on naturally fractured downhole core samples from the East Brae field, see Figure 4-5.
- CO2 exposure experiments, batch and flow through on further caprock samples have been conducted on a wide variety of sources including: St Ninian's shale: carboniferous fluvial deltaic shales, Heletz caprock: Lower cretaceous fluvial marine shales, Kimmeridge Clay - UK North Sea East Brae Field and Miller field caprock: Jurassic submarine fan shales and Boulby mine evaporite: Permian / Triassic Zechstein sea deposits, Figure 4-6..
- CO2 flow through experiments on Heletz sandstone, Stuben sandstone and Clashach sandstone, Figure 4-6.
- Porosity and permeability measurements obtained for the caprock and reservoir rock samples. The measurements were taken using a conventional helium porosimeter and nitrogen permeameter. Table 1 presents a summary of the average bulk density, porosity and permeability results obtained and Figure 4-7presents the complete porosity results. The permeability results reveal the East Brae caprock to have an average permeability of 0.07mD. The Heletz caprock is higher than this at 13.15mD; however this is due to the samples being from a silty transitional area of the depositional sequence rather than pure shale which will have a significantly lower permeability. The porosity values show consistency between individual field samples with the East Brae having the lowest

average porosity at 0.44%, and the Heletz caprock has an average porosity of 7.32%, again this is higher than expected due to the silty nature of the samples. The two reservoir sandstones have high porosities of 15.5% for the Clashach and 21.47% for the Heletz reservoir sandstone.

- The mineralogy of the caprock samples has been determined using X-ray diffraction (XRD). Table 2 presents the average XRD mineralogy results for the caprock and sandstone samples. The primary expected mineral reactions with CO2 are: dissolution of feldspars; anhydrite removal; infilling of secondary porosity in K-feldspars by kaolinite; barite precipitation; mica splaying in open porosity; dolomite / ankerite as a pore filling cement and the dissolution of ankerite. These chemical reactions will be accelerated by high temperatures and under flow. The mineralogy results from the caprock samples, Figure 4-8, indicate that all of these chemical reactions are possible within the experimental program: the Heletz caprock and sandstone will be most vulnerable to the dissolution of feldspars; the Boulby evaporites susceptible to anhydrite removal and all have some degree of ankerite available for reaction.

- **THMC flow experiments:** The effect of THMC processes on the fractured caprock samples are investigated using the high pressure and temperature flow rig. This facilitated Temperature, Hydraulic (flow rate) and Mechanical (pressure) parameters to be controlled experimentally for each rock type during CO2 and CO2 enriched brine flow through experiments. Before, during and after experimentation the rock samples were subjected to a range of experimental techniques to fully investigate the chemical processes affecting the caprock including: Scanning Electron Microscope (SEM) imaging, EDS (energy dispersive) X-ray analysis and X-Ray Diffraction (XRD) analysis.
- **TMC batch experiments**: The chemical effect of scCO2 and CO2 enriched brine exposure on caprock in-situ pressure and temperature is under investigation using the high pressure batch vessel. For the batch experiments powdered caprock is exposed to scCO2 only, brine and scCO2 and brine only under 13.7MPa (2000psi) pressure and 40ºC. The samples are being held in the batch vessels in an oven for 6 months. The samples are then subjected to XRD and SEM investigation to identify any changes in the caprock mineralogy before and after CO2 exposure.
- Table 3 presents the full suite of THMC coupled process investigations conducted through the experimental program for each of the rock samples.

4.1.2 Task 2: THMC parameterization of non-homogeneous dissolution processes expected in the vicinity of the injection

CNRS is the main contributor to this task. Equipment have been built and experiments have been performed by CNRS and CSIC.

High pressure and temperature flow rig (CNRS) designed to deliver up to 20MPa confining pressure and fluid pressure has been designed and built for the MUSTANG project. It delivers up to 200ºC fluid and rock temperatures and CO_2-saturated brine fluid flow with fluid flow rates from 0.021ml/min to 1 ml/min. It comprises a specific port for in situ Raman Spectrometry measurements. This apparatus constructed for performing flow of CO2-rich brine reproducing far-field conditions (i.e. monophasic fluid) through cylindrical cores of 9mm diameter, 18 mm long cylindrical rock sample (Figure 4-3). The experimental device consists in: 1) a motorized dual-piston pump system that produces the flow of brine, 2) a motorized piston pump containing liquid-phase CO2 cooled at 5 °C that deliver the amount of CO2 required to reach the desired partial pressure, 3) the CO2-brine mixing system, 4) the temperature-controlled confinement cell holding the sample, and 5) the system of servo-controlled valves and hydro-pneumatic tanks used to control

the back-pressure and to deliver samples of the outlet fluid. The sample is installed in the confinement cell (Figure 4) into a silicon jacket. A controlled confining pressure is applied to mimic natural confinement conditions and balance changes in the fluid injection pressure to avoid deviatoric stresses that may damage the sample irreversibly during loading and unloading phases. In the experiments, axial and radial pressures were maintained at an equal value of 112% of the inlet pressure using a mechanical pressure multiplier. This equipment was used in Tasks 1 and 2.

A set of experiments have been performed and results published on different limestone and sandstone samples (Figure 4-4).

- Limestone rock dissolution experiments have been performed at different partial pressure of CO_2 ($0.034 \leq PCO_2 \leq 6$ MPa) displaying distinctly different poro-perm changes. Experiments were performed at T= 100°C and P = 12 MPa, mimicking average values for the expected CO_2 storage in deep saline aquifers. X-ray microtomography (XMT) images were used to characterize the changes in the structural properties from pore scale to Darcy scale, while time-resolved pressure loss and chemical fluxes allow determining the sample-scale change in the porosity and permeability. Two sets of data were performed using two different limestone rocks (Luquot and Gouze, 2009; Gouze and Luquot, 2011; Luquot etal, 2014). We used these sets of data to test the newly developed skeletonization algorithm (see description in section 2) and characterize the dissolution features.

- We also realized two sets of sandstone dissolution experiments: We first realized CO2 percolation experiments through chlorite/zeolite-rich sandstone samples from the Pretty Hill Formation (Otway Basin, Australia), see Luquot etal, (2012). The percolation experiment was setup to reproduce, at laboratory scale, the in situ temperature and pressure conditions (T = 95 °C and P = 10 MPa). The fluid injected at constant flow rate is a rock-equilibrated brine subsequently enriched in CO2 up to partial pressure of 6 MPa. The main objectif was to explore the reaction processes occurring in Fe-rich geological reservoirs, while reproducing the conditions for CO2 injection and storage in geological formations. These experiments allow us to study the relationship between the time-resolved changes of the rock composition, porosity and permeability induced by the mass transfers during the percolation. The methodology combines chemical analysis of the fluid, continuous measurements of sample permeability, and pore-scale characterization of the rock by ESEM and TEM analysis. Then, we reproduce CO2-rich brine percolation through Heletz samples (Heletz, Isreal). We did five different flow-through experiments changing the flow rate and the injected brine composition (sulfate content). The main objective was to predict permeability and porosity change due to CO2-rich brine interaction in Heletz in situ conditions.

4.1.3 Task 3: Determination of the parameters which are essential for constraining SACS-adapted numerical models

- **Task 3.1** Kinetic control of interfacial processes in scCO2/brine/rock systems during & after injection(s) (UGOE)

UGOE has been contributing to this task. The progress made is as follows:

- **Synthesis of new esters:** The overall objective was to identify suitable tracers for quantifying the interface between H_2O and $scCO_2$ during CO_2 sequestration and possibly identify residual saturation of CO2 after flushing. Therefore, the reaction kinetics of most suitable tracers at the boundary conditions of CO2 injection sites were investigated. Initially, commercially available phenol esters were believed to be suitable tracers, but did not show the expected behavior. Therefore, new compounds based on naphthalenesulfonic acid esters were designed, synthesized, and purified in order to adapt the reaction speed to the required timescale of the experiments. Especially the influence of molecule properties on the polarity and the reaction kinetics were studied. The new compound 2-naphthalenesulfonic acid chloro-phenyl ester (2-NSAPhCl) was expected to be most suitable for laboratory scale experiments. A faster interface reaction speed compared to 2-naphthalenesulfonic acid phenyl ester (2-NSAPh) was expected due to the negative inductive effect of the chlorine atom in the phenolic substructure.
- **Static batch experiments:** During the project, static analogue experiments (*n*-octane as analogue for $scCO_2$) with a constant interfacial area size were conducted for studying the two-phase behavior of potentially suitable KIS tracer compounds. The experiments allow the determination and comparison of kinetic constants for the phase-transfer-reaction of different hydrolysable compounds (Figure 4-10 in 48 month report) and are vital to assess the role of newly introduced molecule moieties or molecule parameters under defined conditions.
- **Dynamic batch experiments:** After the experimental setup of the dynamic analogue studies with a variable interfacial area size (for details see Milestone M044) was finally designed and built, first experiments with the self-synthesized compounds were performed.
- **Modeling of KIS tracers in two-phase systems:** A mathematical model for interface sensitive tracer transport and reaction has been developed and can be used for the evaluation of the interfacial area size between two fluid-phases (i.e. CO2 and brine). The focus was to extend and support the laboratory work and to create a sophisticated mathematical model that is able to describe the behavior of KIS tracers and its kinetic and thermodynamic properties in two-fluid-phase porous media systems (CO2-brine) and to account for the fluid-fluid interfacial areas. This model is necessary in order to determine required reaction rates for different experimental setups, which can be considered as target parameter within the tracer synthesis.

- **Task 3.2** Thermodynamic properties of CO2 solubility in brine and design of on-site pumping and sampling equipment for Heletz (KIT)

KIT is contributing to this Task. In order to fulfill the experimental requirements for online analysis of the liquid phase at high pressures and temperature, the MUSTANG-HP high pressure lab scale apparatus has been designed, constructed, built and put to operation. It consists of a high pressure visual cell valid for pressures up to 500 bar and temperatures up to 200°C, 2 syringe feed pumps, and 2 online sampling devices for online analysis of the gas phase via gas chromatography and of the liquid phase via ion analysis, as shown in **Fel! Hittar inte referenskälla.**. This high pressure high temperature lab scale apparatus has been used for extensive high pressure calibration tests for the ions to be regarded as relevant for the Heletz site in order to investigate the behavior of a saline aquifer during and after CO2 injection. The thermodynamic and kinetic measurements via online sampling and analysis of

the liquid phase have been prepared. During these tests, a corrosion problem of the autoclave emerged despite the fact it had been built by Hastelloy. This alloy had been chosen because of its well-known corrosion resistivity against solutions with high salt concentrations. A fault analysis together with the manufacturer showed a construction defect within the movable piston sealing. Hence, it had to go to an entire revision. Afterwards, a new calibration of the system turned out to be necessary. Here, defect of the ion analysis came up. A fault analysis together with the manufacturer showed a general problem with the ion chromatograph because of the unusually high salt concentrations, which have to be applied in the experiments. After an exchange of the entire system, a new calibration had been performed and tested. Now the MUSTANG-HP system is ready to start the measurements for MUSTANG.

- **Task 3.3** Effective dissolution-precipitation rates and proper parameterization in the system CO2-enriched brine/rock, i.e. far-field conditions.

A main issue concerns the parameters that control the occurrence of negative porosity-permeability, while the great majority of laboratory experiment dealing with carbonate dissolution displays positive correlations. Certainly, the microstructure heterogeneity is a critical parameter, but we envisage that the degree of under-saturation of the flowing solution should have a significant impact on the occurrence and the sustainability of the negative correlation between the porosity and the permeability in the course of dissolution. In this letter, we first present the result of a flow-through experiment using the same rock and procedure as Luquot and Gouze (2009), but with a CO2-rich brine displaying a lower partial pressure of CO2; a negative correlation between the porosity and the permeability changes is measured. Then X-ray tomography is used to investigate the redistribution of mass within the rock sample and to conclude on its effect on the permeability decrease.
The change of permeability in the course of CO2 injection in carbonate reservoir is a major issue because of the high reactivity of these environments at low pH. The increase of permeability and the formation of preferential paths such as experimented by Luquot and Gouze (2009) who investigated the mechanisms of dissolution at high pCO2 expected in the vicinity of the injection well, is viewed as favoring both the pressure dissipation and the spreading and mixing of the CO2. However, the experiments of the core-flood experiment performed in the same conditions of dissolution but with lower pCO2 showed much more complex mechanisms that caused the sustainable decrease of permeability.
Specifically, the experiment consisted in injecting a CO2-rich brine in calcite limestone for conditions representative of underground storage (P = 12MPa and T = 100°C) in order to explore the dissolution mechanisms arising at moderate CO2 partial pressure (0.3 MPa). An increase of the total porosity accompanied by a persistent permeability decrease was measured. The mechanisms controlling this atypical anti-correlated relationship were investigated from the analysis of high-resolution X-ray micro-tomography images of the sample acquired before and after the experiment. All the evidences converges to the conclusion that the ubiquitous decrease of permeability measured during the 44 hours of dissolution is due to the clogging of a fraction of the macro-porosity by micro-porous material triggered by the rearrangement of the detached undissolved particles. This mechanism results in the development of low permeability zones bridging the macro-porosity and increasing the tortuosity and decreasing the sample-scale effective hydraulic radius.

4.1.4 Task 4: THMC analysis of seal integrity in CO2 analogues

UEDIN is the main contributor to this task.

- Completion of deliverable D045 and finalisation of the analogue work.
- Geomechanical facies interpretation of the Miller field into caprock genetic units. The key to a successful CO_2 storage project is appropriate selection criteria and a proper

understanding of how to manage the risks of geological uncertainties. It is essential to define the required storage site attributes selection criteria based on determining the likelihood of adequate storage formation, suitable caprock thickness and extent and quantified fracture network. This will determine the data and analysis requirements necessary to provide the knowledge that the storage site has the required attributes for successful CO_2 storage. We propose using a geomechanical facies approach as a first order assessment tool to determine CO_2 storage site attributes and suitability. To address this, we explore the governing processes of CO_2 storage and propose the notion of geomechanical facies, where storage formation quality, caprock integrity, stress state and fracture patterns are governed by original tectonic setting controlling the sedimentary depositional settings, and thereafter compaction, subsequent stress overprint and preservation potential.

- Workflow model that other CCS projects may utilise to populate 3D caprock models when only well data is present. Based on Petrel multifacies caprock model of the Miller field.
- Core analysis and logging of Heletz Well H-18 – report on MUSTANG intranet.
- Risk matrix of caprock leakage.
- Further development of the strata bound sequential fracking model, Figure 4-13. This is an analytical model that creates a fluid pressure builds up underneath layered sedimentary system (cap), increased pressure caused fracking in layers in cap. New fracks exert extra horizontal confining pressure in cap to develop further fractures.
- A numerical model has also been developed for stress factors using elastic model this extra pressure can be evaluated using an influence factor. This allows a normalized spacing of fracs against increased pressure to be evaluated, Figure 4-14.
- Finally a Hybrid Analytical Numerical Model was created with the integration of normalised curve into fluid pressure models to evaluate fracking patterns to simulate fracking due to reservoir pressure build up in overlying multilayer sedimentary sequences, Figure 4-15.

4.2 Main results and achievements

4.2.1 Task 1

The conclusions we can draw from the experimental work undertaken on the hydro-chemical alteration of claystone / mudrock and evaporate cap-rocks due to CO2 seepage in hydraulic discontinuities are that:

- The clay matrix remains unchanged in in Heletz, St Ninians, Miller Kimmeridge clay, East Brae Kimmeridge clay and boulby mine evaporites under all experimental pressure, temperature and CO2 exposure conditions.
- No new minerals were precipitated in Heletz, St Ninians, Miller Kimmeridge clay, East Brae Kimmeridge clay and Boulby mine evaporites under all experimental pressures, temperatures and CO2 exposure conditions.
- Minor Calcite and Pyrite dissolution is observed in Heletz, St Ninian's, East Brae Kimmeridge clay and Miller Kimmeridge clay caprock samples under all experimental temperatures, pressures and CO2 exposure conditions.
- Looking at more detail at the metal oxides (the most likely to react with CO_2) CaO, MgO, K_2O, Fe_2O_3 and Al_2O_3 follow a linear and unchanging mineral weight percentage trend for the Mimmeridge clay, Figure 4-16and Heletz caprock samples at all rages of temperature, pressure and flow rates.
- These results indicate that under the experimental timescales the general mineralogy along the caprock fractures and microcracks do not experience any mineralogical changes on exposure to gas phase CO_2.

- Supercritical CO_2 did not flow through the tight natural caprock fractures in the East Brae caprock under supercritical reservoir conditions.
- When the temperature and fluid pressure were reduced to below the critical point, CO_2 in its gas phase did flow through the tight natural caprock fractures (even with a constant pressure difference between the confining pressure and the upstream fluid pressure of 15MPa under both supercritical and gaseous conditions) for two naturally fractured East Brae caprock samples, Figure 4-17and Figure 4-18.
- The contradictory experimental observations are linked to the complex interplay between the fluid conductivity response of the CO_2 phase to the fracture properties, the influence of stress on the fracture aperture, the chemical interaction between the rock minerals and the CO_2 fluid, the fluid pressure influencing the fracture permeability, the influence of CO_2 phase on the capillary entry pressure and the relationship between CO_2 phase on the wettability, interfacial tension and contact angle, Figure 4-19.
- Calculations indicate that there is a large decrease in hydraulic conductivity as the aperture size reduces, indicating that it is aperture size that is the dominant controlling factor in fracture flow of CO_2. It is possible that there is a critical threshold of fracture aperture size which controls CO_2 flow along the fracture. Above the critical aperture size $scCO_2$ and gaseous CO_2 will flow, on or near the critical fracture aperture size we see gaseous flow but not $scCO_2$ flow and below the critical aperture size we would see little or no gas or $scCO_2$ flow along the fracture and flow would become matrix dominated.
- This has significant implications for the planning of CO_2 storage projects in the North Sea basin, in that the CO_2 should be stored at pressures and temperatures (depth) comfortably above the CO_2 critical point.
- The main result concerning the experiment displaying low partial pressure of CO_2 is that permeability decreases while porosity increases (**Fel! Hittar inte referenskälla.**). This phenomenon is poorly discussed in the literature, but is observed as well for low temperature carbonate dissolution. This is specific of carbonate reservoirs that are usually an assemblage of micritic grains of distinctly different dissolution kinetic due to distinctly different reaction surface area. The decrease of permeability is induced by the detachment of the grains in the pores and their re-deposition in the throats. This phenomenon is not observed for high P_{CO2} because the gains are quickly dissolved before the redeposition occurs.

4.2.2 Task 2

- Limestone reservoir:

We show that the k-ϕ function at location **x** in the reservoir is determined by the reactivity of the fluid that first percolates this portion of the rock. Although the measured power law relationship between permeability and porosity is in agreement with several observations from measurements on samples collected in sedimentary layers and Kozeny-Carman-based model. The analysis of XMT data gives physical meaning to the constitutive relationships that relate porosity to permeability. Specifically, XMT data allowed us to determine the relative importance of tortuosity and pore enlargement that rules the permeability-porosity law for the different regimes of dissolution. We also used the XMT data to characterize the wormhole morphology (Figure 4-10). We also proposed a phenomenological relationship between the reactive surface area and the porosity change used and validated recently by Luhmann etal (2014), with another carbonate rock and by numerical modelling.

- Pretty Hill sandstone:

We showed that the Pretty hill sandstone from Otway basin strongly reacts during the CO_2-rich brine. Minerals such as feldspar, chamosite and laumontite are dissolved and the precipitation of kaolinite and silica is observed. Carbon storage is also recorded as the formation of Fe/Ca-rich carbonate minerals (ankerite, siderite) and as amorphous carbon precipitation coupled

with Fe-oxyde (Figure 4-11). These results testify that CO_2 can be efficiently stored in such sandstone reservoirs and show that amorphous carbon must be considered as a possible means for storing carbon in such Fe-rich reservoirs. We observed that hydrated minerals precipitation such as kaolinite induces permeability decrease. Finally, we concluded that the heterogeneous spatial distribution of mixing, triggered by the variability of the velocity field in pores, promotes the development of chemical microenvironments where the fluid composition is different from the bulk concentrations.

- Heletz sandstone:

We observed that whatever the brine composition and the flow rate, the sample permeability increased during CO2-rich brine flow-through experiments. Nevertheless, we observed that for high flow rates, the permeability increase is faster than during lower flow rate injection (Figure 4-12). We also characterized that the permeability increase is less important when the injected fluid is equilibrated with respect to gypsum (high sulfate content). In Heletz sandstone samples, the permeability increase is explained by the dissolution of the dolomite and feldspar composing the rock sample. Some precipitation of clay was observed as during experiments with Pretty Hill samples, nevertheless, the clay precipitation did not clogged the main path-ways (Figure 4-13). This mechanism is explained in the Heletz samples by the initial high porosity, permeability and pore diameter in comparison with the Pretty Hill samples. During, high sulfate content brine injection, the delay on permeability increase can be explained by gypsum precipitation.

4.2.3 Task 3

- **Static batch experiments:** The results from the static batch experiments with the newly synthesized compounds confirm the KIS tracer concept, because a linear concentration increase and, thus, a zero-order reaction kinetics could be identified. The comparison of the investigated compounds indicates that the combined kinetics (mass transfer across interface and hydrolysis reaction) is in the same order of magnitude for both synthesized compounds despite the introduction of an additional chlorine atom. Thus, further molecule modifications will be necessary for adapting the reaction speed to the experimental requirements.
- The results from the dynamic batch experiments show that an increase of the interfacial area causes a response in the measured concentration curve (Figure in 48 month report). Unfortunately, the fluorescence signal was too weak (strong noise) in order to determine the kinetic constants, compare them with the static experiments, and correlate the observed curves with the interfacial area change. For increasing the sensitivity of the optical measurements, the setup was slightly modified and a new flow-through cell with a bigger aperture size was purchased. However, the new cell also did not lead to a lower limit of quantification. Therefore, the setup has to be further optimized in order to meet the requirements for studying the interface mass transfer processes in a dynamic system.
- **Modeling of KIS tracers in two-phase systems:** The measurement of the interfacial area is a hard task and cannot yet be done experimentally in a porous medium with the solid phase also to be taken into account. Therefore, the new model follows the approach of calculating the interfacial area size by means of pore-network models. Pore network models are a very useful tool to obtain a fundamental understanding of the physics of flow and transport in porous media. As a result, the spatial and temporal distributions of the non-wetting phase saturation can be calculated and hence the specific interfacial area can be derived. The KIS tracer reaction was implemented and coupled with a function for the interfacial area size. Subsequently, the modeling of different scenarios allows investigating the KIS tracer behavior in more complex systems and gaining information on the required timescale of the reaction kinetics for the problem to be solved. However, additional efforts have to be undertaken in order to obtain and validate the underlying capillary pressure-saturation-interfacial area functions, since the model results are beside the reaction rate very sensitive to this assumed function. This in turn facilitates the further tracer design.

- **Thermodynamic properties of CO2 solubility in brine:** The MUSTANG-HP high pressure lab apparatus has the capability to perform direct lab simulations of real insitu solubility behavior for the CO2 storage experiments. Therefore, the injection of CO2 into a synthetic – or if available a real – aquifer can be simulated at reservoir conditions (150-180 bar, 65°C). The results are online measurements of CO2 dissolution in aquifer solution as a function of time in order to detect the concentration changes as a function of time and to analyze potential precipitates. The investigations are possible on short term or long term scale. The expected exploitation of these results are seen in the application for the dimensioning and the practical approach for CO2 storage experiments in the field. They can also be used for modelling purposes. In detail, the dissolution kinetics of CO_2 in aquifer solution at reservoir conditions are measured and the following questions can be answered: (i) how does the CO_2 behave in the reservoir during and after injection? (ii) How fast does the CO_2 dissolve in the aquifer? (iii) What types of reactions occur between CO_2 and aquifer? (iv) Are precipitates formed by contact between CO_2 and aquifer? If yes, which types? (v) Is a difference between short term and long term formation of precipitates?
  The experimental results are also important for other WPs, as they influence WP5 (Process Investigations) and WP7 (Modeling and Model development), but also WP6 (Simulation of CO2 injection has direct impact on the ”real” injection experiment).
  By the lessons learned so far, even the analysis of online samples taken at downhole conditions (high pressure, high temperature, high salinity) is now under development. The expected innovations concering the solubility behavior are the answers to the following questions: (i) How much CO2 can dissolve in the aquifer at reservoir conditions? (ii) How long does it take to achieve thermodynamic equilibrium? (iii) Do precipitates occur? (iv) If yes: Detection of type, amount and composition.

- **Far-field mass transfers in limestone reservoirs**: We measured an increase of the total porosity accompanied by a persistent permeability decrease during the low CO2 concentration injection. The mechanisms controlling this atypical anti-correlated relationship were investigated from the analysis of high-resolution X-ray micro-tomography images of the sample acquired before and after the experiment. All the evidences converges to the conclusion that the ubiquitous decrease of permeability is due to the clogging of a fraction of the macro-porosity by micro-porous material triggered by the rearrangement of the detached undissolved particles. This mechanism results in the development of low permeability zones bridging the macro-porosity and increasing the tortuosity and decreasing the sample-scale effective hydraulic radius.

4.2.4 Task 4

Results from the analogues studies

- A study of several analogues for CO2 storage with a focus on the identification of coupled processes // positive feedback processes which may lead to failure of the storage system.
- A caprock model was constructed of the East Brae field, subdivided into generic units based on the analysis of some 38 wells, Figure 4-21. The caprock is divided into three main genetic units which can be found throughout the whole of the East Brea field. Some uncertainties still exist within (1) the quality of the stage 1 model interpretation based on a limited number of wells; (2) fault geometry; and (3) accuracy of the 3D geometry of the model. Despite this our stage 2 model incorporating 38 wells appears to closely match real data.
- This study demonstrates a workflow that other CCS projects may utilise to populate 3D caprock models when only well data is present, Figure 4-22. Models built within Petrel can be viewed as a good means to visually understand the structural geometry of the KCF

caprock, outline the genetic unit facies within the primary seal and show where they are likely to pinch out, as well as, situating this in the context of an overlying secondary seal.

- It is noteworthy that the thickness maps are most reflective of the generalized thickness trends. However, these do not incorporate faults N1 – N3 and so are not reflective of localized points with large thickness variation.
- The study highlights data sensitivity issues suggesting that in the absence of seismic data, sites require moderate well coverage (20 wells) to yield a model that is reasonably representative of the true geological structure. In data poor areas as would be typical of most fields, the resultant model smoothes out even large scale features, due to spatial aliasing effects, and yields a model that poorly reflects the true structural geometry and GU horizons
- A new numerical method and modelling study completed on the effects of heterogeneity on the migration of scCO2 in a two-phase brine CO2 system.
- A new conceptual approach coupled with a modelling approach for natural fluid fracking, and relate this to analogue field observations. Directly applicable to the effect of increasing reservoir fluid pressure due to fluid injection.
- Initial application of **a geomechanical facies approach** to considering key risk scenarios based on the consideration of THMC processes operating under generic, but distinctive in terms of deposition environment and tectonics, proposed storage sites, paper nearing completion.

Caprock leakage risk model

Identification and assessment of the potential leakage pathways (risks) was undertaken, figure 4-23. A number of leading academic experts from the MUSTANG project completed risk assessment questionnaires based on the scale of the potential leakage (severity) and the probability of any leakage (timescale) for each leakage risk factor, Figure 4-24. This led to the development of a site characterisation tool with a ranked hierarchy for data collection based on the highest data quality requirements linked to the highest leakage risk, designed to prioritise risk and improve cost efficiency during site characterisation. Our summary findings of the CO_2 leakage risks from the risk questionnaire and subsequent risk matrix are:

- The geology, fracture network and well environment were identified as the areas having the highest perceived leakage risk
- The highest leakage risks identified were:
  - improperly abandoned wells (most significant risk)
  - poor sealing of the injection well
  - injection rate and position
  - hydraulic fracturing
  - injection pressures
  - lithological discontinuities in the caprock
  - fracture density
  - high permeability lithological conduits in the caprock
  - caprock and storage reservoir dipping to surface
  - fracture permeability
  - fluid pressure changes
- As the timescale decreases (increased probability value) the severity of the leakage increases. This is important as it indicates that the highest and most severe leakage risk period is during the initial stages of the injection process. It highlights the importance of greater effort at the beginning of the project on the higher risk areas and the resultant monitoring and mitigation procedures.

- For lower risk factors the average severity and probability (timescale) assigned by the experts for each leakage risk factor are similar to each other, indicating that they perceive that if the severity of the leakage is low the leakage will happen over a longer timeframe.
- For the higher leakage risk factors the expert assigned severity of the risk is generally higher than the expert assigned probability (timescale of the leak) of the risk. This indicates the possibility that if the severity of the leakage is high it will happen over a shorter timeframe.
- The expert perceived results indicate that small scale (micro (*pore*) to macro (*Darcy*)) risk factors have a lower risk categorization and that large scale (macro (*Darcy*) to field scale) factors have higher risk factors. The implication is that when constructing the CO_2 storage site model the field scale geology and fracture networks must be very well constrained and that the smaller scale information can be less well constrained.

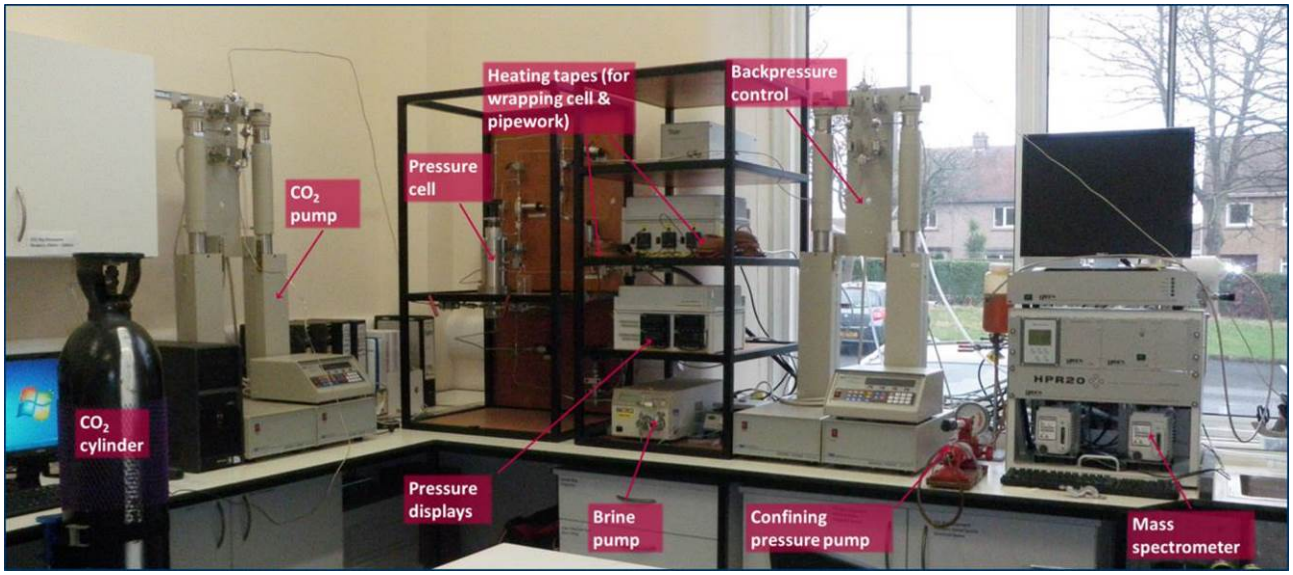

Figure 4-1. High temperature and pressure rig

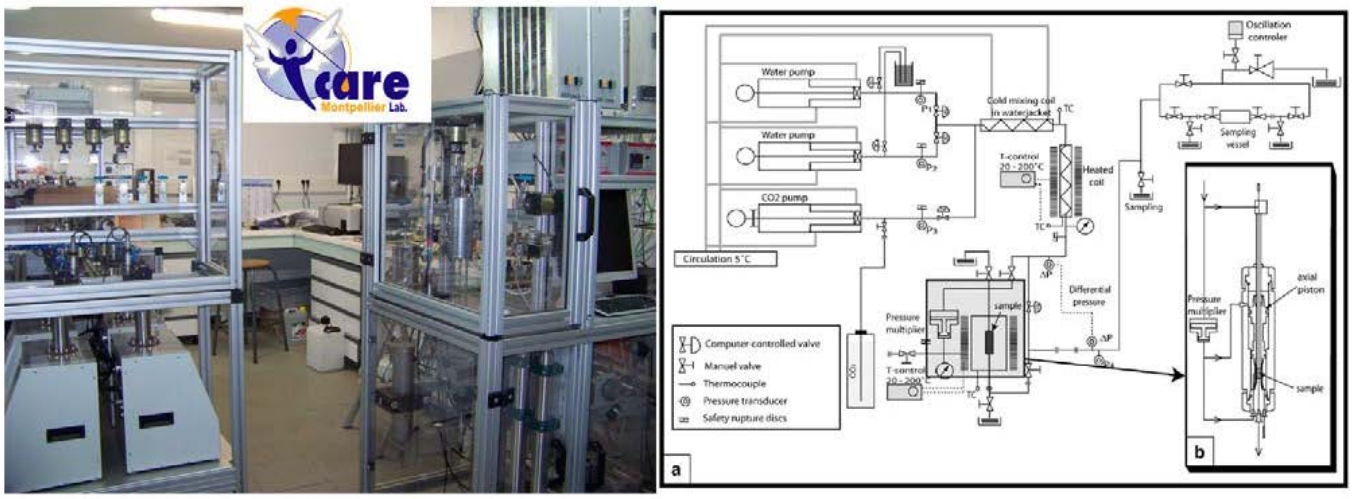

Figure 4-2. Left: the CNRS high pressure / high temperature ICARE-Lab. Right: the diagram of the ICARE-1rig used for reservoir samples.

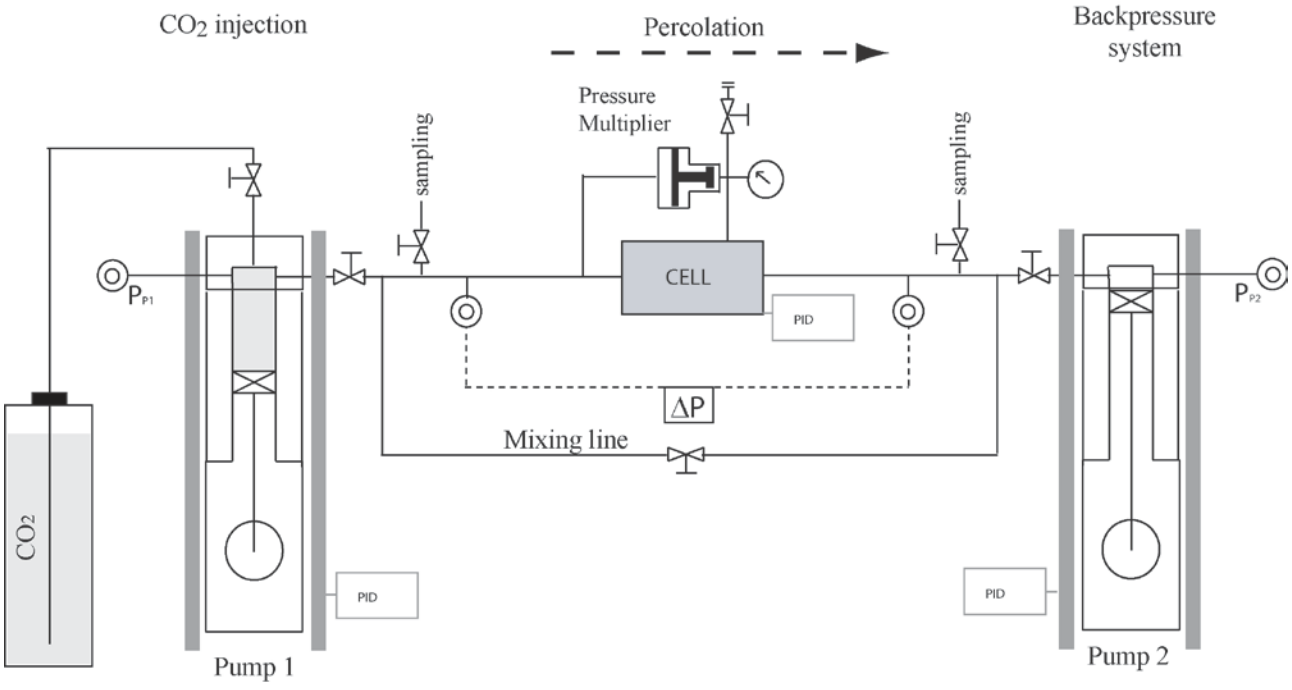

Figure 4-3. The diagram of the ICARE-2rig used for reservoir samples.

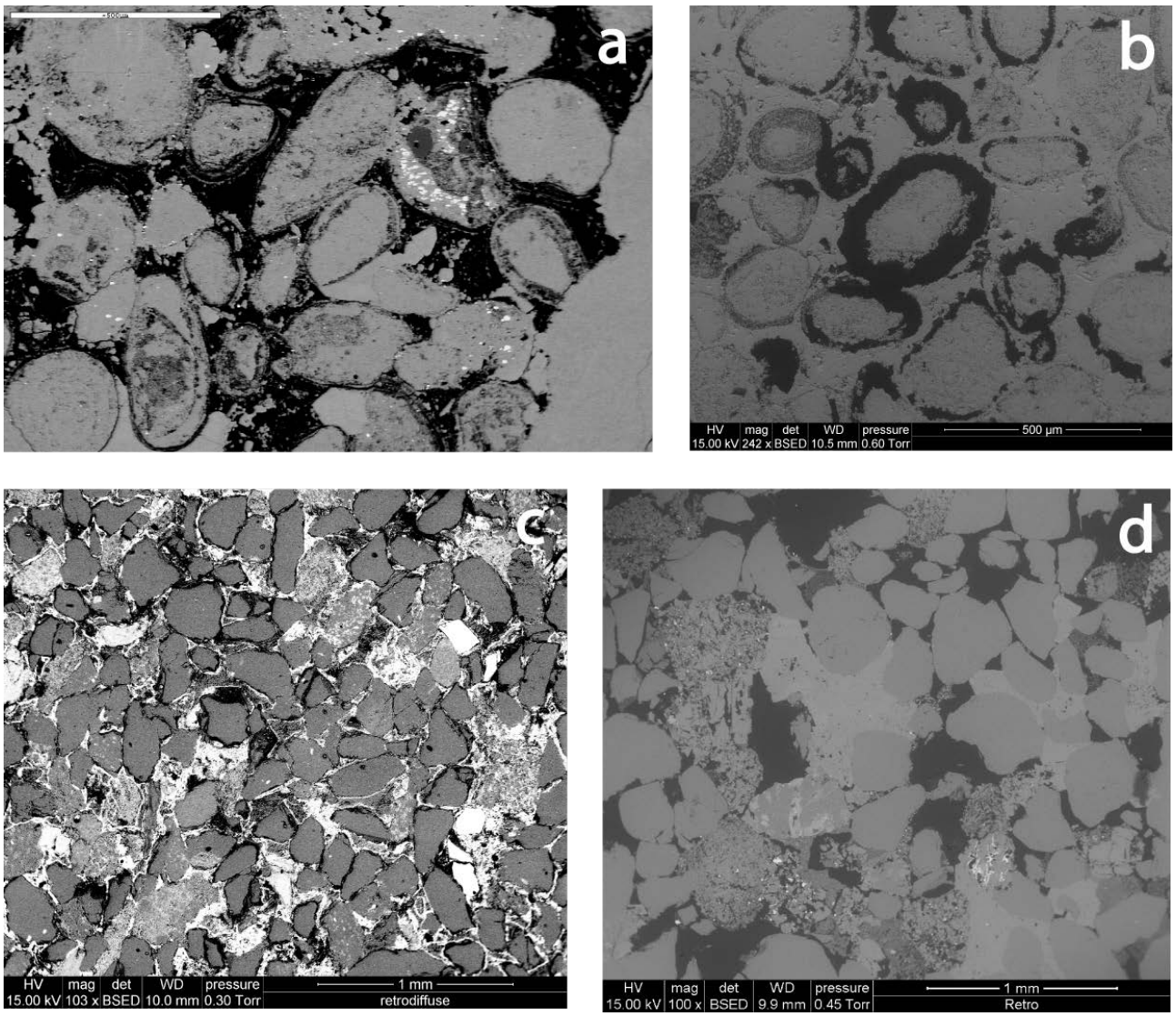

Figure 4-4. SEM picture of the different limestone and sandstone rock studied during the Mustang project (a: Mondeville sample in Luquot and gouze, 2009; Gouze and Luquot, 2011; Mangane etal 2013; b: Port sample in Luquot etal, 2014; c: Pretty Hill sample in Luquot etal, 2012; Heletz sample).

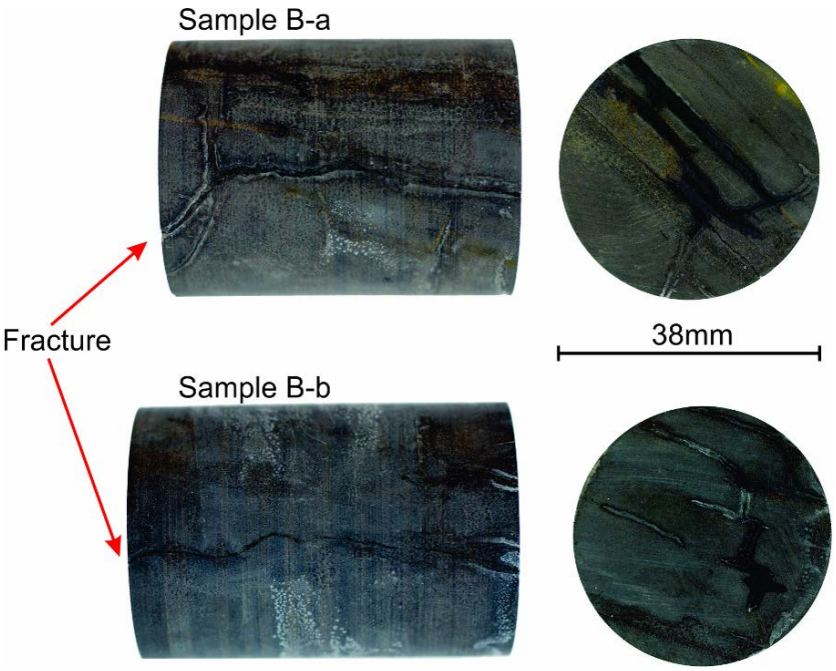

Figure 4-5. Naturally fractured East Brae

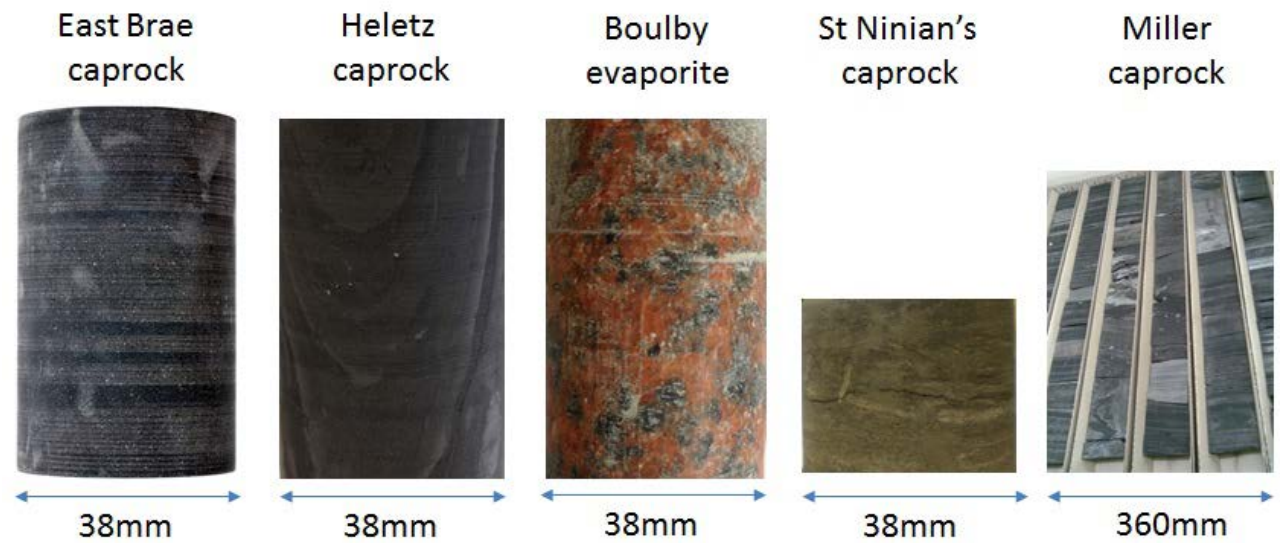

Figure 4-6. Further caprock samples

Figure 4-6. Heletz and Clashach sandstone

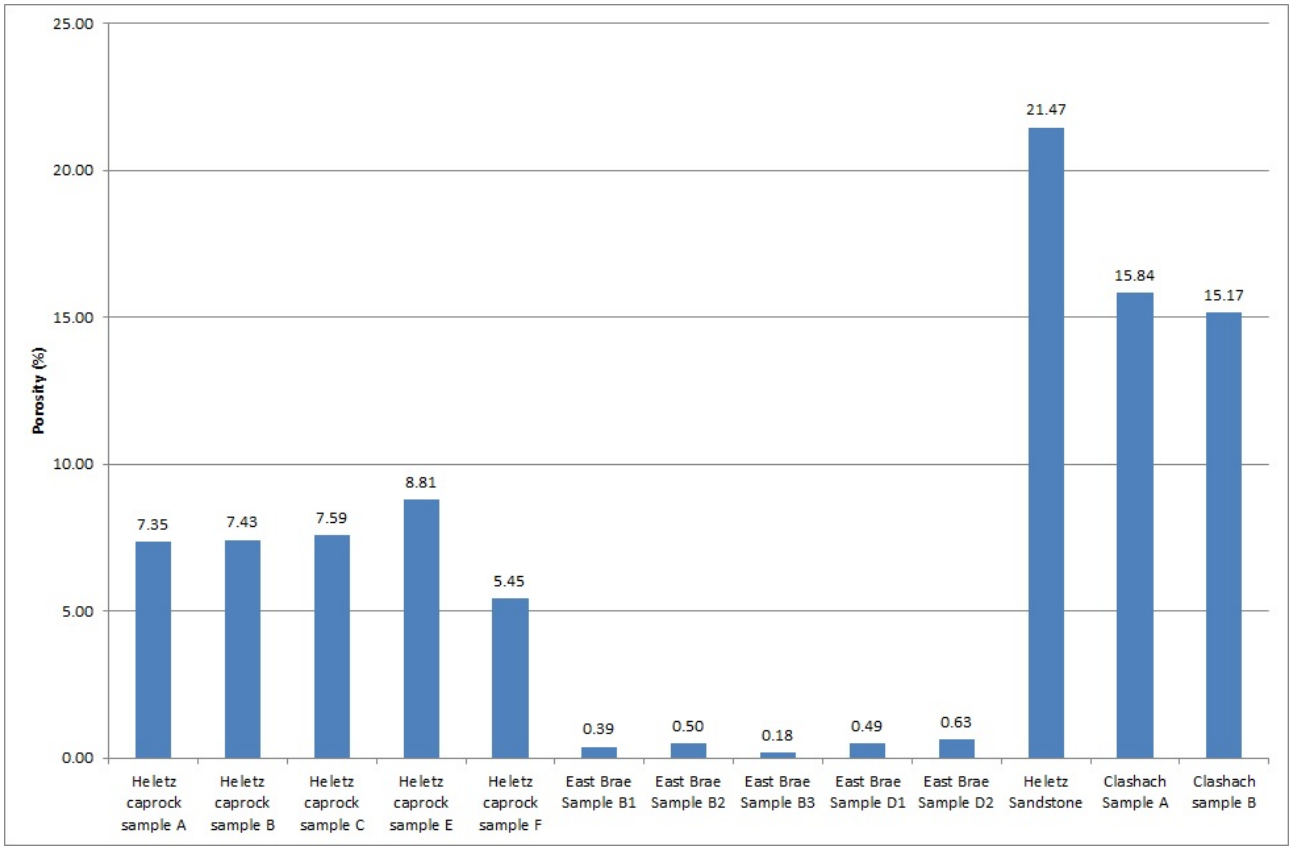

Figure 4-7. Porosity results

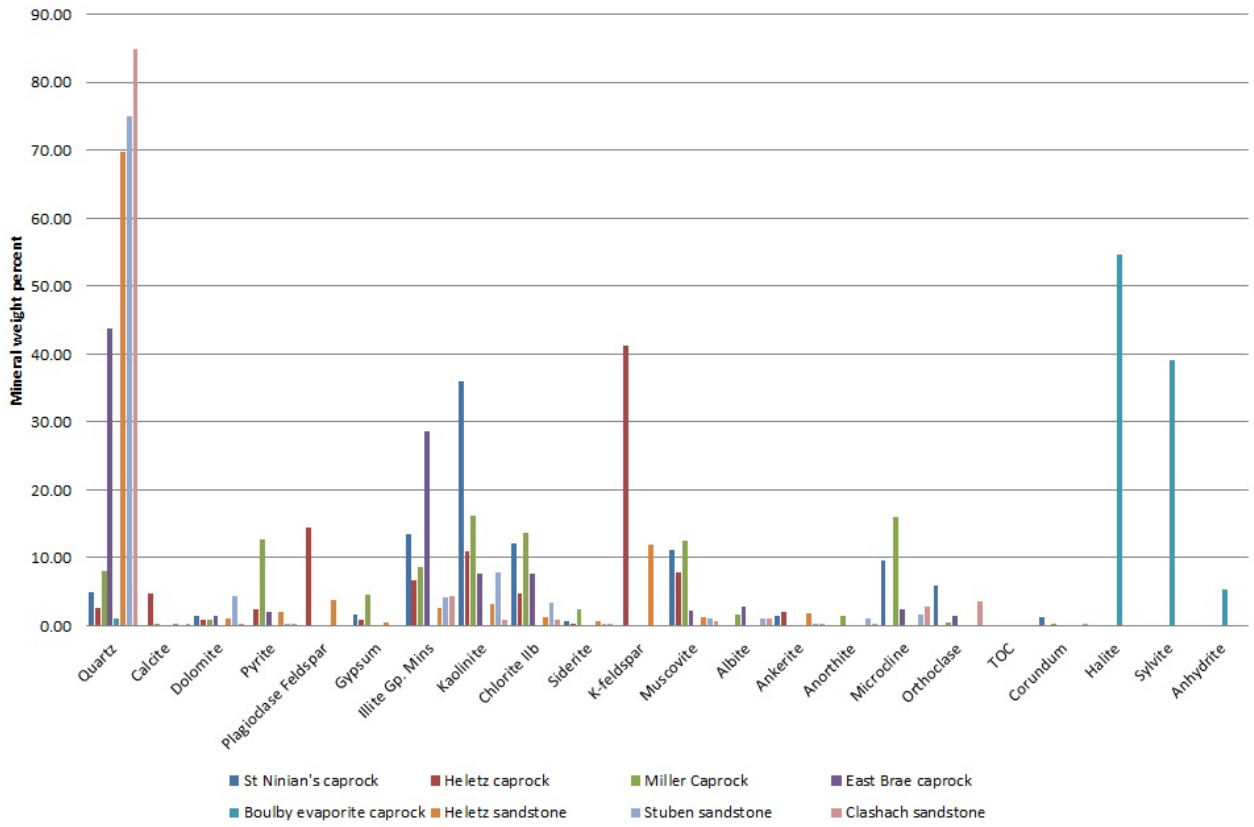

Figure 4-8. Mineralogy results

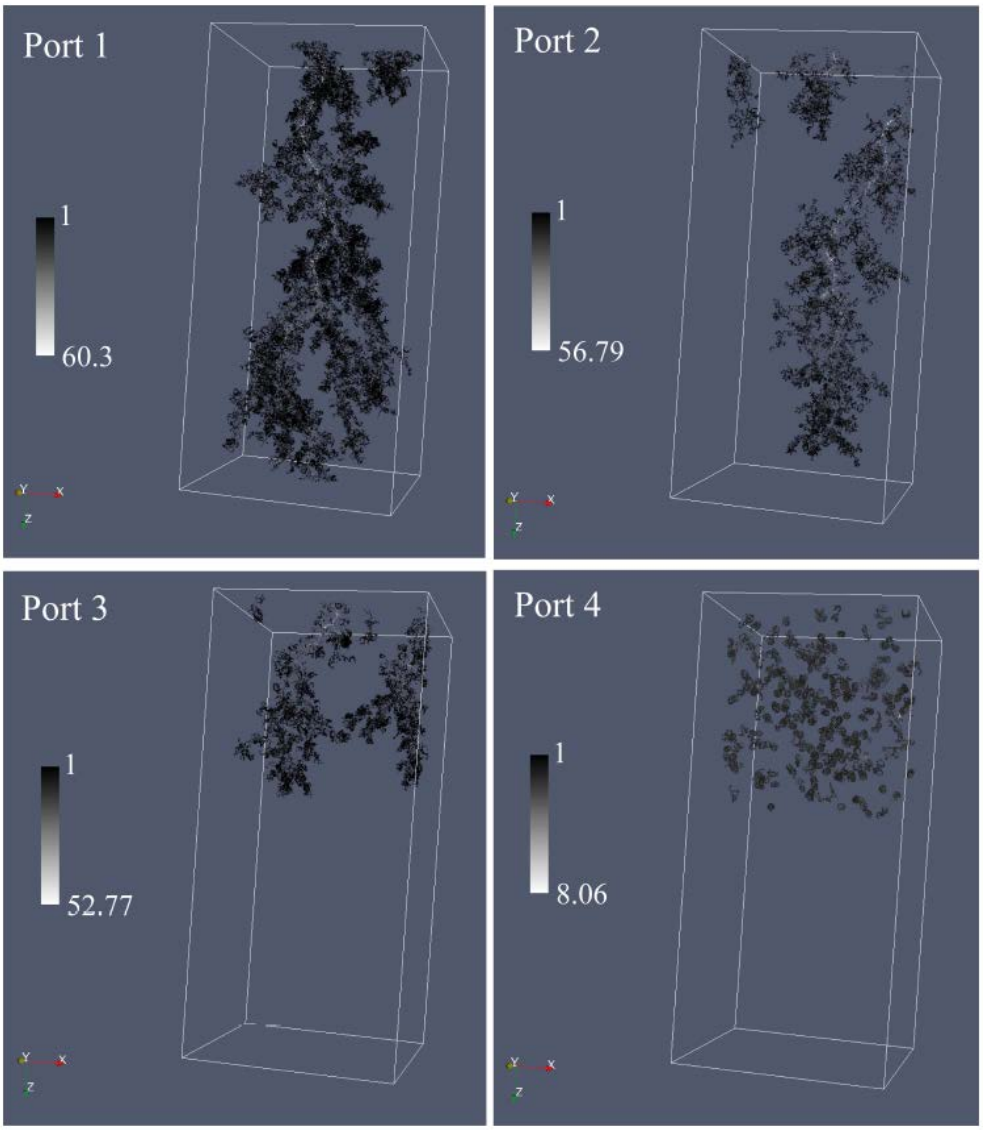

Figure 4-9. Representation of the nodes of the main components of the skeleton, i.e. parts of the skeleton coinciding with connected components of the void space that were exposed to dissolution at macroscopic scale. The grayscale colors correspond to the radius of the largest sphere centered at each node inscribed inside the void space (brightest points correspond to largest radii, logarithmic scale in voxel unit).

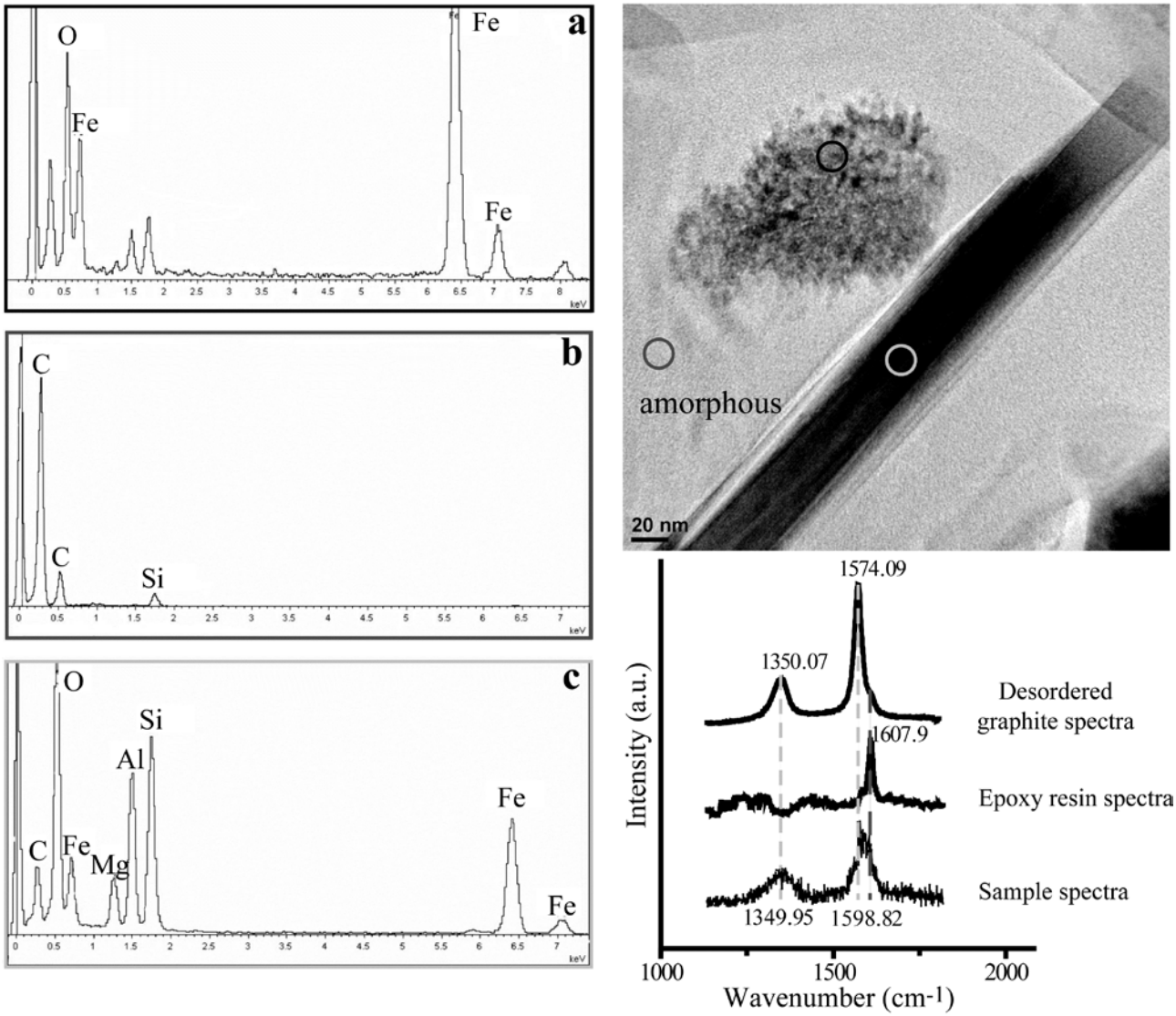

Figure 4-10. TEM image of the chlorite fibres and precipitated magnesite surrounded by amorphous and poorly crystallized carbon. On the left: Chemical analysis associated with the TEM image, A: magnetite chemical analysis, B: carbon chemical analysis and C: chamosite chemical analysis. Raman spectra of precipitated carbon near chlorite compared with epoxy-resin spectra and disordered carbon spectra.

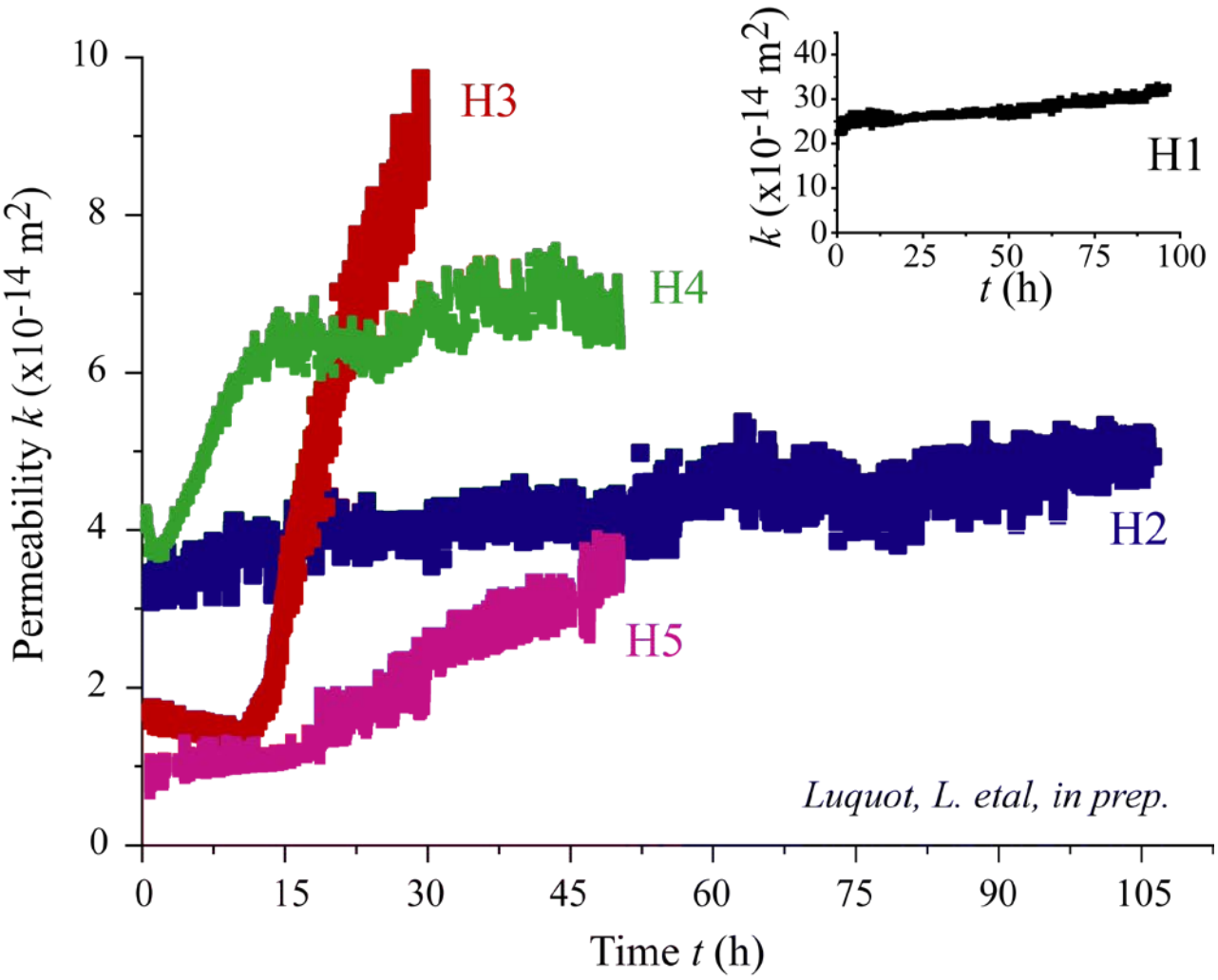

Figure 4-11. Permeability change during the five flow-through experiments through Heletz samples (H4 and H5 with equilibrated gypsum brine, H3 and H4 with high flow rate).

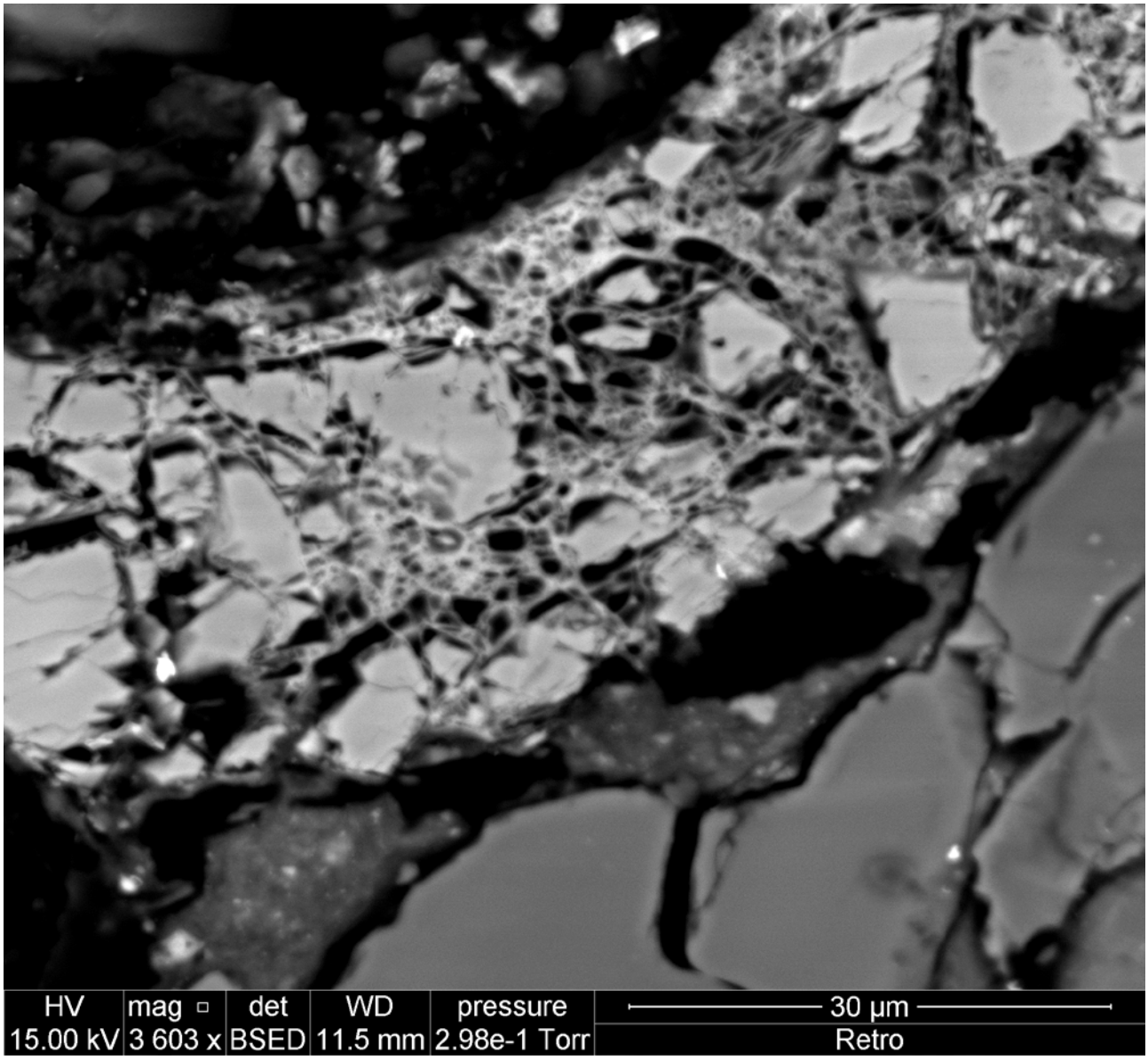

Figure 4-12. SEM image of Heletz sample after CO2-rich brine percolation, where we can observe clay precipitation.

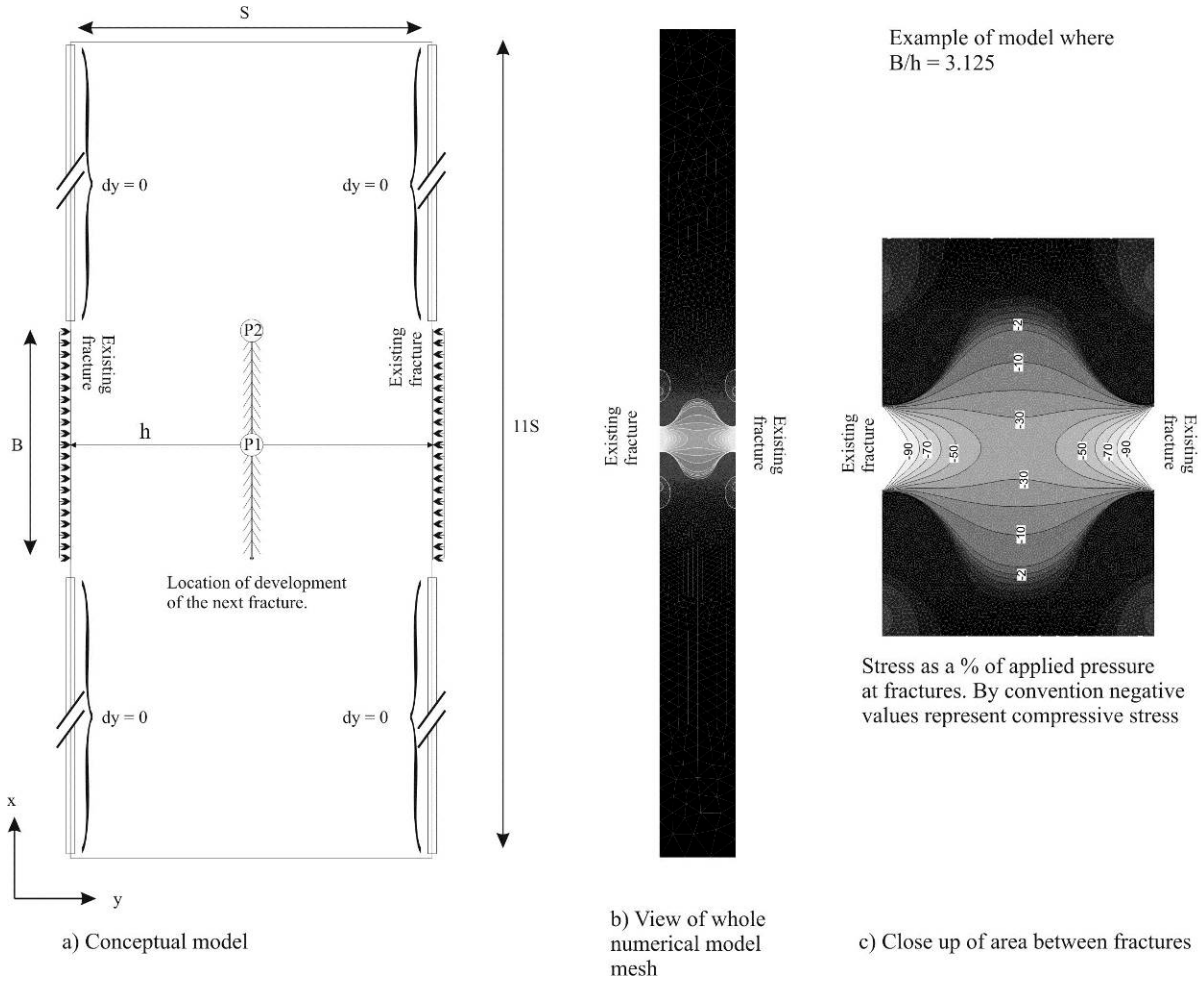

a) Conceptual model

b) View of whole numerical model mesh

c) Close up of area between fractures

Figure 4-13. Strata bound fracturing model

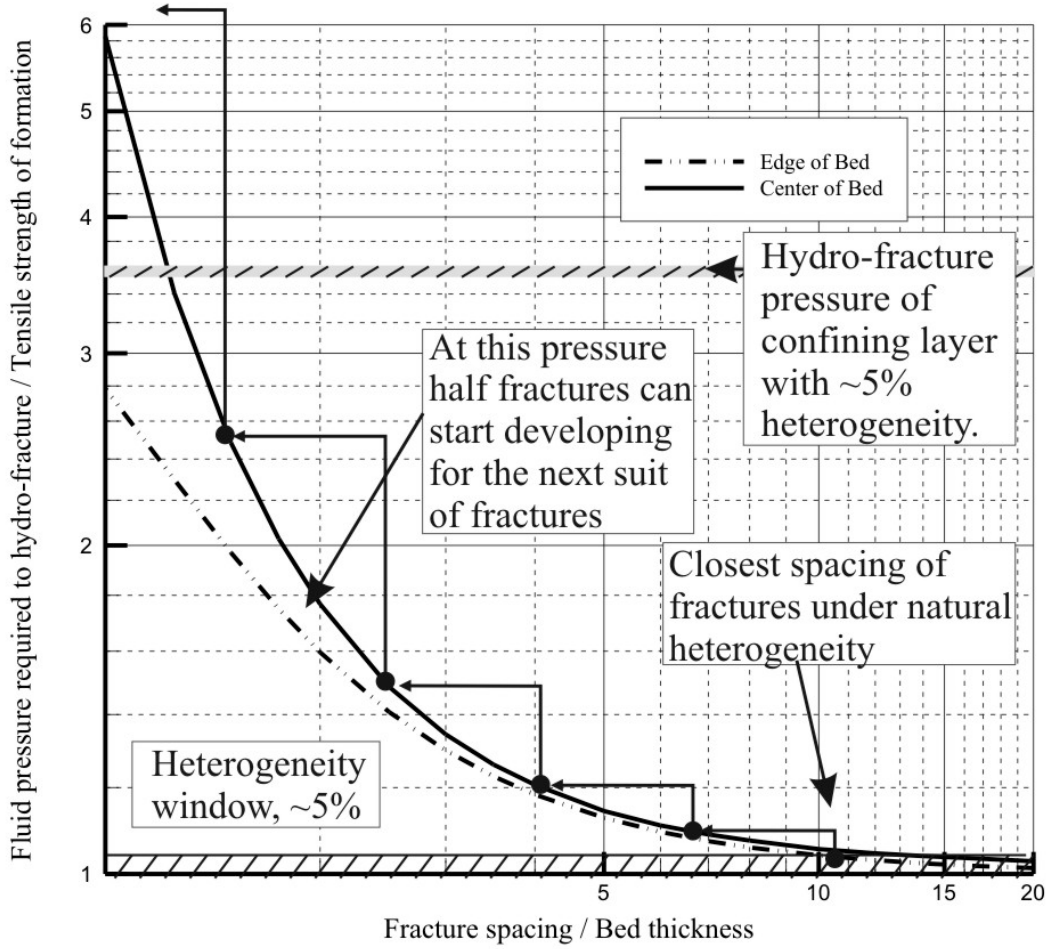

Figure 4-14. Normalised curve for fracturing in strata bound systems

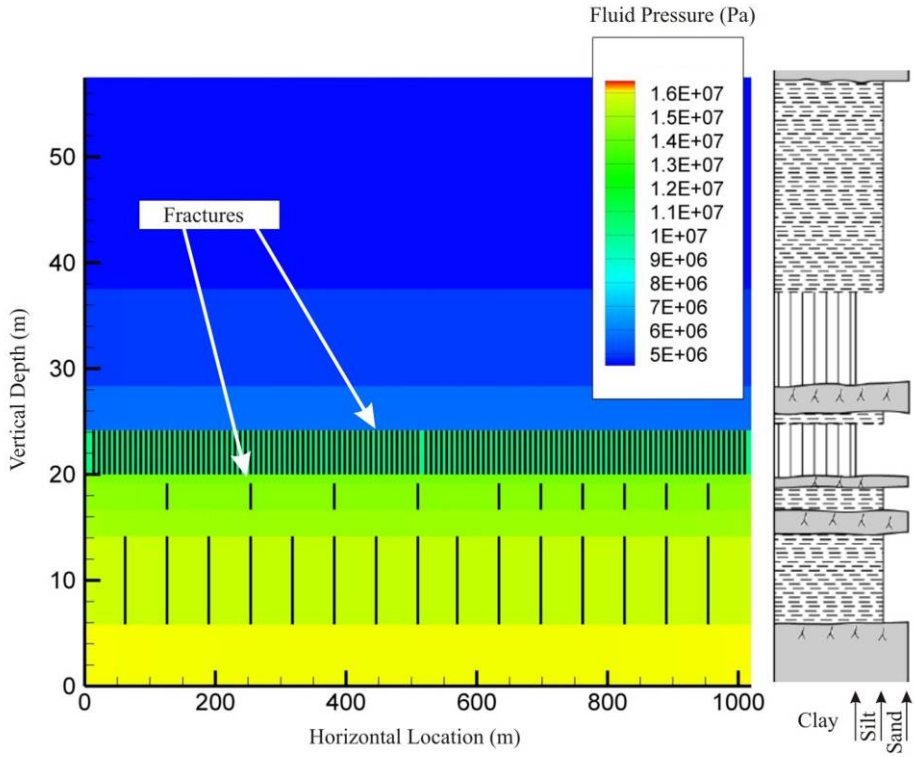

Figure 4-15. Hybrid Analytical Numerical Model

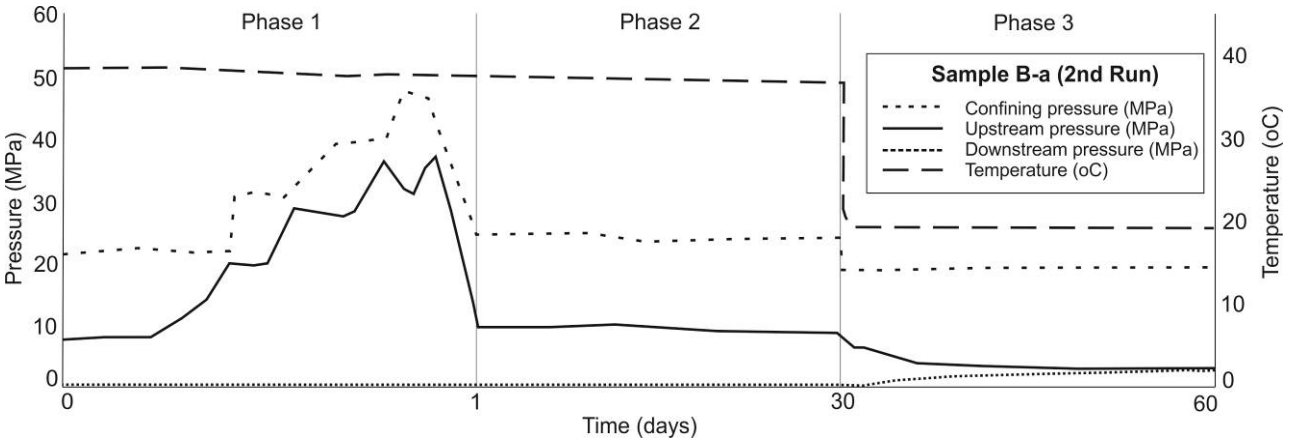

Figure 4-18. Results of the fractured caprock sample B-b, plotted as confining pressure (MPa), upstream pressure (MPa), downstream pressure (MPa) and temperature (ºC), with time

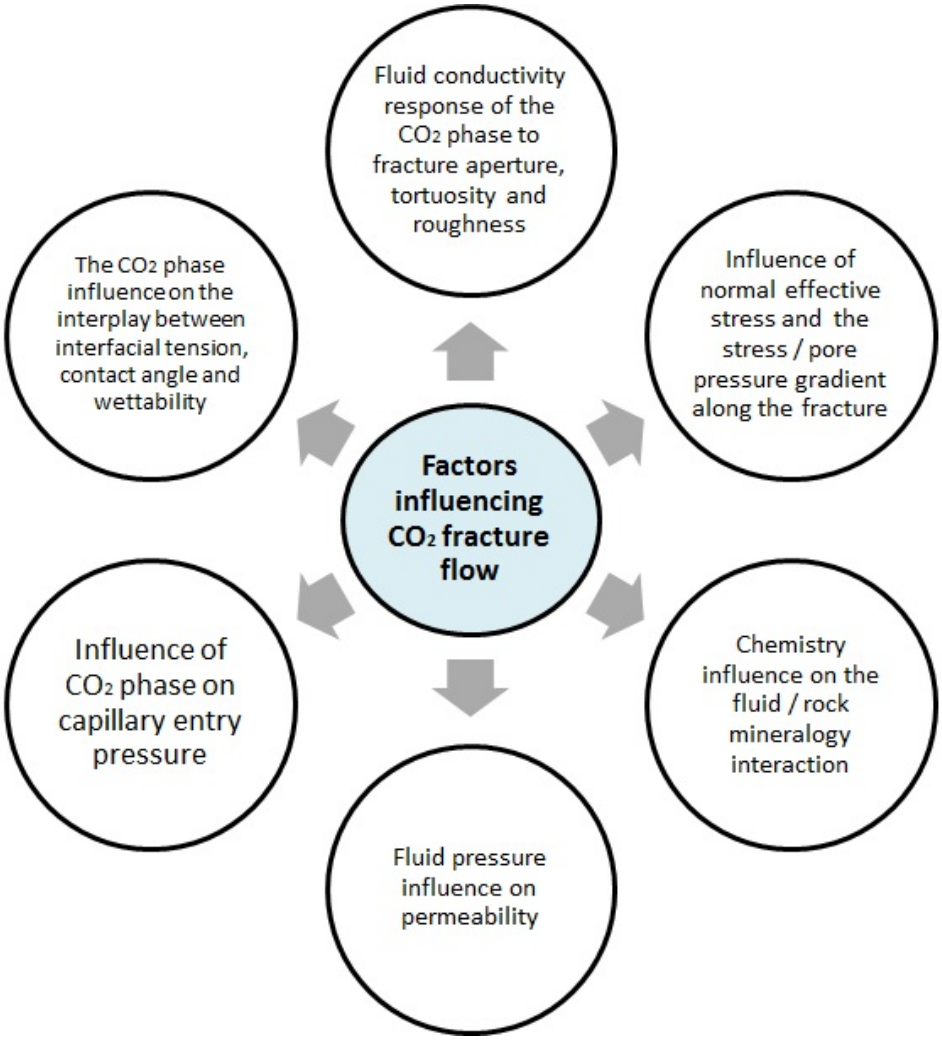

Figure 4-19. Factors influencing the flow of CO_2 along a fracture.

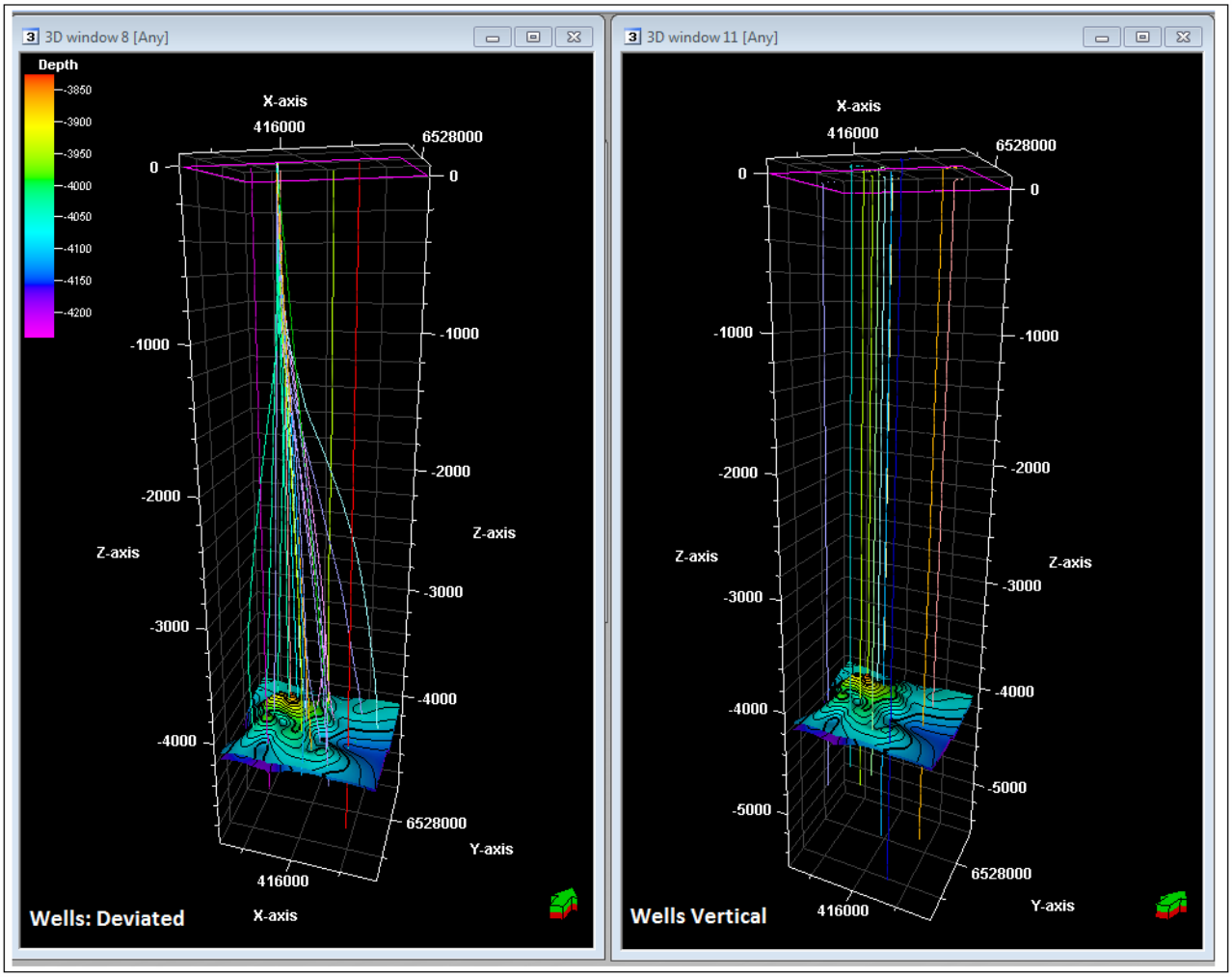

Figure 4-21. 3D perspective of both (left) deviated and (right) Vertical well paths (multi-coloured lines) intersecting the top KCF surface.

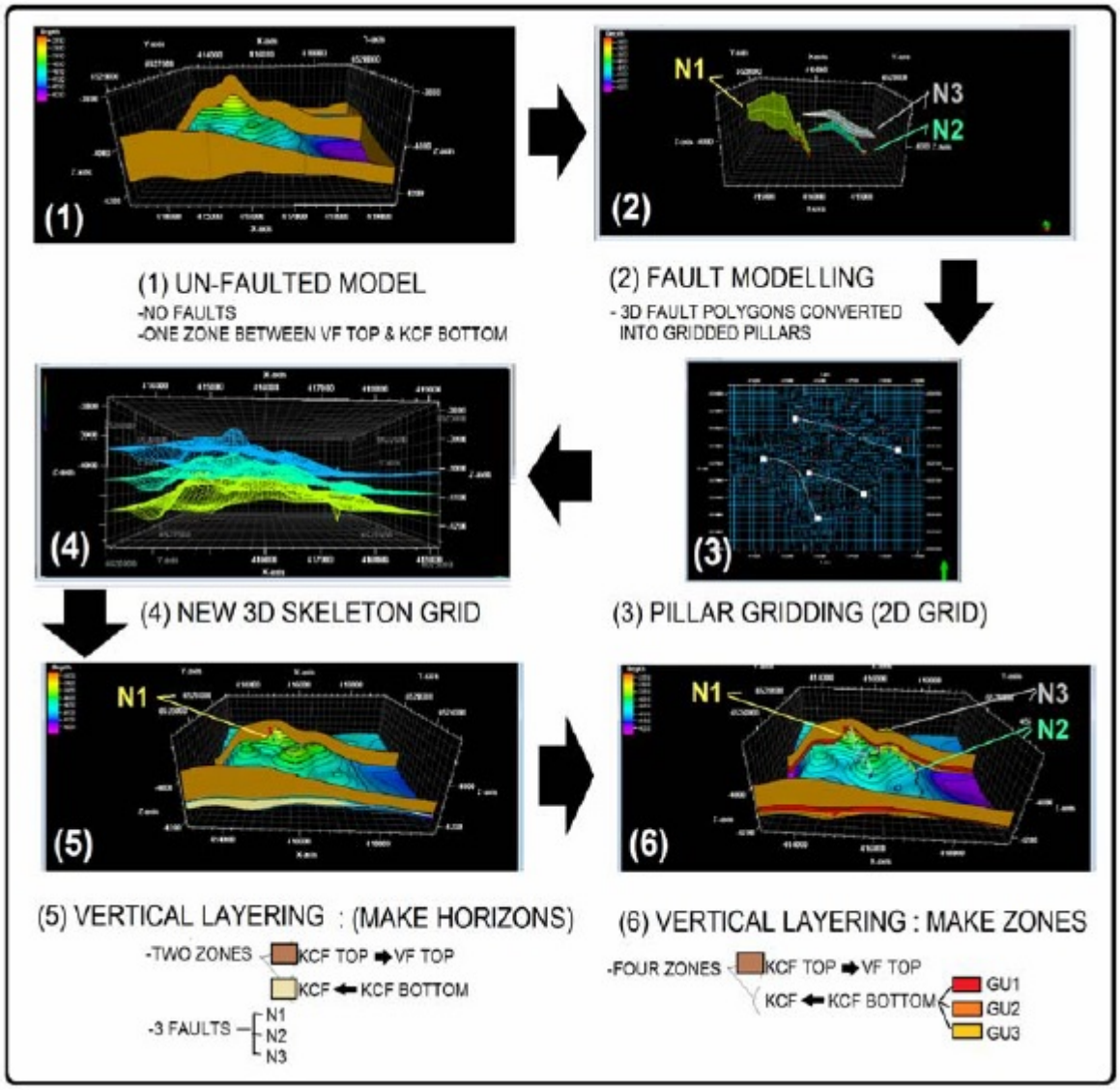

Figure 4-22. Flowchart detailing Petrel workflow for Structural Modelling of the faulted KCF Caprock in stages from (1) Un-faulted model, (2) Fault modelling, (3) Pillar Gridding, (4) New 3D Skeleton Grid creation, (5) Vertical Layering make horizons to (6) the final model to include zones.

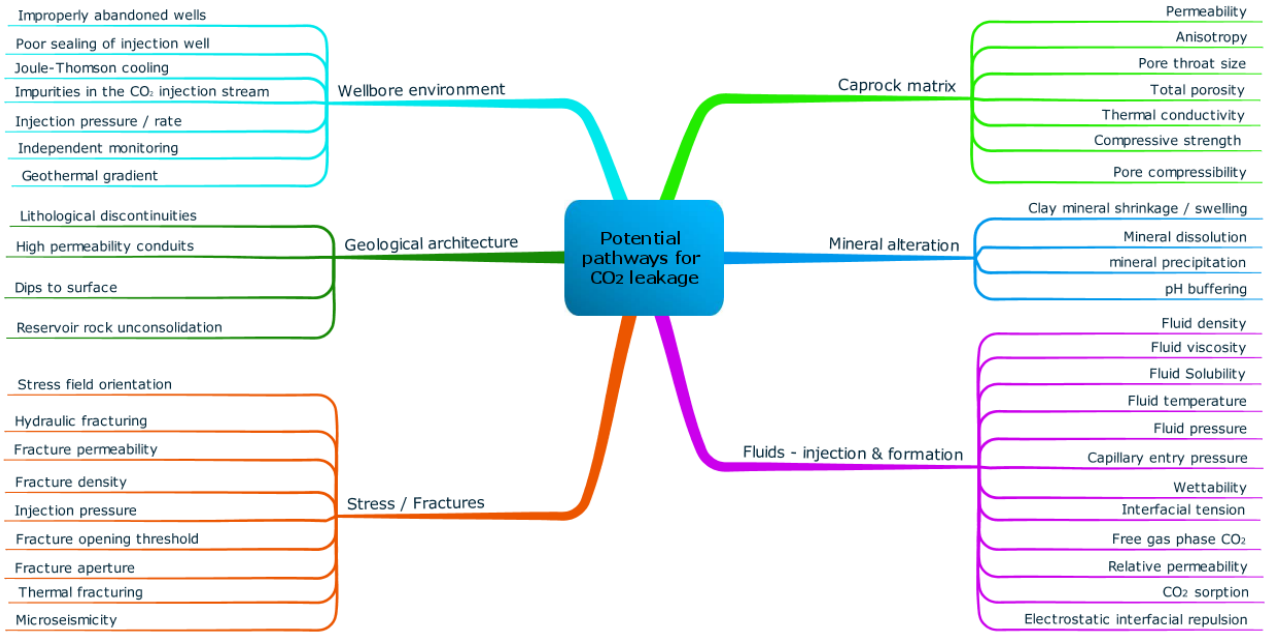

Figure 4-23. The potential CO_2 leakage pathways and leakage impact factors (risks) influencing caprock leakage grouped by primary category.

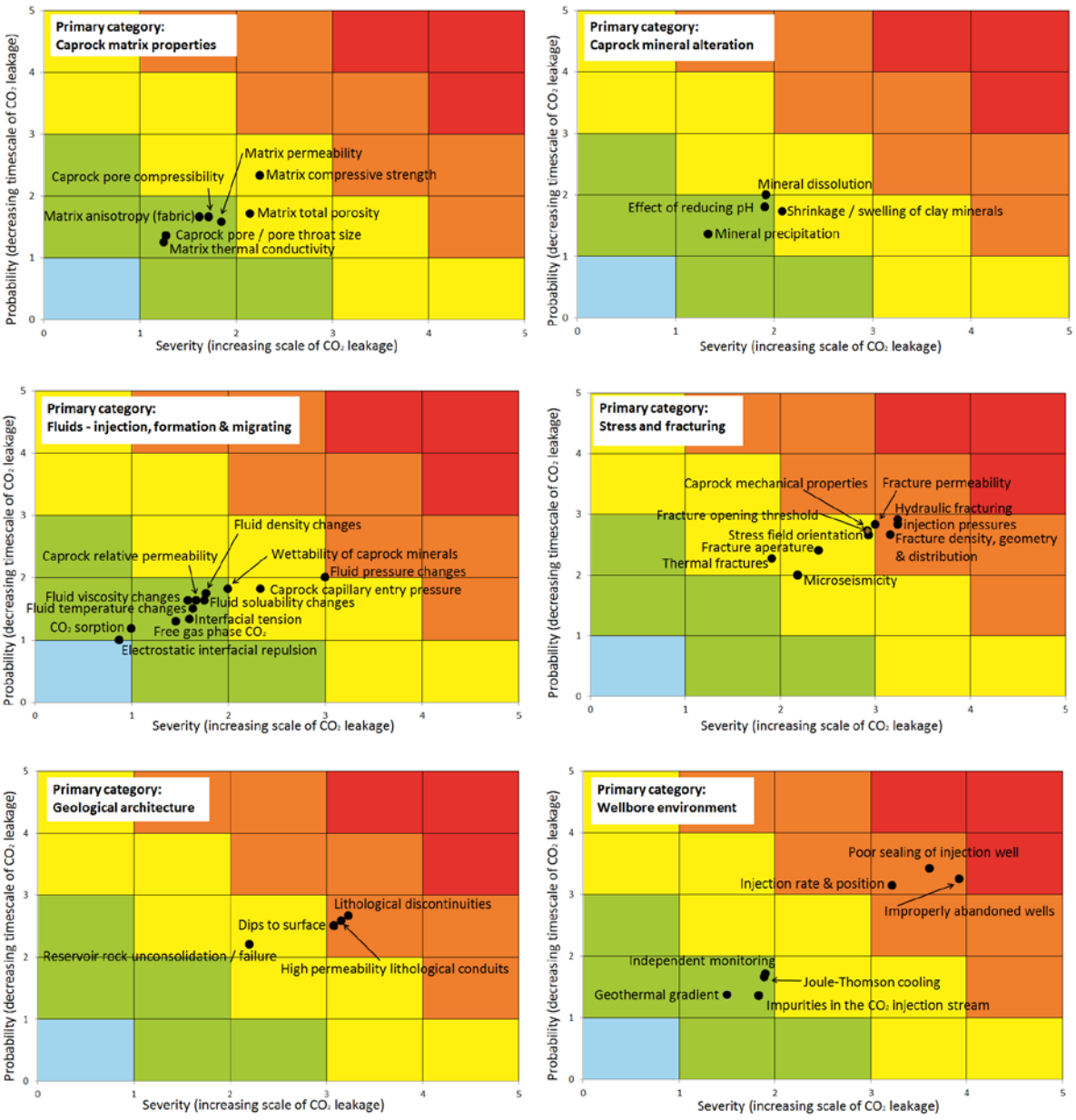

Figure 4-24. Risk matrix plot for CO_2 leakage (dark grey denotes extreme risk and the pale grey denotes low risk).

Table 4-1. Average bulk density, porosity and permeability results from the caprock and reservoir rock samples.

Rock type	Average bulk density (g/cc)	Average porosity (%)	Average Klinkenberg permeability (mD)
East Brae caprock	2.46	0.44	0.07
Heletz Caprock	2.36	7.32	21.9 *(samples are silty caprock so higher permeability than expected)*
Clashach sandstone	2.20	15.50	291.95
Heletz sandstone	2.19	21.47	Sample too small

Table 4-2. Mineralogy results for the caprock and sandstone samples used in the MUSTANG project.

	St Ninian caprock	Heletz caprock	Miller Caprock	East Brae caprock	Boulby evaporite	Heletz sst	Stuben sst	Clashach sst
Quartz	4.90	2.62	8.00	43.70	1.05	69.7	75.00	84.90
Calcite	0.00	4.70	0.27	0.00	0.00	0.1	0.00	0.11
Dolomite	1.50	0.95	0.80	1.50	0.00	1.1	4.30	0.15
Pyrite	0.00	2.39	12.70	2.00	0.00	2.0	0.25	0.04
Plagioclase Feldspar	0.00	14.55	0.00	0.00	0.00	3.9	0.00	0.00
Gypsum	1.60	0.94	4.50	0.00	0.00	0.4	0.00	0.00
Illite	13.40	6.72	8.70	28.70	0.00	2.6	4.10	4.40
Kaolinite	36.00	11.03	16.20	7.60	0.00	3.2	7.90	0.86
Chlorite	12.20	4.75	13.70	7.60	0.00	1.4	3.40	0.91
Siderite	0.70	0.34	2.46	0.00	0.00	0.7	0.16	0.11
K-feldspar	0.00	41.28	0.00	0.00	0.00	12.0	0.00	0.00
Muscovite	11.10	7.78	12.60	2.20	0.00	1.2	1.10	0.77
Albite	0.00	0.00	1.70	2.80	0.00	0.00	1.15	1.03
Ankerite	1.50	1.94	0.00	0.00	0.00	1.8	0.13	0.30
Anorthite	0.00	0.00	1.40	0.00	0.00	0.00	1.00	0.04
Microcline	9.70	0.00	16.10	2.50	0.00	0.00	1.62	2.90
Orthoclase	5.90	0.00	0.40	1.40	0.00	0.00	0.00	3.50
TOC	0.00	0.00	0.00	0.00	0.00	0.00	0.00	0.00
Corundum	1.30	0.00	0.10	0.00	0.00	0.00	0.00	0.09
Halite	0.00	0.00	0.00	0.00	54.55	0.00	0.00	0.00
Sylvite	0.00	0.00	0.00	0.00	39.15	0.00	0.00	0.00
Anhydrite	0.00	0.00	0.00	0.00	5.25	0.00	0.00	0.00

Table 4-3. The THMC parameters measured for each rock type

Rock type	Experiment type	Temperature (°C)	Flow rate (g/min)	Pressure (MPa)
St Ninian's	Batch	80	NA	13.7
Miller caprock	Batch	55	NA	13.7
Heletz caprock	Batch	80	NA	13.7
Naturally fractured East Brae	Rig- flow through	20 / 40	1 / 2 / 3 / 4 / 5	20 / 30 / 40 / 50
Artificially fractured Heletz caprock	Rig - flow through	20 / 40	1 / 2 / 3 / 4 / 5	20 / 30 / 40 / 50
Boulby Evaporite	Batch	20 / 40	NA	13.7
Heletz sandstone	Batch		NA	13.7
Stuben sandstone	Rig - flow through	20 / 40	1 / 2 / 3 / 4 / 5	20 / 30 / 40 / 50
Clashach sandstone	Rig - flow through	20 / 40	1 / 2 / 3 / 4 / 5	20 / 30 / 40 / 50

Table 4-4. Summary of the risk matrix results in ranked order.

Risk Category	Risk Ranking	Risk factor
Extreme leakage risks	-	None
High leakage risks:	1	improperly abandoned wells (**most significant risk**)
	2	poor sealing of the injection well
	3	injection rate and position (*injection rate above poorly defined capillary entry pressure or caprock tensile / compressive strength*)
	4	hydraulic fracturing (*if fracture propagation values are lower than expected*)
	5	injection pressures (*above capillary entry pressures or fracture propagation*)
	6	lithological discontinuities in the caprock (*caprock less continuous*)
	7	fracture density (*unexpectedly high fracture density*)
	8	high permeability lithological conduits in the caprock
	9	caprock and storage reservoir dipping to surface (*reservoir has surface outcrop*)
	10	fracture permeability (*unexpectedly high fracture permeability*)
	11	fluid pressure changes (*increase to cause fracturing / movement*)
Medium leakage risks:	12	caprock mechanical properties (*lower than expected*)
	13	fracture opening thresholds (*lower than expected*)
	14	stress field orientation (*improperly evaluated*)
	15	fracture aperture (*larger than expected*)
	16	caprock matrix compressive strength (*lower than expected*)
	17	reservoir rock unconsolidation / collapse
	18	thermal fracturing (*occurring*)
	19	micro seismicity (*occurring*)
	20	caprock capillary entry pressure (*lower than expected*)
	21	matrix total porosity (*higher than expected*)
	22	clay mineral shrinkage (CO_2 *dehydration or occurring in the presence of* CO_2)
	23	mineral dissolution (*higher than expected*)
	24	Wettability (*lower than expected*)
Medium Low leakage risks:	25	Reducing pH (*of formation fluids*)
	26	Independent monitoring (*does it increase confidence or data quality*)
	27	Joule Thomson cooling (*during any depressurisation*)
	28	Fluid density changes
	29	Matrix permeability (*wrongly characterised*)
	30	Fluid solubility changes (*wrongly characterised*)
	31	Pore compressibility (*wrongly characterised*)
	32	Matrix anisotropy (*wrongly characterised*)
	33	Caprock relative permeability to CO_2 (*wrongly characterised*)
	34	Fluid viscosity changes (*wrongly characterised*)
	35	Fluid temperature change
	36	Impurities in the CO_2 stream (*above the percentage tolerance*)
	37	Interfacial tension (*lower than expected*)
	38	Geothermal gradient (*significantly different to expected*)
	39	Free phase gas CO_2 (*present*)
	40	Mineral precipitation (*wrongly characterised*)
	41	Pore / pore throat size (*wrongly characterised*)
	42	Thermal conductivity(*wrongly characterised*)
	43	CO_2 sorption (*does not occur*)
	44	Electrostatic interfacial repulsion (*poorly defined clays*)
Low leakage risks:	-	None

5 WP 05 – Processes

The objective of this WP is to provide a comprehensive framework, in the form of process models, for the description and investigation of the major processes occurring during the injection of CO_2 into a brine-containing formation and the interactions that will take place between the injected CO_2, the solid matrix and the indigenous liquid in the formation. This will enable the investigation of (i) the relative significance of the various processes under different conditions, and (ii) the behavior of the system as a whole, in response to various scenarios. Specific objectives are: 1) Investigate the coupled flow, transport, chemical, geo-mechanical, and thermodynamic phenomena that occur in the subsurface brine formation into which CO_2 is injected; Evaluate their relative significance and dominance; 2) Construct a comprehensive description of the processes in form of conceptual models.

Partners contributing to this task are IIT, UU, EWRE, UGOE, CNRS, CSIC, UNOTT, KIT UEDIN, and UCAM.

The work is divided into four specific tasks

A- Process description
B- Process models
C- Process analyses and study of coupled phenomena
D- Synthesis of the results

5.1 WP 05 - Summary of work (IIT, CNRS, CSIC, UNOTT, KIT, UGOE, UCAM, EWRE, UU)

5.1.1 Comprehensive description of all processes

The properties of the CO_2 and brine were reviewed, including the equation of state of the CO_2 and constitutive relationships for the relevant properties of the CO_2 and the brine and their mixture (density, viscosity and enthalpy) and their dependence on state variables (temperature, pressure and concentration).

A review of possible interactions in the system rock matrix-CO_2 (various phases) and brine was suggested, allowing the identification of the coupling between them. This represents backbone of the processes to be formulated, particularly the relevant couplings.

Formulation of the processes that need to be taken into account during various phases of the CO2 injection and storage in a saline formation, including: two-phase fluxes (advection, dispersion and diffusion); heat fluxes; dissolution processes (brine in CO2 and CO2 in brine); interphase mass exchanges and transfer; chemical reactions and phase partitioning; Hydro-mechanical effects and fracture generation; mixing and spreading and the associated fingering resulting from density, viscosity and capillary forces contrasts; and finally hydrothermal and thermo-mechanical processes.

The injected super-critical CO2 (scCO2) has a lower density and viscosity than the reservoir fluid and therefore it is prone to hydrodynamic instabilities, arising from density and viscosity stratification. When the scCO2 is in contact with the formation fluid, dissolution will occur at

the interface between the two phases, which will have a fingered structure due to viscosity contrasts, thus resulting in a relatively large interface area between the two phases.
Dissolution of CO2 injection into saline aquifers causes an unstable high-density diffusive front. This unstable front of dissolved CO2 into brine will strongly affect the dissolution trapping mechanism.

Major knowledge and information gaps were identified, including:
• **Instabilities** (viscous, gravity, capillarity, dissolution: Their interactions still remain to be fully understood.
• **Pore scale processes**: Processes have been described on a continuum (porous medium) scale. Experience is lacking in many of the processes involved in CO2 storage, particularly with regard to chemical reactions and their interactions with other phenomena, such as mechanical deformation.
• **Heterogeneity**: This is the most singular feature of natural permeable media. The descriptions presented here acknowledge variability through the spatial dependence of the controlling parameters.
• **Coupled processes at varying scales**: couplings, which are essential to CO2 storage, add new dimensions of complexity, especially when dealing with varying scales. For example, CO2 injection may cause increases in fluid pressure and mechanical stresses that are well described macroscopically, but which may activate small scale processes, such as micro-fracturing, and dissolution-precipitation.

This description of all processes is presented in Deliverable D051.

5.1.2 Development of process models

Based on the formulations in the previous step, a complete and detailed description, in form of mathematical models, was formulated that describes the relevant processes of CO_2 spreading and trapping in geological formations. This includes two-phase flow of water and CO_2, in heterogeneous deformable porous media, under non-isothermal conditions. Each of the two phases is compressible and is comprised of a number of chemical species, possibly interacting. Solid matrix dissolution is also taken into account, with possible reactions that can lead to precipitation of reaction products. A discussion is provided on the effect of precipitation on coefficients that are related to the size of the pores, e.g. effective permeability. Special attention is given to solid matrix deformation that may occur as consequence of increased fluid pressure, and consequently, change in effective stress, which may cause damage to the impervious sealing formation.

A well-posed model requires information on the initial and boundary conditions of the system of interest. Discussion is included of such conditions, as may be encountered in practice. For any specific case to be modelled, the actual numerical values of the various coefficients appearing in the model need to be provided. Often these are expressed in form of constitutive relations that relate e.g. changes in fluid properties to changes in pressure, temperature and concentrations of dissolved constituents. Such relationships must also be provided. All the relevant coefficients and constitutive relations are presented. These models are presented in deliverables D052 and D053, which were combined into one deliverable, as this became a more natural entity for a report.

5.1.3 Process analyses and study of coupled phenomena

In this task the main focus has been in two topics, namely modelling of immiscible supercritical CO_2 plume movement including the effects of compressibility and carbonate precipitation and the effect of viscous and density fingering

Modeling of vertical and lateral viscous fingering and the effect of density stratification (UNOTT, CSIC, UEDIN)

In CO_2 sequestration, the injected supercritical CO2 displaces the surrounding liquid brine as an immiscible fluid phase. Supercritical CO_2 has a lower density and viscosity than the surrounding brine and therefore it is prone to hydrodynamic instabilities, due to density and viscosity stratification, as the supercritical fluid displaces the surrounding liquid brine. The onset and evolution of instabilities that occur in the displacement of the interface between two immiscible fluids with different viscosities is known as viscous fingering (interface instabilities). Besides, the supercritical CO2 plume in contact with the brine at the immiscible inter-phase dissolves in the liquid phase. As the immiscible CO2 plume dissolves into the saline water formation, the total carbon concentration in the liquid phase increases. The higher the CO2 content, the higher brine density; brine with dissolved carbon dioxide is heavier than the surrounding fresh brine. The unstable layering, heavier brine over lighter brine, is maintained until a small perturbation disturbs the system and triggers fingering of the CO2 saturated brine (volume instabilities). The Deliverable D054 gives a report of the study of these interface and volume instabilities, including the main associated processes occurring during the evolution of the injected CO2.

Mathematical description and numerical simulation of the motion of the immiscible supercritical CO2 plume during the injection period and related coupled phenomena (IIT, CSIC, UCAM)

Deliverable D055 summarizes several topics related to complex coupled processes of CO2 injection, which are discussed below

Carbonate precipitation in THMC modeling (CNRS)

In D055 we introduce a procedure to add CO2-chemistry to the coupled hydro-thermo-mechanical multiphase flow simulation model Code-Bright. By simplifying the chemical problem, we are able to express the entire chemical system as a function of the state variables of the code: Liquid pressure (Pl) for water balance, gas pressure (Pg) for air balance, porosity (f) for halite balance, temperature (T) for energy balance, and displacement (u) for momentum balance.
Then, in each time step the chemical system can be calculated without the need for specific subroutines and solvers. Examples of simulation results are shown in the Deliverable as well as in summary of WP 07 (Modeling).

Cold CO2 injection (CSIC)

Implications of cold CO2 injection into deep saline aquifers are also investigated by numerical modeling. It is shown that when cold CO2 is injected into a deep storage reservoir, the CO2 is typically colder than the formation. The subsequent exchange of heat between the injected cold CO2 and the porous matrix results in a non-isothermal current with a cold region near the injection well and a hot region ahead of a thermal front in the current. For buoyancy-driven flow, the non-isothermal current, in comparison to an isothermal current injected at aquifer temperature, has an increased depth near the well owing to the relatively slow up-slope

velocity of cold, viscous and dense CO2. This increases the storage potential in the near source region. It also leads to different leakage behaviour through the seal rock.

Dissolution of porous media by buoyancy-driven flow

Dissolution of porous media by buoyancy-driven flow has been also studied experimentally. A rich range of buoyancy transitions and associated flow morphologies that arise from the dissolution of a soluble inter-grain cement into an invading under-saturated fluid is demonstrated. Also, interesting cases of reversing buoyancy are produced where injectate has a double-flood front, with buoyant under-saturated injectate propagating upslope along an upper boundary and dense saturated injectate propagating downslope along a lower boundary.

Other process analyses (CSIC, UU)

Other work on complex processes requiring numerical modeling and listed in Task C in DOW has included in particular work on *coupled hydromechanical modelling* to evaluate the stability of the caprock during CO2 sequestration (Vilarrasa et al, 2011a) as well as development of a methodology to assess the stability of the caprock and to measure the mechanical parameters of the storage formation and the caprock by means of a high-pressure injection test. (Vilarrasa et al, 2011b). We have also addressed the question of *capillary trapping* from different points of view; Firstly, by deepening our conceptual understanding by looking at the concept of capillary pressure from the first principle. Since the various dissolved species are transported also by dispersion, we have also deepened our understanding of modeling the dispersive flux (Bear et al 2012a,b). Second, we have addressed the issue of capillary trapping by means of significant numerical modeling of various scenarios of CO2 injection at Heletz site, to analyze this phenomena and to characterize it with different measurement methods like tracers and hydraulic testing (documented in WP 07, works by Fagerlund et al., Rasmusson et al.)

5.1.4 Synthesis and relevance of various processes to key questions of geosequestration (UU)

The final stage of work was to develop an approach to relate the various processes and rheri relevance to key key questions of geosequestration. In the approach taken we first identify and define objectives, issues of concern, or **key questions (KQ)** associated with CO2 geosequestration. We call all of them KQs. We then list the **processes, features, and technical issues**, **P, F and Ti**, associated with each KQ. For this, we draw on input from MUSTANG partners, previous deliverables in this WP and the current state of knowledge.

Particular attention will be paid to effects of **couplings** between thermal, hydraulic, mechanical and chemical processes. For KQs with similar groups of P, F, and Ti, comparative tables can be formed with KQs as headings on columns and P-F-Ti on the rows. Below are some examples how we implement our approach.

Key Questions (KQ): We define the Key Questions to 1) Performance related, which are Capacity, Injectivity and Containment and 2) Risk-related, which are Induced seismicity, Focused leakage, Diffused leakage, Large-scale flow, Brine displacement, Pressure propagation, Leaching and transport of minerals and chemicals from rock matrix to shallow groundwater. List of **Processes (P)** and their description is extensive and will not be repeated here. **Features (F)** includes, among others, Geometry of the target layer and the caprock, Structural roughness of the caprock (increases trapping), Heterogeneity, permeability

correlation structures, hydraulic compartmentalization, Geologic structures such as faults, folds and fracture zones, Preferential pathways and Boundary conditions (open/closed boundary).

Examples of linking two example 'Key Questions' to the relevant 'Processes, Features and Operational Strategy questions' is given in **Tables WP 05-1** and **WP 05-2** below. The Deliverable D056 'Evaluation of the effect of individual processes and relative dominance of various processes' presents the approach as whole

Table 5-1. Example of Features (F) and Processes (P) relevant to Example Performance Key Question (KQ) 'Capacity'

F	Porosity: Lateral and vertical extent of storage formation; boundary conditions; caprock structure — structural trapping; presence of sealed or conductive faults and of leakage paths; heterogeneity, and flow compartmentalization…
P	Buoyancy flow, flow fingering at CO_2-water interface and at CO_2-saturated brine and formation-brine interface; CO_2 solubility in brine and solution rate; mineralization and rate; residual saturation and hysteresis in relative permeability characteristics
Coupled Process	Hydromechanical effects on porosity and on fault or fracture permeability; hydrochemical effects on dissolution and mineralization
Remarks on Operational Strategy	Site characterization and selection is needed. The controlling parameter is pressure rise in the storage formation due to CO_2 injection and storage; it must be kept below a regulatory maximum. Pressure management methods may be applied.

Table 5-2. Example of Features (F) and Processes (P) relevant to an example Risk Key Question (KQ) 'Focused Leakage'

F	Fault and fracture structure; connected fractures; heterogeneity-induced channeling; multiple caprock layers; abandoned wells and imperfectly constructed injective wells, formation pinch-out areas
P	Multiphase flow in faults, connected fractures, and heterogeneity-induced channeling paths; vertical leakage through multilayer caprock; potential for accelerating leakage rate, degassing
Coupled Process	Coupled thermohydrological effects (e.g., cooling) on multiphase flow through vertical leakage paths; coupled thermo-hydro-chemical and thermo-hydro-mechanical effects on permeability and leakage paths
Remarks on Operational Strategy	Site evaluation and selection; Monitoring plan and response strategy needed

5.2 WP 05 - Main results and achievements

1) Development of a comprehensive description of the process models relevant to CO2 spreading
2) Development of a comprehensive description of CO2 spreading processes in form of mathematical models
3) Process analyses and study of coupled phenomena, including
   a. Development of a coupled model for carbonate precipitation in coupled THMC modeling
   b. Model for cold CO2 injection
   c. Models for viscous and density fingering.
   d. Coupled HM modelling and related testing
   e. Capillary trapping modelling and observation by measurement (see WP 07)
   f. Modeling effects of heterogeneities on the flow of buoyant CO2 – experiments and theory to quantify the lateral dispersion from a point well injection
   g. Modeling the effects of the confinement of an aquifer during the injection of CO2 when the aquifer is inclined and when both injection pressure and buoyancy have important impact on the flow
   h. Modeling the mixing produced by oscillatory flow from tidal oscillations and the effect on enhancing dissolution of CO2

i. Modeling the buoyancy driven dispersion of co2 in a multilayer system, as the co2 spreads laterally in the different layers subject to buoyancy forcing

4) Developing a framework for relating the processes to key questions of geosequestration.

The main achievements for previous periods have been summarized in the previous periodic reports as well as the comprehensive deliverables (D5.1 to 5.5) from these periods, and will be summarized as whole in the final report due at the end of the project. The main result of this period is the establishment of the framework and the synthesizing assembly of the relevance of various processes in terms of the key questions of geosequestration. The relevant deliverable (due the next period) is practically completed and will be submitted as scheduled.

6 WP 06 - Validation experiment

Within the mustang project two experimental sites are operated: Maguelone (France) and Heletz (Israel). Maguelone is aimed at demonstrating the use of various MMV technologies at shallow depth, while Heletz is deep injection experiment of a small quantity (up to 1,000 tons) of super-critical CO_2.

The Heletz experiment is a scientifically motivated CO2 injection experiment to a target layer at 1600 m depth. The objectives are 1) to gain understanding and develop methods to determine the two key trapping mechanisms of CO2, namely residual trapping and dissolution trapping, at field scale. Furthermore, the experiment should provide data for the validation of predictive models, and measurement and monitoring techniques. This experiment is by far the major financial component of the MUSTANG project.

The Maguelone experiment, led by CNRS, is aimed at demonstrating the use of various MMV technologies at shallow depth based on CO2 gas injection.

6.1 Heletz

6.1.1 General description

Heletz is a depleted oil reservoir with saline water at it is edges. The experiment is situated in the saline part of the reservoir (Figure 6-1). The reservoir comprises a dolomite layer (LC11), sandstone layers (“K”, “W” and “A”, the Heletz sands) and the Kochav sands. These layers are separated by shale intercalations. The reservoir is bounded from above a relatively thick layer of shale and marl. The target layers for the experiments were “K”, “W” and “A” as these were extensively investigated for oil exploration and substantial information was available about their properties and their behaviour.

Prior to any field activity partner GII gathered all the available information and created a picture of the site geology, relevant hydraulic, properties (porosity, permeability), chemical composition of the formation water and cumulative thickness of the conductive layers and of the caprock. The selection of the location for the experiment was driven by two criteria: 1) the area had to be “dry” (no presence of oil); 2) prior hard information had to be available, in form of an abandoned well with potential for re-entry. Re-entry efforts were unsuccessful and finally two deep wells (wells H18A and H18B) were drilled at the selected site (well H18). Prior information included a relatively detailed description of the geology, layer thicknesses and topography as well as initial estimates of the permeability (~100 md) and of the porosity (~15-20%).

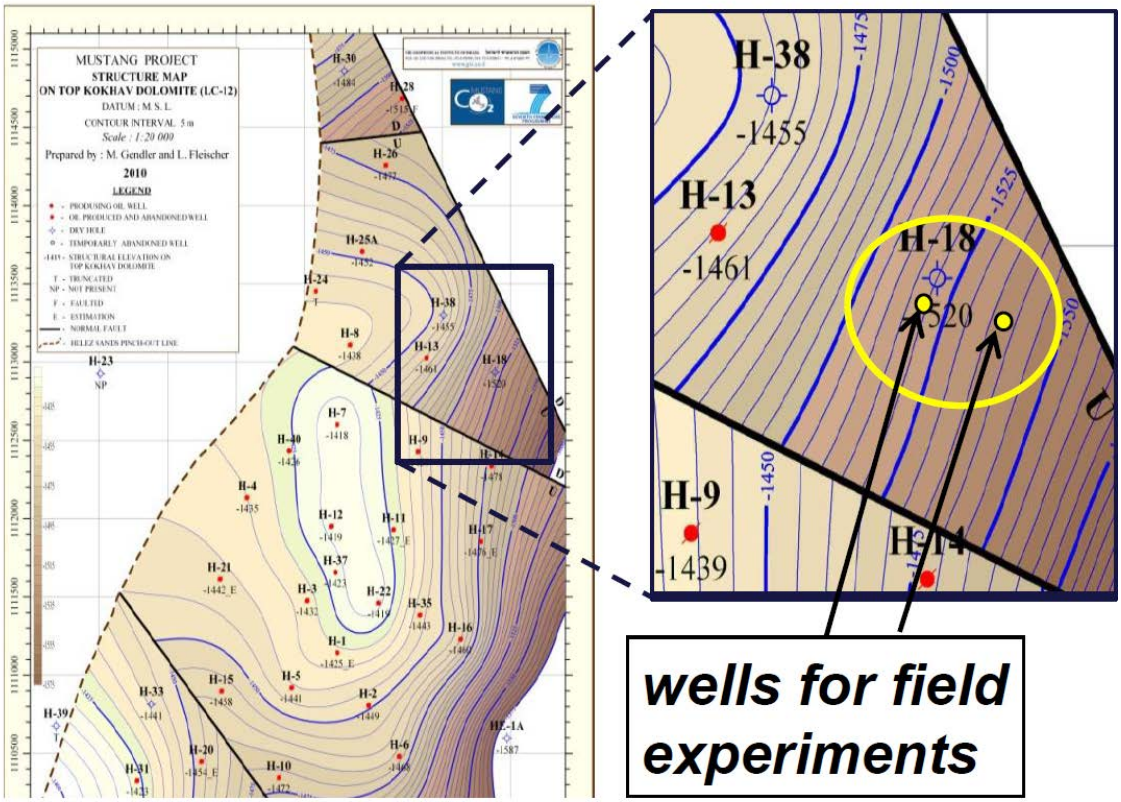

Figure 6-1. Site layout for Heletz experiment.

6.1.2 Experiment principle and predictive modelling

The original plan was as identified in DOW was to conduct a dipole injection of CO2, by injecting in one borehole and monitoring in another. This plan was later extended to consist of (1) essentially a single-well push-pull experiment (still with monitoring in the monitoring well), to investigate the in-situ residual trapping and (2) two-well dipole injection, for determining residual and dissolution trapping in the presence of heterogeneity. Conceptual pictures of the experimental setup are given in Figure 6-2. In both sequences, the first of which closely follows the Otway push-pull sequence, the principle is to use a number of indirect measurement techniques (hydraulic, thermal and tracer tests) before, after and during the injection, to evaluate the in-situ values of residual and dissolution trapping.

Extensive modelling has been carried out to design the experiments, test different test scenarios and finally produce detailed test protocols for the experiments. Modeling has been carried out with TOUGH2 family of codes and the models have been continuously updated as more data has come from the field and laboratory. Example modelling is presented in Deliverables of WP06 and also in e.g Rasmusson et al. (2014a, b) and Fagerlund et al. (2013 a, b). Example of a simulated test sequence for the push-pull experiment is shown in Figure 6-3, indicating how different values of residual trapping can influence the hydraulic, thermal and tracer response of a test. Figure 6-4 shows how the tracer enrichment in CO2 during the dipole can be linked to the in-situ dissolution.

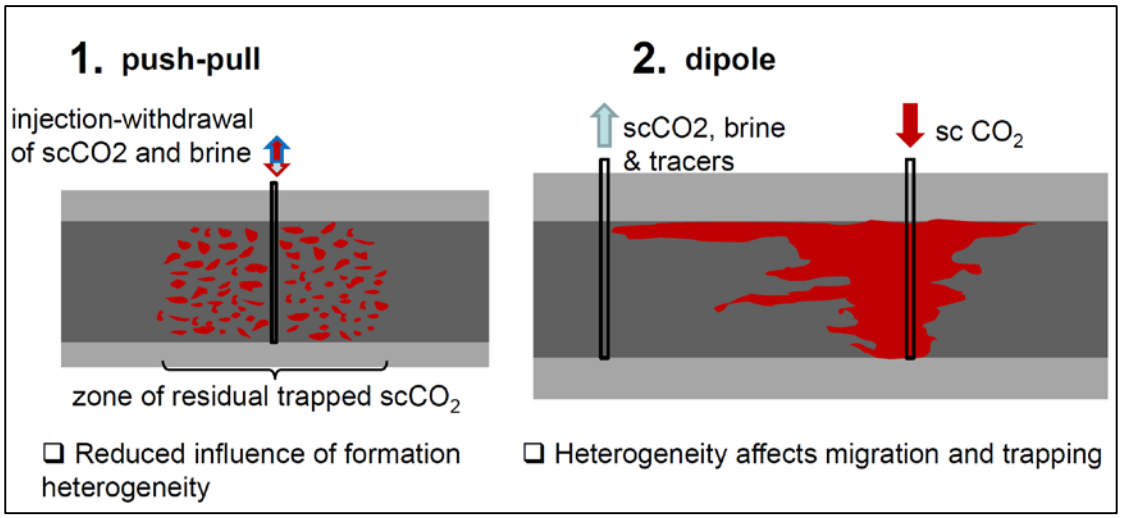

Figure 6-2. Principle of the CO2 test scenarios at Heletz.

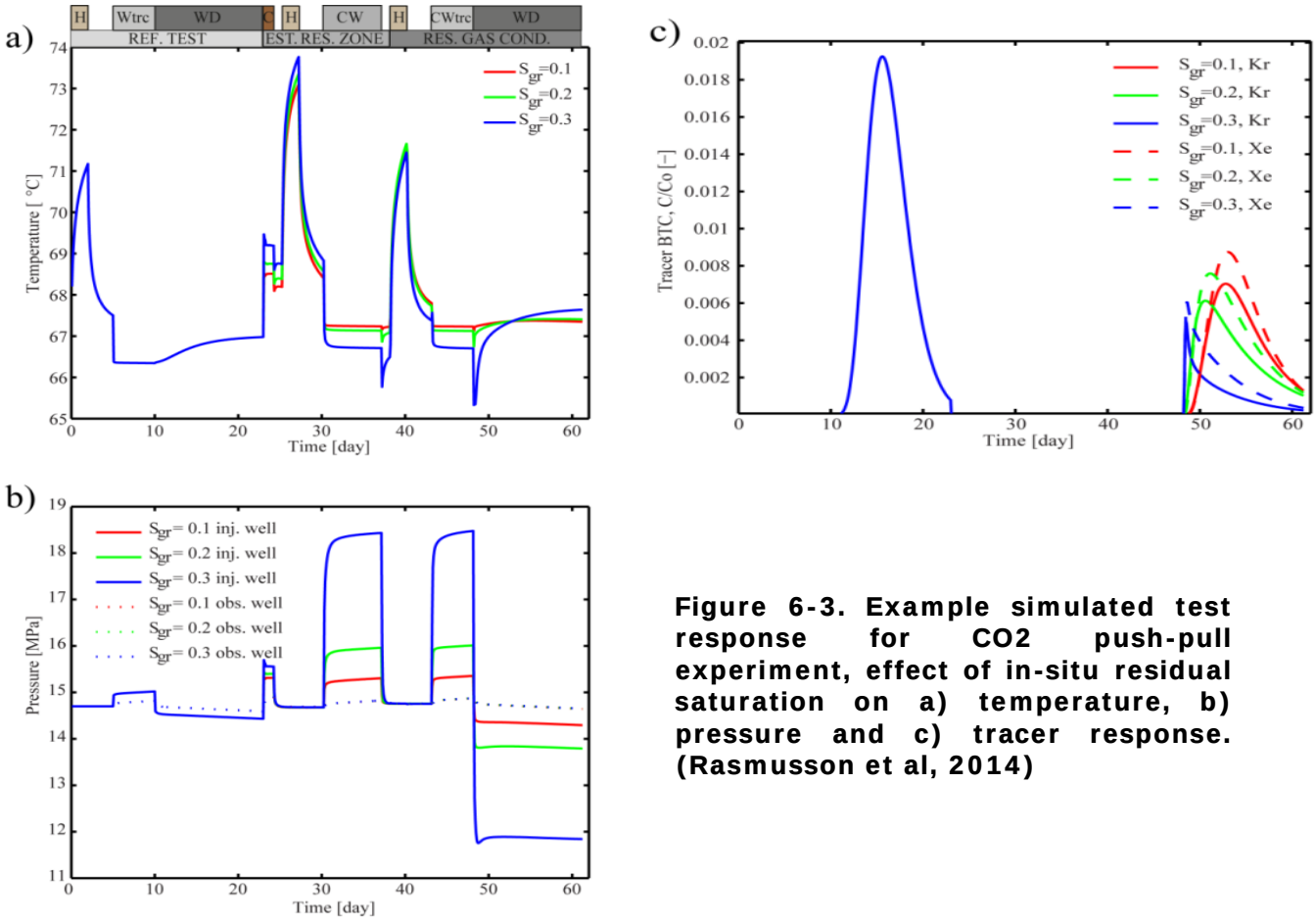

Figure 6-3. Example simulated test response for CO2 push-pull experiment, effect of in-situ residual saturation on a) temperature, b) pressure and c) tracer response. (Rasmusson et al, 2014)

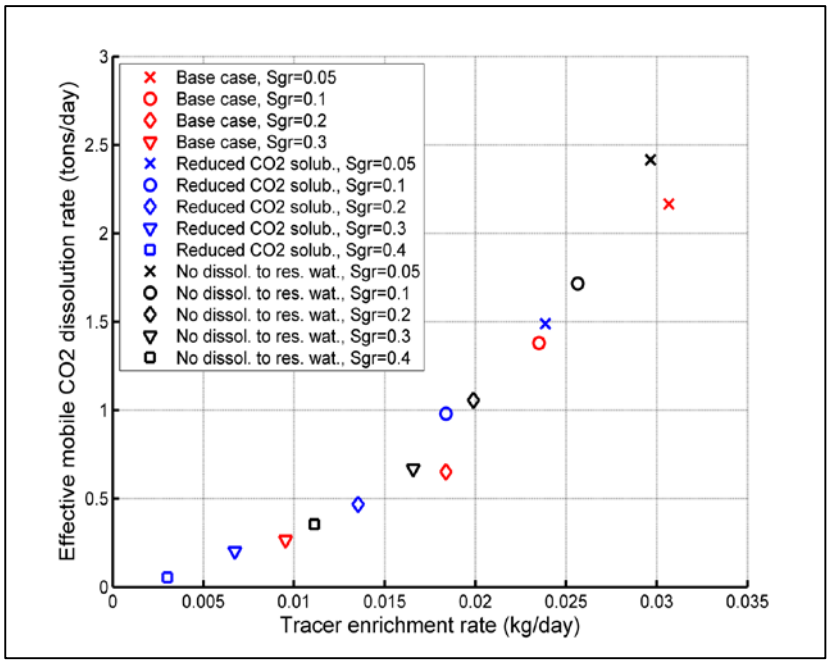

Figure 6-4. Example simulated test response for CO2 dipole experiment, mobile scCO2 dissolution as a function of tracer enrichment showing a strong correlation (Fagerlund et al, 2013)

6.1.3 Characterization and monitoring program

Characterizatrion program

The characterization program of the reservoir includes:

1. Coring the reservoir and the caprock of each well;
2. Core analysis;
3. Executing logs;
4. Inferring logs;
5. Seismic survey;
6. Hydraulic testing;
7. Tracer testing;
8. Thermal recovery;

Cores were taken from the reservoir and from the caprock in both wells. They were sent for analysis to a number of institutions: CNRS for chemical reactivity, UEDIN for hydraulic mineralogy characterization, UGOE and LIAG for hydraulic characterization and to Stanford University for the determination of H_2O-CO_2 capillary pressure and relative permeability curves. There was a common agreement that reservoir material is poorly cemented and easily disintegrates in presence of brine, that the hydraulic properties may be higher that the predicted ones (Stanford measured a permeability of 100 md while LIAG measured was of ~450 md).

An extensive set of logs was conducted in both wells, including Electric Resistivity, Gamma Ray, Neutron, Spontaneous potential and caliper. The logs were interpreted by GSI and CNRS and

provide the key information: 1) the layer structure is consistent with the picture that was built based on available data; 2) only the “W” and “A” layers are suitable for injection as the “K” layer could have poor hydraulic properties.

From these activities we gained a substantial amount of information that partly changed our program. The poor cementation of the reservoir layers implied that there was a need to case and cement the well H18, activity that was not initially planned. The hydraulic properties of the reservoir seem to be better than originally expected. GSI conducted a seismic survey in order to prepare a baseline picture of the reservoir. The reservoir and caprock were identified.

A program for the hydraulic testing was established. It included:

1. Pumping tests, aimed at determining the transmissivity of the reservoir
2. Flowing fluid electrical conductivity (FFEC) test aimed at determining the vertical variability of the permeability.

Pumping tests showed that the reservoir layers are far more conductive than expected, even from the core analysis: we obtained a permeability of ~720 md and an anisotropy of 1:6. The FFEC log could not be undertaken so far, due to sand accumulation in the well and the need to prioritize the well completion (instrumentation) activities. The FFEC will be carried out after the execution of the push-pull experiment.

The plan for a tracer test comprised the injection of water and tracers in the injection wells and water abstraction in the monitoring well. Due to the relatively long time needed for breakthrough and tail monitoring we plan to conduct this experiment after the first CO2 injections. Thermal recovery is aimed at determining the heat transfer between the borehole and its surroundings. It consists in injecting water of substantially lower temperature in the borehole and measure the heating rate in order to deduct the coefficient of heat transfer and its vertical variability along the borehole. This activity was intentionally postponed until the wells are completed, as the installed monitoring technologies allow a straightforward measurement of the temperature.

During the pumping tests we also sampled the formation water and sent for extensive chemical analysis. The results show a full compatibility between the chemical composition measured during the drilling of well H18 (in 1955) and the water recently sampled.

Monitoring program

Down-hole monitoring

As previously stated the monitoring program was driven by the objectives of the planned experiment and by dictated by budget considerations too. The monitoring instrumentation of the wells included:

1. Downhole high precision and robust pressure and temperature sensors;
2. Fluid sampling;
3. Optical Fiber (OF) for continuous temperature sensing.

Pressure and temperature sensing are crucial in determining the state of the injected CO_2. In the injection well we installed P/T sensors in the bottom and top of the reservoir layers, while in the monitoring well only P/T sensor was installed. Fluid sampling will provide information on the fluid composition, subsequent to CO_2 injection, CO_2 dissolution, and mixing via the tracer analysis. Continuous temperature sensing will allow conducting the thermal recovery test, detect CO_2 leakage and also infer the CO_2 saturation, when coupled with a heating process (also available in both wells). A second seismic survey is planned after CO_2 injection and this completes the monitoring program of MUSTANG.

Above-the ground monitoring program

The CO_2 injection system above the ground includes a set pressure and temperature sensors distributed along the line between the CO_2 storage tank and the well head. These enable to determine to what measure the CO_2 is within planned conditions of pressure and temperature and in case this is needed to determine the measures that have to be taken in order to achieve them. Additionally we have installed continuous CO_2 sensors at the vicinity of the injection kit, connected to an alarm system, in order to detect and provide warning about any possible CO_2 leak.

6.1.4 Drilling, logging, casing and cementation of wells (LAPIDOTH, EWRE, UU and GII)

Well opening attempts

The original plan of the Heletz experiment was to re-enter an abandoned well (H-18) and to drill a new one at a distance to be determined by the experimental design. The work started on October 10th, 2010 and continued until January March 1st, 2011. During this period, LAPIDOTH staff attempted to re-enter the well, i.e., prepare the well so it would be possible install a 7 inch casing, cement the well and instrument it for injection. Work progressed until a fracture was identified in the casing, at a depth of ~720 meters. In this depth the geological section is composed of a karst, with a substantial proportion of cavities. Additionally, the formation water is saline from this depth and thus is potentially corrosive to the carbon-steel existing casing. Part of the casing in this depth penetrated the karst, thus making the re-entry of H-18 unfeasible, even after 71 days of efforts. On April 1st, 2011, we commonly decided to abandon the well and halt the design of the well completion until a decision could be taken on how to proceed.

We then decided to search for a new candidate well for re-entry. Together, with GII, we identified the well H-35. This well had better hydraulic properties than H-18, but had the drawback of having been an oil production well. H-35 was drilled in 1967 and the oil production ceased in 1988, when the abstracted fluid comprised over 90% brine. The activities for the re-entry of well H-35 started in May 2011 and continued until mid-July. This time LAPIDOTH was able to drill the cement plugs and reach the target layer, at a depth of 1580 m, by mid June 2011. However, while performing cleaning operations, the drilling head hit the casing and broke it a depth of ~270 m. Here too, the broken casing was moved aside towards the karst. Many attempts were made to redress the deviated part of the casing but without success. Fearing to reach the same situation as for H-18, we decided to abandon the well.

Drilling of the two wells

During the summer of 2011, we explored with LAPIDOTH possible solutions to the situation. In order to save the project, LAPIDOTH agreed to drill two new wells, provided that the consortium would agree on a budget increase of 200,000 Euros. This agreement was reached during the fall of 2011. The drilling of the new well (Heletz-18A) started on January 3rd, 2012 and was completed in May 13th, 2012. The drilling of the monitoring well started on May 29th, 2012 and ended on August 8th, 2012. The Location of the wells is presented in Figure 6-5.

Figure 6-5. Areal view of the site and location of the two wells drilled

In order to allow for more flexibility in the installation of pump in this well (in order to meet space constraints as reported by SOLEXPERTS, at that time the selected provider of the wells instrumentation), we tried to install a larger casing in the upper part: 1) from the ground surface to a depth of 300 m – $7^{5/8}$ inch casing and from 300 m to bottom 7 inch casing. 300 meters of $7^{5/8}$ inch casing were purchased The $7^{5/8}$ inch casing and a cross-over aimed at allowing the diameter transition was purchased by the end of December 2011. However, during the cementation of the lower portion of the well, the lower clearance left between the 95/8 casing and the $7^{5/8}$ casing did not allow for a proper cementation. We had then to remove the $7^{5/8}$ inch casing and install the 7 inch casing from ground surface to well bottom.

Cores and logs

Cores were taken: 1) one core from the caprock; 3) 3 cores from the target layers, both in the injection and monitoring wells. Cores from the caprock were put in an epoxy resin in order to protect them from alterations. A core “party” took place in September 2012. Samples of these cores were sent to the University of Stanford laboratories, for the determination of the capillary pressure and relative permeability curves; to UEDIN for the analysis of the caprock; to CNRS for the execution of flow-through experiments and determination of chemical reactivity; 4) to UU for the determination of the mechanical properties and to UGOE/LIAG for visualization of the structure and for the measurement of the hydraulic properties.

Logs were conducted in the lower part of the borehole, from the depth of 1222 m to the well bottom (1655 m). The following logs were conducted: DLL, CDL, CNL, SONIC and GR, by Metsada. The logs were interpreted by CNRS (Philippe Pezard group). The analysis suggested that out the sandstone K, W and A layers, only W and A should have favorable hydraulic properties. We then decided to perforate on the suggest horizons.

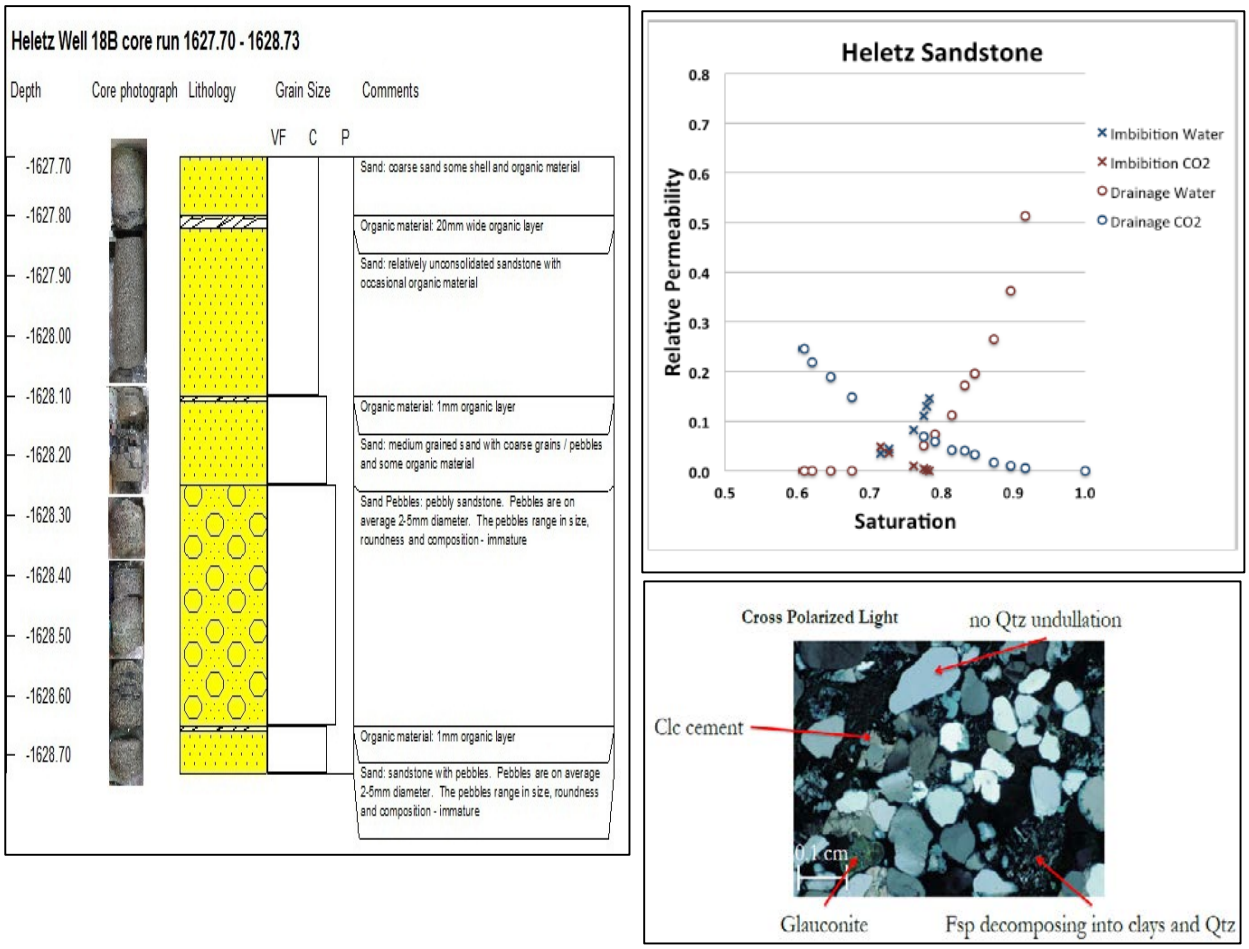

Figure 6-6. Example core sequence and interpretation (Edlmann, 2012) and example laboratory results (relative permeability function and example petrography (Benson et al, 2013)

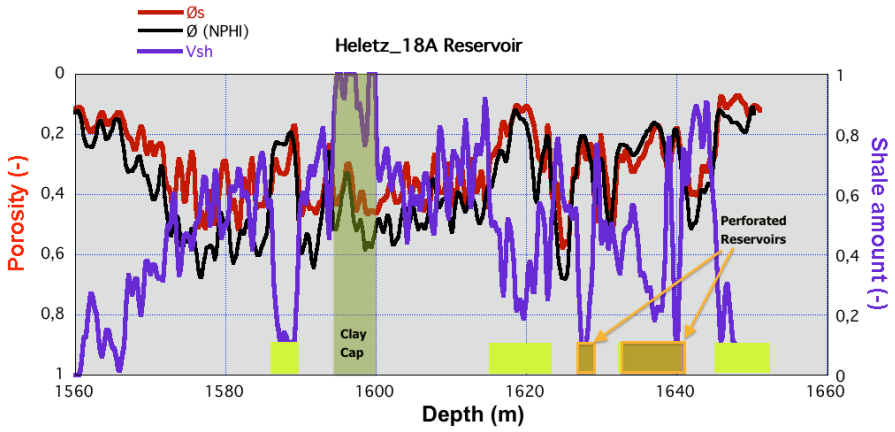

Figure 6-7. Borehole logs for Heletz 18-A indicting the perforated reservoir sections (after Pezard, 2012)

Cementation

In May 2012, the cementation of the lower part of the well 18-A (from the depth of 1222 meters to the well bottom and for the annulus between the 7 inch casing and the $9^{5/8}$ inch casing, was carried out by Lapidoth, under the supervision of UES (Universal Energy Services, a subsidiary of Halliburton) and with the CO_2 resistant CORROSACEM cement (all the consumables were supplied by Halliburton Italy).

A cement bond log (CBL), aimed at checking the quality of the cementation was executed by Metsada. It shows a good quality of the cementation, at least in the open section of the well (from 1655 m to 1222 m). Above this depth, the presence of the second, outer, $9^{5/8}$ casing prevents from having a good picture of the cementation. However, post-cement calculations provided by Halliburton show that the cementation was successful and the cement reach a depth to ~200 m below ground surface. The perforation of the injection well took place in August 2012. The perforating gun comprised 10 shots/foot. According to the findings of the logs analysis we perforated only the W and A horizons as follows:

Table 6-1. Depth of the reservoir layers in the injection well H18A

Layer	Lithology	Top Depth	Bottom Depth
Caprock	Shale	1572	1616
LC11	Dolomite	1616	1621
Heletz Sands	Sandstone-K	1622	1624
	Sandstone-W	1627	1629
	Sandstone-A	1632	1641

The drilling of the monitoring well ended in August 8th 2012. According to the plan the borehole was left open from the depth of ~1200 m to the well bottom. The analysis of the logs unraveled a lithology identical to the one of the injection well, slightly more elevated topographically. The reservoir layer were identified at the following depths:

Table 6-2: Depth of the reservoir layers in the monitoring well H18B

Layer	Lithology	Top Depth	Bottom Depth
Caprock	Shale	1567.0	1610.0
LC11	Dolomite	1610.0	1615.0
Heletz Sands	Sandstone-K	1616.5	1617.5
	Sandstone-W	1621.0	1626.0
	Sandstone-A	1627.0	1635.0

The analysis of the cores had pointed at a poor cementation of the reservoir rock, which disintegrated in presence of brine. This lack of stability did not allow to leave monitoring well as an open borehole. We therefore procured a 7 inch casing and proceeded with its installation and cementation using standard Portland cement. This activity took place in February 2013 (as there was a need to procure the 7 inch casing).

Soon after the cementation we proceeded with the perforation of the well. Here too, only the W and A horizons were perforated, the send density of charges. At this point the drilling of both wells was completed and perforated.

As a post-cementation work, and prior to the perforation of the wells, the casing was washed with freshwater, in order to remove the remnants of the cementation work.

6.1.5 Hydraulic testing and well stimulation

First tests

In parallel to the field activities we worked on at the formulation of comprehensive hydraulic testing suite. The tests included:

1. Slug injection;
2. Pumping test;
3. Flowing Fluid Electrical Conductivity (FFEC) log;
4. Single well tracer test;
5. Two well tracer test.

In May 2013 we started the hydraulic testing sequence. We installed a submersible pump at a depth of ~270 meters. This pump (Grundfos SP5) has a discharge capacity of ~5 tons/hour at that head. To this end we installed a generator for power supply and a control cell for the online measurement of the electric conductivity and the PH. After a few hours, it had to be concluded that the well was clogged.

Injection pressure test at wells H18A and H18B, were conducted during the month of July 2013: a packer was installed at the depth of ~1000 m in the well and attempts were made to inject water at increasing pressures with the aim to determine the pressure needed to achieve water entry. During the test conducted in 2013 even an injection pressure of 2,500 psi (~172 bars). Therefore the wells were heavily clogged.

Well stimulation

During the summer of 2013 we consulted two companies: Fangmann (Germany) and Halliburton for advice concerning the clogging of the wells. Both companies suggested that the clogging was the result of the flushing with freshwater of the wells after the cementation and this could have led to swelling of clay lenses present in the formation, bacteria growth at the perforation, hydroxide precipitation and therefore the clogging. A well stimulation program comprising a large number of stimulating chemicals, the cost of which was beyond our resources (over two hundred thousand euros for the chemicals only).

We finally decided adopt a more affordable approach as follows:

1. Equilibrate the water in the borehole with KCL (salt);
2. Conduct a second perforation of the well;
3. Conduct a series of swab suctions (suction of water from the well).

The operations started in November 2013. About 5 tons of KCL were mixed with fresh water and injected into the H18A and H18B in order to achieve a concentration of ~1,050 Kg/m^3 in the boreholes. Then we perforated well H18A, using a gun of hollow charges (10 charges per foot). A few days after the perforation Lapidoth installed the system aimed at conducting the swab suctions.

The suction operation consists in withdrawing a volume of water from the borehole under a high suction pressure. This has the effect to create a lower pressure at the perforated section and thus stimulates the flow of water from the formation to the borehole. The efficiency of the operation is measured via the recovery rate of the water table in the well. Each suction withdraws a volume of ~0.5 m^3, resulting in a drawdown of 250 meters of the water table in the 7 inch tube installed in the well. The recovery rate is the time taken for the water table to rise to 80% of the original level. As the suctions were conducted we observed a dramatic reduction of the

recovery rate, which was of 40 seconds. Then we conducted a pressure injection test and observed that we were able to inject water at a rate of 30-40 m^3/hour, which clearly indicated that the well stimulation succeeded. Encouraged by the success of the stimulation of well H18A, we decided to skip KCL and perforations steps at well H18A and directly performed swab suctions in H18B. We conducted ~20 suctions and observed an even better recovery rate than for well H18B. Here too, we conducted a pressure injection test and found out that we could inject water at a rate of ~80 m^3/hour.

Second set of hydraulic tests and fluid sampling

After the successful well stimulations, in December 2013, hydraulic tests were conducted again at well H18A. This required once again the installation of the pump at a depth of ~270 meters. The interpretation of these pumping tests indicated that the properties of the formation are far dramatically higher than previously assumed (>700mD horizontal and >100 mD vertical, against the earliest estimations of 100mD and the laboratory values between about 100mD and 400mD). Water samples were taken and send for chemical analysis. The results are highly similar to the water quality data we had from the nearby well H18 (1955). The concentration of suspended solids was very high (~60g/l).

6.1.6 Well completion (EWRE, UU and SIRAB)

A tender was issued by UU for the instrumentation of the injection and monitoring wells. The SOLEXPERTS (SE) company was selected for the instrumentation of the injection and monitoring wells. The contract was signed in the last quarter of 2010. In January 2011, SE submitted the first version of the design of the instrumentation of the injection well. The submitted document was reviewed, during February and March 2011, at our request, by Dr. B Freifeld (LBNL) and Dr. S. Sharma (CO2CRC), members SIRAB, among the most qualified experts in the design of well completion for CO_2 injection related experiments. The reviewers raised a number of concerns in many aspects of the design and these were then forwarded to SE. However due to the failed attempts of re-entry of well H-18, we decided, in agreement with SE, to put on hold their work, until a new well for re-entry is identified and successfully re-entered. Accordingly, SE activity was halted until the summer of 2011, when the decision to drilling two new wells at the location of the former H-18 well was finally consolidated. SE work resumed then in the early fall of 2011. The second version of the completion design was submitted in January 2012 and reviewed by the same team. In this second round, the reviewers expressed a number of concerns too, partly related to the safety of the system, partly related to guaranteeing the well-functioning, and partly to the durability (which related to the materials to be used and thus to the budget). The MUSTANG team in charge of the experiment decided consequently to formulate a number of requests to be met by SE and to prepare an update of the design and also to submit the updated document for review by Halliburton experts. The update design was received from SE in April 2012 and reviewed by Halliburton in two phases (May 2012 and June 2012). Halliburton review expressed a number of concerns, which were also raised by the reviewers from the SIRAB.

Based on the expert reviews and exchange of information with CO2CRC team who had been working on similar experiment, it was concluded that there was a need to update part of the components of the well completion, namely:

1. Duplicating the downhole pressure and temperature sensors;
2. Installing an additional pressure and temperature sensors midway in the injection tube, in order to detect the eventuality of phase change;
3. Using more resilient materials for the tube in which water and CO_2 could be in contact (injection and pumping tubes);
4. Making sure that the selected pressure and temperature sensors are suitable to the field conditions (depth, pressure, temperature and salinity)

5. Making sure that the suggested sealing packer would perform according to the design;
6. Taking care of the temperature and pressure conditions at the well head during pumping;
7. Making sure that the materials used for the communication lines are suited to the thermodynamic conditions that will prevail in the borehole.
8. Using alloys for the injection and pumping tube that resistant to combined action of water and CO_2.

SOLEXPERTS was not able to match these requirements with reasonable budget changes, or alternatively to prove that they were not needed and that the proposed design was capable of meeting the project objectives and satisfy the safety constraints. In view of this situation, the contract with SOLEXPERTS was cancelled in early 2013.

We then approached SageRider/Class VI solutions companies as a replacement. These companies provided completion designs that met the experiment needs, while satisfying strict safety constraints. The layout of the wells is shown in Figure 6-8.

The instrumentation of the injection well H18A was completed in early February 2014. The process was smooth and all the installed technologies worked properly. The instrumentation of the monitoring well took place early in May 2014. In this case communication with the pressure and temperature sensors and one of the two sampling system did not work and were lost for all practical purposes. While the loss one sampling system was a relatively minor drawback (as one system works) the loss of the pressure and temperature sensors presented a major problem. SageRider suggested to install an alternative pressure and temperature sensor through the inner $2^{7/8}$ inch tubing. The process was completed in June 2014. The installed P/T sensor worked and provided data.

Pictures 6-9 show the instrumentation of the injection well, Figure 6-10 the U-tube sampling system in operation.

6.1.7 Injection permit (EWRE and Lapidoth) and storage permit (EWRE)

Israel Water Authority (IWA) is the permitting authority regarding the injection permit. The Oil and Mines authority expressed its support (letter of Dr. Jacob Mimran, then head of this institution) and IWA had expressed interest in the experiment. In February 2013, we presented the project to the IWA personnel. The purpose was to help the IWA determine the modalities and legal framework for submitting the permit of injection. It was decided to submit the permit of injection to the Injection Committee of IWA (which usually deals with water injection in wells). A formal permit of injection was awarded in the spring of 2014.

There was need to obtain a permit for the onsite storage of CO_2 and tracers from the Ministry for the protection of the environment (MPE). The MPE policy is to regard all chemicals as hazardous and delivers permits for their storage / utilization. A formal request was submitted to the MPE and a formal permit was obtained in June 2014.

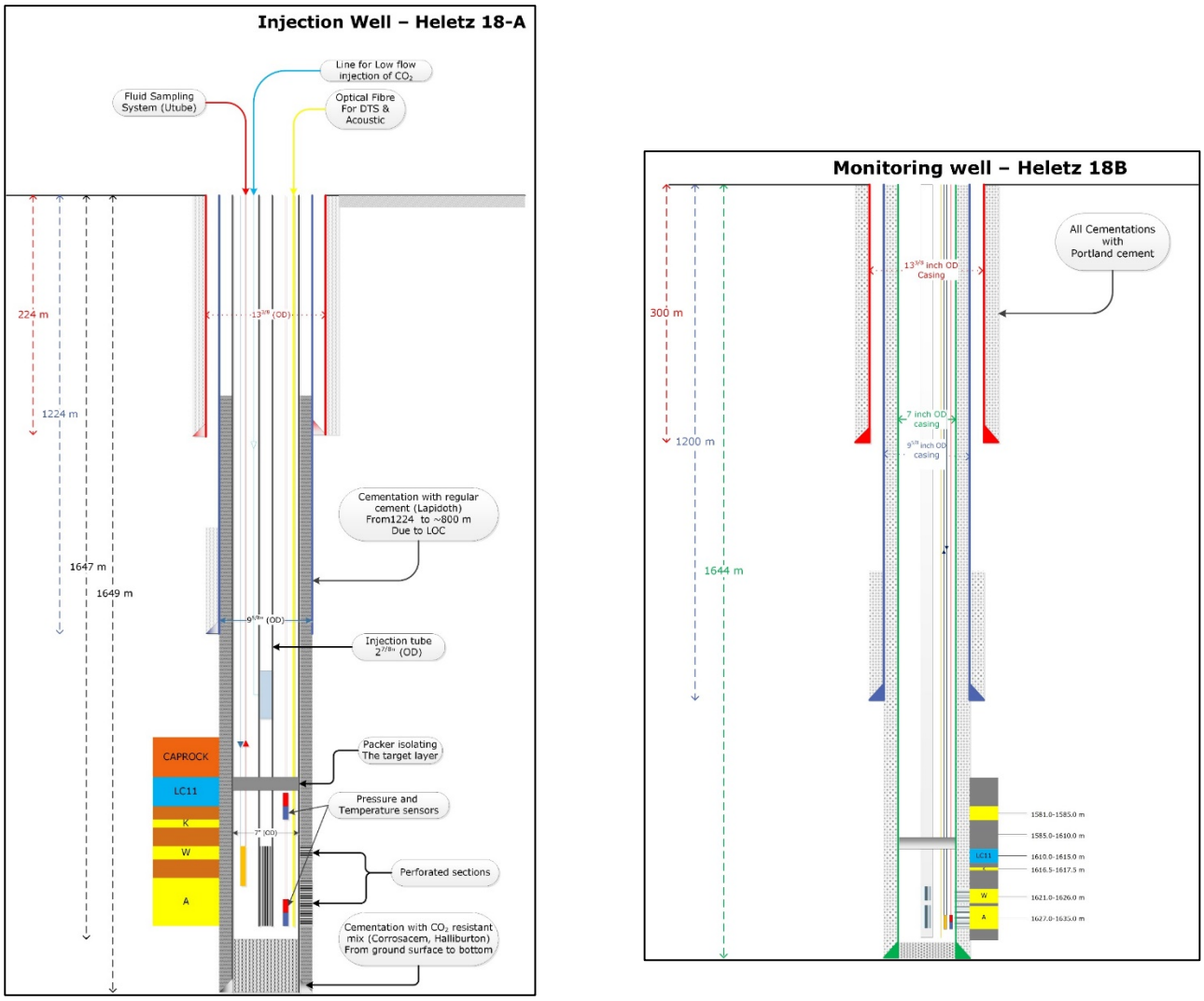

Figure 6-8: Layout of the injection well H18A and monitoring well H18B (implemented by Class VI Solutions and SageRider).

Figure 6-9: Injection well well-head (upper left), U-Tube sampling in progress (upper right), 'above-the-ground' facilities for the U-tube sampling (middle) and instrumentation of the injection well underway (lowest panel)

6.1.8 Design of the facilities on the ground, injection module (EWRE, UU and KIT)

The original CO_2 injection system was planned to be a very limited and suited to the original set of CO_2 injection experiments suggested in the DOW. However, the evolution of the planned CO_2 injection experiments, which are far more sophisticated, and the fact that we were awarded the TRUST project implied a re-thinking and design of the CO_2 injection system (mainly with funds from the TRUST budget).

The first step was to visit sites where CO_2 injection occurs such as the Ketzin and the Otway sites. Although these projects were far larger in scope and in budget than MUSTANG, we were able to understand the basic engineering needs and determine a suitable scale and configuration of the CO_2 injection system needed at Heletz, and subsequently terms of reference for the system. The main identified components of the injection system included:

1. CO_2 supply lines: one for the injection of CO_2 as a single phase, with a discharge of up to 4 tons/hour under a pressure of 90 bar and 35 degrees Celsius, high-flow system, and one for the injection of CO_2 for the dissolving it into water, smaller discharge pump, low-flow system.
2. Possibility to mix tracers in the CO_2.
3. Possibility to add impurities.
4. Interfacing with other systems at the wellhead of the injection well.
5. A heat exchanger for increasing the CO_2 temperature, as we were informed by the CO_2 suppliers that the CO_2 would be supplied low pressure cold (in contradiction to the initial information we received about a high pressure and hot CO_2).
6. Water supply line.
7. The abstraction line (of water and or a mixture of water and CO_2).
8. CO_2 storage tank (s).
9. Water supply tank (s).
10. Tank for the collection of the fluid to abstracted (also for degasing).
11. Easy and semi-automated operation.
12. High safety.
13. Online reporting.

KIT identified NATEX of Austria, with proven experience in high pressure CO_2, mainly for the food industry. They prepared a preliminary design (presented in the special deliverable prepared by KIT in the frame of this WP). Linde of Germany suggested a design similar to the one implemented in Ketzin. After two visits to Otway (the last one in early May 2011) we reached the conclusion that the design implemented at Otway was the most cost-effective and suitable to the experiment conditions at Heletz. Accordingly, we approached the TRIMERIC Company of Budda, Texas, USA. This company designed the Otway CO_2 injection system and had a rich experience and know-how in the design and manufacturing of the CO_2 injection systems (over 6). Additionally, the cost (which was higher than the original price quotation) was substantially lower than the prices suggested by NATEX (written proposal) and Linde (Oral communication). The discrepancy between the original price estimation of TRIMERIC and the final cost is due to the fact there is a very high degree of activity in the USA, due to the intensive shale gas exploration and production and enhanced oil recovery, all using similar technologies and components.

The fine design of the system, including the preparation of HAZOP (Hazard operation manual) and an operation manual was prepared by TRIMERIC. The constraints and conditions were discussed during two meetings held in Budda (in May 2013 and in September 2013).

From the CO_2 storage tank the module comprises a booster pump (to increase pressure and thus keep the CO_2 in liquid state), a low-flow pump (up to 0.5 ton/hour flow-rate) and a high-flow pump (up to 4 tons/hour flow-rate). The CO_2 is then flowed to the heat exchanger for increasing the temperature. The module include a relatively large number of online pressure and temperature sensors, pressure regulators, check valves, valves and shutoff valves in order to enable an adequate control of the pressure and temperature conditions of the CO_2. Near the wellhead end an online Coriolis flow-meter for the CO_2 is installed. A bypass is installed in the heat exchanger, in case we plan to inject cold CO_2. At the wellhead the module connects to a spooling unit, which enables to inject CO_2, water, mix tracers in the water and in the CO_2 and impurities. Pictures of the injection module (injector) are presented in Figure 6-10.

Additional facilities include a system for fluid abstraction via air-lift, comprising a powerful air-compressor, high pressure tubing from the compressor and the two wells, a pressure regulator, a check valve, pressure relief valves and valves. The abstracted fluid is then transferred to an operational tank, having a storage volume of 15 m^3, used for solid particles deposition and degasing (in case of CO_2 presence).

Power supply is ensured via a 165-KVA (130 KW) diesel generator. Power is consumed by the injection module, the CO_2 tanks (their cooling system), the CO_2 supply trucks, the lightning system, the air and nitrogen compressors, the heating system and the control room.

The control room comprises the sampling system panel (to which converges the TiT systems from the injection and monitoring wells), the DTS systems of both wells, Pressure and temperature readings, the heating system and the monitoring of the injection module.

6.1.9 Conditioning of the CO_2 at the well head (IIT, UU, EWRE)

Work on the conditioning of the CO_2 at the well head and the coupling to the behaviour of the target layer was further investigated, using a combination of the TOUGH/ECO2N code for the target layer and of a semi-analytical, steady state, model of the flow in the injection tube (based on the paper of Lu and Connel) and an transient implementation of the flow in the injection tube from the TOUGH/T2Well code (LBNL).

6.1.10 Overview of project parameters

Table 6-3 summarizes the project parameters for the Heletz injection as of today, according to the template used by IEAGHG (2013) to summarize small-scale injections. The injection was supposed to take place summer 2014 and thereby be included into this report, but due to the force major conditions (war) in the area this summer we were not carry out the work or even enter the site. The work has now resumed and the experiments will be carried out in autumn 2014. Relevant MUSTANG reports will be updated accordingly as data comes available.

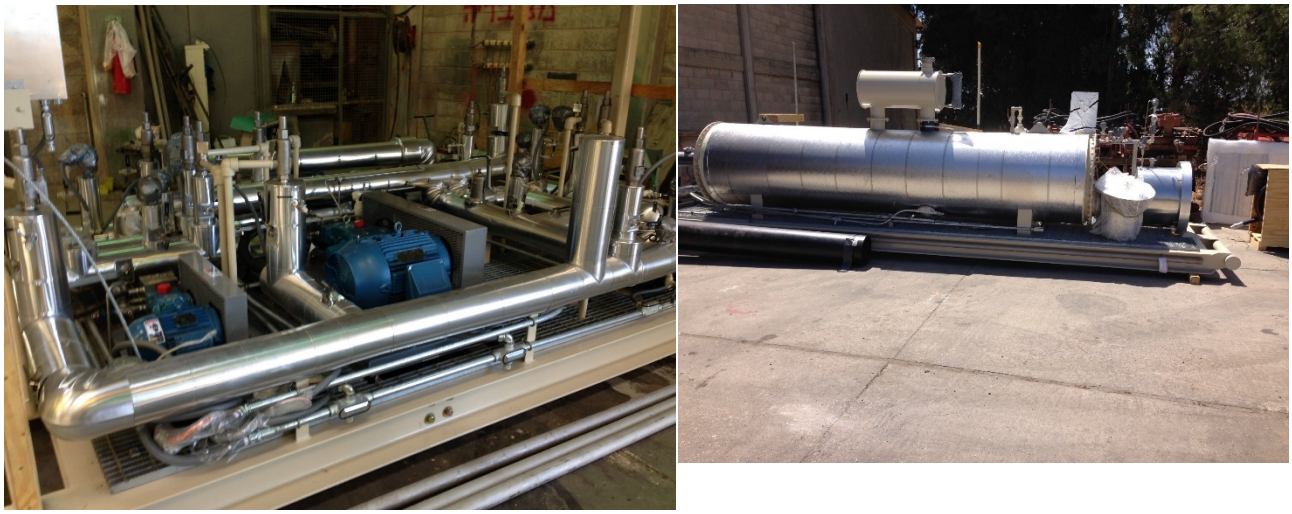

Figure 6-10. The injection module and heat exchanger

Table 6-3 Project summary Heletz site

Project Summary		**Project Parameters**	
Project name	MUSTANG	Planned Injection Volume	up to 4000 tons
Project Organization		Total Volume Injected	
Location	Heletz (Israel)		
Project Type	Scientifically driven	Reservoir porosity	20-25%
Project Scale	small	Reservoir permeability	500-750 md
Type and depth of reseroir	Sandstone, 1630 m		
Type of Seal	marl and shale ~ 50 m	**Monitoring**	
Year of First Injection	2014	Seismic Monitoring	YES
Current Status	final preparations	Gravity Studies	NO
		Water Monitoring	YES
Project Details		Pressure logging	YES
Project Operator	EWRE	Soil Monitoring	YES
Project Contact	Jacob Bensabat	Thermal logging	YES
Project contact phone and email	+972-4-8383919 - jbensabat@ewre.com	Atmospheric Monitoring	NO
Project Location	Heletz - Israel	Wireline logging	NO
Injection site coordinates	ITM - (166900,612925)	Ecological Monitoring	NO
CO2 Source	Food grade CO2	Obserwation well	YES
CO transport/Delivery	Trucks	Tracer Analysis	YES
Project Planning start	Q4 of 2014	Geochemical research/fluis sampling	YES
Duration of Injection	3 years	Electromagnetic	NO
Injection rate	up to 3.5 tons/hour	inSAR	NO
Injection Pressure	up to 90 bar at wellhead - 158 bar at well bottom		
Planned Injection Volume	up to 4000 tons	**Reservoir Studies**	
Total Volume Injected		Reservoir Studies	YES (Modeling)
		Geologic Model	YES
Reservoir porosity	20-25%	Coring	YES
Reservoir permeability	500-750 md	Seismic	YES
		Other Technologies	Hydraulic testing, FFEC, thermal recovery

6.1 Maguelone

The Maguelone site is operated by partner CNRS.

6.1.1 Overview of the CO2 and N2 injection experiments (CNRS)

Prior to **CO_2 injection** in 2013, a series of **N_2 injection** experiments were undertaken at Maguelone in 2012, in order to evaluate the site response to gas injection. N_2 was chosen because of the reducing nature of the in-situ environment, precluding O_2 injection to avoid massive bacterial developments. For three nitrogen injection experiments in March, June and November of 2012, the gas plume was successfully detected by all monitoring techniques (pressure, electrical resistivity, sonic logging and seismic monitoring). The response to gas propagation was immediate. During nitrogen injection, noises coming from gas bubbles were also heard in several holes, leading to a re-inforcement of the down-hole experimental set-up from cement injections around each of the injection/monitoring holes.

During **CO_2 injection** at 13 to 16 m depth, a similar surface and down-hole hydrogeophysical monitoring set-up was deployed. A volume of 111 m^3 of CO_2 was injected during 3.5 hours. The gas plume is successfully detected by all monitoring techniques, and the response to gas propagation was also immediate. Pressure recorded at 7.9 m depth was the most directly impacted by CO_2 injection. After a short period of resistivity increase due to the presence of free gas, electrical resistivity monitoring and down-hole induction logging show a comparable reduction in resistivity, possibly due to the CO_2 dissolving in pore fluid water. The seismic monitoring appears to be also very sensitive to gas storage, with clear and gradual changes as soon as the injection begins. For sonic logging, changes in amplitude were obtained over the injection time, while Vp was measured to change very little. Before, during and after CO_2 injection experiment, pore fluid samples were taken in order to follow changes in water chemistry during the experiment. A decrease in pH on the order of one pH unit was measured at the depth of 7.9 m from the beginning of the CO_2 injection, also pointing at CO_2 dissolving in pore fluid.

In summary, as for N_2 injection experiments, the CO_2 storage happened mostly in thin sand beds located close to the surface (~7-8 m) under the Late-Holocene lagoonal sediments (mostly impermeable dark green clays) forming an impermeable seal overlying homogeneous fine-grained Pliocene continental deposits. Signs of the CO_2 plume were successfully obtained and characterized by a full suite of coordinated monitoring techniques, either from surface or downhole. All methods appear to be extremely sensitive to the presence of CO_2 in the shallow subsurface. In summary, the shallow injection at Maguelone shows that a coordinated set of observatories can provide valuable information to monitor in-situ CO_2 geological storage and to detect near-surface migration pathways indicative of CO_2 transport.

6.2.2 The Maguelone experimental site

Hydrogeological and petrophysical context

An experimental setup for shallow subsurface hydrogeophysical monitoring has been installed at the Maguelone site, located along the Mediterranean lido of the Gulf of Lions near Montpellier, France. The experimental site was developed in the context of MUSTANG and has been presented in the previous periodic reports. The field spread includes an injection hole, a logging hole (TLL), a downhole hydrodynamic observatory based on a pore fluid sampling completion from WestBay (SWS), two permanent downhole electrical resistivity observatories (imaGeau), a downhole

seismic observatory, plus surface seismic and electrical resistivity observatories. This coordinated set of observatories should lead to the design of integrated sensors and methods for the monitoring of gas injection in deeper reservoirs (*Pezard et al., 2012*). The site is limited to the north by the Prevost coastal lagoon and to the south by the sea, this site offers a natural laboratory to study porous coastal reservoirs in a clastic and clay-rich context saturated with saline fluids. Continuous geological samples and geophysical data from shallow boreholes at Maguelone have leaded to identify two depositional sequences:

- Near the ground surface (0-9 m), a thin Late-Holocene sequence (< 5000 yrs B.P.) is constituted with lagoon sediments with impermeable dark green clays topped by grey shelly beach sands. This sequence forms an impermeable seal overlying the Pliocene sequence with an unconformity.
- Pliocene sequence, from ~ 9 m to the base of MAG1-DSO (60 m). This sequence consists mainly in relatively homogeneous fine grained continental deposits (clays and silts). Locally, some marine An experimental setup for shallow subsurface hydrogeophysical monitoring has been installed at the Maguelone site, located along the Mediterranean lido of the Gulf of Lions near Montpellier, France.

In the Pliocene sequence, a single remarkable depositional unit is located from about 13 to 16 m depth and consists in a porous and permeable conglomerates and sands interpreted as fluvial deposits. The conglomerates, clearly identified downhole from low natural gamma radioactivity values, are correlated laterally with boreholes located at a km distance, showing the lateral extension of this unit. Sedimentary facies, geophysical measurements and hydrological testing indicate a high permeability ($K = 4.10^{-3}$ m/s), salinity (34 g/l) and porosity for these conglomerates, also bounded above and below by clay-rich horizons. Hydrogen sulphite (H_2S) encountered in a repetitive fashion during coring and drilling operations near 15 m depth confirms the presence of a small reservoir at this depth. The possibility of the conglomerate forming a 3 m-thick gas-rich reservoir may consequently be envisaged, this anomaly resulting from lagoonal organic matter decomposition. From a hydrological point of view, the electrical resistivity (opposite to electrical conductivity) data show that the sedimentary column is saturated with seawater to brackish water from surface down to 32 m.

Shallow gas injection monitoring experiments

The field spread (Figure WP 06-12) for gas injection includes an injection hole GIH, a time-lapse logging hole TLL, two downhole electrical observatories imaGeau (DEO), a downhole hydrodynamic observatory based on a multipacker completion from WestBay (SWS) DHO, a downhole seismic observatory DSO, plus surface seismic (SSO) and electrical resistivity observatory (SEO).

Prior to gas injection, a whole set of pre-injection experiments have been conducted in order to prepare, test, and calibrate the Maguelone site for later experiments. The initial physical properties of the study site have been successfully characterized using downhole geophysical measurements (gamma ray, electrical and acoustical logging), followed by surface (electrical and seismic tomography) and surface-to–borehole (seismic) surveys. N_2 injection experiments were undertaken in order to measure the site response to gas injection. N_2 was chosen because of the reducing nature of the in-situ environment present in the shallow subsurface at Maguelone, precluding O_2 injection to avoid bacterial developments. Three N_2 injection experiments were made at the Maguelone study site in March, June and November 2012 from the injection hole GIH (Figure WP 06-12) at a depth of 13-16m (fluvial conglomerates and sands).

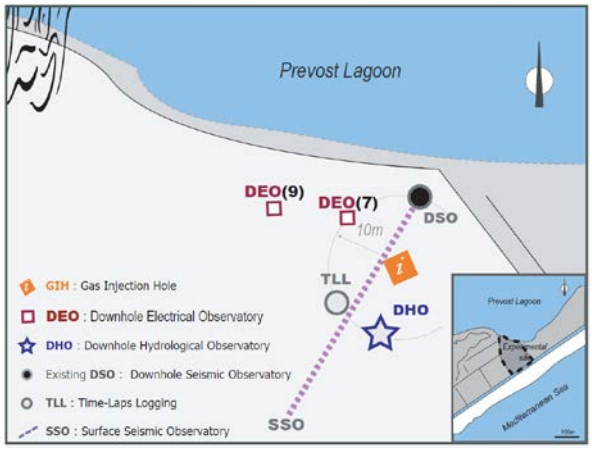

Figure 6-12. Field spread at the Maguelone experimental site for the SIMEx integrated monitoring experiments in 2012 (nitrogen injection) and 2013 (CO2 injection).

The shallow CO_2 injection experiment took place on January 21-25, 2013. The experiment consisted in a single CO_2 injection on January 22. A total volume of 111m^3 of CO_2 was injected during 3.5 hours at 2 bars. Due to rain overnight and in the morning on January 23, a second CO_2 injection experiment was abandoned in order to give priority to the post-injection monitoring during 3 days.

6.2.3 Pressure monitoring and fluid sampling from WestBay system

WestBay hydrochemical monitoring completion

The downhole hydrodynamic observatory (DHO, **Figure 6-7**) is a multilevel ground water device based on a multi-packer completion from WestBay (SWS), including packers in order to provide fluid samples, temperature and pressure records during injection and thereby time/space calibration points from tracers (i.e. precise boundary conditions) to numerical modelers. At the Maguelone site eight zones are equipped for fluid sampling and monitoring down to a depth of 49 m. For experimental purpose as part of SIMEx, two of these zones were located within the reservoir (at 13.9 and 15.5 m), one was located above (at 7.9 m) and a fourth one below (24.9 m) the reservoir.

Gas injection experiments

The shallow CO_2 injection experiment took place on January 21-25, 2013. Pressure profiles were acquired before, during and after the injections with 30 minutes – 1 hour time slots during injection . Only three zones within reservoir (7.9 m, 13.9 m and 15.5 m) were affected by injection. **Figure WP 06-8a** provides the results of pressure monitoring for the 3 levels, the upper level being the most affected by gas injection as for previous N2 injection in 2012. The pressure values increase during two injection periods, and decrease between and after injections. Pressure recorded at the depth of 13.9 m and 15.5 m shows slight increase during injection. For the 3 N_2 injection experiments, the pressure returned to the initial background after the end of the experiment. It also appears that the gas was stored mostly close to the surface (~ 7-8 m), under the Late-Holocene lagoonal sediments.

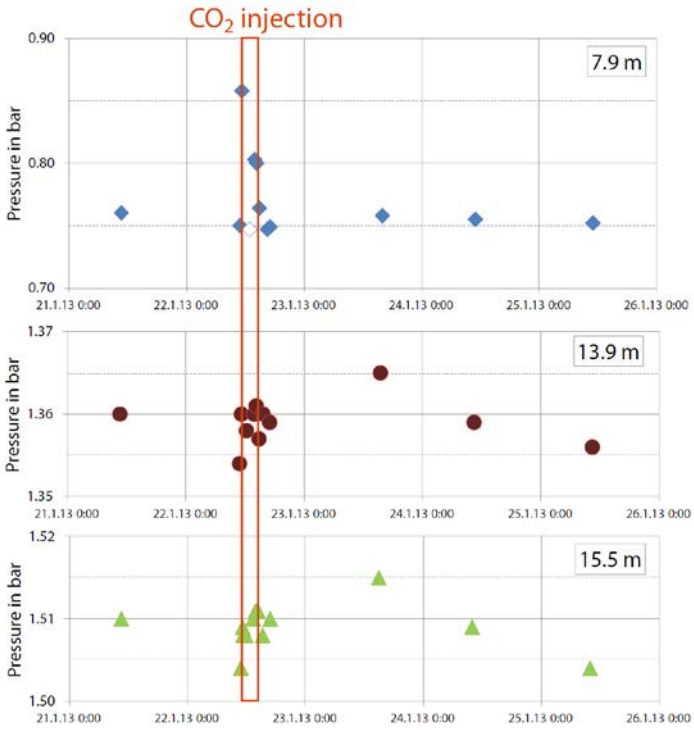

Figure 6-13a. CO_2 injection experiment (January 2013). Pressure monitoring in MAG5 from the WestBay completion at 7.9 m, 13.9 m and 15.5 m depths.

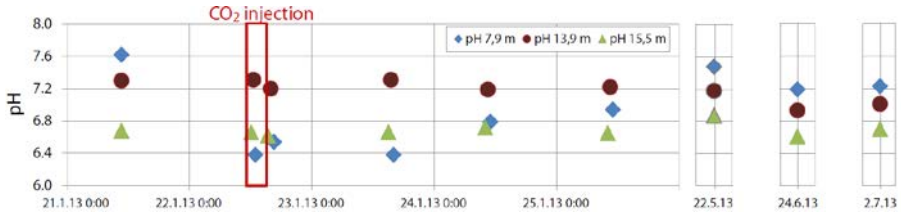

Figure 6-13b. pH monitoring in MAG5 at 7.9 m, 13.9 m and 15.5 m depth. Left: CO_2 injection experiment (January 2013). Right: pH monitoring in the following months (May to July, 2013).

Before, during and after CO_2 injection experiment pore fluid samples were taken at the depth of 7.9 m, 13.9 m and 15.5 m in order to follow the changes in water chemistry during experiment. A decrease in pH closer to 1 pH units (**Figure WP 06-8b**) was measured at the depth of 7.9 m just after the beginning of the CO_2 injection. This decrease in pH seems to confirm the hypothesis of CO_2 dissolution. The analysis of pore fluid will permit to validate the CO_2 dissolving during injection.

6.2.4 Downhole time-lapse monitoring

Induction logging

Repeated logging measurements (induction) were performed in the TLL (time-lapse logging) borehole (PVC cased and 20 m deep) before injections (for référence and calibration), during and after gas injection experiments in 2012 and 2013 with the EM51 induction resistivity probe from Geovista. The data acquisition was performed up and down with a 5 cm spacing. Only the up logs are used in the analyses, with thirty minutes time slots on the day of injection

(22/01/2013), one measurement per day on January 23 and 25 and three measurements per day on January 24 for post-injection monitoring (**Figure 6-14**). On January 21, before the start of CO_2 injection, a baseline measurement was recorded.

In summary :

- as for nitrogen injection experiment, the gas appears to accumulate under the Late-Holocene lagoonal sediments (mostly impermeable dark green clays) acting as an impermeable seal overlying homogeneous fine-grained Pliocene continental deposits,
- an increase in resistivity is observed at this depth just after the beginning of injection, inferring the presence of free gas at this stage of the experiment. After the end of the CO_2 injection, resistivity starts to decrease and reaches a minimum on the last day of monitoring (25/01/2013). The gradual resistivity decrease is associated with progressive CO_2 dissolution within the pore fluid,
- a slight resistivity decrease was measured later on January 23-25 at about 6-7 m depth suggesting progressive upward migration of the injected CO_2.

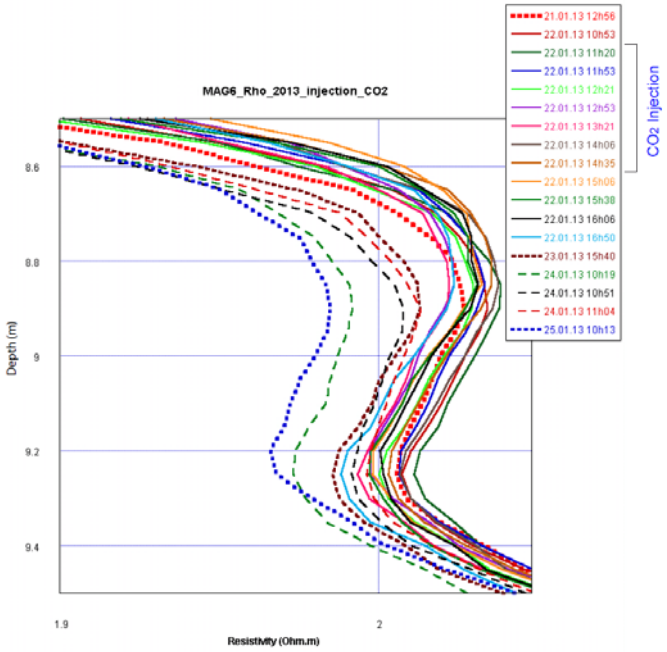

Figure 6-14. Time-lapse monitoring in MAG6 from induction logging before, during and after CO_2 injection (January 2013 at ~ 8-9 m depth).

ImaGeau observatories

The subsurface observatories (DEO7 & DEO9, **Figure 6-12***)* were built from down-hole electrodes located along the external surface of a PVC pipe. The electrodes are made of gold plated copper to reduce the corrosion process. The technical specificities for the DEO9 (MAG9) apparatus are: 17.80 m depth capacity, 0,35 m electrode spacing. The technical specificities for the DEO7 (MAG7) apparatus are: 18.15 m depth capacity, 0,70 m electrode spacing from surface to 13.0 m depth, 0.10 m electrode spacing from 13.0 m to 16.4 m depth and 0.70 m depth from 16.4 m to 18.15 m depth. The observatories work in an automatic mode with electrical resistivity profiles acquired once a day. During and between the injection of the N_2 and CO_2, profiles were acquired every hour. Before and after injection (pre- and post-injection monitoring), profiles were acquired every two/three hours. In this report, the results of resistivity monitoring from DEO9 are presented. The high frequency acquisition during injections allowed to follow in 2D (z,t) the resistivity changes over time due to the nearby gas injection (**Figure WP 06-15**). The results are presented in terms of the resistivity difference relative to the baseline measurement before injection.

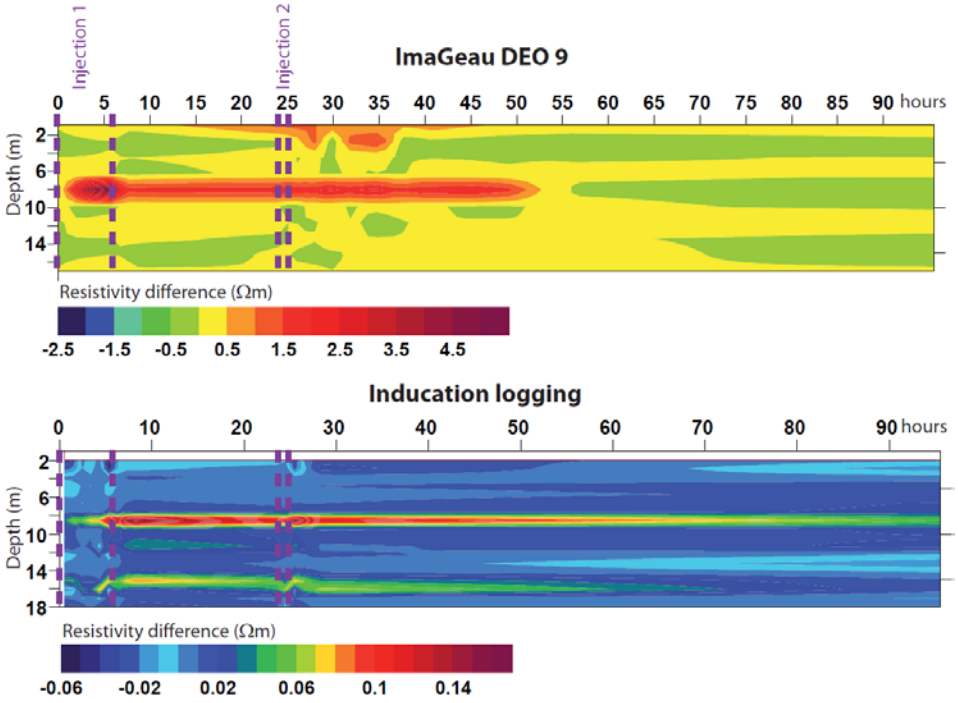

Figure 6-15. Time-lapse single hole electrical monitoring (June 2012). Differences overtime in electrical resistivity relative to the baseline measurements. Above: imaGeau observatory DEO9. Below: time-lapse induction logging in MAG6.

Resistivity differences relative to the baseline were measured in the DEO9 and TLL holes after the beginning of N_2 injection in June, 2012. An increase in resistivity is measured at ~ 8m depth just after the start of injection in both holes. This increase due to N_2 propagation is observed to continue at this depth during first and second injection periods, as well during 25 hours after the end of 2nd injection for the DE0 observatory and ~70 hours for the TLL hole. The increase in resistivity due to the gas injection is more significant for the imaGeau observatory then for the TLL hole. A second very slight increase in resistivity is obtained at ~15 m depth at TLL hole, starting later than the first one, after about 4 hours of injection (*Pezard et al., 2012*).

Sonic logging

Repeated downhole sonic measurements were also performed occasionally (1 to 3 times per day) in the TLL and DSO holes before, during and after N_2 and CO_2 injection (June and November 2012, & January 2013). The data were obtained with a 20kHz Full Waveform Sonic probe (from Mount Sopris) every 5 cm while logging up. Little changes over injection time in sonic signal amplitude and Vp were obtained from first arrival picking during the CO_2 injection, with changes in amplitude.

6.2.5 Seismic time-lapse monitoring from surface

CO_2 injection experiment

The seismic time-lapse monitoring was made before (for calibration and baseline), during and after injection (January 21-25, 2013). The seismic acquisition set-up and timing was :

- 4 downhole components "28 Hz" geophones, including a vertical component and two perpendicular horizontal components installed at 4, 8, 12 and 16 m in the DSO.
- a surface seismic antenna composed of 29 "50 Hz" vertical geophones, spaced every meter, along a line spanning from DSO to TLL (NE/SW), starting 14 m from DSO

- a surface geophone located 3 m from DSO for reference and synchronization (cross-correlation),
- the source (hammer blow) kept at a fixed position along the same line, 2 m from the well head,
- sequences of 5 successive shots were acquired with 15 minutes time-lapse. A total of 245 shots were recorded during the 5 days experiment in January 2013.

Gradual changes in waveforms are obtained through the injection experiment (**Figure 6-16**).

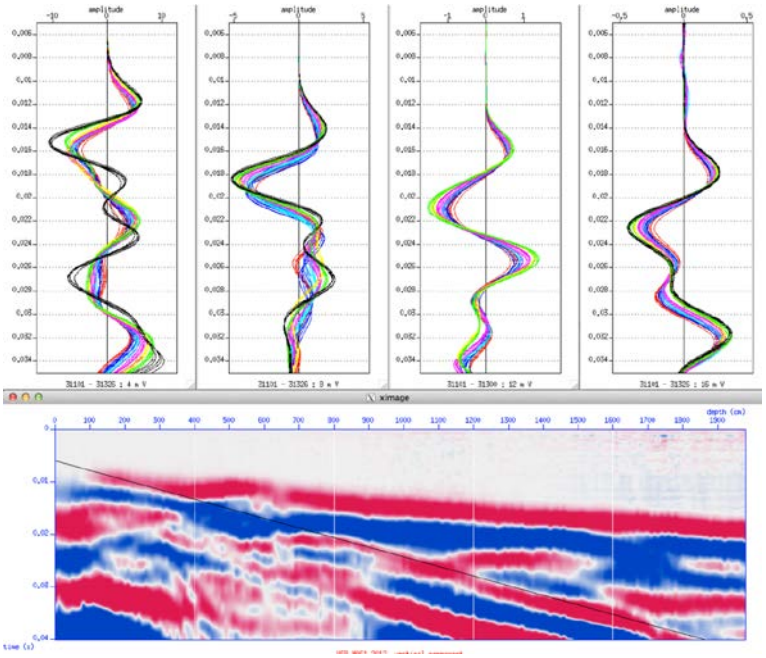

Figure 6-16. Downhole measurements. Seismic time-lapse monitoring (January 2013). Above: Records obtained at 4, 8, 12 and 16 m depth with downhole geophones (vertical component). Seismic traces recorded before (red), during (blue) and after injection (magenta, yellow, green, black). Changes in waveforms are gradual through the injection experiment. Below: Vertical seismic profiling (baseline) recorded before CO_2 injection. Black line: tube wave arrival. White lines: depth of downhole geophones.

6.2.6 Electrical resistivity tomography (ERT) monitoring from surface

Repeated electrical resistivity tomography (ERT) profiles were performed before injections (calibration), during and after N_2 and CO_2 injection experiments. During the first N_2 injection (March 2012), two perpendicular profiles were recorded with a Wenner-Schlumberger array. During the folowing N_2 injections (June & November 2012) and the CO_2 injection (January 2013), the surface electrical resistivity monitoring was performed with one 235 m-long profile using Wenner-Schlumberger and Dipole-Dipole arrays. For the ERT monitoring, the acquisition was performed with 1 to 2 hours time-lapse. The data were inverted using the Res2Dinv software.

Figure 6-17 shows resistivity difference relative to this baseline measurement from data inversion. A slight increase in resistivity that could be related to the gas propagation is obtained after the end of the first injection (at about 8 m depth on Figure 38, 07.06.12 12:00). After the

end of the second injection on the next day (08.06.12 11:12&15:25 on Figure 16), the zone affected by the gas injection increase in width and became more resistive.

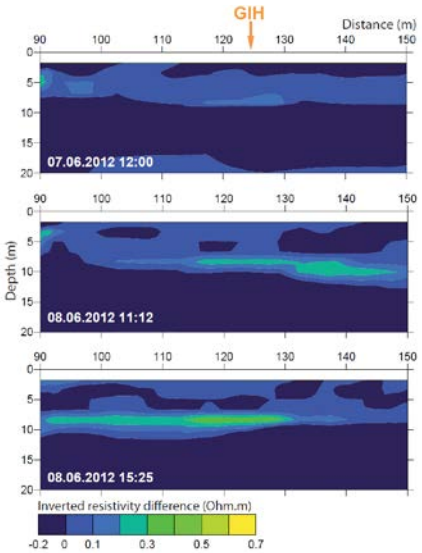

Figure 6-17. ERT monitoring during N_2 injection (June 2012). Inverted resistivity difference related to the baseline (07.06.2012 09:00). Wenner-Schlumberger array.

6.2.7 Preliminary modeling of the experiment (UU)

To analyse the experimental results, we use TOUGH2/EOS7CA model to simulate the injection-monitoring experiments carried out at Maguelone, France, during 2012 and 2013. The aim is to improve our understanding of gas transport in the shallow subsurface as well as to develop and validate the model to monitor it. So far the modelling results are preliminary in character **(Figure 6-18)** and the agreement between the model and the first data set is not yet sufficient, the main hypothesis being that the leakage through one of the wells is not yet sufficiently accounted for. Some leakage has been sealed in the later experiments and work is presently going on to further process the data from these experiments as well as to incorporate that into the numerical simulations [Basirat at al, 2013].

6.2.8 Concluding remarks

It can be concluded that all hydrogeophysical monitoring methods deployed at Maguelone, either from surface or downhole at shallow depth have proven to be effective in the detection of gas after injection. For purely geophysical approaches, while seismic and acoustic methods appear to be sensitive to the presence of free gas but not to slight changes in the ionic charge of the pore fluid, electrical methods are observed to be sensitive to both. These two unknowns might consequently be inverted from a joint analysis of electrical and seismic methods, providing that coupled measurements can be performed at similar scales. This inversion might also be greatly improved from the continuous monitoring of fluid parameters such as pressure, temperature, electrical conductive or pH, for example.

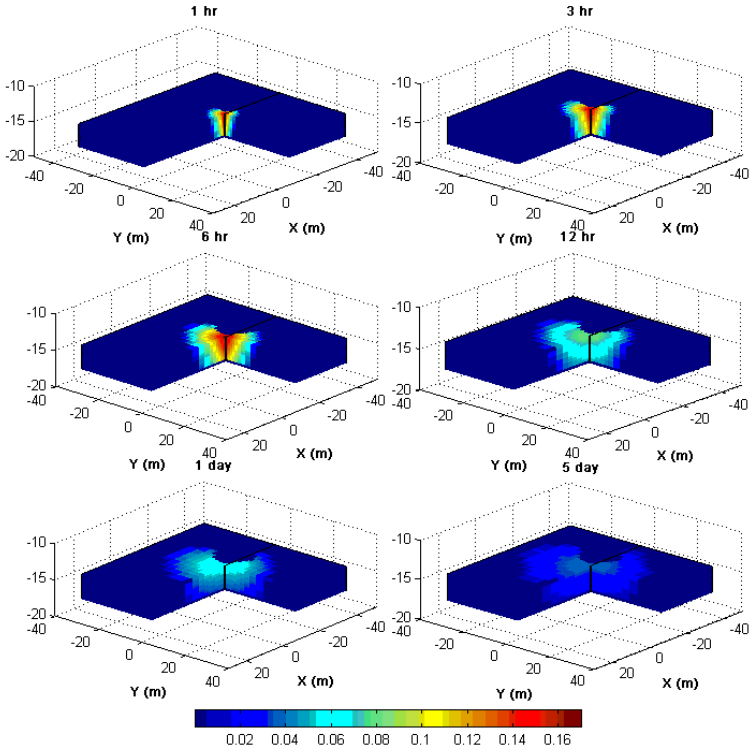

Figure 6-18. N_2 plume evolution model during gas injection (0 to 6 hr) and after the injection period (until 5 days)

7 WP 07 - Modeling

7.1 Introduction

The overall objective of MUSTANG modelling and model development work has been provide a comprehensive modelling approach and associated numerical tools for the simulation of flow, transport, reactive transport, thermal and chemical processes occurring to the fluids and to the rock matrix during the injection and storage of CO2, with special emphasis on the coupled effects, multiple scales and uncertainties due to heterogeneity.

More specifically, the main objectives, according to the original work plan have been to: (i) Adopt the best available THMC models for the simulation of the CO2 flow and transport processes in deep saline formations and update them as needed according to the findings of the project; (ii) Apply these models to the validation experiment in Heletz and to the other MUSTANG test sites and (iii) Update existing codes by incorporating innovative numerical schemes (e.g. meshless approaches) able to quantify the impacts on seal integrity resulting from the injection of CO2.

The main reservoir modelling tools have been CSIC-UPC CODEBRIGHT-RETRASO model that has during the course of the project been updated for CO2 storage specific scenarios, including treatment of THMC processes. The other main tool has been the LBNL TOUGH2/ECO2N code that was already suited to CO2 storage simulations at the onset of the project and its different modules have been extensively applied in the project and combined with other approaches. In addition to these main reservoir simulation tools, several new numerical and analytical models have been developed and applied for various case studies and site specific analyses. This Deliverable summarizes the main model development and modeling work of the project. It is not intended to give any details of the work but work more as a road-map to the relevant reports and publications.

7.2 Development of Field Scale Numerical Simulators

The overall objective of MUSTANG modelling work has been to develop and apply approaches and associated numerical tools for the simulation of flow, transport, reactive transport, thermal and chemical processes occurring to the fluids and to the rock matrix during the injection and storage of CO2. Special emphasis has been on (i) on coupled THMC (Thermo-Hydro-Mechanical-Chemical) effects (ii) multiple scales and (iii) uncertainties due to heterogeneity

7.2.1 Development of Coupled Models for THMC processes

Updates of the CODEBRIGHT – RETRASO reservoir simulator

CODE_BRIGHT, a finite element code for THM (thermo-hydraulic-mechanical) problems including multiphase flow, was modified for CO2 injection. For this, first, some equations of state were added relevant for the (supercritical) CO2 phase. Second, the code was changed to incorporate the chemical reactions relevant for CO2 injection in saline carbonate aquifers. It redefines the components of multiphase flow codes (traditionally, water and CO2) so that they are conservative for all reactions of the chemical system. Chemical composition can be deduced from

the concentrations of these components. This way, a model code was obtained, capable of simulating all HTCM processes in a coupled way. This modified code was applied to a number of cases of CO2 injection. The effect of CO2 injection on mechanical properties was studied by HM models (Vilarrasa et al., 2010b; Vilarrasa et al., 2011). Also HM were used to study microseismicity induced by CO2 injection and to propose a hydromechanical characterization tests (Vilarrasa, 2013b). THM models were used to analyze the advantages and disadvantages on energy efficiency and mechanical stability of injecting CO2 in liquid instead of supercritical state (Vilarrasa, 2013b). More details on updates are given in the following chapters.

Coupled Hydromechanical Modeling

The possible overpressure resulting from CO2 injection may promote reactivation of sealed fractures or the creation of new ones in the caprock seal. This could lead to escape routes for CO_2. In order to assess the probability of such an event, we model an axisymmetric horizontal aquifer–caprock system, including hydromechanical coupling. We study the failure mechanisms, using a viscoplastic approach. Simulations illustrate that, depending on boundary conditions, the least favorable moment takes place at the beginning of injection. Initially, fluid pressure rises sharply because of a reduction in permeability due to desaturation. Once CO_2 fills the pores in the vicinity of the injection well and a capillary fringe is fully developed, the less viscous CO_2 displaces the brine and the capillary fringe laterally. The overpressure caused by the permeability reduction within the capillary fringe due to desaturation decreases with distance from the injection well. This results in a drop in fluid pressure buildup with time, which leads to a safer situation. Nevertheless, in the presence of low-permeability boundaries, fluid pressure continues to rise in the whole aquifer. This occurs when the radius of influence of the injection reaches the outer boundary. Thus, caprock integrity might be compromised in the long term.

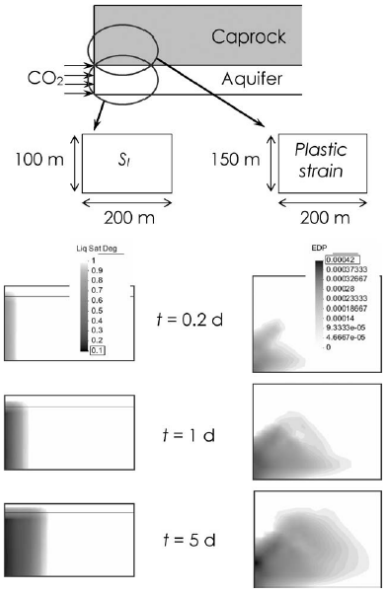

Figure 7-1. Plastic strain (*EDP*) in the caprock (left) and liquid saturation degree, S_l, in the aquifer (right) for different injection times. Plastic strain propagates as CO_2 advances at the beginning of injection. (Vilarrasa et al, 2010)

Incorporating Chemical Reactions into multiphase flow models for CO2 storage

CO_2 injection and storage in deep saline aquifers involves many coupled processes, including multiphase flow, heat and mass transport, rock deformation and mineral precipitation and

dissolution. Chemical coupling is especially critical in carbonate aquifers, where minerals will tend to dissolve in response to the dissolution of CO_2 into the brine. The resulting neutralization will drive further dissolution of both CO_2 and calcite. This suggests that large cavities may be formed and that proper simulation may require full coupling of reactive transport and multiphase flow. We show that solving the latter may suffice whenever two requirements are met: (1) all reactions can be assumed to occur in equilibrium and (2) the chemical system can be calculated as a function of the state variables of the multiphase flow model (i.e., liquid and gas pressure, and temperature). We redefine the components of multiphase flow codes (traditionally, water and CO_2), so that they are conservative for all reactions of the chemical system. This requires modifying the traditional constitutive relationships of the multiphase flow codes, but yields the concentrations of all species and all reaction rates by simply performing speciation and mass balance calculations at the end of each time step. We applied this method to the H_2O–CO_2–Na–Cl–$CaCO_3$ system, so as to model CO_2 injection into a carbonate aquifer containing brine. Results were very similar to those obtained with traditional formulations, which implies that full coupling of reactive transport and multi-phase flow is not really needed for this kind of systems, but the resulting simplifications may make it advisable even for cases where the above requirements are not met. Regarding the behavior of carbonate rocks, we find that porosity development near the injection well is small because of the low solubility of calcite. Moreover, dissolution concentrates at the front of the advancing CO_2 plume because the brine below the plume tends to reach high CO_2 concentrations quite rapidly. We conclude that carbonate dissolution needs not to be feared.

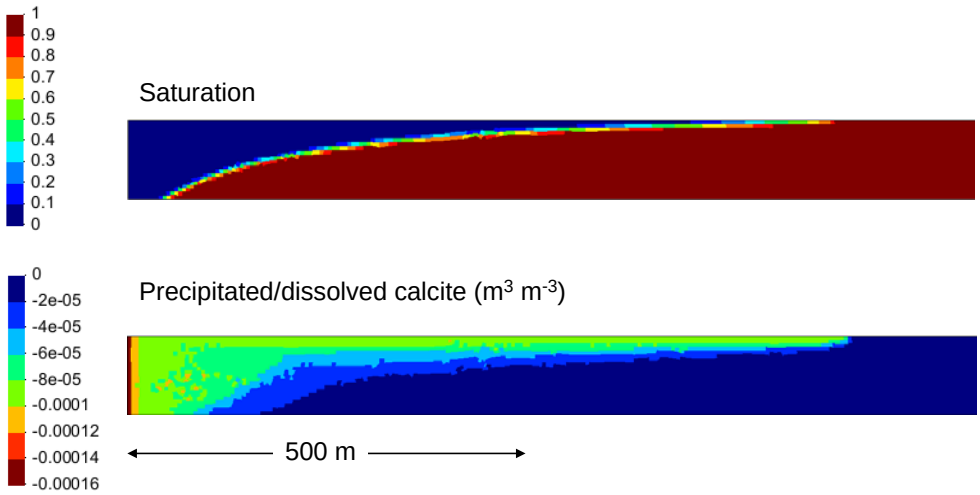

Figure 7-2. Saturation (above) and dissolved calcite (below) after one year of CO_2 injection. CO_2 is injected at the left boundary. Calcite dissolves in the vicinity of the CO_2 plume.(Saaltnik et al, 2013)

A coupled hydro-mechanical model for predicting cap-rock fracturing

A new hydromechanical model was also developed (McDermott et al, 2013) predicting the spacing of fracturing in overlying caprocks due to fluid pressure increase in the reservoir. Predicting the spacing of tensile-fractures due to fluid pressure increase in a multilayered sedimentary sequence comprising different typical sedimentary deposits such as mudstones, siltstones and sandstones is important whilst considering the integrity of a sealing unit. During normal burial and tectonic conditions, strata will undergo both extensional forces and increase in fluid pressures. This model addresses the effects of the diffuse fluid pressure increase, and is useful for engineered applications such as the injection of fluid into a reservoir thereby causing an increase of fluid pressure beneath a caprock, and for sedimentary sequences during normal digenetic processes of burial and fault activation. Analytical and numerical elastic stress strain

solutions are compared to provide a robust normalised standard relationship for predicting the spacing of fractures. Key parameters are the local minimum horizontal stress, variability of the tensile strengths of the layers of a sedimentary sequence and the thickness of the beds. Permeability and storage are also shown to impact the fracture spacing. The model predicts many of the field observations made about strata bound fracture systems, and should also prove useful in consideration of the impact of raised reservoir fluid pressures on caprock integrity.

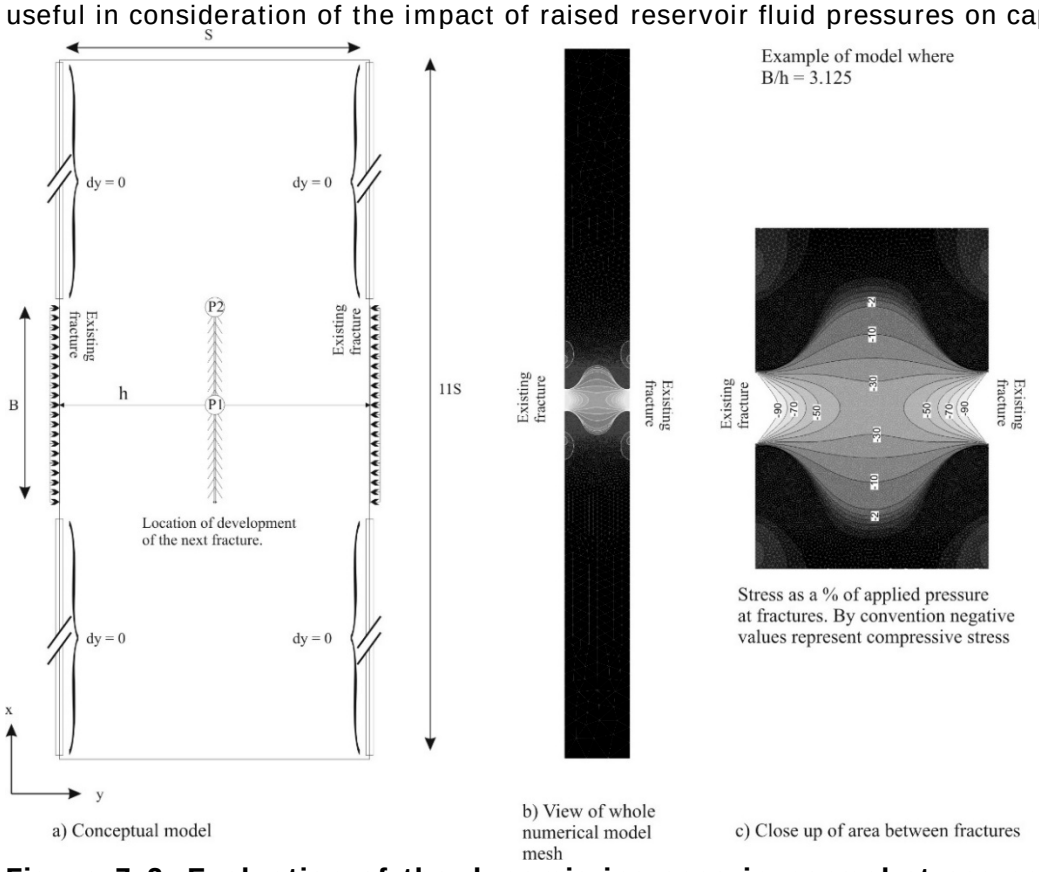

Figure 7-3. Evaluation of the dynamic increase in normal stress as a result of new fracture development (Mcdermott et al, 2013)

7.2.2 Development of Advanced Flow and Transport Models for CO_2 systems

A numerical model of tracer transport in a non-isothermal two-phase flow system for CO_2 geological storage characterization

For the purpose of characterizing geologically stored CO2 including its phase partitioning and migration in deep saline formations, different types of tracers are being developed. Such tracers can be injected with CO2 or water, and their partitioning and/or reactive transfer from one phase to another can give information on the interactions between the two fluid phases and the development of their interfacial area. Kinetic rock-water interactions and geochemical reactions during two-phase flow of CO2 and brine have been incorporated into numerical simulators (e.g. Xu et al., 2004). However, chemical equilibrium between the fluid phases is typically assumed, and multi-component, multiphase, non-isothermal codes for CO2-brine systems that incorporate kinetic mass-transfer of tracers between the two fluid phases are not readily available. New models or further developments of existing models are therefore needed to provide the capability

for interpreting the signals of novel tracers, including tracers with kinetic/time dependent interface transfer.

Therefore, in the frame of MUSTANG a new numerical model of tracer transport in a non-isothermal two-phase flow system was developed (Tong et al, 2013). The model consists of five different governing equations describing liquid-phase (aqueous) flow, gas (CO2) flow, heat transport and the movement of the tracers within the two phases, as well as allowing kinetic transport of the tracers between the two phases. A finite element method is adopted for the spatial discretization and a finite difference approach is used for temporal discretization. Some special technologies and solution strategies are adopted for increasing the convergence, ensuring the numerical stability and eliminating non-physical oscillations. The new numerical model is validated against the code TOUGH2/ECO2N as well as some analytical/semi-analytical solutions. Good agreement between the simulated and analytical results indicates that the model has capability to simulate two-phase flow and tracer transport in a non-isothermal two-phase flow system with high confidence. Finally, the capability to model transport and kinetic mass-transfer of tracers between the two fluid phases is demonstrated through examples.

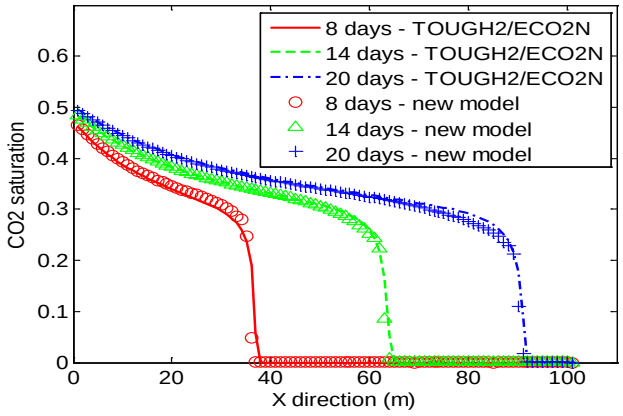

Figure 7-4. Comparison of CO2 saturation profiles at different times as simulated using the new model and the numerical model TOUGH2/ECO2N.(Tong et al, 2013)

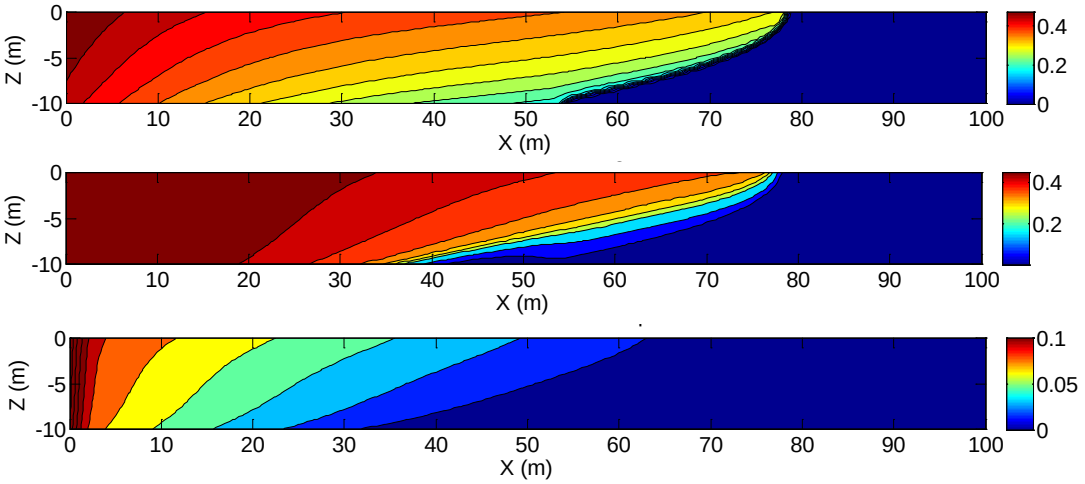

Figure 7-5. Example simulation of CO_2 migration with tracer partioning between CO_2 and brine. The tracer (0.52 mol/kg) is injected with CO2 from the left-hand side. Top: CO_2 saturation after 16 days. Middle: tracer concentration in the gas phase after 16 days. Bottom: tracer concentration in the liquid phase after 16 days. (Tong et al, 2013)

Front Tracking Approach for Two-Phase Flow applied to Supercritical CO_2 Replacing Brine in a Heterogeneous Reservoir and Caprock

A new simulation approach was developed for modelling the flow of supercritical CO2 in heterogeneous porous media whilst tracking the CO2 brine interface at a subgrid scale. Predicting fluid replacement by two phase flow in heterogeneous porous media is of importance for issues such as supercritical CO2 sequestration, the integrity of caprocks and the operation of oil water/brine systems. When considering coupled process modelling, the location of the interface is of importance as most of the significant interaction between processes will be happening there. Modelling two phase flow using grid based techniques presents a problem as the fluid-fluid interface location is approximated across the scale of the discretisation. Adaptive grid methods allow the discretisation to follow the interface through the model, but are computationally expensive and make coupling to other processes (Thermal, Mechanical, Chemical) complicated due to the constant alteration in grid size and effects thereof. Interface tracking methods have been developed that apply sophisticated reconstruction algorithms based on either the ratio of volumes of a fluid in an element (Volume of Fluid Methods) or the advective velocity of the interface throughout the modelling regime (Level Set Method). In this paper we present an "Analytical Front Tracking" method where a generic analytical solution for two phase flow is used to "add information" to a finite element model. The location of the front within individual geometrical elements is predicted using the saturation values in the elements and the velocity field of the element. This removes the necessity for grid adaptation, and reduces the need for assumptions as to the shape of the interface as this is predicted by the analytical solution. The method is verified against a standard benchmark solution and then applied to the case of CO2 pooling and forcing its way into a heterogeneous caprock, replacing hot brine and eventually breaking through.

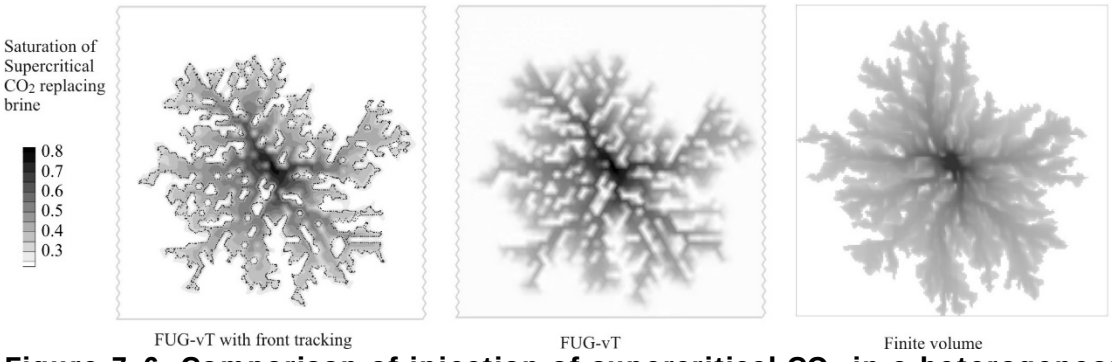

Figure 7-6. Comparison of injection of supercritical CO_2 in a heterogeneous reservoir rock, with finite element with front tracking, finite element without front tracking, and a finite volume solution. (McDermott et al, 2011)

7.2.3 Model for Heterogeneous Systems and Uncertainty Analysis using Gaussian Process Emulator

Simulations of CO2 sequestration in geological formations are subject to uncertainties from a number of sources. For simulation to make a useful contribution to the understanding of CO2 migration and its associated storage, these uncertainties must be identified, characterized and their consequences quantified. This part of the project deals with the uncertainties quantification on modelling evolution of the CO2 plume during the injection process due to the lack of detailed

knowledge of the spatial variation of the permeability field, and so this uncertainty about the permeability thus makes uncertain in the expected evolution of the plume.

In the analysis the permeability is modeled as a lognormal random field with an exponential correlation structure. A truncated Karhunen-Loève (KL) expansion of the logarithm of the permeability field is used so that the input to the calculation can be characterized by a finite number of parameters, which are the coefficients in the KL expansion. In this way, a Monte-Carlo simulation is effectively achieved by running the emulator many times with the input parameters (the KL coefficients) drawn from the appropriate multivariate normal distribution. To mitigate the computational cost of a Monte Carlo scheme, a Gaussian process emulators (GPE) is implemented. In a traditional Monte-Carlo method the full simulation has to be run for a large number of realizations, whereas in the GPE approach a relatively small number of realizations of the full problem are run first with the TOUGH2 simulator to train the emulator. The basic idea is that the GPE produces a good approximation to the output of the full simulation from where the statistical properties of the output can be computed from the emulator runs. We also used the TOUGH2 simulation results to evaluate the emulator performance.

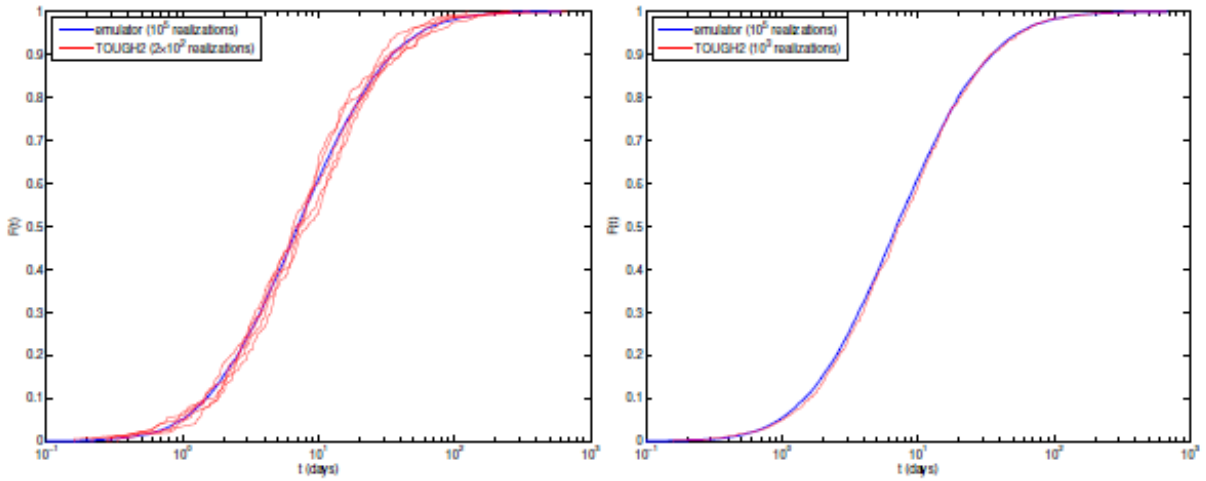

Figure 7-7. Comparison of the CO2 break-through time as calculated with TOUGH2 Monte Carlo simulations and Gaussian emulator runs. Heterogeneous system. (Wilkinson et al, 2014)

7.3 Process Analyses and Process Models – Small Scale

7.3.1 Coupled Hydro-Mechanical Processes and Fracturing

Development of Advanced Meshless Numerical Methods

During the course of the MUSTANG project, several new so-called meshless numerical methods have been developed. These methods are designed to allow high-resolution solutions to a number of complex physical processes that are of interest during CO2 injection. Each of these methods is based on the local collocation of radial basis functions. Radial basis functions are typically used to interpolate scattered data, offering a powerful alternative to polynomial collocation. In the literature, several approaches exist for local Radial Basis Function (RBF) methods that replicate the formulation of existing numerical methods (such as finite difference and finite volume method), which are based on the use of RBF interpolants in place of polynomials. In this way these methods are able to operate on irregular datasets.

The developed methods extend the local RBF concept by introducing the full RBF PDE interpolation machinery into the local systems. The full-domain PDE interpolation procedure is popular within the literature for solving small-scale problems on complex datasets. During this work different methods for incorporating the PDE-interpolation procedure into a local RBF framework were investigated.

Most of the RBF finite difference approaches described in the literature are based on the use of RBF interpolation instead of traditional polynomial interpolation in a finite difference type of scheme, with the solution of the PDE driven by global reconstruction of partial differential operators. While the method allows solutions to be obtained on irregular datasets, in contrast to polynomial-based finite difference methods, it suffers from many of the traditional drawbacks of such methods (limited spatial convergence rate, requirement to form upwind-biased stencils in convective-dominant scenarios etc.).

The first approach considered in this work was an “enhanced finite difference” method (RBF-FD+). Here the PDE governing operator is enforced within the local stencil at auxiliary points, along with any boundary operators that may be required. This allows the method to be stabilised during convective-dominant scenarios, without introducing artificial upwinding. As with all finite difference methods, the solution of the PDE is obtained by reconstructing the partial derivatives from the underlying interpolation systems. As alternative approach and completely innovative, the RBF finite collocation approach (RBF-FC), was also developed resulting in a very efficient and accurate scheme, which appears to be the best local RBF method reported in the literature. Here the PDE governing operator is enforced throughout the stencil interior, not only at auxiliary points, with any boundary operators enforced at the domain periphery. In this way, any data reconstructed from the local systems automatically respects the governing and boundary PDEs, and therefore no global reconstruction of partial differential operators is required; the solution field may be assembled directly. The obtained results with this method have shown high spatial convergence rates (in excess of seventh order), and a relative insensitivity to variations in basis function flatness in comparison to other RBF methods. Moreover, the method is highly stable in convective-dominant scenarios, and is able to accurately capture shocks and other discontinuities while retaining a centred stencil.

These new local RBF numerical schemes were implemented to solve several of the complex processes encountered during CO2 sequestration, as described in the sections.

Material damage through generation of micro-fractures

Using the RBF-FC approach outlined above, the generation of micro-fractures and micro-fissures within a poroelastic domain was investigated, due to the high-pressure injection of fluid. Following the classical continuous Damage Formulation of damage mechanics, the presence of micro-fractures was considered by introducing a continuum damage parameter, D, which quantifies the volumetric proportion of the material that is occupied by micro-fissures. The presence of material damage weakens the material (by reducing the bulk modulus), and increases the porosity and permeability of the material. In this type of approach, the evolution of damage is described as a function of the local shear strain. Damage may only form where the material is dilatational.

To validate the numerical results the case of propagation around an injection well was considered. In this case the high-pressure injection leads to the formation of damage around the injection well, which in turn increases the hydraulic conductivity and therefore reduces resistance of the material to any future injected fluid.

Macroscopic fracture propagation

In this part of the project a meshless numerical solution of the propagation of fractures through a poroelastic domain was developed. Propagation of fractures is a process driven by the stress singularity that occurs at the crack tip. The behaviour on approach to this singularity may be described using a stress-intensity formulation, with the stress intensity factors determining the speed and direction of the crack tip propagation.

By using the integrated RBF-FC approach, also developed as part of this project, a local RBF collocation system can be defined around the crack-tip, encompassing the singularity within a local boundary integral domain. In this way, it is extended the behaviour of the method on approach to the singularity without bringing the singularity itself into the local RBF collocation systems. The approach is able to accurately predict the exact stress intensity factors for benchmark problems

Leakage of CO_2 through fissures and faults

The flow and transport of a CO2-brine mixture through a porous fissure, and its coupling to a surrounding heterogeneous porous medium, was studied. By considering a thin-film approximation to the flow within the channel, via Reynold's equation, and a Darcy flow within the surrounding porous medium, the two domains are coupled by introducing the correct matching conditions into each domain. The transport of CO2 through the fissure is then considered as a coupled transient problem, with the transport within the fissure again taken using a width-averaged thin-film approximation. By using a multi-zone implementation of the RBF-FC approach previously developed, the presence of geological layers is considered (i.e. a heterogeneous porous medium), along with dispersion of the transported CO2 within the porous medium. Besides, the effect of time variation of channel width, due to possible mineral precipitation and/or dissolution was also included in the analysis.

References: *Stevens et al, 2013;.Bustamante,et al (2013); Stevens et al, (2013), Stevens, D et al (2014 a,b, c and d)*

7.3.1 Two-phase flow of CO_2 and brine

Viscous fingering and dissolution during CO_2 injection

Viscous fingering occurs due to instability at the interface of two immiscible fluids, due to the displacement of a fluid by another fluid of lower viscosity. As part of the MUSTANG project, the study of the injection of a low-viscosity fluid, such a gaseous or supercritical CO2, into a higher-viscosity fluid, such as brine, within a Hele Shaw cell was undertaking. Particular attention was given to the dissolution of the injected fluid (CO2) into the surrounding brine, and the effect of this process on the pattern of fingering. By using a boundary element method (BEM) to describe the evolution of the fluid interface, different possible injection scenarios were considered. The presence of dissolution is characterised by a bubble-shedding mechanism; the bases of viscous fingers are slowly eroded by the dissolution, leading to the breaking of viscous fingers. These broken fingers are shed from the main injection bubble, and move outwards with the velocity of the surrounding fluid. Over time these detached bubbles dissolve entirely. New fingers then evolve, with their concurrent breaking, resulting in the possibility of a cascade of travelling and dissolving bubbles, rather than a continuous fingering structure such as occurs without the presence of dissolution. In order to take into account the dissolution process in the mathematical formulation of the problem, a modification to interface boundary conditions and the required adaptation for the BEM are described. In addition, a methodology is described for reconstructing the fluid pressure at any location within the fluid domain, by exploiting the properties of the BEM. (*Power, H et al, 2013)*

7.4 Process Analyses and Process Models – Field Scale

7.4.1 Two-phase flow of CO_2

Dispersal of buoyancy-driven flow in porous media with inclined baffles

From some real sites, seismic images of geological CO_2 storage show the rise of CO_2 is influenced by horizontal shales. The buoyant CO_2 spreads beneath impermeable barriers until a gap allows its upward migration. The large number and small scale of these barriers makes the prediction of the CO_2 migration path and hence the magnitude of CO_2 trapping very challenging.

A new model has been developed to follow the motion of a CO2 plume in a complex permeable rock accounting for the presence of shale baffles which provide local barriers to the flow and the porous matrix. This leads to prediction of the shape of the plume and its dispersal. The key fascinating result is that there is significant horizontal spreading of the plume as it rises through the formation, owing to the diversion of the flow around the baffles. A simple analytical model has been developed to describe the shape of the plume and the spreading around the baffles, using an approximate gravity current model for each baffle. The predictions of the model have been compared with laboratory experiments. In the case of baffles which are inclined to the horizontal, there is a net spreading of the plume in the direction of inclination with a final steady shape being established in which the plume rises at an angle to the vertical as all the CO2 runs under the baffles and flows from the upper end of the baffle. The model leads to a new prediction of the effective permeability in this generic rock morphology, characteristic of many turbidite and other layered rocks in which fine grained sediment accumulates between successive deposits of the more permeable larger grains.

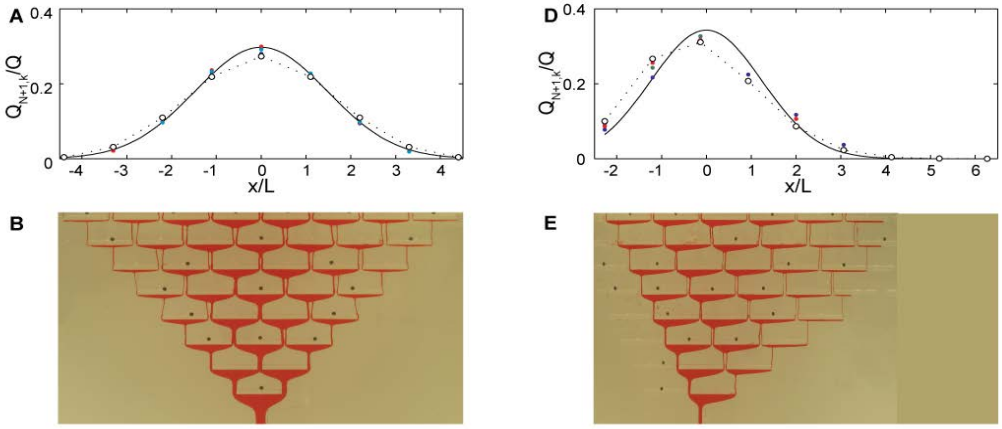

Figure 7-8. *Dispersal of buoyancy-driven flow in porous media with inclined baffles. (Rayward-Smith et al, 2011)*

CO_2 Spreading in Layered Aquifer

A new model has been developed to follow the shape of the plume at the Sleipner field in Norway by assuming that in each layer of the formation, the plume spreads within a confined permeable layer from a constant source of CO2 at the well. There are nine layers at the Sleipner field and so this model includes nine separate layers. The balance of gravity driven flow and pressure driven flow leads to the prediction of different plume shapes in the layers depending on the volume flux supplied to each layer. We then develop the model in an attempt to invert the field data and predict the fraction of the supply flux which flows into each layer. This leads to an interesting problem in that the main measurable from field data is the radius of the plume in each layer, as obtained by seismic. This radius in fact corresponds to the radius at which there is seismic resolution in the signal which requires a plume of CO2 about 1m thick. As a result, there are typically two inverse models for the layer permeability for a given supply flux , corresponding to a low permeability pressure driven flow and a higher permeability gravity driven flow, both of which have the same depth at a distance where the depth is 1m. We show that this non-uniqueness in the inversion for each layer leads to an underresolved inverse problem for nine layers at Sleipner. There are special inverse solutions which can be constructed assuming the well pressure is either hydrostatic or CO2 static, and we illustrate how these lead to similar predictions of the flow partitioning between layers but not the permeability of the layers.

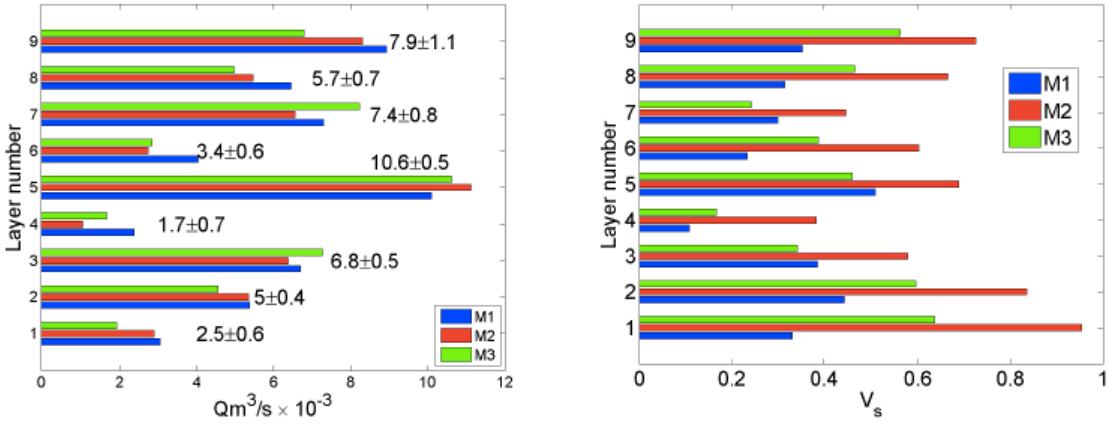

Figure 7-9: Partitioning of (a) the flux and (b) the permeability at Sleipner as predicted by the inverse model (Dudfield, P and Woods, 2013)

Propagation of non-isothermal gravity currents in an inclined porous layer

It was also considered the buoyancy-driven flow in an inclined porous layer. The thermal inertia of the porous matrix leads to a transition in the temperature of the injectate as it spreads from the well and heats up to reservoir temperature. Since the buoyancy and viscosity of the injectate change across this thermal transition, the alongslope characteristic speed of the current also changes. Density and viscosity typically decrease with temperature and, so, for injectate that is positively buoyant at reservoir temperature, the changes in density and viscosity with temperature have complementary effects on the characteristic speed. The change in characteristic speed, combined with the change in buoyancy across the thermal transition, leads to a series of different flow morphologies with the thermally adjusted injectate either running ahead of or lagging behind the original injectate. By approximating the thermal transition as a discrete jump, the leading-order structure of these currents for the different possible cases was derived. Then build on this to develop a more detailed boundary layer description of the thermal transition based on the theory of thin gravity driven flows in porous media. Under certain injection conditions, it was found that the thermal transition is gravitationally unstable and that this may lead to mixing across the thermal transition. (Rayward-Smith and Woods, (2011)

Distribution of injected CO_2 in a stratified saline reservoir accounting for coupled wellbore-reservoir flow

Alternating high and low permeability strata are common in prospective CO2 storage basins. The distribution of injected CO_2 among such layers affects e.g. CO_2 storage efficiency, capacity and plume footprint. A numerical study on the distribution of injected CO_2 into a multi-layered reservoir, accounting for coupled wellbore-reservoir flow, was carried out using T2Well/ECO2N. A site-specific case, reflecting the properties of Heletz site, as well as a more general case were considered.

Properties and processes governing the distribution of sequestrated CO_2 were identified and the potential to operationally modify the distribution was investigated. The distribution of CO_2 was seen to differ from that of injected water, i.e. it was not proportional to the transmissivity of the layers.

The results indicate that caution should be taken when performing numerical simulations of CO_2 injection into layered formations. Ignoring coupled wellbore-reservoir flow and instead adopting a simple boundary condition at the injection well, such as an inflow rate proportional to the transmissivity of each layer, may result in significant underestimation of the proportion of CO_2 ending up in the shallower layers, as not all relevant processes are accounted for. This discrepancy has been thoroughly investigated and quantified for several CO_2 sequestration scenarios. (Rasmusson et al, 2014)

Effects of CO_2 Compressibility

The injection of supercritical CO_2 in deep saline aquifers leads to the formation of a CO_2 plume that tends to float above the formation brine. As pressure builds up, CO_2 properties, i.e. density and viscosity, can vary significantly. Current analytical solutions do not account for CO_2 compressibility. In this article, we investigate numerically and analytically the effect of this variability on the position of the interface between the CO_2-rich phase and the formation brine. We introduce a correction to account for CO_2 compressibility (density variations) and viscosity variations in current analytical solutions. We find that the error in the interface position caused by neglecting CO_2 compressibility is relatively small when viscous forces dominate. However, it can become significant when gravity forces dominate, which is likely to occur at late times of injection.

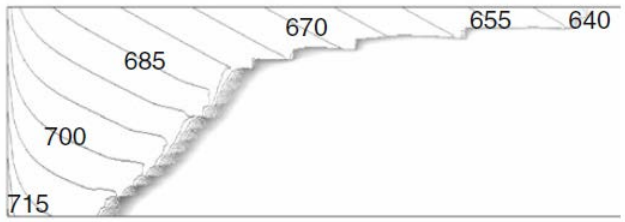

Figure 7-10. CO_2 density (kg/m_3) within the CO_2 plume resulting from a numerical simulation that acknowledges CO_2 compressibility (Vilarrasa et al, 2010)

7.4.2 Hydro-mechanical Effects

Geomechanical Stability of the Caprock

Sequestration of carbon dioxide (CO_2) in deep saline aquifers has emerged as a mitigation strategy for reducing greenhouse gas emissions to the atmosphere. The large amounts of supercritical CO_2 that need to be injected into deep saline aquifers may cause large fluid pressure buildup. The resulting overpressure will produce changes in the effective stress field. This will deform the rock and may promote reactivation of sealed fractures or the creation of new ones in the caprock seal, which could lead to escape paths for CO_2. To understand these coupled hydromechanical phenomena, we model an axisymmetric horizontal aquifer-caprock system. We study plastic strain propagation patterns using a viscoplastic approach. Simulations illustrate that plastic strain may propagate through the whole thickness of the caprock if horizontal stress is lower than vertical stress. In contrast, plastic strain concentrates in the contact between the

aquifer and the caprock if horizontal stress is larger than vertical stress. Aquifers that present a low-permeability boundary experience an additional fluid pressure increase once the pressure buildup cone reaches the outer boundary. However, fluid pressure does not evolve uniformly in the aquifer. While it increases in the low-permeability boundary, it drops in the vicinity of the injection well because of the lower viscosity of CO2. Thus, caprock stability does not get worse in semi-closed aquifers compared to open aquifers. Overall, the caprock acts as a plate that bends because of pressure buildup, producing a horizontal extension of the upper part of the caprock. This implies a vertical compression of this zone, which may produce settlements instead of uplift in low-permeability ($k \leq 10^{-18}$ m^2) caprocks at early times of injection.

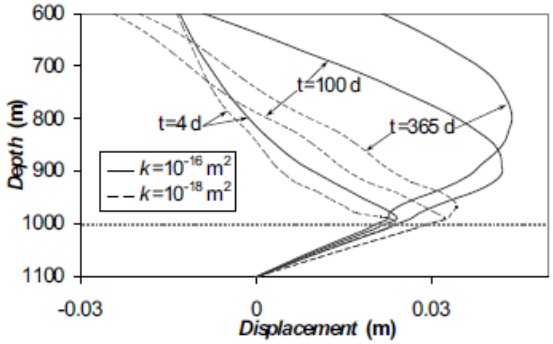

Figure 7-11. Vertical displacement next to the injection well at various injection times and caprock permeabilities. A low-permeability caprock limits the vertical displacement and even produces settlement in its upper part. The dotted line indicates the contact between the aquifer and the caprock.(Vilarrasa et al, 2011)

Microseismicity and Hydromechanical Characterization

Clear understanding of coupled hydromechanical effects, such as ground deformation, induced micro-seismicity and fault reactivation, will be crucial to convince the public that geologic carbon storage is secure. These effects depend on hydromechanical properties, which are usually determined at metric scale. However, their value at the field scale may differ in orders of magnitude. To address this shortcoming, we propose a hydromechanical characterization test to estimate the hydromechanical properties of the aquifer and caprock at the field scale. We propose injecting water at high pressure and, possibly, low temperature while monitoring fluid pressure and rock deformation. Here, we analyze the problem and perform numerical simulations and a dimensional analysis of the hydromechanical equations to obtain curves for overpressure and vertical displacement as a function of the volumetric strain term. We find that these curves do not depend much on the Poisson ratio, except for the dimensionless vertical displacement at the top of the caprock, which does. We can then estimate the values of the Young's modulus and the Poisson ratio of the aquifer and the caprock by introducing field measurements in these plots. Hydraulic parameters can be determined from the interpretation of fluid pressure evolution in the aquifer. Reverse-water level fluctuations are observed, i.e. fluid pressure drops in the caprock as a result of the induced deformation that undergoes the aquifer-caprock system when injecting in the aquifer. We find that induced microseismicity is more likely to occur in the aquifer than in the caprock and depends little on their stiffness. Monitoring microseismicity is a useful tool to track the opening of fractures. The propagation pattern depends on the stress regime,

i.e. normal, strike slip or reverse faulting. The onset of microseismicity in the caprock can be used to define the maximum sustainable injection pressure to ensure a permanent CO_2 storage.

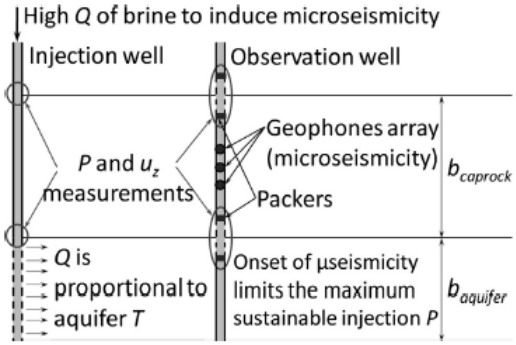

Figure 7-12. Schematic representation of the hydromechanical characterization test. A sufficiently high water flow rate so as to reach the maximum sustainable injection pressure is injected for several hours. Fluid pressure and displacements or strains are monitored in the aquifer and caprock in as many places as possible (preferably in both the injection and the observation well, but at least in one well). (Vilarrasa, 2013)

7.4.3 Injection Strategies and Effects

Liquid CO_2 injection

CO_2 will remain in supercritical (SC) state (i.e. p > 7.382 MPa and T > 31.04 ◦C) under the pressure (p) and temperature (T) conditions appropriate for geological storage. Thus, it is usually assumed that CO_2 will reach the aquifer in SC conditions. However, inflowing CO2 does not need to be in thermal equilibrium with the aquifer. In fact, surface operations are simpler for liquid than for SC CO_2, because CO_2 is transported in liquid state. Yet, problems might arise because of thermal stresses induced by cold CO_2 injection and because of phase changes in the injection tubing or in the formation. Here, we propose liquid CO_2 injection and analyze its evolution and the thermo-hydro-mechanical response of the formation and the caprock. We find that injecting CO_2 in liquid state is energetically more efficient than in SC state because liquid CO_2 is denser than SC CO_2, leading to a lower overpressure not only at the wellhead, but also in the reservoir because a smaller fluid volume is displaced. Cold CO_2 injection cools down the formation around the injection well. Further away, CO_2 equilibrates thermally with the medium in an abrupt front. The liquid CO_2 region close to the injection well advances far behind the SC CO_2 interface. While the SC CO_2 region is dominated by gravity override, the liquid CO_2 region displays a steeper front because viscous forces dominate (liquid CO_2 is not only denser, but also more viscous than SC CO_2). The temperature decrease close to the injection well induces a stress reduction due to thermal contraction of the media. This can lead to shear slip of pre-existing fractures in the aquifer for large temperature contrasts in stiff rocks, which could enhance injectivity. In contrast, the mechanical stability of the caprock is improved in stress regimes where the maximum principal stress is the vertical.

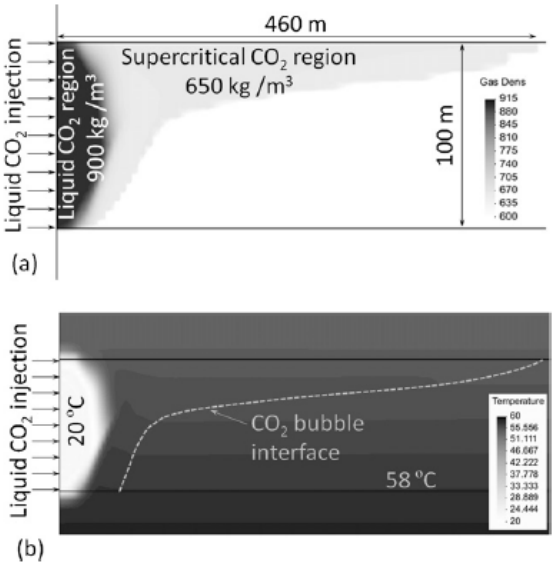

Figure. 7-13 (a) CO_2 density and (b) temperature after 8 months of liquid CO_2 injection. CO_2 remains in liquid state close to the injection well, leading to a steep front because viscous forces dominate gravity forces. Once the CO_2 thermally equilibrates with the medium, CO_2 stays in SC state, leading to a CO_2 plume interface dominated by gravity forces. (Vilarrasa et at, 2013)

Results from an analytical model - Implications of cold CO_2 injection

An analytical model was used to study some of the implications of cold CO2 injection in saline aquifers and the conclusions are presented in Rayward-Smith and Woods (2011). When CO2 is injected down a well, the temperature at the bottom of the well depends on surface conditions, heat exchange with the wall of the well and pressure work within the well. Typically, the temperature of the CO2 at the bottom of the well is lower than the local geothermal temperature. As this relatively cold CO2 flows into the porous matrix, local thermal equilibrium manifests a thermal front, behind which the porous matrix and CO2 adjust to the cold injection temperature. As the temperature of the injected CO2 increases across the thermal front, the CO2 becomes less viscous and less dense. In relatively high permeability rock, as the flow spreads from the well, it becomes buoyancy-driven, and so at the thermal front, the flow adjusts from a deep, slow flow to a relatively shallow, fast flow. The increased depth in the near source cold region has two significant implications. First, it increases the near source storage potential as more rock is flooded with CO2, but it may also enhance the leakage into the seal rock which occurs in regions where the current is sufficiently deep for the pressure to exceed the capillary entry pressure. (Rayward Smith and Woods, 2011)

7.5 Model Applications to Site-Specific Studies

7.5.1 Modeling of Heletz Deep CO_2 Injection Experiments

Field testing is a critical step to improve our knowledge on in situ-trapping mechanisms of CO2 injected in geological formations, their relative importance and monitoring. Both single-well push-pull experiments and inter-well experiments between two wells will be carried out at the Heletz site, Israel, which experiments are also a key component of the MUSTANG project. The target layer, an about 10 m thick sandstone layer composed of three layers, is located at a depth of 1600 m and extensive investigations have and are being carried out on the site in preparation of the experiments. Numerical modeling has been a key component in designing these experiments.

Modeling of the push-pull test for characterizing residual carbon dioxide saturation

Modeling results of different single-well push-pull (injection-withdrawal) test designs have been analyzed for their ability to determine residual trapping of CO2 in-situ. The modeling aims to improve the design of a CO2 push-pull test part of the field experiment conducted at the Heletz site, Israel. Single-well experiments complement two-well injection-monitoring tests in that they offer a way of reducing heterogeneity effects on CO2 transport in comparison to two-well tests. The test scenarios simulated combine thermal, hydraulic and tracer tests in line with the work by Zhang et al (2011), where the test sequences have three main stages divided into (i) reference tests, (ii) creation of a zone of residual gas saturation and (iii) testing during residual gas saturation conditions. One of the main interests is to compare different ways of creating the residual zone, the two principal approaches being to push the mobile CO2 away by injecting CO2 saturated water, thus leaving the residual zone behind or by pumping the mobile CO2 back. Inverse modeling with the iTOUGH2 simulator and the EOS7c module were used to analyze the ability of the competing test designs to accurately determine parameters of main interest during CO2 sequestration, in particular the residual gas saturation. Results from e.g. sensitivity analysis and parameter estimation were used to compare alternative test designs (Figs. 1-3) in the ability to accurately estimate the parameters of interest. The residual gas saturation can be derived from measurable responses in temperature, pressure, mass fraction of CO2 in the aqueous phase or tracer breakthrough curves (Figs. 4-6) during the test.

A new alternative way to create residual gas conditions in-situ incorporating withdrawal and a novel indicator-tracer approach was investigated. Further the value of additional pressure measurements from a nearby passive monitoring well was evaluated. Results show that the indicator-tracer approach could be used to create residual conditions without increasing estimation uncertainty of residual gas saturation. Additional pressure measurements from a passive observation well would reduce the uncertainty in the residual gas saturation estimate. The findings of the study can be used to develop field experiments for site characterization.

The push-pull modeling and comparison study resulted in articles (Niemi et al., 2012; Rasmusson et al., 2014a, b), several conference submissions/presentations (Niemi et al., 2011, 2013; Rasmusson et al., 2010, 2011, 2012b) and progress reports (Bensabat et al., 2010; Fagerlund et al., 2011; Rasmusson et al., 2012a).

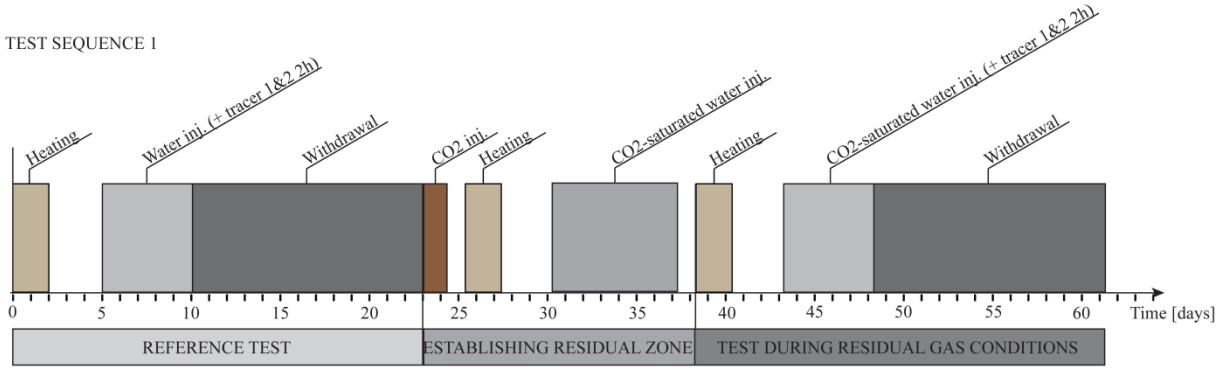

Figure 7-14a. Test sequence 1.

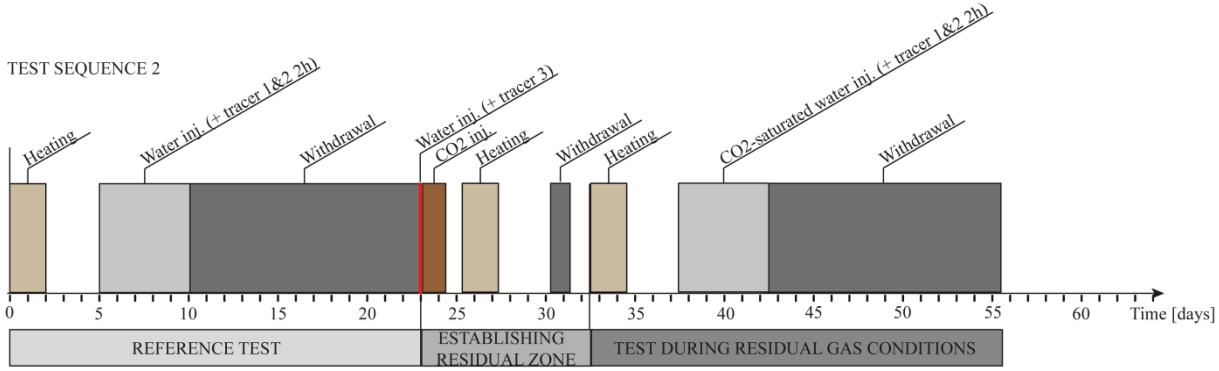

Figure 7-14b. Test sequence 2. Incorporates the indicator-tracer approach to create a residual zone.

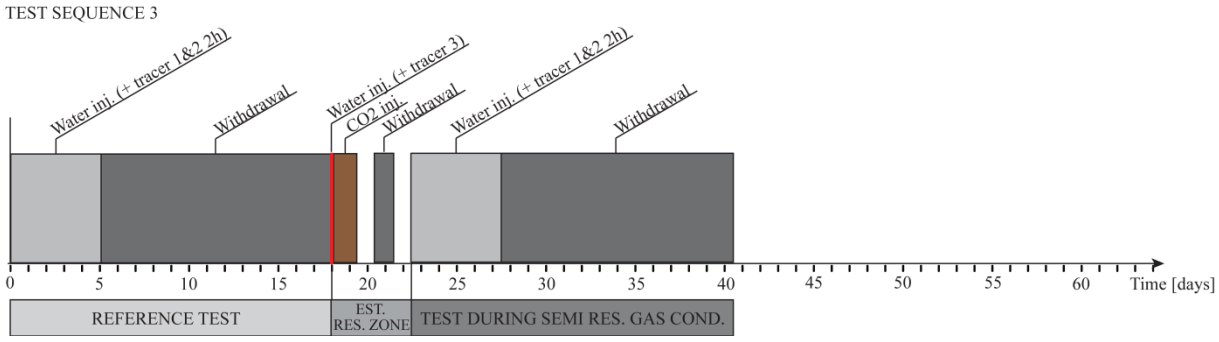

Figure 7-14c. Test sequence 3. Incorporates the indicator-tracer approach to create a residual zone. No thermal tests included. (Rasmusson et al, 2014)

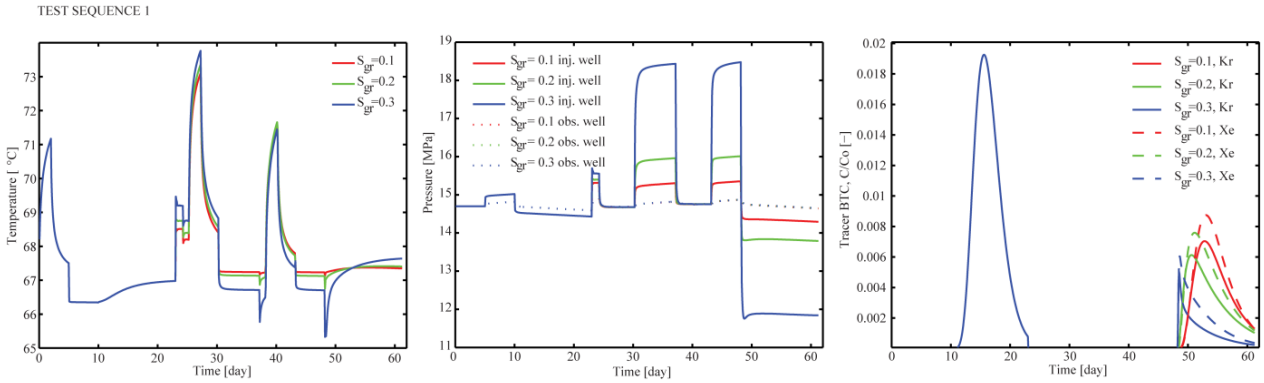

Figure 7-15a. Simulated (temperature, pressure and tracer concentration) responses for test sequence 1.

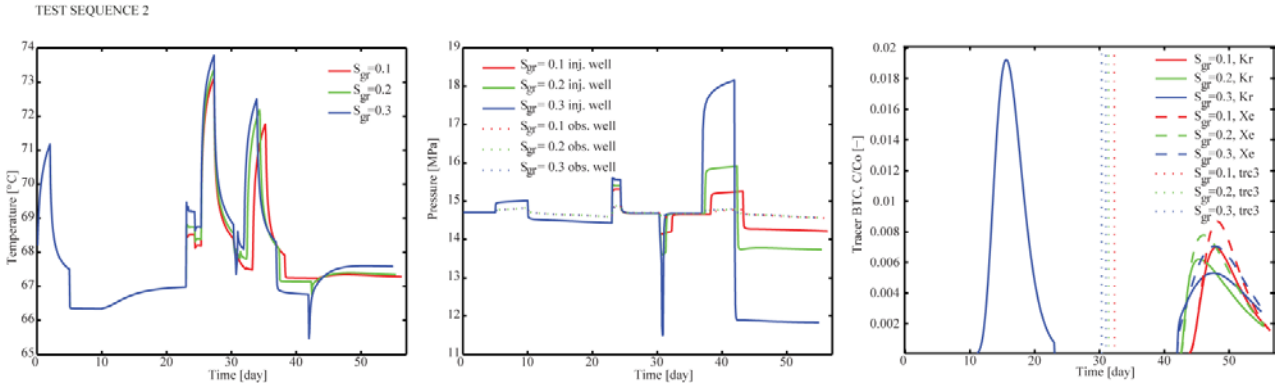

Figure 7-15b. Simulated (temperature, pressure and tracer concentration) responses, for test sequence 2.

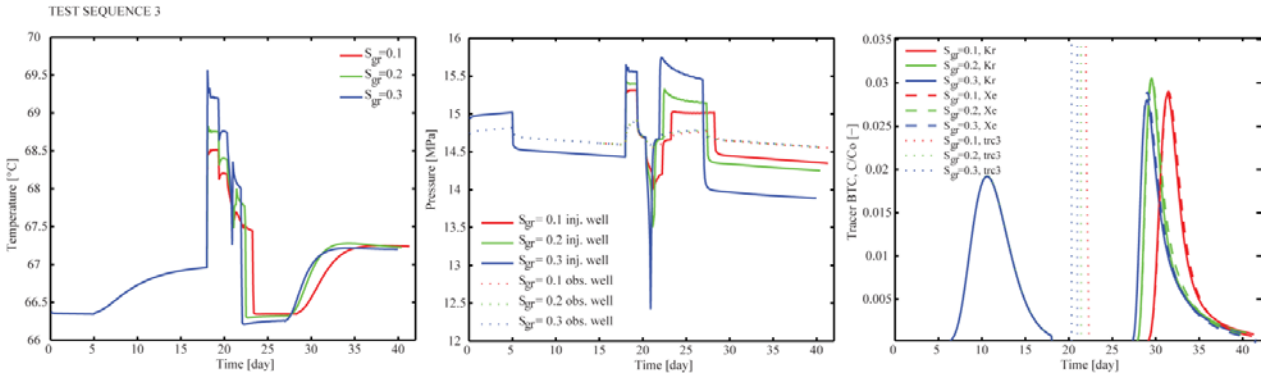

Figure 7-15c. Simulated (temperature, pressure and tracer concentration) responses for test sequence 3. (Rasmusson et al, 2014)

Interwell test to quantify residual and dissolution trapping

A two-well test sequence aimed at quantifying field values of both residual and dissolution trapping of CO2 has been developed and applied to the Heletz site using numerical modelling (Fagerlund et al., 2013a,b). The sequence includes a hydraulic test to measure residual scCO2 saturation and a novel tracer technique, together with measurements of abstracted fluid compositions for quantification of the rate of CO2 dissolution in the reservoir. The proposed

tracer technique uses a tracer with negligible aqueous solubility, which is injected with the scCO2 and enriched in the scCO2 phase as CO2 dissolves. As illustrated in Figure 1, we show that this tracer can provide direct information about the dissolution of mobile scCO2. We also show that the rate of abstracted dissolved CO2 can be used to predict the total rate of CO2 dissolution, provided that the amount of dissolved CO2 in the formation stabilizes, and that this can be achieved with the proposed abstraction scheme. We conclude that the combination of these measurements is a promising tool for detailed field-scale characterization of residual and dissolution trapping processes.

Effects of test-design options and geological parameters were also investigated using numerical modelling (Fagerlund et al., 2013b). It was found that the interwell distance has large influence on the feasibility of the test both in terms of creation of a zone of residually trapped CO2 and detection of the time when such zone has been created. The optimal distance is site-specific and depends on formation properties. Alternating CO2 and brine injections slightly increased residual trapping, but did not facilitate creation of a well-defined zone of trapping. (Fagerlund, et al, 2013 a, b, Niemi et al, 2011)

7.5.2 Modeling of Maguelone Shallow Injection Experiments

Maguelone experiment (SIMEx) is a part of Mustang project consists of a series of Nitrogen and CO_2 injection experiments in shallow aquifer, including application of different monitoring techniques (Lofi et al, 2012). We used TOUGH2 code with module EOS7CA (Pruess et al, 1999) to simulate the injection-monitoring experiment carried out during 2012 and 2013. Our main objectives are to improve our understanding of gas transport in the shallow subsurface as well as to develop and validate the model to monitor it (Oldenburg et al, 2003). The Module EOS7CA is including the equation of states to treat a two phase flow (gas and liquid), five components (water, brine, CO_2 or N_2, a gas tracer, and air) system in near ambient pressure/ temperature conditions. According to the site information, a series of axisymmetric 2D and 3D numerical simulations, with three different geological layers, were done. The host layer in the bottom and top layer have high hydraulic conductivity and the middle layer is impermeable to fluid flow. Leaky path near injection well connects to permeable layers and injected gas can also flow into the top layer. The modelling represents the results toward the N_2 injection in Nov 2012 and CO_2 injection in Jan 2013 (Fig.1). Numerical Simulations with TOUGH2 show a good agreement with the pressure data from WestBay systems (Fig.2). The CO_2 gas plumes from modelling are qualitatively supports the monitoring techniques. Work is presently going on to incorporate the experimental data into the numerical simulation further.

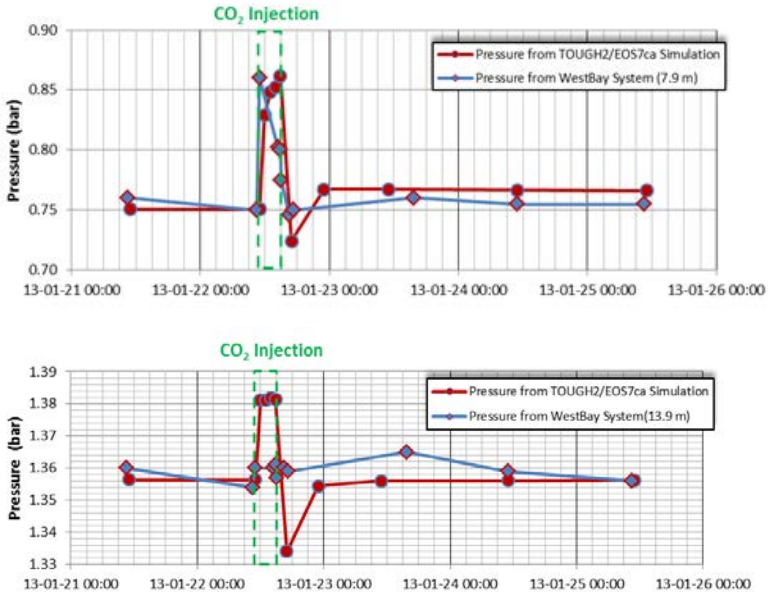

Fig. 7-16 Simulated and measured pressure at observatory well (Mag 5) (a) at depth of 7.9 m (b) at depth of 13.9 m (Basirat et al, 2013, Lofi et al, 2012)

7.6 Large-Scale Modeling of Mustang Test Sites

For the MUSTANG project, five sites with different geological and geographical settings were selected for detailed analysis. These sites are South Scania, Heletz, Horstberg, Hontomin and Valcele. Comprehensive data analysis and construction of conceptual/geological models were carried out and are reported in the Deliverables of WP2 and model simulations were carried out to consider their suitability for large scale CO2 storage.

Here a brief summary is given concerning the modelling results. The full models can be found in Deliverable D7.3, which also give all the underlying references. Due to the different characteristics and conditions of each site, different modeling approaches have also been used, as will be described.

South Scania site, Sweden, is a saline aquifer with a sequence of alternating reservoir and sealing layers. Considerable data exists from previous investigations for purposes other than CO2 storage. Here, a potential CO2 injection from an existing well is modeled and capacity estimates for this scenario presented. A three-step modeling approach is used where first a semi-analytical approach (extended from Mathias et al, 2011, 2013) is used to determine a viable injection rate, followed first by simulations with a multi-layer vertical equilibrium model (based on Gasda et al., 2009, 2011; Nordbotten et al. 2009) to explore the spatial and temporal scale of the injected CO_2 and a finally, by full simulation with the massive parallel version of the TOUGH2 code, TOUGH2MP/ECO2N to calculate the CO_2 inventory in greater detail. In the tested injection scenario injection took place from one existing well to all the layers and the limiting factor for storage showed to be transport in the high-permeability ‘primary trap’ layer. Based on the result, alternative injection scenarios that might be more beneficial and use the total capacity of the site are also suggested.

Heletz site, Israel, is a depleted oil field, with saline water on its edges. It is also the site where the small-scale scientifically motivated MUSTANG CO2 injection experiments take place and extensive local modeling has been previously carried out for this purpose. Here the entire Heletz structure, both in reservoir layers and in geographical extent, is modeled in terms of the capacity of the site for larger scale injection. The modeling approach is numerical modeling with PFLOTRAN code. The results indicate that Heletz structure, section 1, appears to be suitable for CO_2 storage, provided that open boundary conditions prevail at the eastern edges of the reservoir. The other sections do not seem to be suitable for massive CO_2 injection as they are bounded by faults, thus creating small closed sub-reservoirs. In general, the character of the bounding fracture zones is uncertain and could greatly influence the capacity estimates.

Horstberg site, Germany, is unique for its low-permeable Jurassic sandstone formations. Here the effects of supercritical CO_2 injection into a tight sandstone reservoir under the high pressure and temperature conditions are investigated using a numerical FE-model ROCKFLOW. In particular, the impact of hydraulic fracturing on the development of the pore pressure and the cap rock were investigated. A comprehensive set of hydraulic and tracer data was available for model calibration. The simulations consider the amount of supercritical CO_2 that could be stored within the area without exceeding the threshold set for the cap-rock, both with and without hydraulic fracturing. The simulations also show that below a certain limit range of permeabilities, the hydraulic stimulation is of great advantage for the storage capacity of the respective reservoir. This limit range, from which stimulation will be effective, varied between 3 – 10 mD to 1 – 4 mD, depending on the size of the reservoir considered. The results show that for reservoir dimensions realistic for Horstberg, a reservoir can be created with nearly tight sandstone formations, appropriate for $scCO_2$-storage.

Hontomin site, Spain, is a large-scale pilot storage site for the so-called Compostilla CCS project, where CO2 will be injected 1600 m depth. A large number of experiments have been carried out and/or are planned both for site characterization and for injection technology development. The site has two singular features; the permeability and porosity are very low and the storage formation is made of carbonate rocks. Here the evolution of the plume shape and bottom whole pressure are modelled. While some of the properties are based on data from the site, others are obtained from the literature to perform sensitivity analyses due to the uncertainties in permeability. Evolution of the CO2 plume and pressure for various combinations of permeability are considered and the results analysed for different gravity numbers. To study the plume evolution, the semi-analytical solution for compressible CO_2 injection (Vilarrasa et al., 2013) and compressibility corrected analytical solutions of Nordbotten et al. (2005) and Dentz and Tartakovsky (2009) are used and to analyse the evolution of pressure the method Vilarrasa et al. (2010) to account for CO_2 compressibility in the analytical solutions of Nordbotten (2005) and Dentz and Tartakovsky (2009) are used.

Valcele site, Romania, is an oil structure and deemed suitable as geological trap for CO2 as oil and gas reserves have been exploited in a proportion of 70%. Significant data base exists with 241 drilled boreholes along with complete geophysical investigations and 3D seismic work. Due to the large amount of boreholes and data available, special emphasis in the modeling work presented here is put on geostatistical modeling of site properties and analysis of related uncertainty by multivariate geostatistical tools. The corresponding uncertainty distribution in pressure was studied by simulating water injection by hydrodynamic modeling. The main aim of hydrodynamic model is to evaluate the area affected by injection.

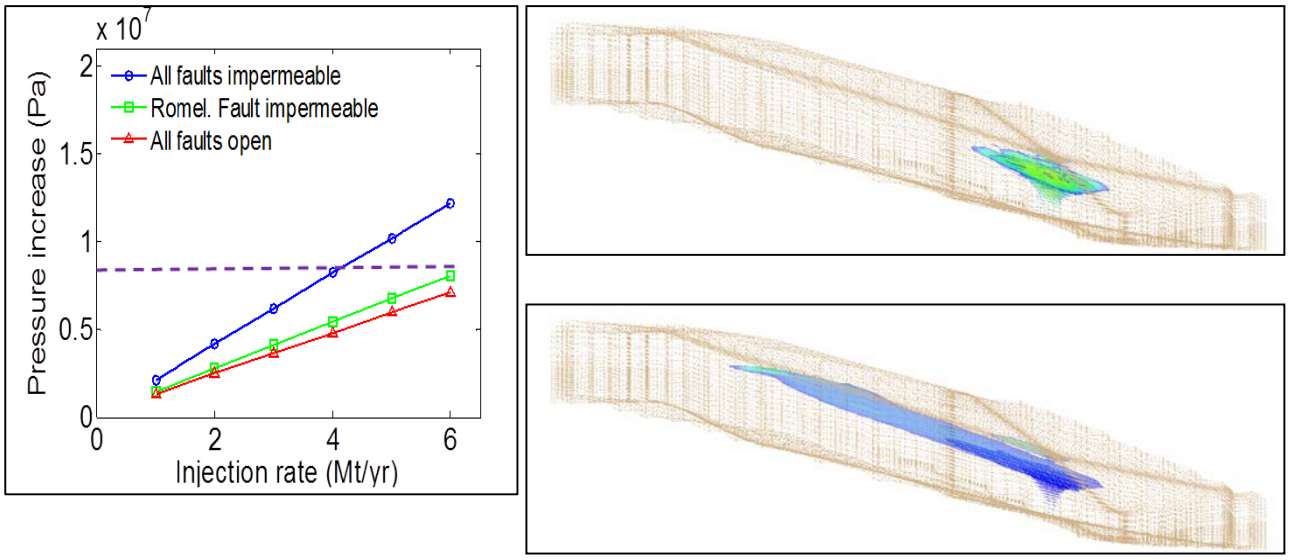

Figure 7-17. Example simulation results from the MUSTANG Site Models: Pressure increase as a function of injection rate in preliminary scoping calculations (left panel) and aimulated CO2 saturation after 50 and 1000 years; 50 years injection (right panel). South Scania site, Sweden. (Deliverable D073)

8. WP 8 - Scale Effects

The overall objective of WP 8 is to quantify scale effects in flow, transport and reaction due to spatial heterogeneities and temporal fluctuations which are relevant for understanding and modeling of CO2 spreading and for evaluation of performance and risk assessment. This includes the quantification of front dispersion during the displacement of brine by supercritical CO_2, the evaluation of mixing of CO_2-rich water and brine and the quantification of reaction efficiency to assess the sequestration potential and possible storage risks. Heterogeneity manifests itself in terms of scale effects in flow, transport and reaction coefficients, on one hand, and in modified process laws on the other hand. The latter implies that the evolution of the system state (flow, transport, reaction) is on the large scale in general different from the local scale. This is due to incomplete mixing within the large scale support volume, which in general leads to so-called non-Markovian processes.

8.1 Overview

The overall objective of WP 8 is to quantify scale effects in flow, transport and reaction due to spatial heterogeneities and temporal fluctuations which are relevant for understanding and modeling of CO_2 spreading and for the evaluation of performance and risk assessment. We highlight the following key findings:

8.1.1. Flow

The roughness and therefore the spreading of the front during CO_2 injection can significantly increase as a consequence of the interaction of spatial heterogeneity and buoyancy. This behavior can be upscaled in terms of a macrodispersion coefficient to be used in large-scale multiphase flow simulations.

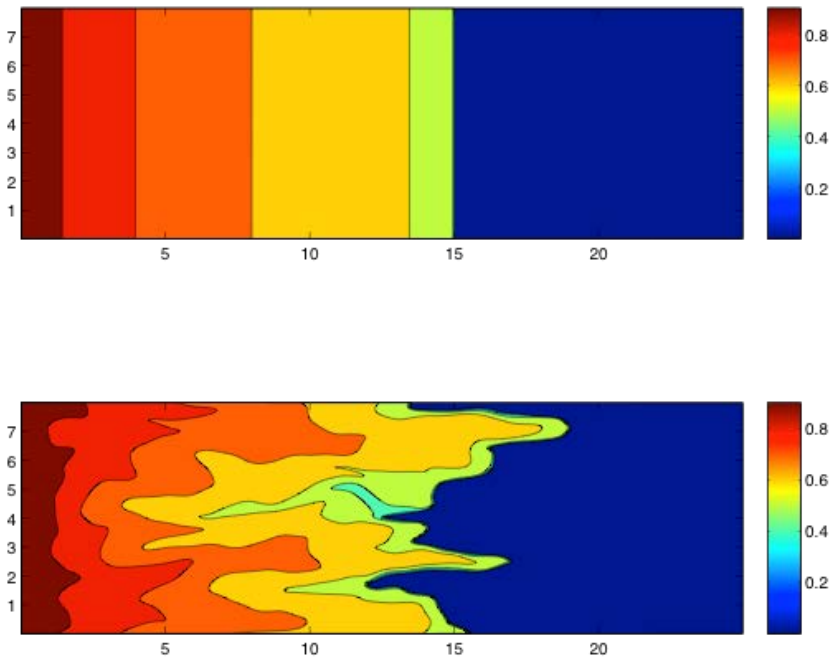

Figure 8-1. Saturation distribution for immiscible displacement in (top) homogeneous porous medium and (bottom) heterogeneous porous medium. The roughening of the displacement front can be described by an effective large-scale dispersion coefficient (from Bolster et al., Water Resour. Res., 2009).

For highly heterogeneous media, such as fractured formations, the macrodispersion concept is not sufficient to quantify the two-phase flow dynamics. We find that the evolution of saturation shows similar evolution patterns as found for passive solute transport in single phase flow, which allows parameterize the large scale dual porosity model based on, much easier accessible, tracer data.

8.1.2 Transport

The medium structure (correlation) and heterogeneity distribution (physical and chemical properties) impact on large scale transport in different ways. Both lead to anomalous transport patterns, which may be similar in terms of the spreading behavior but quite different in terms of the spatial evolution of the dissolved CO_2 and travel times. This behavior has been quantified for the large scale in terms of a coupled continuous time random walk model.

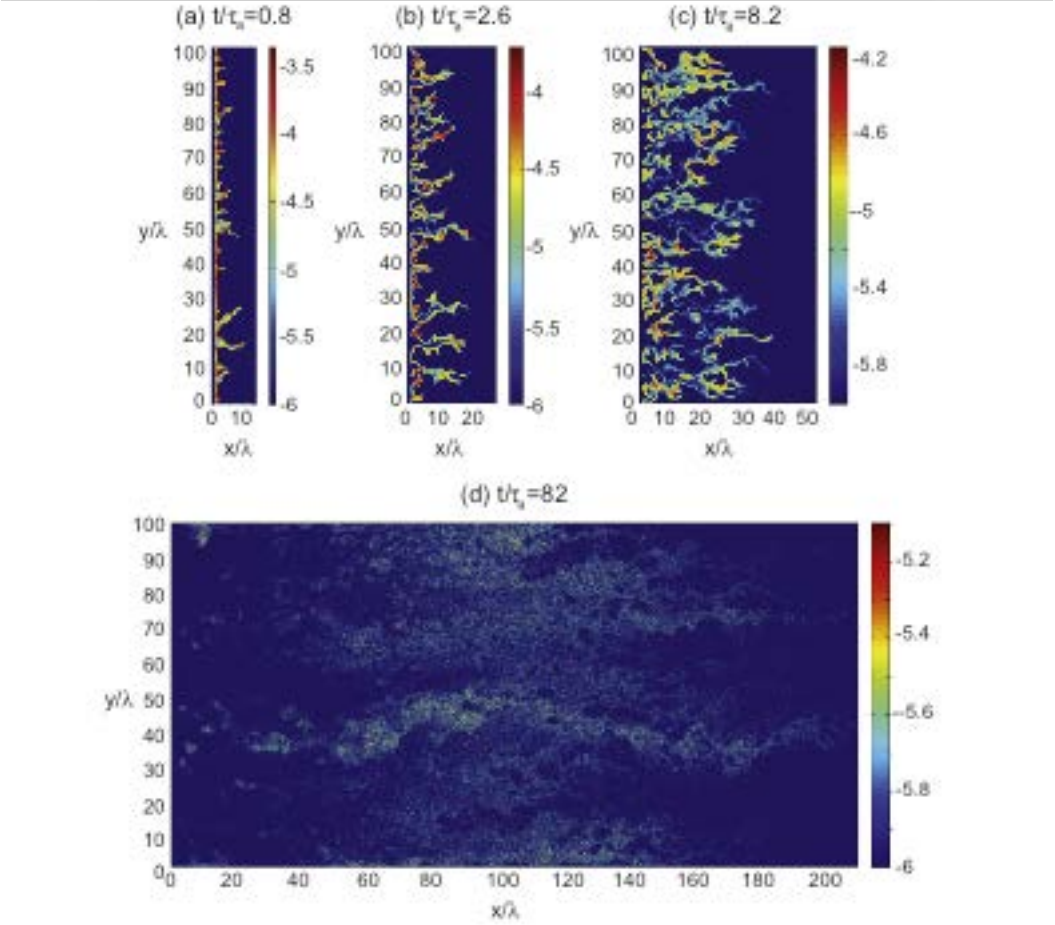

Figure 8-2. Concentration distribution of a dissolved substance evolving from an initial line source in a heterogeneous porous medium at different times. The deformation action of the heterogeneous flow field on the material line leads to a (multi)-fractal organization of the concentration field. The steepening of concentration gradients in the line and eventual merging of line segments due to folding leads to increased mixing (from Le Borgne et al., Adv. Water Resour., 2010).

The mixing behavior of waters of different chemical composition is dramatically affected by spatial heterogeneity, and cannot be described in a Fickian paradigm due to molecular diffusion only. Spatial medium heterogeneity induces fractal structure of the distribution of the dissolved substances, which accelerates mixing due to the steeping of concentration gradients. The temporal evolution of the mixing efficiency reflects the fractal dimension of the concentration field. This effect is particularly relevant for upscaling reactive transport.

8.1.3 Reaction

Spatial heterogeneity has a dramatic impact on the efficiency of chemical reactions. Mass transfer limitations lead to a significant reduction of reaction rates compared to well-mixed laboratory scenarios, and induces large scale reaction kinetics that are different from the ones for a homogeneous medium. A multi-continuum reactive transport model was developed and implemented in order to quantify these effects. The dependence of the upscaled reaction rate constants on the Damköhler number (mass transfer time scale/reaction time scale) was quantified by explicit analytical expression.

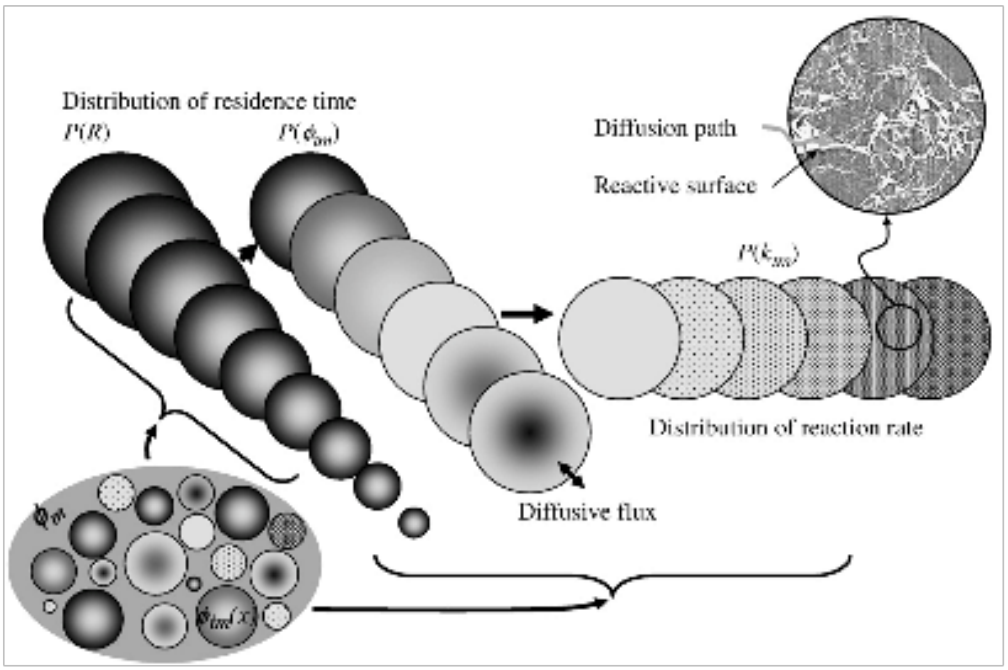

Figure 8-3. Schematic of the multicontinuum reactive transport model developed for the quantification of the impact of physico-chemical heterogeneity in porous media. The two directions indicated in the figure stand for chemical (distribution of kinetic rate coefficient) and physical heterogeneity (the distributions of inclusion sizes and porosity). The CT scan of the rock illustrates the non-resolved subscale. The different sphere sizes stand for the different types of heterogeneity that are unified in the medium, as indicated by the ellipse in the lower left corner (From Dentz et al., J. Contam. Hydrol., 2011).

8.2 Upscaling Analyses

8.2.1 Derivation of effective non-local reaction kinetics for transport in physically and chemically heterogeneous media

The correct characterization of the effective reactive transport dynamics is an important issue for modeling reactive transport on the Darcy scale, specifically in situations in which reactions are localized, that is when different reactions occur in different portions of the porous medium. Medium heterogeneities as expressed by spatial variability of hydraulic conductivity leads to gradients in chemical species concentrations and thus to mass transfer limitations on chemical reactions.

Many laboratory studies of geochemical reactions strive to eliminate such mass transfer limitations by using grinded rock and thus creating well-mixed conditions. As a consequence, laboratory scale reaction rates are systematically larger than the ones measured on the field scale, because the effective reactive surface is in general smaller due to mass transfer limitations between regions of varying permeability and porosity. Under such conditions the conventional approach of homogenizing only the porous medium chemistry is not appropriate. In order to quantify these effects, we studied reactive transport in a porous medium that is characterized by mass transfer between a mobile and a distribution of immobile regions, se the schematic in Figure 8-3.

Chemical and physical heterogeneities are reflected by distributions of kinetic reaction rate constants and residence times in the immobile zones. We derived an effective reactive transport equation for the mobile solute that is characterized by non-local physical mass transfer and reaction terms. Specifically, chemical heterogeneity was upscaled in terms of a reactive memory function that integrates both chemical and physical heterogeneity. Mass transfer limitations due to physical heterogeneity yield effective kinetic rate coefficients that can be much smaller than the volumetric average of the local scale coefficients.

These results help to explain and quantify the often reported discrepancy between observed field reaction rate constants and the ones obtained under well mixed laboratory conditions. Furthermore, these results indicate that transport under physical and chemical heterogeneity cannot be upscaled separately. The results of this work have been published in the Journal of Contaminant Hydrology (Dentz, M., P. Gouze and J. Carrera, Effective Non-Local Reaction Kinetics for Transport in Physically and Chemically Heterogeneous Media, J. Cont. Hydrol., doi:10.1016/j.jconhyd.2010.06.002, 2010). A review paper on "Mixing and Reaction in Heterogeneous Media" has been published in Journal of Contaminant Hydrology (Dentz, M., T. Le Borgne, Englert, A. and B. Bijeljic, Reactive Transport and Mixing in Heterogeneous Media: A Brief Review, J. Cont. Hydrol., doi:10.1016/j.jconhyd.2010.05.002 2010.).

8.2.2. Upscaling of Multiphase Flow

General Approach

Spatial heterogeneity in conjunction with gravity forces impacts on the spreading of the saturation front of carbon dioxide that displaces brine.

We studied the influence of buoyancy and spatial heterogeneity on the spreading of the saturation front of a displacing fluid during injection into a porous medium saturated with another, immiscible fluid, see Figure 8-4. To do so we used a stochastic modeling framework. We derive an effective large-scale flow equation for the saturation of the displacing fluid that is characterized by six nonlocal flux terms, four that resemble dispersive type terms and two that have the appearance of advection terms. From the effective large scale flow equation we derived measures for the spreading of the saturation front. A series of full two phase numerical solutions are conducted to complement the analytical developments. We find that the interplay between density and heterogeneity leads to an enhancement of the front spreading on one hand and to a renormalization of the evolution of the mean front position compared with an equivalent homogeneous medium. The quantification of these phenomena plays an important role in the design and assessment of carbon sequestration injections. The increase of the surface area between phases as measured by the front dispersion impacts on the dissolution and entrapment efficiency. Our study provides a theoretical basis for the design of injection strategies to optimize the sequestration of carbon dioxide. The results of these work are published in the journal Water Resources Research (Bolster, D., I. Neuweiler, M. Dentz, J. Carrera, The Impact of Buoyancy on Front Spreading in Heterogeneous Porous Media in Two-Phase Immiscible Flow, accepted, Water Resour. Res., 2010). This work allowed to quantify the impact of heterogeneity on the spreading of the interface between the displacing and the displaced fluid.

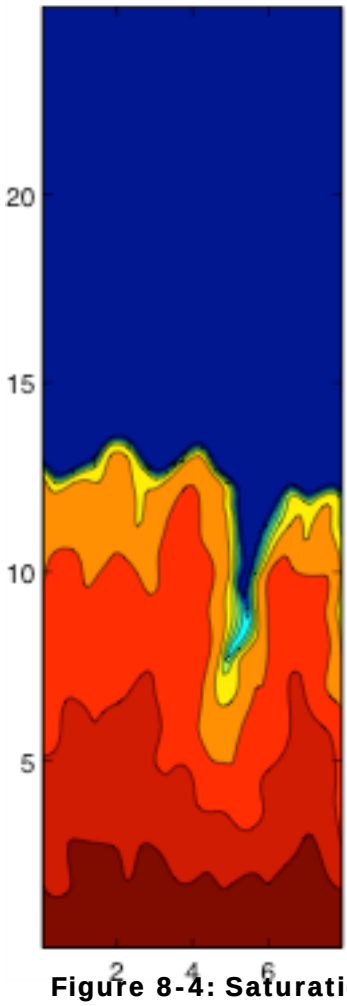

In general, the behavior of multiphase flow in heterogeneous media is different from the one found in homogeneous environments. As seen above, spatial heterogeneities can lead to increased spreading of the interface between the different fluids, and thus may increase the dissolution capacity due to an increased interface length. Strong medium contrasts can cause the entrapment of fluid in low permeability regions, and slow mass transfer processes between different regions of the medium. We considered two approaches to quantify large scale multiphase flow, (i) an effective parameter model, which assumes that the flow system is locally at equilibrium, (ii) a double continuum model, which accounts for non-equilibrium effects at the local scale. In the first approach, the spreading of the interface between different fluids can be quantified by a macrodispersion coefficient, which depends on the correlation length of the medium and the variance of log-hydraulic conductivity, similar to single phase flow and passive solute transport. Thus, if local equilibrium exists, large scale multiphase flow in heterogeneous media can be parameterized by a macrodispersion coefficient. For the case of local scale non-equilibrium as can be expected in media with strong contrasts in the hydraulic properties, we derived a double continuum approach that explicitly models the (slow) mass exchange between portions of the medium characterized by strong contrasts. This model is parameterized by a memory function that quantifies mass exchange between mobile and immobile medium fractions. This memory function can be traced back to the one for single phase flow, which simplifies the model parameterization significantly. We also developed a numerical approach for upscaling two-phase flow of CO2 in complex heterogeneity (Yang et al., 2013)

Figure 8-4: Saturation profile in sample realization.

Numerical upscaling for complex geological heterogeneity

Numerical upscaling is needed for cases with complex heterogeneity. A macroscopic invasion percolation (MIP) model is developed, based on the assumption of capillary force dominance. Comparison of the MIP model with the numerical simulator TOUGH2/ECO2N for simulations of large-scale drainage capillary pressure curves shows a reasonably good match between results from the two models. We consider a two-dimensional heterogeneous section which is composed of a rectangular array of cells. The array is assigned a local permeability value to each cell, assuming that the permeability follows a multimodal distribution. Based on the well log data from deep borehole FFC-1 at the South Scania Site (Sweden), we generate realizations of the heterogeneous medium using geostatistical methods. Large-scale constitutive relationships are obtained through simulation procedures of CO_2 displacing brine in multimodal heterogeneous media for ten cases with different geostatistical parameters. The large-scale constitutive relationships are mainly controlled by the proportion and the permeability variability of the background (framework) material, while the existence of the non-framework materials and their permeability variabilities may contribute, in a complex way, to the uncertainty in the large-scale constitutive relationships. In addition, the Leverett equation may well describe the relationship between the large-scale capillary pressure and absolute permeability when the sandstone (background material) proportion is high (>0.7). For cases with smaller sandstone proportions

it may not be appropriate to link capillary pressure and absolute permeability through the Leverett equation.

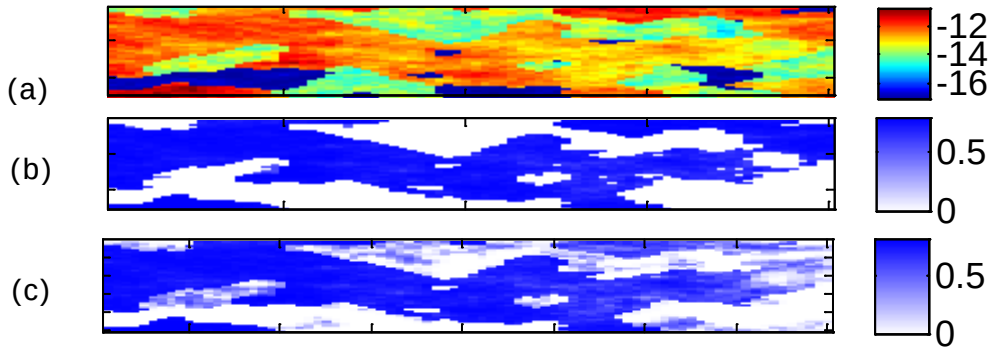

Figure 8-5. (a) Example ($\log_{10} k$) permeability field realization for a multimodal heterogeneous medium. (b) CO_2 saturation distribution obtained from the percolation model for an externally applied pressure difference of 20000 Pa between the invading CO_2 and the formation brine. (c) CO_2 saturation distribution obtained from TOUGH2/ECO2N simulation.

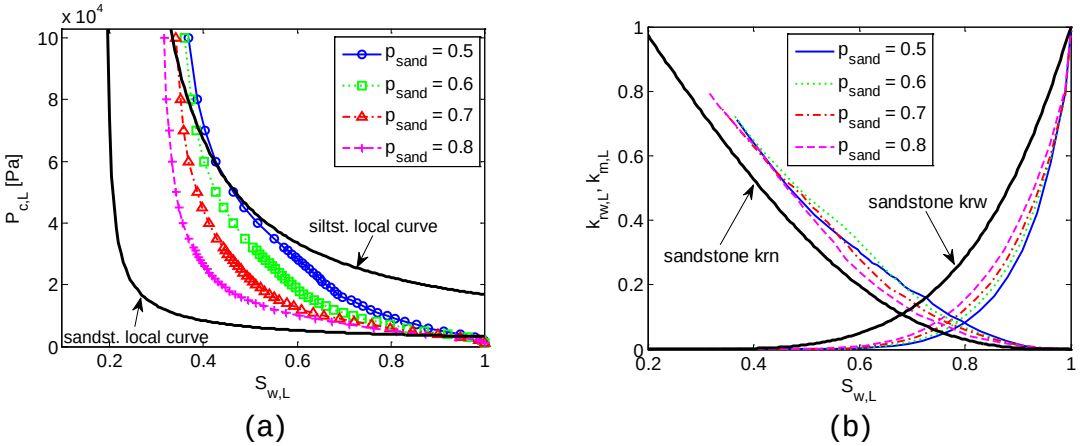

Figure 8-6. Comparison of ensemble average capillary pressure and relative permeability curves for different material proportions. (Yang et al, 2013)

8.2.3 Quantification of mixing in heterogeneous media

We investigated the temporal scaling properties of mixing in heterogeneous permeability fields with variances ranging from very small (0.01) to very large (9). We quantified mixing by the scalar dissipation rate, which we estimate over a large range of temporal scales. For an initial pulse line injection (see Figure 8-5), we find that moderate and strong heterogeneity induce anomalous temporal scaling of the scalar dissipation rate, which we call non-Fickian mixing. This effect is particularly relevant for upscaling reactive transport as it implies a non-Fickian scaling of reactive transport. Although spreading and mixing are intimately coupled, we find that their scaling properties are not directly related in general.

In the non- Fickian mixing regime, the temporal scaling of the scalar dissipation rate depends on the complex spatial distribution of the concentration field that generates transverse mixing.

For times larger than the characteristic diffusion time associated with one permeability field correlation length, the heterogeneity of concentration in the plume is attenuated and progressively erased by diffusion. Thus, at large times, the temporal scaling of mixing and spreading can be related through a simple analytical expression. These results are reported in the journal Advances in Water Resources (Le Borgne, T., M. Dentz, D. Bolster, J. Carrera, J.-R. de Dreuzy, P. Davy, Non-Fickian scaling of mixing in heterogeneous velocity fields, Adv. Water. Resour., doi:10.1016/j.advwatres.2010.08.006, 2010).

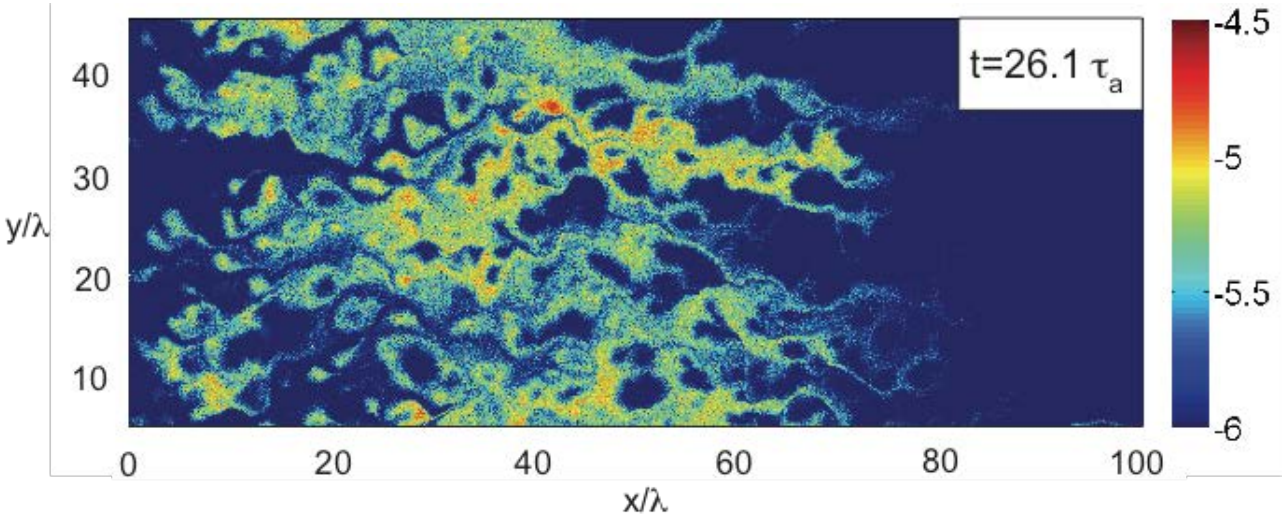

Figure 8-7. Concentration distribution evolving from a line source at t = 0 at x =0 after t = 26 advection times. One can clearly distinguish advective spreading and actual mixing.

Furthermore, we studied the evolution of the scalar dissipation rate and thus mixing in confined stratified media. We find an approximate, but accurate expression (when compared to numerical simulations) to evaluate mixing. These results shed some new light on the mechanisms that lead to large scale mixing and allow for a distinction between solute spreading, represented by the mean concentration, and mixing, which comes from both the mean and deviation concentrations, at pre-asymptotic times. The work is published in Journal of Contaminant Hydrology (Bolster, D., F. J. Valdés-Parada, T. Le Borgne, M. Dentz and J. Carrera, Mixing in confined stratified aquifers, J. Cont. Hydrol., doi:10.1016/j. jconhyd.2010.02.003, 2010.)

We also studied the effect of long range mass transfer on mixing and chemical reactions. We find that the reaction rates far from the reactant source are greater for long-range mass transfer than for purely advective diffusive mass transfer; however, the globally integrated reaction rate decreases with longer range mass transfer. Reaction products can be found in places precluded by Fickian dispersion, and overall reaction rates are suppressed. This study has been published in Physical Review E (Bolster, D., D. A. Benson, T. Le Borgne and M. Dentz, Mixing and Reaction Modeled by the Space-Fractional Advection-Dispersion Equation, Phys. Rev. E, 82, 021119, 2010).

In order to study mixing dynamics in heterogeneous porous media, we quantified the effective mixing state by the integral of concentration squared over the spatial domain. We defined the potential mixing in terms of the mixing state of a Gaussian plume that has the same longitudinal dispersion coefficient as the actual solute distribution. In case that the average concentration can be well approximated by a Gaussian, the difference between the effective and potential

mixing state quantifies the concentration variance. In general, however, this is not true. Nevertheless, we will refer to this quantity in the following as concentration variance.

The so defined concentration variance normalized by the potential mixing traduces the lag of diffusion to homogenize the concentration structure generated by the dispersion processes. In the following it will be denoted by cv. This definition makes full use of dispersion for quantifying mixing and restricts the analysis of mixing to the difference of the effective and potential mixing states. In cases for which the mean concentration can be assumed Gaussian, we use the balance equation for the concentration variance to show that the difference of mixing states depends solely on the macrodispersion coefficient (spreading rate) and the recently developed mixing scale, which is defined as the smallest scale over which concentration can be considered uniform, and which quantifies the internal plume disorder. Numerical simulations to show that cv turns has a simple scaling form that depends on neither the heterogeneity level nor the Peclet number. A very similar scaling form is recovered for Taylor dispersion. This generic characterization of mixing can offer new ways to set up transport equations that honor not only advection and spreading but also mixing. These results have been published in the journal Water Resources Research (Dreuzy, J.-R., J. Carrera, M. Dentz, and T. Le Borgne, Time evolution of mixing in heterogeneous porous media, Water Resour. Res. 48, W06511).

8.2.4 Multirate Mass Transfer and Random walk Models of non-Fickian transport in heterogeneous media

Many flow and transport phenomena, ranging from delayed storage in pumping tests to tailing in river or aquifer tracer breakthrough curves or slow kinetics in reactive transport, display non-equilibrium (NE) behavior. These phenomena are usually modeled by non-local in time formulations, such as multi-porosity, multiple processes non equilibrium, continuous time random walk, memory functions, integro-differential equations, fractional derivatives or multi-rate mass transfer (MRMT), among others. We developed a MRMT formulation that can be used to represent all these models of non-equilibrium. The formulation can be extended to non-linear phenomena. Here, we develop an algorithm for linear mass transfer, which is accurate, computationally in- expensive and easy to implement in existing groundwater or river flow and transport codes. We illustrate this approach by application to published data involving NE groundwater flow and solute transport in rivers and aquifers. This work has been published in Hydrol. Earth Syst. Sci. (Silva, O., J. Carrera, S. Kumar, M. Dentz, A. Alcolea and M. Willmann, A general real-time formulation for multi-rate mass transfer problems, Hydrol. Earth Syst. Sci., 13, 13991411, 2009.)

Derivations of continuum nonlocal models of non-Fickian (anomalous) transport require assumptions that might limit their applicability. We developed a particle-based algorithm, which obviates the need for many of these assumptions by allowing stochastic processes that represent spatial and temporal random increments to be correlated in space and time, be stationary or non-stationary, and to have arbitrary distributions. The approach treats a particle trajectory as a subordinated stochastic process that is described by a set of Langevin equations, which represent a continuous time random walk (CTRW). Convolution- based particle tracking (CBPT) is used to increase the computational efficiency and accuracy of these particle-based simulations. The combined CTRW–CBPT approach enables one to convert any particle tracking legacy code into a simulator capable of handling non-Fickian transport. The results of this work are reported in the Journal of Computational Physics (Srinivasan, G., D. M. Tartakovsky, M. Dentz, H. Viswanathan, B. Berkowitz, and B. Robinson, Random Walk Particle Tracking Simulations of Non-Fickian Transport in Heterogeneous Media, J. Comp. Phys., 229, 43044314, 2010).

We developed an efficient method for the simulation of diffusion processes in heterogeneous media characterized by heterogeneous trapping (chemical or physical trapping). The method is

based on the time-domain random walk (TDRW) framework. We (i) demonstrate the exact equivalence of the TDRW method and the finite volume discretization of the heterogeneous diffusion equation, (ii) based on the constructive nature of this demonstration, we derive the TDRW model for diffusion and heterogeneous trapping. The developed TDRW method is an efficient tool for the numerical simulation of diffusion problems in pixelized maps obtained from XMT-imaging of heterogeneous rock samples in combination with heterogeneous trapping, see Figure 8-8.

Specifically, the TDRW approach provides an ideal framework for the integration of particle based simulations and chemical reactions.
Thus, the random walk method was extended for the simulation of diffusion processes in heterogeneous media characterized by spatially distributed sorption-desorption reactions and solute immobilization due to trapping in low conductivity zones. The method is based on the time-domain random walk (TDRW) framework, which we derived rigorously from a finite volume discretization of the diffusion equation, and generalized to account for chemical reaction and trapping. We furthermore developed an TDRW scheme for advective-diffusive transport in any spatial dimension. This random walk particle tracking method is used for the implementation of particle based reactive transport, specifically for the efficient pore scale simulation of dissolution-precipitation reactions. The main results of these studies have been published in the research paper on Diffusion and Trapping in Heterogeneous Media: An Inhomogeneous Continuous Time Random Walk Approach, Dentz, M., P. Gouze, A. Russian, J. Dweik, and F. Delay, Adv. Water Resour. 49, 13-22, 2012.

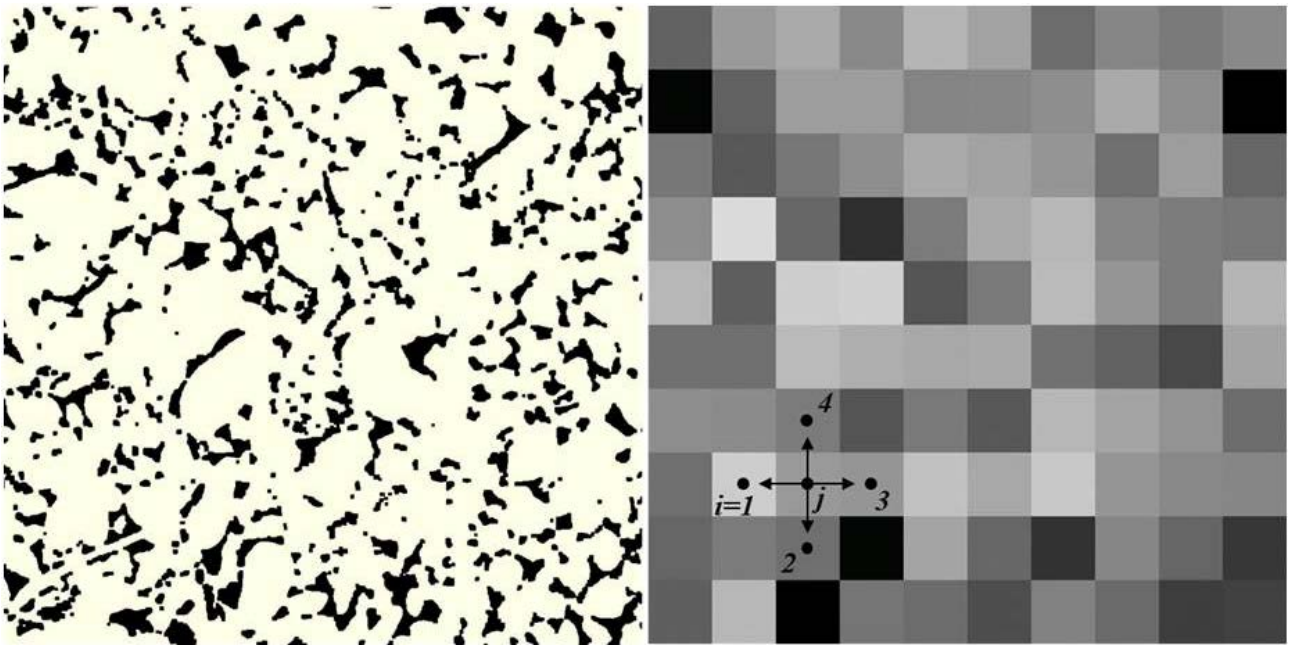

Figure 8-8. Left: Numerical cross-section of a connected pore cluster obtained from a d = 3 dimensional XMT image (5 mm × 5 mm limestone sample), the black color indicates pore space. Right: Equivalent upscaled porosity map. The arrows indicate possible particle transitions to nearest neighbors.

8.3 Main results and achievements

The main findings and results include:

(i) Quantification of the increased CO2 front spreading due to the interaction of spatial heterogeneity and buoyancy in terms of effective dispersion coefficients. Development of a dual porosity model for two-phase flow in heterogeneous media.

(ii) Derivation of effective reaction kinetics for reactive transport in heterogeneous media and evaluation of the impact of heterogeneity on the reaction efficiency. Reaction rates in heterogeneous media are in general smaller than in homogeneous laboratory settings due to mass transfer limitations.

(iii) Identification of the local scale mass transfer and heterogeneity processes that control mixing and their quantification in terms of the scalar dissipation rate. This description allows for the separation between mixing and spreading processes, which are often equalized for transport in heterogeneous media. Identification of a scaling form for the concentration variance in heterogeneous media.

(iv) Efficient simulation techniques for the modelling of non-Fickian large scale transport processes as described by the multirate mass transfer and continuous time random walk frameworks. Development of an efficient simulation algorithm for diffusion in heterogeneous media under multiple trapping.

(v) Development of numerical upscaling for complex, multimodal geological heterogeneity.

9 WP 9 - Certification

The global objectives of WP 09 are to

- Develop a generic methodology for performance and risk assessment related to CO2 storage in saline aquifers;
- Application of the methodology in one of the MUSTANG test sites;
- Develop measures for the performance evaluation of the CO2 storage in a specific reservoir.
- Outline a set of practical guidelines for the quantification of a specific site for CO2 storage.
- Develop a decision support system in order to assist the decision making process both at the scientific level and the decision making level.

9.1 Development of the Decision Support System (UB)

The main objective of the DSS is to assist the decision maker, the regulator and the scientist/engineer in the evaluation and quantification of potential sites for CO2 injection and storage in deep saline aquifers. The architecture of the system developed involves one database and a modular application composed by: (1) a visualization module, (2) an analysis module, (3) a guidelines module, and (4) a risk assessment module. The analysis module will allow the user to perform certain analysis like Injectivity, Containment and Capacity analysis. The Risk Assessment module focuses on the site risk matrix approach. The Guidelines module will contains the methodologies of CO2 injection and storage into deep saline aquifers guidelines, provided by the Mustang partners. The MUSTANG DSS web application can be reached via internet site.

Because of the multiple aspects of processes involved, the web solution must be flexible and compliant with different type of data. Here are the main features of the MDSS.

The core server application. The main server application that manages all the informational fluxes is a Java based Open-Source technology (GlassFish). Under the application server many powerful java technologies are put together (AAS < Java Authentication and Authorization Service>, EJB3 <Enterprise Java Bean>, JSF <JavaServer Faces>, JSP <JavaServer Pages>, Servlets3). Also under the GlassFish work 2 GIS based OpenSource Technologies: (1) Geoserver – for geospatial data publishing and management and (2) GDAL <Geospatial Data Abstraction Library – for geospatial raster based data analysis and transformation.

The Database Actually the MDSS comes with 2 databases: (1) an intern use database that manages all the users, roles and rights – this database is not design to be access or managed by the users, only by application administrators, and (2) the Mustang Database – in which all the specific data are stored (spatial data, attributes, time series, etc). The technology used for the database is PostgreSQl and PostGIS (for spatial data).

The application interface. Based on a powerful open-source technology (PrimeFaces) the interface brings the desktop application experiences to the web. The modular structure is based on different panels that can be minimized and maximize in order to let the user construct a

specific layout. Inside the web interface the user will find the 4 main conceptual modules of the application: (1) Visualization (2) Analysis, (3) Guidelines and (4) Risk Assessment.

Visualization. Data can be visualized in three different formats: (1) geospatial visualization – trough the implementation of a 3D geospatial environment provided by Google Earth API, (2) table view and (3) graphic view (for time series). An important feature developed to facilitate the data interpretation and analysis is the styling of raster based data. The user can upload ASCI geospatial files (ASCI grid) to the application and to style them accordingly to his needs (Fig 9-1).

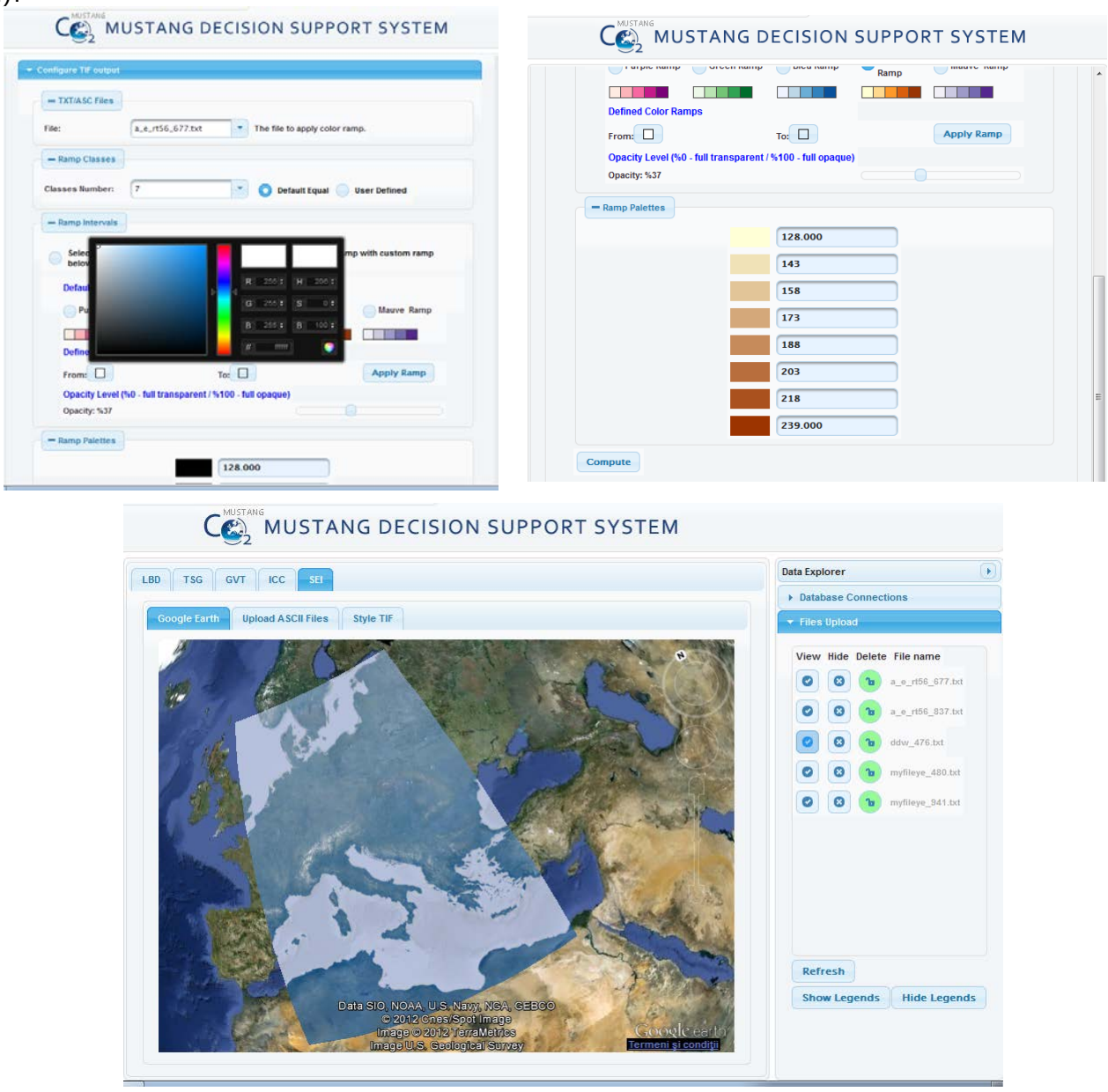

Figure 9-1: Styling data

Analysis. Injectivity, Capacity and Containment analysis is already developed. The analysis is flexible and is not constraining the user to create the analysis upon data from the database. The

data coming from the database are also display in the input data forms of the analysis, but this aspect gives to the user the needed information if there are no other sources (Fig. 9-2).

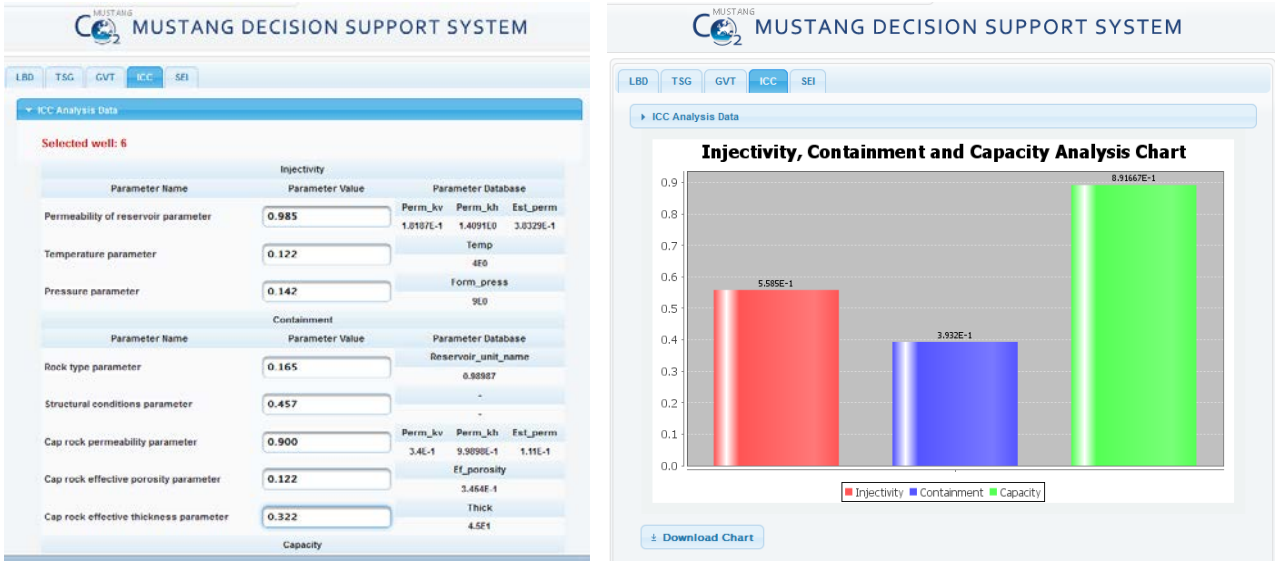

Figure 9-2. ICC analysis.

Another developed analysis is the Time Series Generator. The time series are plotted taking account the spatial point (the well, and the depth), the time period (the user will define a time period) and the parameters (the user can select to plot one parameter or many parameters (Fig 9-3).

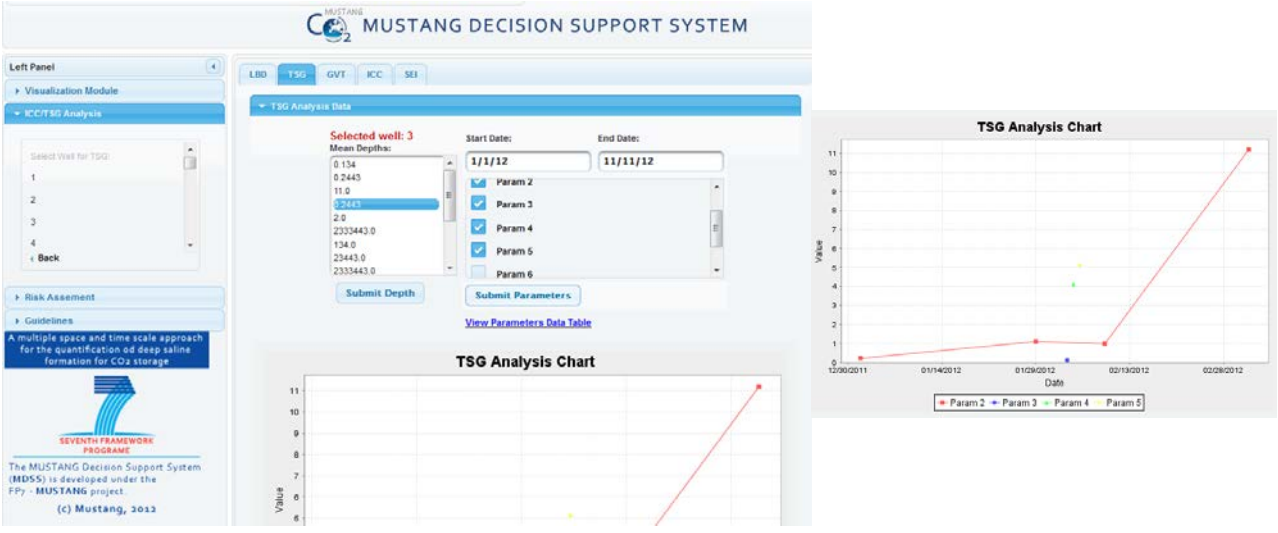

Figure 9-3. Time Series Analysis

Guidelines. For guidelines module the application provides the framework to upload, store and view specific technical and scientific material in PDF or Video Format (Fig. 9-4).

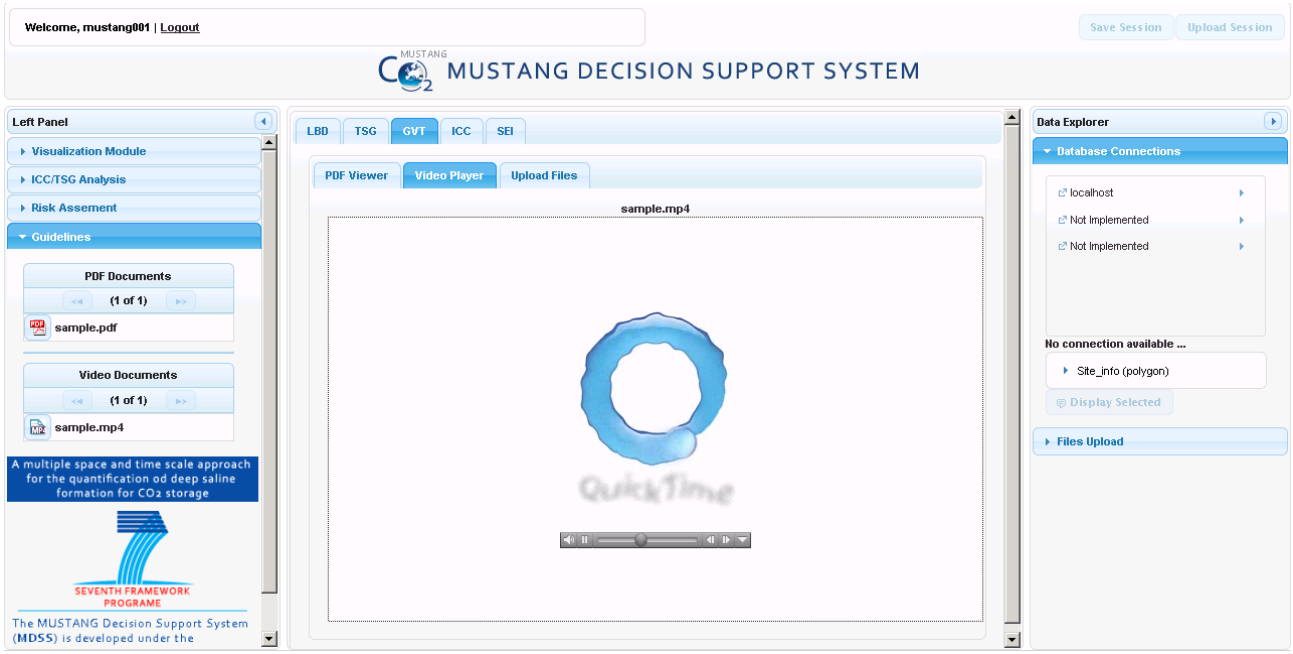

Figure 9-4. Guidelines

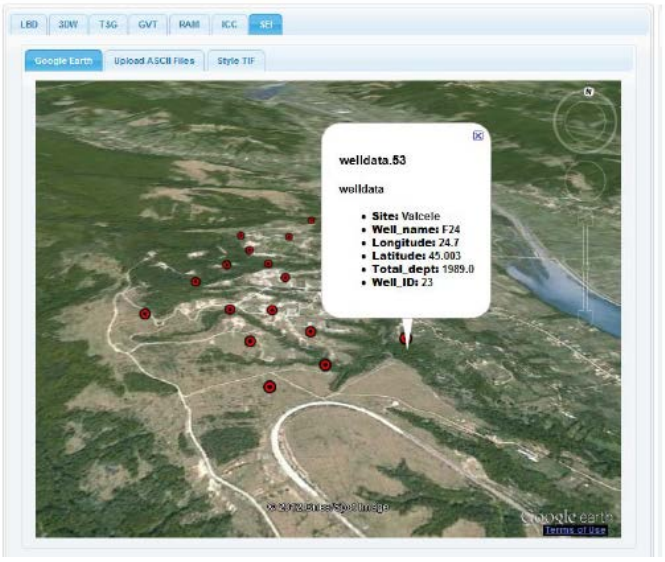

Figure 9-5. Spatial data visualization of the MUSTANG DSS

9.2 Risk Management System (Oxand)

The final deliverable summarizing the key findings for guideline of the risk management methodology to a CO2 deep saline aquifer storage (Deliverable D096) was delivered month 58. This document illustrates application of the risk management approach described in a previous deliverable (D091), for a generic storage site in deep saline aquifer. The objectives of WP9 work package for Risk Management are as follows:

- Adapt methodology for performance and risk management for CO2 Storage Project (Framework)
- Adapt approach for measures for the risk-based performance evaluation
- Outline a set of guidelines for the risk management of a specific site for CO2 storage

The application of the risk management approach has been performed for a generic storage site in deep saline aquifer such as the storage in Heletz.

The objective of the last stage of this WP9 done was to summarize the work done as part of 'Risk Management' Section of MUSTANG project and provide guideline for any actors in a CO2 geological storage project for risk management including risk assessment and their treatments to secure project performance. It gives also some elements to identify key challenges and improvements to be performed for the future studies on technological risks management over project lifecycle for future CO2 storage projects.

A methodological framework is proposed to structure a set of actions and rules to achieve the desired results.

The main results of this Work Package are:

- Consolidate the Methodological Guide by applying it to specific cases studies for a CO2 storage project;
- To formulate some improvements on risks treatments, propose measures to control the risk, and collect feedback and assessment of the likelihood (or probability).
- Update the methodology in particular through the integration of monitoring measures and treatment parameters of interest and risks in the guideline ;
- Formulate some key lessons learned from the application to cases studies to assess the difficulties and strengthen its practical use.

9.2.1 Implementation of the Risk Assessment

The application of the risk management approach has been performed for a generic storage site in deep saline aquifer. The main objective of such approach is:

- Improve risk management of future CCS projects
- Share and improve knowledge on risks
- Establish a risk framework for CCS
- Create a risk database for CCS projects with characterization of causes and consequence
- Ensure the major risks are mitigated from relevant treatment action and Monitoring program (MVA)

A workflow has been proposed (see Figure below).

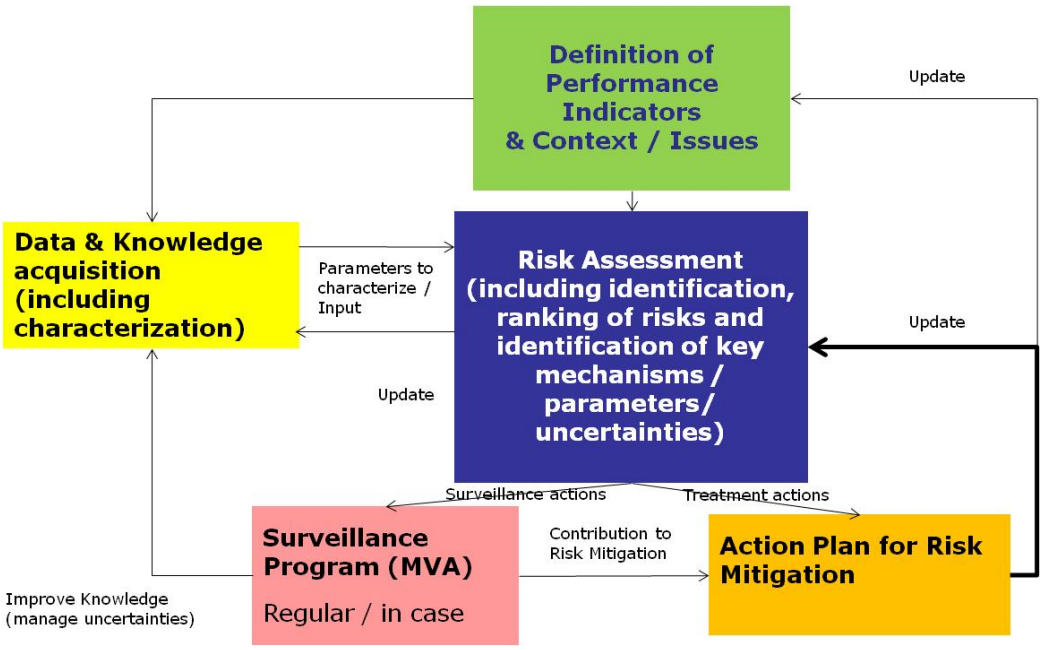

Figure 9-6. Workflow for Risk Management for a CCS Project.

Technical risk identification and estimation have been defined for some components of a CO_2 storage in a deep saline aquifer, following steps below:

1. *Failure mode and effect analysis (FMEA) of components of a CO_2 storage similar to Heletz site.*

The achievement of a functional model of the studied system allows to have an overview of the system and to show the different elements to consider for the functional analysis and then for the risk identification. The objectives of the functional analysis are:

- To identify the functions of the system (and sub-system) regarding the storage;
- To set the contribution of each component with respect to these functions;
- For each component, to identify the potential failure modes, causes and consequences.

2. *Method to visualize risks scenarios, examples of scenarios selection*

Functional analysis coupled with a failure mode and effects analysis (FMEA) allows to create a preliminary risk register. This comprehensive list of risks must be validated by project leaders and/or by experts with good knowledge of the storage site and of CCS technology.

In order to select the most relevant risks for a specific project, bow-ties can be built. This approach allows visualizing, for a main event (or failure mode), all causes and associated effects (see illustration in figure below). Impacts on vulnerable targets (aquifers, atmosphere) also appear in the bow-ties diagrams.

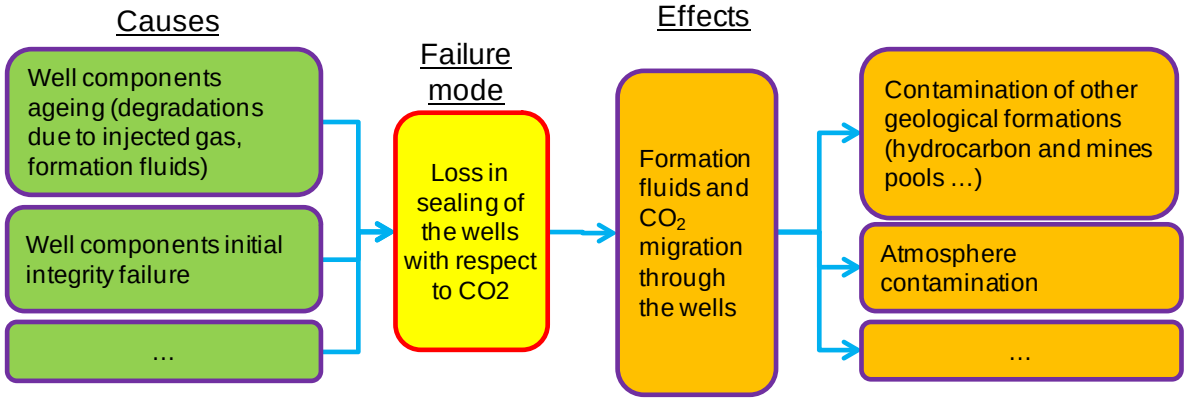

Figure 9-7: Example of Bow-Tie for the Central Event "Loss in sealing of the well with respect to CO2".

3. Risk estimation methods for a generic component

Estimations of risks were based on Oxand's feedback and description of Heletz site. The estimation has been made for a list of possible risks than can occur in the injection well and the caprock. To go in details, a scenario should be a combination of cause and a consequence however, to limit the number of risks; a scenario can also be a combination of several causes and consequences for a given failure mode. Results show that:

- Injection well has the highest levels of risk, this can be explained by :
  - A low knowledge level of the injection well, combined with the fact that, for the purpose of the Heletz experiment, the well will be completed with specific equipment not commonly used in the industry.
  - The pressure will be the highest in the close vicinity of the injection well.
- Risk levels for the caprock are lower, mainly explained by:
  - The quantity of CO_2 to be injected in the reservoir is low, and impacts on the geology should be very limited, over a short period of time.

The final outcome of risk estimation is to be able to rank the risks according to the criticality levels. This ranking will support the definition of priorities (risk with higher criticality value should have priority in the treatment) in the definition of treatment actions, if treatment actions are found to be required.

Figure below illustrates a map of the macro risks associated with Heletz (as an illustrative example based on a first assessment with first available data). For more details see Deliverable D-094. On this map, points represent the estimation of the macro-risks associated to the projects.

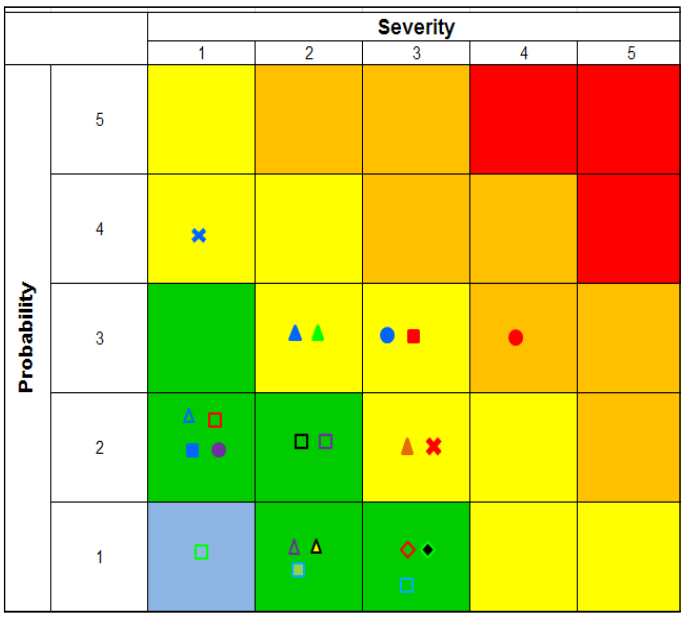

Scenarios (as illustrative)

- CO2 migration through P&Aed wells (well integrity)
- CO2 migration through monitoring wells (well integrity)
- CO2 migration through injection wells (well integrity)
- Lateral migration of CO2 plume
- CO2 migration across caprock (caprock integrity)
- Pressure change affecting above geological formation
- Loss of injectivity
- Risk of Insufficient Storage Volume
- ...

Figure 9-8: Macro Risks Maps for Heletz Project – Based on a First Assessment (with limited data and first set of assumptions for the project)

4. Risks treatment

Risk treatment has to be structured from 3 distinct plans:

- The risk-based treatment plan
  - This plan is built to define actions with respect to critical risks and to reduce their values below an acceptable level. Actions could act on probability of occurrence level or on severity level (impact on consequences). Some examples of actions could be: Change injection strategy, close the leaky well ….
- Regulatory requirements Plan –
  - This plan will be dependant of national regulatory requirements. It could impact the needs in terms of monitoring, especially in:
    - Surface monitoring (soil, air, rivers…)
    - Shallow subsurface (usable water aquifer protection, vadose zone pollution…) monitoring
- The **risk-based MVA program** dealing with
  - Time dimension: frequency, project phases…
  - Spatial dimension : Locations of the new wells drilled Monitoring wells spacing, sensors, measurements locations …

The MVA program (Figures below) runs from the end of the pre-operational phase of the project (baseline data acquisition) to the beginning of the post-closure phase (end of the operator liability period) and therefore covers the injection phase and the post-injection phase.

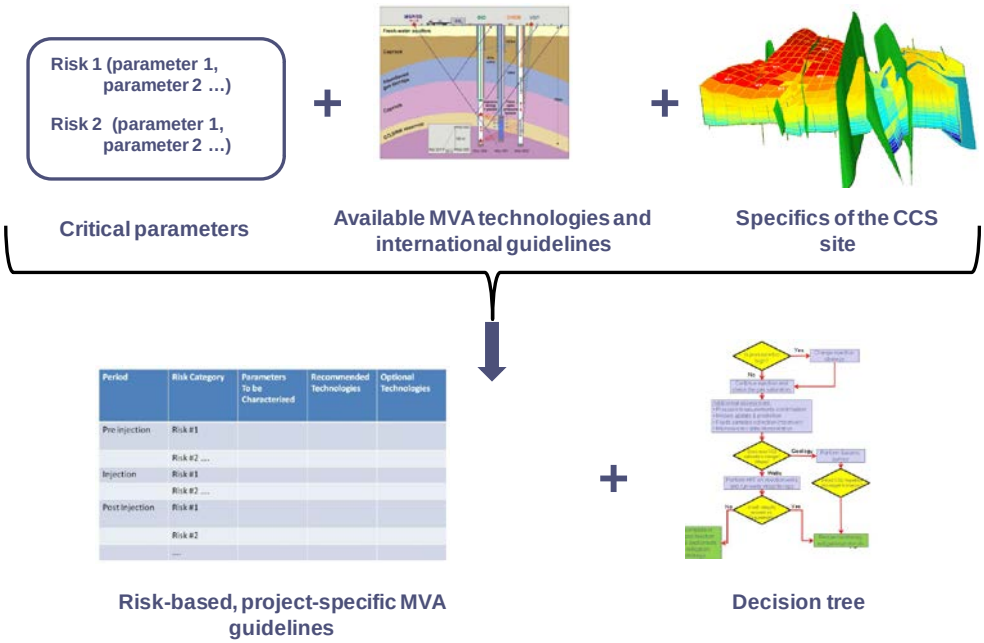

Figure 9-9: Risk-based MVA – Key Principles

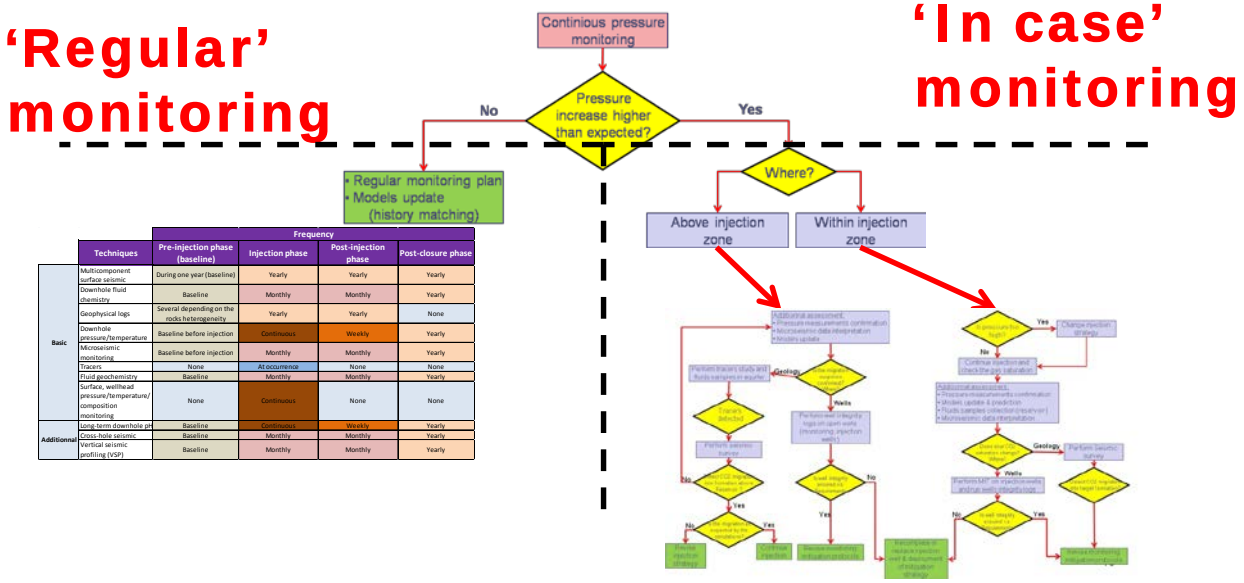

Figure 9-10. Overall Decision-Tree for the monitoring of a CO2 geological storage Project, (a) Start of the Decision-Tree and "regular" MVA Plan, (b) Decision-tree Associated with Abnormal Pressure Increase Within Injection Zone, (c) Decision-tree Associated with Abnormal Pressure Increase Above Injection Zone

	Techniques	Frequency			
		Pre-injection phase (baseline)	Injection phase	Post-injection phase	Post-closure phase
Basic	Multicomponent surface seismic	During one year (baseline)	Yearly	Yearly	Yearly
	Downhole fluid chemistry	Baseline	Monthly	Monthly	Yearly
	Geophysical logs	Several depending on the rocks heterogeneity	Yearly	Yearly	None
	Downhole pressure/temperature	Baseline before injection	Continuous	Weekly	Yearly
	Microseismic monitoring	Baseline before injection	Monthly	Monthly	Yearly
	Tracers	None	At occurrence	None	None
	Fluid geochemistry	Baseline	Monthly	Monthly	Yearly
	Surface, wellhead pressure/temperature/ composition monitoring	None	Continuous	None	None
Additionnal	Long-term downhole pH	Baseline	Continuous	Weekly	Yearly
	Cross-hole seismic	Baseline	Monthly	Monthly	Yearly
	Vertical seismic profiling (VSP)	Baseline	Monthly	Monthly	Yearly

Figure 9-11: Overall Decision-Tree for the monitoring of a CO2 geological storage Project, (a) Start of the Decision-Tree and "regular" MVA Plan, (b) Decision-tree Associated with Abnormal Pressure Increase Within Injection Zone, (c) Decision-tree Associated with Abnormal Pressure Increase Above Injection Zone

It is important to note that the Heletz CCS project is in an exploratory phase. As a result, the first-round risk assessment was based on preliminary data from a single test well and no laboratory results. By drilling additional test wells, acquiring additional seismic data, and getting the complete results from the laboratory work and associated analyses of samples from all wells, a much better representation of the geologic model and potential risks can be achieved. Also, it is important to note that risk assessment is an iterative and live process. The results of this first round of risk assessment are not meant to be final and will be updated periodically as more data become available. So, on this basis, it may well be used by operators of sites for geological storage of CO2 or engineering companies that assist them, for the constitution of regulatory reports for authorization, guidance efforts for characterization and monitoring sites and operations. This guide may also be useful to the authorities in the process of project certification. It thus aims to provide a common reference and recognized framing the risk analysis, and support for dialogue between the different stakeholders on these issues and decision making.

9.3 Recommendations and guidelines (EWRE)

Based on the results of MUSTANG and review of existing guidelines Deliverables D095 and D097 (Guidelines for the quantification of deep saline formations for CO_2 storage and Quantitative criteria and measures for assessing the performance of deep saline formation for CO_2 storage) have been prepared. Many projects, conducted in parallel to MUSTANG,have addressed these issues and there is abundant literature available. Accordingly, recommendations with regard to the quantification of deep saline formations and quantitative measures for the assessing performance are suggested. Most of them are quite compatible to the ones suggested in the

literature (and developed in parallel to MUSTANG). In our recommendations, however, emphasis is given to the experience obtained from MUSTANG field sites.